Springer Series in Solid-State Sciences 195

Teruo Matsushita

Superconductivity and Electromagnetism

Springer

Springer Series in Solid-State Sciences

Volume 195

The Springer Series in Solid-State Sciences features fundamental scientific books prepared by leading and up-and-coming researchers in the field. They strive to communicate, in a systematic and comprehensive way, the basic principles as well as new developments in theoretical and experimental solid-state science.

We welcome submissions for monographs or edited volumes from scholars across this broad domain. Topics of current interest include, but are not limited to:

- Semiconductors and superconductors
- Quantum phenomena
- Spin physics
- Topological insulators
- Multiferroics
- Nano-optics and nanophotonics
- Correlated electron systems and strongly correlated materials
- Vibrational and electronic properties of solids
- Spectroscopy and magnetic resonance

More information about this series at http://www.springer.com/series/682

Teruo Matsushita

Superconductivity and Electromagnetism

Springer

Teruo Matsushita
Kyushu Institute of Technology
Iizuka, Japan

ISSN 0171-1873 ISSN 2197-4179 (electronic)
Springer Series in Solid-State Sciences
ISBN 978-3-030-67567-7 ISBN 978-3-030-67568-4 (eBook)
https://doi.org/10.1007/978-3-030-67568-4

This Springer imprint is published by the registered company Springer Nature Switzerland AG
The registered company address is: Gewerbestrasse 11, 6330 Cham, Switzerland

Preface

Today, MRI systems with superconducting magnets are commonly used in hospitals, and commercial superconducting linear maglev trains that connect Tokyo and Nagoya in Japan in 40 min are scheduled to start in 2027. Thus, superconductivity has become well-known. In addition, it is known by people who are interested in our global environmental problems that the introduction of superconducting instruments and power cables has great potential to contribute to suppression of CO_2 emissions.

Superconductivity is a peculiar phenomenon in which electrical resistance disappears when a superconducting material is cooled down to very low temperatures. Thus, it has been investigated for a long time in solid-state physics, and many scientists have received Nobel prizes for work based on superconductivity. For example, the idea of symmetry breaking in the field of elementary physics by Dr. Youichiro Nanbu was derived from the theory of superconductivity.

Thus, the phenomenon of superconductivity may seem to be special. Even so, almost half of all elements show superconductivity. This means that superconductors are not minor substances. In addition, the ***E*-*B*** analogy, the main principle in present electromagnetism, can be made more rigorous by the introduction of superconductivity into Maxwell's theory, which was completed before the discovery of superconductivity. In other words, the existence of substances with zero resistivity, i.e., superconductors, could have been predicted in the 19th century.

Electromagnetic phenomena in superconductors can be described by first principles that assume the minimization of the relevant energy, since the phenomenon is reversible because of zero resistivity. On the other hand, irreversible phenomena such as electrical resistivity can be easily found in the world. The mechanism of irreversibility has not yet been proved theoretically. In this sense, superconductors are pure materials from the viewpoint of physics. Even so, the electromagnetic phenomena in superconducting wires used for electric power instruments, etc. are irreversible. This irreversible nature is largely different from irreversible phenomena such as electrical resistance in normal metals but similar to friction: When an object does not move due to friction under a driving force, there is no energy dissipation. If a driving force that exceeds the friction moves the object, energy dissipation occurs.

The situation is similar in superconductors. When a constant direct current flows in a superconductor and quantized magnetic flux lines do not move, there is no energy dissipation, but when an alternating current flows or when an alternating magnetic field is applied, quantized magnetic flux lines move, and energy is dissipated in the superconductor. In particular, the loss energy in a unit cycle of applied AC magnetic field is independent of the frequency, and the loss is iron type in nature. Since the loss energy is proportional to the area of the closed magnetization curve, this is called hysteresis loss. On the other hand, the loss energy in most metals is copper type and proportional to the frequency. The irreversibility associated with the copper-type loss comes from the breaking of time reversal symmetry of the equation of motion, although the mechanism has not yet been proved theoretically.

The irreversibility in superconductors can be proved theoretically, as shown in this book. Then, the force balance equation used in the phenomenological critical state model that describes irreversible phenomena in superconductors can be derived using first principles. Here it should be noted that the flux pinning that is responsible for hysteresis losses originates from the interaction between flux lines and pinning potentials. Hence, this interaction is essentially reversible in nature. In fact, if we watch carefully, reversible electromagnetic phenomena can be observed. It is also proved that, if the displacement of flux lines exceeds a reversible regime, the phenomena become irreversible. The essence of the irreversibility in the critical state in superconductors can be summarized by the statement that the force of defects works to prevent flux lines from being driven by the Lorentz force. This results from a biased statistical distribution of flux lines inside innumerable potentials in the superconductor. A certain phenomenon, i.e., an instability of flux motion in a pinning potential well, is inevitable for realization of the biased distribution, as shown in this book. This is quite analogous to friction and hysteresis in ferromagnetic materials. In this sense, it can be said that theoretical understanding on irreversibility is slightly advanced in the field of superconductivity.

In addition, it can be emphasized that a certain electromagnetic phenomenon in superconductors is not widely known. This is the longitudinal magnetic field effect observed in a current-carrying superconductor in a parallel magnetic field. The peculiarity is represented by a dramatic increase in the critical current density, i.e., the maximum non-dissipative current density, and the appearance of negative voltage. It is empirically known that the force-free state ($\boldsymbol{J} \times \boldsymbol{B} = 0$) is achieved in this field configuration. That is, the current density $\boldsymbol{J}$ and the magnetic flux density $\boldsymbol{B}$ are parallel to each other. Research on this phenomenon started in 1963 and has been conducted on metallic low-temperature superconductors. The high-temperature superconductors were discovered in 1986; however, and attention of most researchers was attracted to these new materials. In addition, an appreciable longitudinal magnetic field effect was not observed in high-temperature superconductors fabricated at that time due to weak-link grain boundaries that disturb current flow. For this reason, the longitudinal magnetic field effect has not been investigated for a long period, and only small number of researchers know about this effect now.

The characteristic point of this effect is that the magnetic flux density $\boldsymbol{B}$ and vector potential $\boldsymbol{A}$ are parallel to each other in the static force-free state. That is, the static magnetic helicity is not zero in this state. This can be achieved only in superconductors with zero electrical resistivity. When Maxwell's theory was completed in the 19th century, superconductors had not been discovered. Hence, the state with nonzero static magnetic helicity was not considered during the process of completion of Maxwell's theory. In addition, such a peculiar state has not been theoretically investigated from the viewpoint of electromagnetism. Hence, it is expected that we can open a new pathway to unknown physics through investigating the peculiar electromagnetic phenomena in superconductors. One of these new phenomena is the appearance of a magnetic generalized force, i.e., a torque, in spite of zero Lorentz force. That is, the driving torque on flux lines is not equal to the moment of the Lorentz force. The appearance of torque in the condition of no force cannot happen in dynamics.

The characteristic points of electromagnetic phenomena in superconductors are briefly introduced here. First, it is shown in this book not only that the diamagnetism in the superconductors harmonizes with Maxwell's theory, which was completed before its discovery, but also that the dominant $\boldsymbol{E}$-$\boldsymbol{B}$ analogy in the present electromagnetism loses perfection without the superconductor. Secondly, it is shown that the flux pinning that brings about the beneficial feature of non-dissipative current in DC condition causes special irreversibility in the AC condition. We have proved only experimentally that if there is no energy dissipation in the superconductor caused by the breaking of time reversal symmetry, it contradicts the thermodynamic principle on energy conservation. This is now proved theoretically based on Maxwell's theory, since the irreversibility in the superconductor is theoretically derived. Thirdly, the longitudinal magnetic field effect that is only known to a small number of researchers is introduced, and it is shown that this phenomenon leads to a new development of Maxwell's theory. Thus, the electromagnetic phenomena in the superconductor are deeply associated with electromagnetism over a wide range from the primary level to new profound matters. The validity of Maxwell's theory for all of them will be clarified in this book.

This book will be recommended to people who are interested in science, especially in superconductivity. It seems to be enough to read Chaps. 1–3 to gain knowledge over a wide area. If the relationship with other related phenomena such as friction or the application of superconductors in the future is interesting, Chap. 7 will also be useful.

All of this book is recommended as an introduction to students or young scientists who are interested in applied superconductivity, especially in power applications. Then, if they are interested in practical electromagnetic phenomena such as flux pinning mechanisms and flux creep in superconductors, it is desirable to move to more technical books.

Many appendices will help the readers to understand the methods of derivation of the equations. These will also be useful to clarify this particular way of thinking.

It is expected that this book will give its readers a useful introduction to superconductivity.

Iizuka, Japan Teruo Matsushita

Contents

Chapter 1
Introduction

1.1 Superconductor

Superconductors, the materials that can carry a current without electric resistance, may be unfamiliar to people. This is because the superconducting state can be realized only at very low temperatures. It is necessary to cool down a superconductor with liquid nitrogen at 196 °C to realize the superconducting state, even for the "high-temperature superconductors" discovered in 1986. There is no material that achieves superconductivity at room temperature. Thus, superconductors are usually placed within special metallic containers to keep their temperatures low, and hence, people seldom see them. Superconducting wires are fabricated to carry current, and some of them are shown in Fig. 1.1.

The role that superconductors play is now gradually increasing around the world. For example, electromagnets in the Magnetic Resonance Imaging (MRI) systems that physicians sometimes use in medical examinations are made of superconducting wires (see Fig. 1.2). The Central Japan Railway Company is planning to connect Shinagawa in Tokyo and Nagoya, which are separated by 285.6 km, with a 40 min journey on a **S**uper**c**onducting **Mag**netic **Lev**itated (SCMAGLEV) Train by the latter half of the 2020s (see Fig. 1.3). Superconducting magnets are used to levitate and drive the train at very high speed. The prediction of the Higgs boson was awarded the Nobel Prize in Physics in 2013. The highly developed Japanese technology of superconducting magnets that compose particle accelerators supported the successful observation of the Higgs boson. Large-scale integrated circuits (LSI) are now installed in various devices such as computers and home electrical appliances. Large single crystals of high-purity silicon for LSI cannot be made without strong magnetic fields produced by superconducting magnets. Such a wide variety of applications for superconducting magnets are owing to their property of no electrical resistance. For example, the very strong magnetic field produced by superconducting magnets is useful to levitate heavy trains or to prevent hot melted silicon from moving by convection and introducing impurities. For MRI, a very stable magnetic field is a key point.

T. Matsushita, *Superconductivity and Electromagnetism*, Springer Series in Solid-State Sciences 195, https://doi.org/10.1007/978-3-030-67568-4_1

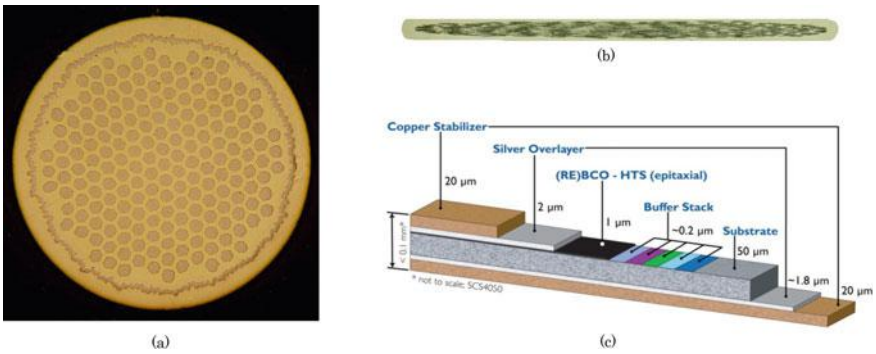

Fig. 1.1 Cross-sections of superconducting wires: **a** multi-filamentary Nb_3Sn wire (provided by Showa Cable Systems Co., Ltd.), **b** Bi-2223 tape (provided by Sumitomo Electric Industries, Ltd.), and **c** rare-earth barium copper oxide (REBCO) coated conductor (provided by Furukawa Electric Co., Ltd. and SuperPower Inc.)

Fig. 1.2 3 T superconducting MRI system (provided by Canon Medical Systems Corporation)

Superconductivity is a peculiar phenomenon in solid state physics. For this reason, almost half a century was needed for solution to the mechanism of superconductivity after its discovery in 1911. In the meanwhile, the theory of quantum mechanics was completed in the 1920s. The great physicists who contributed to the development of quantum mechanics could not solve the problem of superconductivity. This was because the appearance of superconductivity was contradictory to the Pauli exclusion principle based on symmetry of the wave functions of particles. Superconductivity is a phenomenon of electrons that carry non-dissipative current. The superconducting state was speculated to be one of condensed states in which many electrons stay in the same state with the same energy. Such a state is only achieved, however, for Bose

Fig. 1.3 LO series SCMAGLEV train (provided by Central Japan Railway Company)

particles but electrons, which are Fermi particles, cannot achieve such a condensation. A long time was needed to solve this problem. It was clarified by Bardeen, Cooper, and Schrieffer in 1957 that superconductivity occurs by the formation of pairs of electrons, which behave similarly to Bose particles. This is called pair condensation. Based on this discovery, it was predicted that liquid ^{3}He composed of two protons and one neutron, which is a Fermi particle, would achieve superfluidity without viscosity, in a similar way to liquid ^{4}He containing two neutrons, which is a Bose particle. This prediction was experimentally proved later. Thus, solid state physics was significantly advanced by the solution of the mechanism of superconductivity in the 20th century.

In spite of such a complicated mechanism, almost half of the elements show superconductivity if cooled sufficiently, including under high pressure conditions or in thin films. Hence, the elements that show superconductivity are not rare and special. Most metallic compounds show superconductivity, and some organic compounds do also. Some insulating materials also become superconducting on the introduction of a small amount of carriers. Thus, we can say that superconductors are common.

Magnetic materials are commonly used substances with magnetic moment. Among them, the ferromagnetic materials that are used for permanent magnets lose their ferromagnetic property when heated above the Curie temperature due to the now random orientation of magnetic moments. This is a kind of phase transition similar to the change of ice to water when heated above 0 °C. When the temperature of a superconductor is increased above the critical temperature, the superconducting state with zero resistivity turns into the normal state with resistivity. A similar phase

transition occurs in ferroelectric materials, which are a type of electric materials. Thus, the superconducting transition can be regarded as just one of the general phase transitions, and its one exceptional point is a very low transition temperature. If a room temperature superconductor is discovered in the future, the idea of peculiarity will be weakened. Recently, it was discovered that H_3S became superconducting at 203 K ($-70\,^{\circ}$C) under a very high pressure of 155 million atm. In addition, LaH_{10} showed superconductivity at 250–260 K (-23 to $-13\,^{\circ}$C) under a similar high pressure. These discoveries create the strong impression that the discovery of a room temperature superconductor is not a pipe dream.

1.2 Zero Electrical Resistance

Here we discuss the zero resistivity, which is the most outstanding property of a superconductor, from various aspects. Firstly, the zero resistivity is proved theoretically. Then, we try to check if it is possible to prove it experimentally. It is necessary to measure the voltage drop V across a specimen when a current I is applied to it. The resistance is obtained as $R = V/I$. This measurement is applied to a square rod made of high purity copper with a cross-sectional area of 1 cm^2 and length of 10 cm that has been cooled down to liquid helium temperature $-269\,^{\circ}$C. The electrical resistivity ρ_r of pure copper at this temperature is about $1 \times 10^{-11}\,\Omega$m, and the electrical resistance is estimated from Ohm's law as $R = \rho_r l/S = 1 \times 10^{-6}\,[\Omega]$, where l and S are the length and cross-sectional area, respectively. Hence, when a current of 1 A is applied, the potential drop is $1\,\mu\mathrm{V}\left(= 1 \times 10^{-6}\,\mathrm{V}\right)$. Thus, the measurement is possible. When the electrical resistivity is smaller by two orders in magnitude, the measurement is difficult due to the noise in the voltmeter. That is, it is difficult to measure a resistivity smaller than $1 \times 10^{-13}\,\Omega$m by this measurement method. Thus, it is impossible to prove the zero resistivity in superconductors.

Then, we try to measure the resistivity by another method. We assume a closed circle 10 cm in diameter (D) made of a round wire 1 mm in diameter (d). The electrical resistance of this closed circle is $R = 4\rho_r D/d^2$ and the self-inductance[1] is

$$L \cong \frac{\mu_0 D}{2} \log \frac{8D}{d} \cong 4.2 \times 10^{-7}\,[\mathrm{H}], \tag{1.1}$$

where $\mu_0 = 4\pi \times 10^{-7}\left[\mathrm{N/A^2}\right]$ is the magnetic permeability of vacuum, the unit of the inductance H is the Henry, and N in the magnetic permeability is the Newton. When a current is induced in the closed loop by magnetic induction, the current decays with time t as

[1] The magnetic flux that penetrates a closed circuit is denoted by Φ, when current I is applied to the circuit. The coefficient $L = \Phi/I$ is the self-inductance.

$$I(t) = I(0)\exp\left(-\frac{t}{t_0}\right), \tag{1.2}$$

where t_0 is the time constant given by

$$t_0 = \frac{L}{R}. \tag{1.3}$$

Hence, the electrical resistivity can be estimated by measurement of t_0. When the closed loop is made of high purity copper, we have $R \cong 4 \times 10^{-6}\ \Omega$ and t_0 is estimated to be 0.11 s. In the case of the usual copper, t_0 is below 1/10,000 s.

When this measurement is performed for a superconductor, a decay of the current is not observed for three years. Hence, we can say that the electrical resistivity of superconductors is very small. However, it is not possible to prove that the electrical resistivity is exactly zero. If the uncertainty of the measured value of the decay rate is 10^{-4}, the time constant is estimated to be larger than 30,000 years $\cong 9.5 \times 10^{11}$ s. Hence, we can say that the electrical resistivity of the superconductor is below $1 \times 10^{-24}\ \Omega$m. Thus, our estimation is limited. A time constant of over 30,000 years, however, can be regarded as infinity in the time scale of our lives. Thus, we can substantially regard the electrical resistivity of superconductors as zero. This is similar to the case where we regard the continents on the earth as stationary, although they move a few mm in a year.

Secondly, we will consider the physical aspect of electrical resistivity. When we apply a current to a substance with a finite electrical resistivity, the electrical energy changes to heat. The reversal process, however, i.e., a direct change from heat to electrical energy, is not possible. Although we can obtain 100 Wh of heat from electrical energy of 100 Wh, the electrical energy obtained from 100 Wh of heat using a heat engine is fairly small. Thus, the generation of heat by electrical resistance is an irreversible phenomenon. We know of various other irreversible phenomena. Spilled water from a glass cannot be brought back into the glass. A drop of ink that has fallen into water is diffused, but it does not happen that diffused ink coheres to a point as the time is reversed. Such things occur commonly in our daily life, and we are accustomed to irreversible phenomena.

Nevertheless, such irreversibility has not been theoretically proved. The essence of physical phenomena is the equation of motion that describes the movement of matter. This holds also for the movement of particles in a many body system. The equation of motion is symmetric with respect to time reversal. This may indicate that a phenomenon can be reversed like movie film run backwards. In reality, most phenomena are irreversible, and such a reversal does not occur. Electrical resistance is also one of the irreversible phenomena. When we apply a voltage across a substance like a metal, electrons are accelerated by the Coulomb force. The motion of the electrons is interrupted by ions, and the velocity decreases. As a result, the velocity of electrons is approximately constant under the acceleration and scattering, if averaged over a certain period. Thus, the steady condition of current is fulfilled. Electrons obtain kinetic energy by Coulomb interactions and lose it by the scattering. On the

other hand, ions acquire the kinetic energy of electrons, which leads to heat. It is possible to derive electrical resistance and Ohm's law by introducing a phenomenological viscous force into the equation of motion, although the viscous force has not been proved theoretically.

Now we go back the superconductor. Since the electrical resistance is zero, the electromagnetic phenomena in the superconductor can be derived from first principles, i.e., the minimization of the relevant free energy. First principles cannot be applied to irreversible phenomena accompanied by energy dissipation. This means that the superconductor is a pure material in physics.

1.3 Energy Dissipation in Superconductors

In spite of the explanation above, energy dissipation does occur in superconductors in reality, and electrical resistance appears. Superconductors are used for magnets. When a superconducting magnet is operated, the superconductor is subject to a strong magnetic field, and the magnetic flux penetrates in the form of quantized magnetic flux lines, which are simply called flux lines. When a current is applied to the superconductor that contains flux lines, the Lorentz force works on the flux lines. If flux lines are driven by the Lorentz force, an electromotive force appears. Since the central area of 10–100 nm in diameter in each flux line is in the normal state with a finite resistivity, normal electrons in this area are driven by the electric field, resulting in energy dissipation. This state is called the flux flow. Hence, defects such as normal precipitates or grain boundaries are introduced in practical superconductors used for various devices so that such defects prevent flux lines from moving, even under the Lorentz force. This effect is called flux pinning and defects that are effective for this are called pinning centers. Since the Lorentz force is proportional to the current density, the critical current density, i.e., the maximum non-dissipative current density, is proportional to the strength of flux pinning.

Energy dissipation does not occur in the superconductor due to the flux pinning effect, if the current with a density below the critical current density is applied in a static condition. The flux motion still occurs, however, resulting in energy dissipation under a condition varying with time such as an alternating current or varying external magnetic field. This is similar to friction. In reality flux pinning interactions work against the driving force on flux lines and are irreversible in nature. This seems to be contradictory to the above statement that electromagnetic phenomena can be derived from first principles to minimize the relevant energy. It should be noted, however, that flux pinning originates from the interaction between flux lines and the pinning potentials of defects and is reversible in nature. Reversible phenomena are really observed for very small displacements of flux lines. This corresponds to a play in friction. The irreversibility appears when displacement exceeds a certain level of reversibility in both cases. Variation from reversibility to irreversibility takes place continuously. As will be explained later in this book, therefore, flux pinning

phenomena can be derived from first principles. This fact strongly suggests theoretically that, if there is not energy dissipation, it contradicts the first law of thermodynamics. The contradiction has only been pointed out from the experimental viewpoint. It can be recognized from the above discussion that there are two kinds of irreversibility: One originates from the breaking of time reversal symmetry, in spite of the restriction by the common equation of motion, and the other originates from a difference in the equation between just before and just after unstable motion of flux lines. The irreversibility in superconductors belongs to the latter type. Thus, the electromagnetic phenomena in superconductors are deeply associated with fundamental aspects of physics.

Here, we emphasize a series of special electromagnetic phenomena called the "longitudinal magnetic field effect" in superconductors. One of them represents a significant increase in the critical current density. The magnetic field produced by a current is directed perpendicular to the current. A longitudinal magnetic field is a magnetic field applied parallel to a superconducting wire and it is empirically known that a state in which the local current and the magnetic field are parallel to each other is attained. This state is called the force-free state, since the Lorentz force on the flux lines is zero. If a simple superposition is assumed for the magnetic field between the applied field and the self-field of the current, there is no change in the Lorentz force, resulting in no change in the critical current density. As will be shown later, the longitudinal magnetic field effect is a quite new electromagnetic phenomenon that has not been discussed in terms of the usual electromagnetism, and it will add a new page to electromagnetism. Hence, the introduction of superconductivity is expected to greatly influence electromagnetism.

Thus, the electromagnetic phenomena in superconductors are important, not only from scientific, but also from technological aspects. Even a primitive perfect diamagnetism in superconductors is not described in textbooks of electromagnetism, however. Such a situation should be corrected. In this book it is emphasized how elementary electromagnetism changes by introducing perfect diamagnetism in superconductors. If we reach a conclusion, the analogy between electricity and magnetism becomes perfectly rigid, just as in the case where a picture of a jigsaw puzzle is completed by adding a missing piece. Maxwell's theory was completed in the 19th century. Although superconductivity had not been discovered at that time, the framework of electromagnetism was compatible with superconductivity, as if it had already been discovered. Since the zero resistivity is easily derived for a material with perfect diamagnetism using Maxwell's equations, it was, in principle, possible to predict the superconductor in the 19th century, even if it might be an imaginary material.

1.4 Contents of This Book

The contents of this book are briefly introduced here. It is also recommended to read the introduction at the beginning of each chapter.

In Chap. 2, the fundamental phenomena of elementary electromagnetism, which are needed to understand electromagnetic phenomena in superconductors, are briefly summarized. A special emphasis is placed on describing Maxwell's equation for electromagnetic induction, Poynting's vector, which describes the flow of energy, etc. These are used in other chapters. It may occur that knowledge on these matters is required there. Please utilize effectively the knowledge in this chapter in such a case.

In Chap. 3, the changes that occur in elementary electromagnetism are described, when the magnetic phenomena in the Meissner state, i.e., perfect diamagnetism, are introduced. The essential point is that the present $\boldsymbol{E}$-$\boldsymbol{B}$ analogy becomes more perfect, when the magnetic phenomena in superconductors satisfying $\boldsymbol{B} = 0$ is introduced, which corresponds to the electric phenomena in conductors satisfying $\boldsymbol{E} = 0$. The various advantages obtained by this introduction are introduced. It should be mentioned that, in a substance in which $\boldsymbol{B} = 0$, the electric resistivity must be zero. Although this property might be peculiar from the experimental viewpoint, it can be easily derived from Maxwell's theory.

In Chap. 4, the Ginzburg-Landau theory, which describes electromagnetic phenomena in type II superconductors used for various devices, is introduced. Based on this theory, we study the structure of quantized magnetic flux (the flux line) with a normal conducting region around the center, which is important in electromagnetic phenomena in practical superconductors. Because of this structure, electrical resistance appears when flux lines are driven by the Lorentz force arising from current. On the other hand, this structure contributes to the flux pinning that introduces a non-dissipative current.

In Chap. 5, the flux pinning mechanism that determines the critical current density, i.e., the most important parameter for application of superconductors, is introduced. The pinning interaction between flux lines with spatial structure and defects is originally reversible with respect to the displacement of flux lines. In fact, reversible electromagnetic phenomena can be observed within the range of small displacement of flux lines, if we watch carefully, although practical phenomena are mostly irreversible. The irreversible phenomena can be described using the critical state model that assumes the critical current density as a parameter. Magnetization and AC losses are introduced, for example, as phenomena that can be explained by the critical state model. On the other hand, a theory that estimates the critical current density caused by pinning centers, which is called the summation theory, is reviewed from the aspect of historical development. Summation theory that uses a statistical method is also useful to explain a change from reversible to irreversible phenomena. Based on this knowledge, the basic force-balance equation in the critical state model is derived using first principles for the reversible case, and it is extended to the irreversible case. As a result, the theory that describes the critical state can be obtained. In addition, it is shown that the pinning loss power density calculated using a method equivalent to the statistical method in the summation theory agrees with the prediction of the critical state model. Thus, two theories on the flux pinning, i.e., the summation theory and the critical state theory, are unified. The argument is also discussed that

the irreversibility in the flux pinning phenomena does not originate from the breaking of time-reversal symmetry but from a special mechanism.

In Chap. 6, the longitudinal magnetic field effect is introduced as a peculiar electromagnetic phenomenon in a current-carrying superconductor in a parallel magnetic field. It is well known that the force-free state, i.e., the state with zero Lorentz force because the current and magnetic flux are parallel to each other, is established in the superconductor. In this configuration of magnetic field and current, the critical current density takes on a much larger value than in the usual transverse magnetic field, and Josephson's formula for electric field $\boldsymbol{E} = \boldsymbol{B} \times \boldsymbol{v}$ does not hold, where $\boldsymbol{B}$ and $\boldsymbol{v}$ are the magnetic flux density and velocity of the flux lines, respectively. The flux line lattice has a characteristic distortion, i.e., the force-free strain, in the force-free state, and it is speculated that the driving torque works on flux lines to release the distortion in a similar way to the Lorentz force. The longitudinal magnetic field effect is explained comprehensively from the balance between the driving torque and the pinning torque that works to keep the distortion. The driving torque can be derived from the energy that penetrates the superconductor when the force-free strain is introduced. If we assume that the force-free torque does not exist, it results in a violation of the principle of energy conservation. The important thing is that the flux pinning plays an essential role in the longitudinal magnetic field effect. If there is no pinning effect, the longitudinal magnetic field effect does not appear.

In Chap. 7, the essence of this book is summarized, and we look over the position that electromagnetic phenomena in superconductors occupy in the present field of electromagnetism. In addition, we also discuss what kind of progress is expected in science in the future, based on the above argument. On the other hand, the most attractive point of superconductivity is its technological applications. In this chapter the present status and future possibility of applications in the medical, environmental, traffic, and energy fields are briefly introduced.

Some topics are given in the "Coffee break" column at the end of each chapter. Please enjoy it.

Coffee break (1)

Superconducting oxygen

Oxygen is a chemical element that occupies about 21% of the air on Earth. It is also a common element of the third largest mass fraction in the universe following hydrogen and helium. Oxygen also shows superconductivity. It is one of the most difficult elements, however, to reach superconductivity. Oxygen is condensed to a liquid at 90.2 K and becomes a bluish solid at 54.8 K. The crystalline oxygen has a cubic structure and has a metallic sheen under the very high pressure of one million atmospheres. The transition to the superconducting state is realized at the extremely low temperature of 0.6 K under 1.25 million atmospheres.

Chapter 2
Basic Electromagnetism

Abstract In this chapter we summarize the essential principles associated with electrostatic and magnetic phenomena caused by electric charges and currents, respectively, based on the ***E*-*B*** analogy. These are necessary to understand the usefulness of introducing superconductivity into electromagnetism, which will be done in Chap. 3. Poynting's vector, which will be used to discuss the flow of energy in other chapters, is also described. It is recommended that readers who have not studied electromagnetism for many years read this chapter before proceeding to the next chapter. Since this chapter is compactly summarized, it will be actively utilized further on.

2.1 Electrostatic Phenomena

Here we treat electrostatic phenomena that do not change with time. The source that causes various kinds of electric phenomena is electric charge, and there are two kinds of electric charge. One is the electric charge that flows in a conductor and can be transferred elsewhere, which is also called true electric charge, and the other is polarization charge that is locally bound around a nucleus in a dielectric material and cannot be transferred outside. The densities of these electric charges are denoted by ρ and ρ_{p}, respectively. The electrical distortion that these electric charges cause in a space is electric field. It is represented by a vector $\boldsymbol{E}$. When electric charge Q is placed in this space, the following force is exerted on the charge:

$$\boldsymbol{F} = Q\boldsymbol{E}. \tag{2.1}$$

This force is called the Coulomb force. When the true electric charge is distributed with density ρ at position $\boldsymbol{r}'$ in a region V, the electric field at position $\boldsymbol{r}$ that is caused by the charge is given by

$$\boldsymbol{E}(\boldsymbol{r}) = \frac{1}{4\pi\epsilon_0}\int_{\mathrm{V}} \frac{\rho(\boldsymbol{r}')(\boldsymbol{r}-\boldsymbol{r}')}{|\boldsymbol{r}-\boldsymbol{r}'|^3}\mathrm{d}V', \tag{2.2}$$

T. Matsushita, *Superconductivity and Electromagnetism*, Springer Series in Solid-State Sciences 195, https://doi.org/10.1007/978-3-030-67568-4_2

where $\epsilon_0 \left(= 8.8542 \times 10^{-12}\,\mathrm{C}^2/\mathrm{Nm}^2\right)$ is the permittivity of vacuum and the above integration is carried out with respect to $\boldsymbol{r}'$. Equation (2.2) is called Coulomb's law. In (2.2) the electric field contributed from a point-like charge, $\rho \mathrm{d}V'$, is summed up; $\left(\boldsymbol{r} - \boldsymbol{r}'\right)/\left|\boldsymbol{r} - \boldsymbol{r}'\right|^3$ is a vector directed from the electric charge at $\boldsymbol{r}'$ to the observation point at $\boldsymbol{r}$ and its magnitude is the inverse of the square of the distance between the two points. When the electric field is integrated on a closed surface S, the following relationship holds:

$$\int_{\mathrm{S}} \boldsymbol{E} \cdot \mathrm{d}\boldsymbol{S} = \frac{1}{\epsilon_0} \int_{\mathrm{V}} \rho(\boldsymbol{r}) \mathrm{d}V, \tag{2.3}$$

where V is the space surrounded by S and the elementary surface vector $\mathrm{d}\boldsymbol{S}$ is directed outwards. This is called Gauss' law. While Coulomb's law describes the local electric field produced by electric charge, Gauss' law gives the global relationship between electric field and electric charge.

We consider the case where electric charge Q is placed on the origin ($\boldsymbol{r} = 0$). If S is a spherical surface of radius r with its center on the origin, the electric field $\boldsymbol{E}$ is parallel to the elementary surface vector $\mathrm{d}\boldsymbol{S}$ and its magnitude is a constant value on the surface on the left side of (2.3). Hence, the left side is given by $4\pi r^2 E$. Since the right side is Q/ϵ_0, we have

$$E = \frac{Q}{4\pi \epsilon_0 r^2}. \tag{2.4}$$

This is nothing else than the relationship given by (2.2). That is, Coulomb's law and Gauss' law are relative to each other. The condition of the electric field in this case is shown in Fig. 2.1. The virtual lines in the figure are called electric field lines. These lines are defined as the lines parallel to the electric field and drawn so that the number in a unit area in the normal plane is just equal to $|E|$. Thus, Gauss' law is expressed by the statement that the total number of electric field lines that come out of closed

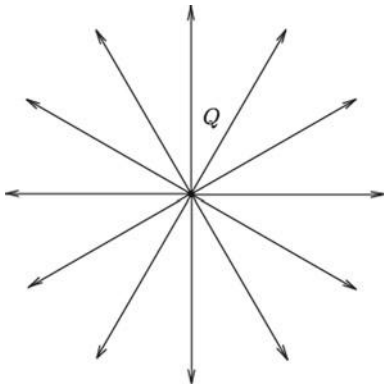

Fig. 2.1 Electric field produced by electric charge Q

surface S is equal to the total electric charge inside S divided by ϵ_0. Hence, the total number of electric field lines in Fig. 2.1 is Q/ϵ_0.

Using Gauss' mathematical theorem, the left side of (2.3) can be rewritten as

$$\int_{\mathrm{V}} \nabla \cdot \boldsymbol{E} \mathrm{d}V = \frac{1}{\epsilon_0} \int_{\mathrm{V}} \rho(\boldsymbol{r}) \mathrm{d}V. \tag{2.5}$$

In the above ∇ represents a differential operator called nabla and is expressed as

$$\nabla = \boldsymbol{i}_x \frac{\partial}{\partial x} + \boldsymbol{i}_y \frac{\partial}{\partial y} + \boldsymbol{i}_z \frac{\partial}{\partial z} \tag{2.6}$$

in Cartesian coordinates (x, y, z), where $\boldsymbol{i}_x$, $\boldsymbol{i}_y$ and $\boldsymbol{i}_z$ are unit vectors along the x, y and z axes, respectively. In (2.5) $\nabla \cdot \boldsymbol{E}$ is also written as div$\boldsymbol{E}$, where div is called the divergence. Since (2.5) holds for an arbitrary region V, the integrands on the both sides are equal to each other:

$$\nabla \cdot \boldsymbol{E} = \frac{\rho}{\epsilon_0}. \tag{2.7}$$

This is called Gauss' divergence law. In Cartesian coordinates the left side of (2.7) is

$$\nabla \cdot \boldsymbol{E} = \frac{\partial E_x}{\partial x} + \frac{\partial E_y}{\partial y} + \frac{\partial E_z}{\partial z}. \tag{2.8}$$

Equation (2.7) shows that electric charge causes a divergence of the electric field. In the case of the point charge shown in Fig. 2.1, for example, the electric field emerges from the origin at which the point charge is located and expands radially. This condition is similar to the light emitted from the point source. An electric field line does not emerge from or terminate at a point where there is no electric charge ($\rho = 0$). That is, there is no divergence ($\nabla \cdot \boldsymbol{E} = 0$).

Here we show an example. Suppose that electric charge is uniformly distributed with density ρ_0 inside a wide slab of thickness $2a$ parallel to the y-z plane (see Fig. 2.2a). The electric field is now calculated using Gauss' law (2.3). In this case the calculation using Coulomb's law is not easy. We assume a closed parallelepiped S, one plane of which stays on the central plane, $x = 0$, as shown in Fig. 2.2b. Then, the electric field must be zero on this plane from symmetry with respect to the x-axis. That is, the same result must be obtained when the right and left sides are reversed. It can be concluded that the electric field has only the x component (E_x) from symmetry with respect to the y- and z-axes. Hence, the electric field is parallel to the surface on the four surfaces parallel to the x-axis, and the surface integral of the electric field on these surfaces is zero. The surface integral only has a nonzero value on the remaining surface. The position and the electric field on this surface are denoted by x and $E_x(x)$, respectively. Then, the right side of (2.3) is $AE_x(x)$, where A

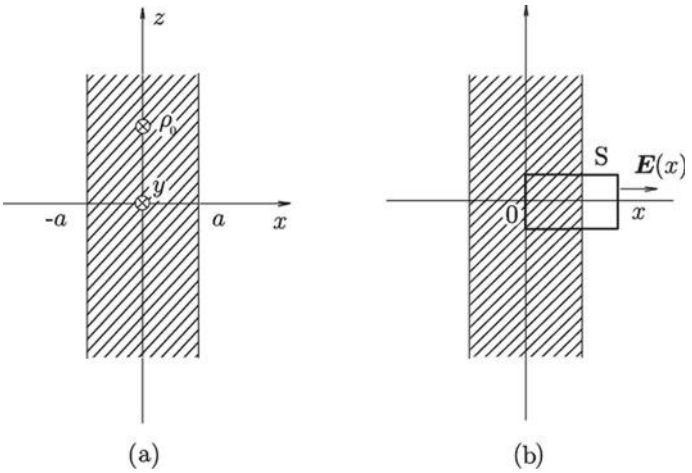

Fig. 2.2 **a** Substance in which the electric charge is uniformly distributed with density ρ_0 and **b** closed parallelepiped S for $x > a$ on which Gauss' law is applied

is the area of the surface parallel to the y-z plane. Now we estimate the total electric charge inside S. A simple calculation leads to $Ax\rho_0$ for $0 \leq x \leq a$ and $Aa\rho_0$ for $x > a$. Thus, we have

$$\begin{aligned} E_x &= -\frac{a\rho_0}{\epsilon_0}; \quad x < -a, \\ &= \frac{x\rho_0}{\epsilon_0}; \quad -a \leq x \leq a, \\ &= \frac{a\rho_0}{\epsilon_0}; \quad x > a, \end{aligned} \tag{2.9}$$

where we have used the symmetry condition with respect to $x = 0$. Substitution of this result into (2.7) leads to

$$\begin{aligned} \nabla \cdot \boldsymbol{E} &= \frac{\rho_0}{\epsilon_0}; \quad -a \leq x \leq a, \\ &= 0; \quad x < -a, x > a. \end{aligned} \tag{2.10}$$

This shows that the electric charge is distributed with density ρ_0 only inside the slab, as assumed in the beginning.

The scalar potential, i.e., the electric potential, ϕ, which causes the electric field is defined as

$$\phi(\boldsymbol{r}) = -\int_{\boldsymbol{r}_0}^{\boldsymbol{r}} \boldsymbol{E} \cdot \mathrm{d}\boldsymbol{s}, \tag{2.11}$$

where $\boldsymbol{r}_0$ is a reference point satisfying $\phi(\boldsymbol{r}_0) = 0$ and is usually taken at infinity. The electric potential that causes the electric field of (2.2) is given by

$$\phi(\boldsymbol{r}) = \frac{1}{4\pi\epsilon_0} \int_{\mathrm{V}} \frac{\rho(\boldsymbol{r}')}{|\boldsymbol{r} - \boldsymbol{r}'|} \mathrm{d}V'. \tag{2.12}$$

It is found from (2.11) that the electric potential difference between point A at position $\boldsymbol{r}_\mathrm{A}$ and point B at position $\boldsymbol{r}_\mathrm{B}$, i.e., the electric potential at point B measured from point A is given by

$$\Delta\phi = \phi(\boldsymbol{r}_\mathrm{B}) - \phi(\boldsymbol{r}_\mathrm{A}) = \int_{\boldsymbol{r}_\mathrm{B}}^{\boldsymbol{r}_\mathrm{A}} \boldsymbol{E} \cdot \mathrm{d}\boldsymbol{s}. \tag{2.13}$$

This value is determined only by the positions of the two points and is independent of the path between them. Hence, when the electric field is integrated along a closed path, we have

$$\oint_{\mathrm{C}} \boldsymbol{E} \cdot \mathrm{d}\boldsymbol{s} = 0. \tag{2.14}$$

Using the electric potential, the electric field is described as

$$\boldsymbol{E} = -\nabla\phi. \tag{2.15}$$

In the above $\nabla\phi$ is also written as grad ϕ. The operator grad is called the gradient and (2.15) is expressed in Cartesian coordinates as

$$\boldsymbol{E} = -\frac{\partial\phi}{\partial x}\boldsymbol{i}_x - \frac{\partial\phi}{\partial y}\boldsymbol{i}_y - \frac{\partial\phi}{\partial z}\boldsymbol{i}_z. \tag{2.16}$$

A virtual surface composed of points with the same electric potential is called an equipotential surface. The electric field lines are normal to the equipotential surface. The equipotential surfaces for the case of the point charge on the origin (see Fig. 2.1) are shown in Fig. 2.3. In this case the equipotential surfaces are spherical surfaces with the centers on the origin.

Using Stokes' theorem (2.14) is written as

$$\int_{\mathrm{S}} (\nabla \times \boldsymbol{E}) \cdot \mathrm{d}\boldsymbol{S} = 0, \tag{2.17}$$

where S is a plane surrounded by closed loop C. In the above $\nabla \times \boldsymbol{E}$ is also written as curl $\boldsymbol{E}$. The operator $\nabla\times$ is called the curl. Using Cartesian coordinates (x, y, z), the integrand in (2.17) is written as

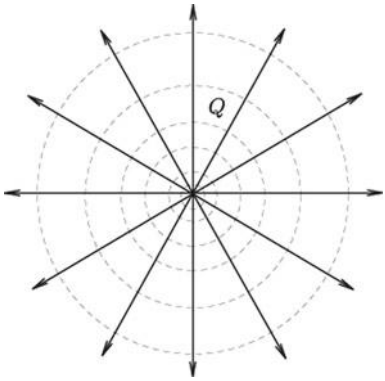

Fig. 2.3 Equipotential surfaces produced by point charge Q (shown by dotted lines)

$$\nabla \times \boldsymbol{E} = \boldsymbol{i}_x\left(\frac{\partial E_z}{\partial y} - \frac{\partial E_y}{\partial z}\right) + \boldsymbol{i}_y\left(\frac{\partial E_x}{\partial z} - \frac{\partial E_z}{\partial x}\right) + \boldsymbol{i}_z\left(\frac{\partial E_y}{\partial x} - \frac{\partial E_x}{\partial y}\right). \tag{2.18}$$

Since (2.17) holds for arbitrary S, we have

$$\nabla \times \boldsymbol{E} = 0. \tag{2.19}$$

This can also be proved mathematically. Using (2.15), the left side of (2.19) leads to

$$-\nabla \times \nabla\phi = -\text{curl grad}\,\phi. \tag{2.20}$$

This is identically equal to 0. Thus, the electric field is a field without a vortex. The electric field lines are not closed.

The essence of the electrostatic field is that it has divergence caused by electric charge but has no vortex. When polarization charge of density ρ_p coexists with electric charge of density ρ, ρ can be replaced by $\rho + \rho_\text{p}$ in the above equations.

2.2 Static Magnetic Phenomena

Here, we treat magnetic phenomena that do not change with time. The sources that bring about various kinds of magnetic phenomena are electric current caused by flow of true electric charges and magnetic moment in magnetic materials. In present electromagnetism, the magnetic moment in magnetic materials is usually expressed using a virtual magnetizing current. This is because magnetic charges, which are similar to electric charges, do not exist, and the resultant field cannot be easily described. The densities of the distributed electric current and the magnetizing current are denoted by $\boldsymbol{i}$ and $\boldsymbol{i}_\text{m}$, respectively. The strength of the magnetic distortion of the space that is caused by these currents is called the magnetic field and is

represented by the magnetic flux density, $\boldsymbol{B}$. When a current $\boldsymbol{I}$ is placed in this space, a force

$$\boldsymbol{F}' = \boldsymbol{I} \times \boldsymbol{B} \tag{2.21}$$

is exerted on a unit length of the current. This force is called the Lorentz force. When an electric current of density $\boldsymbol{i}(\boldsymbol{r}')$ flows at position $\boldsymbol{r}'$ in space V, the magnetic flux density at position $\boldsymbol{r}$ is given by

$$\boldsymbol{B}(\boldsymbol{r}) = \frac{\mu_0}{4\pi} \int_{\mathrm{V}} \frac{\boldsymbol{i}(\boldsymbol{r}') \times (\boldsymbol{r} - \boldsymbol{r}')}{|\boldsymbol{r} - \boldsymbol{r}'|^3} \mathrm{d}V'. \tag{2.22}$$

This is called the Biot-Savart law. In the above, μ_0 is the magnetic permeability of vacuum given by (1.1), and the volume integral is with respect to $\boldsymbol{r}'$. When the magnetic flux density is integrated on a closed line C, the following relationship holds:

$$\oint_{\mathrm{C}} \boldsymbol{B} \cdot \mathrm{d}\boldsymbol{s} = \mu_0 \int_{\mathrm{S}} \boldsymbol{i} \cdot \mathrm{d}\boldsymbol{S}. \tag{2.23}$$

This is called Ampere's law. In the above, S is a plane surrounded by C, and the elementary surface vector $\mathrm{d}\boldsymbol{S}$ points along the motion of a screw when a screw driver is rotated along the direction of the curvilinear integral $\mathrm{d}\boldsymbol{s}$ (see Fig. 2.4). This is the right-hand rule. While the Biot-Savart law describes the local magnetic flux density produced by an electric current, Ampere's law gives the global relationship between magnetic flux density and electric current. This is similar to the relationship between Coulomb's law and Gauss' law.

We consider the case where electric current I flows along the z-axis. Here we estimate the magnetic flux density at point P separated by distance r from the current. Ampere's law is applied on a closed circle of radius r with its center on the z-axis. It is derived that the magnetic flux density is parallel to this circle from (2.22), and its value is constant on the circle from symmetry. Hence, the left side of (2.23) is given by $2\pi rB$. The right side is equal to $\mu_0 I$. Hence, we have

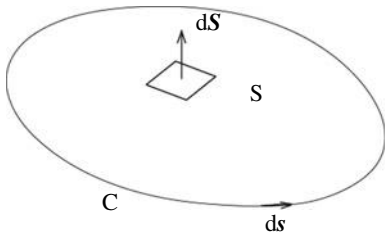

Fig. 2.4 The directions of the elementary surface vector $\mathrm{d}\boldsymbol{S}$ and the curvilinear integral $\mathrm{d}\boldsymbol{s}$ based on the right-hand rule

$$B = \frac{\mu_0 I}{2\pi r}. \tag{2.24}$$

This result can also be derived from (2.22). Since the electric current is concentrated on the line (2.22) leads to the following curvilinear integral:

$$\boldsymbol{B}(\boldsymbol{r}) = \frac{\mu_0 I}{4\pi} \int_{\mathrm{C}} \frac{\mathrm{d}\boldsymbol{r}' \times \left(\boldsymbol{r} - \boldsymbol{r}'\right)}{|\boldsymbol{r} - \boldsymbol{r}'|^3}. \tag{2.25}$$

The coordinates are introduced as shown in Fig. 2.5, and the foot of a line perpendicular to the current from observation point P is set to be $z = 0$. $\mathrm{d}\boldsymbol{r}'$ is a vector directed along the z-axis with magnitude $\mathrm{d}z$. Hence, $\mathrm{d}\boldsymbol{r}' \times \left(\boldsymbol{r} - \boldsymbol{r}'\right)$ is along the azimuthal direction (normal direction of this sheet), and its magnitude is $\left(r^2 + z^2\right)^{1/2} \sin\theta \mathrm{d}z$, where θ is the angle of the observation point measured from the direction of the current. Since all the magnetic flux density produced by the elementary current $I\mathrm{d}z$ is directed along the same azimuthal direction, the integral is simply done and we have

$$B = \frac{\mu_0 I}{4\pi} \int_{-\infty}^{\infty} \frac{\sin\theta \mathrm{d}z}{r^2 + z^2}. \tag{2.26}$$

Using the relationship:

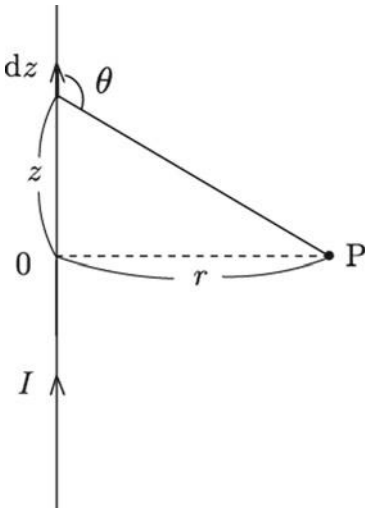

Fig. 2.5 Linear current I and observation point P

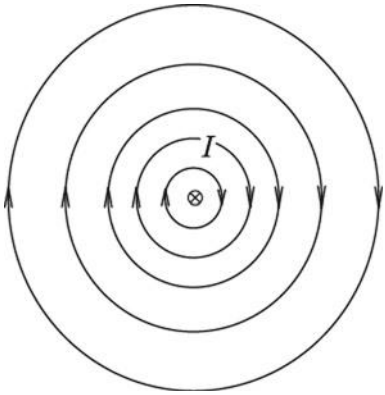

Fig. 2.6 Arrangement of magnetic flux density produced by current I

$$\sin\theta = \frac{r}{\left(r^2 + z^2\right)^{1/2}} \tag{2.27}$$

we have $\mathrm{d}z = \left(r/\sin^2\theta\right)\mathrm{d}\theta$, and (2.26) leads to

$$B = \frac{\mu_0 I}{4\pi r}\int_0^{\pi} \sin\theta \mathrm{d}\theta = \frac{\mu_0 I}{2\pi r}, \tag{2.28}$$

which agrees with the result obtained using Ampere's law. The arrangement of the magnetic flux density produced by the electric current is shown in Fig. 2.6. This arrangement can be visualized by fine iron particles, etc. The virtual lines in the figure are called the magnetic flux lines. These lines are defined as lines parallel to the magnetic flux density and drawn so that the number in a unit area in the normal plane is just equal to $|B|$.

When the right side of (2.23) is rewritten using Stokes' theorem, we have

$$\int_{\mathrm{S}} (\nabla \times \boldsymbol{B}) \cdot \mathrm{d}\boldsymbol{S} = \mu_0 \int_{\mathrm{S}} \boldsymbol{i} \cdot \mathrm{d}\boldsymbol{S} \tag{2.29}$$

Since this equation holds for arbitrary S, the integrands on the both sides are equal to each other:

$$\nabla \times \boldsymbol{B} = \mu_0 \boldsymbol{i} \tag{2.30}$$

This is called the differential form of Ampere's law. It shows that the current produces rotation of the magnetic flux density.

One example is shown here. Suppose that a current flows uniformly along the y-axis with density i_0 inside a wide slab $2a$ in thickness parallel to the y-z plane (see Fig. 2.7a). The magnetic flux density can be easily obtained using Ampere's

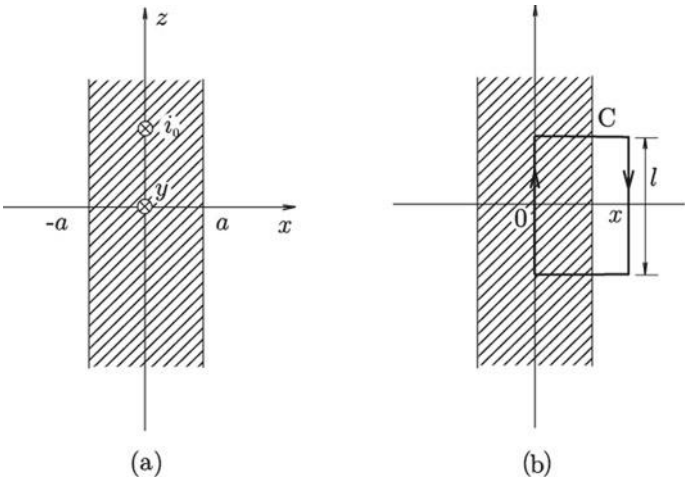

Fig. 2.7 **a** Slab with uniform current of density i_0 and **b** rectangle C in the case of $x > a$

law. If the Biot-Savart law is used, a much longer time is needed for the calculation. Assume a rectangle C with one side on the center, $x = 0$, on the x-z plane, as shown in Fig. 2.7a. From symmetry the magnetic flux density has only a z component, and its value must be 0 at $x = 0$. The magnetic flux density is integrated along rectangle C, as shown by the arrows, so as to be consistent with the current flow along the positive y-axis. Since $\boldsymbol{B}$ is perpendicular to d$\boldsymbol{s}$ on the top and bottom sides of C, the integral is zero there. The left side of (2.23) is $-B_z(x)l$, where l is the length of the side of C along the z-axis. The current penetrating C is lxi_0 for $0 \leq x \leq a$ and lai_0 for $x > a$. From symmetry with respect to $x = 0$ we have

$$\begin{aligned} B_z &= \mu_0 i_0 a; \quad x < -a, \\ &= -\mu_0 i_0 x; \quad -a \leq x \leq a, \\ &= -\mu_0 i_0 a; \quad x > a. \end{aligned} \tag{2.31}$$

The magnetic flux density varies only along the x-axis ($\partial/\partial y = 0$ and $\partial/\partial z = 0$), and the left side of (2.30) has only the y component, $-\partial B_z/\partial x$. Thus, we have

$$\begin{aligned} i_y &= i_0; \quad -a \leq x \leq a, \\ &= 0; \quad x < -a, x > a. \end{aligned} \tag{2.32}$$

This shows that the current flows uniformly in the slab as assumed in the beginning.

Because the magnetic flux lines are closed, as shown in Fig. 2.6, the following relationship holds for an arbitrary closed surface S:

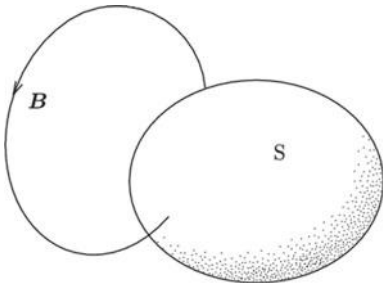

Fig. 2.8 Closed surface S and magnetic flux line

$$\int_{\mathrm{S}} \boldsymbol{B} \cdot \mathrm{d}\boldsymbol{S} = 0. \tag{2.33}$$

Hence, the magnetic flux lines are closed within S, or if the flux line comes into S, it surely goes out of S, as illustrated in Fig. 2.8. If the left side is rewritten using Gauss' theorem, it leads to

$$\int_{\mathrm{V}} \nabla \cdot \boldsymbol{B} \mathrm{d}V = 0, \tag{2.34}$$

where V is the interior of S. Since this holds for arbitrary V, we have

$$\nabla \cdot \boldsymbol{B} = 0. \tag{2.35}$$

This shows that the magnetic flux density has no divergence.

Here, we treat the potential that produces the magnetic flux density. In this case we do not have a procedure to derive the potential from the magnetic flux density. The following relationship holds for an arbitrary vector $\boldsymbol{A}$:

$$\nabla \cdot (\nabla \times \boldsymbol{A}) = \mathrm{div}(\mathrm{curl}\boldsymbol{A}) = 0. \tag{2.36}$$

Since the magnetic flux density obeys (2.35), it can be given in the form of

$$\boldsymbol{B} = \nabla \times \boldsymbol{A}, \tag{2.37}$$

using a vector $\boldsymbol{A}$. This vector is called the vector potential. When a current of density $\boldsymbol{i}$ flows in region V, the vector potential is given by

$$\boldsymbol{A}(\boldsymbol{r}) = \frac{\mu_0}{4\pi} \int_{\mathrm{V}} \frac{\boldsymbol{i}(\boldsymbol{r}')}{|\boldsymbol{r} - \boldsymbol{r}'|} \mathrm{d}V'. \tag{2.38}$$

This is similar to the electric potential caused by electric charge in (2.12). A similar magnetic potential, a kind of scalar potential, is sometimes used, since analysis using

the vector potential seems not to be simple. It is not difficult, however, to use the vector potential. In particular, the vector potential gives a clearer physical concept, as will be shown later. In addition, since the field caused by the magnetic potential is nothing else than a gradient, the field with rotation cannot be given. That is, the use of the magnetic potential is inconveniently limited only in regions where the current does not flow, as in vacuum.

The essence of the magnetic flux density is that it is a rotational field that is caused by current but has no divergence. This characteristic is asymmetrical with respect to the electric field that describes the electrostatic phenomena. When a magnetizing current of density $\boldsymbol{i}_{\mathrm{m}}$ coexists with current density $\boldsymbol{i}$, $\boldsymbol{i}$ can be replaced by $\boldsymbol{i} + \boldsymbol{i}_{\mathrm{m}}$ in the above equations.

2.3 *E-B* Analogy

The electric field $\boldsymbol{E}$ is a general field produced by the electric charge and polarization charge, and the magnetic flux density $\boldsymbol{B}$ is a general magnetic field produced by the current and the magnetic moment. These fields exert the Lorentz force

$$\boldsymbol{F} = q(\boldsymbol{E} + \boldsymbol{v} \times \boldsymbol{B}) \tag{2.39}$$

on a particle with electric charge q and velocity $\boldsymbol{v}$. This phenomenon provides a single connection between electromagnetism and dynamics. The first term is the Coulomb force and the second term is the Lorentz force in the narrow sense. In electromagnetism, the electric field $\boldsymbol{E}$ and the magnetic flux density $\boldsymbol{B}$ are treated as important independent variables, and such a form is called the ***E-B*** analogy.

In the framework of the present electromagnetism, electric substances are roughly classified into conductors and dielectric materials (insulators). Electric charges (electrons) can move freely inside a conductor and keep the interior electric field zero regardless of any condition on the outside. On the other hand, electrons cannot move freely due to bonding by nuclei in a dielectric material. Thus, electrons are slightly displaced when an electric field is applied from the outside, resulting in a partial shielding with a reduced interior electric field. This phenomenon is called electric polarization. In this condition, the electrical neutrality condition is broken, and part of the electric charge appears on the surface of the material. This electric charge is called the polarization charge. The polarization charge cannot be transferred outside. The polarization charge produces the electric field. The electric field produced in the dielectric material is also called the electric polarization and is represented by $\boldsymbol{P}$. This is associated with the polarization charge as

$$\nabla \cdot \boldsymbol{P} = -\rho_{\mathrm{p}}, \tag{2.40}$$

where ρ_{p} is the polarization charge density. It should be noted that the sign is different from (2.7) for the relationship between the electric field and the electric charge

density. This is because the polarization charge always shields in such a way as to weaken the internal electric field. The electric field that is produced by the true electric charge is called the electric flux density and represented by $\boldsymbol{D}$. The relationship between $\boldsymbol{D}$ and $\boldsymbol{E}$ is given by

$$\boldsymbol{E} = \frac{1}{\epsilon_0}(\boldsymbol{D} - \boldsymbol{P}). \tag{2.41}$$

Since $\boldsymbol{P}$ is proportional to $\boldsymbol{E}$ in most cases, there is a proportional relationship between $\boldsymbol{E}$ and $\boldsymbol{D}$, which is expressed as

$$\boldsymbol{D} = \epsilon \boldsymbol{E}, \tag{2.42}$$

where ϵ is the dielectric constant.

Only magnetic materials are treated as substances that show magnetic behavior in the usual electromagnetism. Conductors are non-magnetic materials and are basically the same as vacuum in terms of their magnetic behavior. The sources of the magnetism are current and magnetic moment as mentioned above. The magnetic field produced by the magnetic moment in magnetic material is called the magnetization and is represented by $\boldsymbol{M}$. In classic electromagnetism the magnetization is formally described using the virtual magnetizing current, which can be treated in a similar way to the current. The relationship to the magnetizing current density $\boldsymbol{i}_{\mathrm{m}}$ is given by

$$\nabla \times \boldsymbol{M} = \boldsymbol{i}_{\mathrm{m}}. \tag{2.43}$$

The magnetic field produced only by the current is called the magnetic field and is represented by $\boldsymbol{H}$. Its relationship to the magnetic flux density $\boldsymbol{B}$ is

$$\boldsymbol{B} = \mu_0(\boldsymbol{H} + \boldsymbol{M}). \tag{2.44}$$

Since $\boldsymbol{M}$ is proportional to $\boldsymbol{B}$ in most cases, there is a proportional relationship between $\boldsymbol{B}$ and $\boldsymbol{H}$, which is expressed as

$$\boldsymbol{H} = \frac{1}{\mu}\boldsymbol{B}, \tag{2.45}$$

where μ is the magnetic permeability. The fact that the magnetizing current does not shield most magnetic materials is a characteristic difference from the electrical phenomena. Hence, the sign is different between (2.40) and (2.43).

As discussed above, there is a difference between electricity and magnetism with respect to the component materials. That is, while conductors with electric charge and dielectric materials with polarization charge are treated in electricity, only magnetic materials with magnetizing current are treated in magnetism. It is proposed here to

introduce superconductors, in which current causes magnetic behavior, as one of magnetic substances in such a way as to make electricity and magnetism more equal to each other, which will contribute to advancing the ***E*-*B*** analogy.

2.4 Electromagnetic Phenomena Varying with Time

When electromagnetic fields vary with time, the equations described in Sects. 2.1 and 2.2 do not hold. One of them is the electromagnetic induction. Faraday's law describes how the electromotive force is induced by variation in the magnetic flux with time. That is, if the magnetic flux that penetrates a closed circuit C is denoted by Φ, the electromotive force is given by

$$V_{\mathrm{em}} = -\frac{\mathrm{d}\Phi}{\mathrm{d}t}, \tag{2.46}$$

where the directions of the magnetic flux and electromotive force obey the right-hand rule. The left side of (2.46) is given by the curvilinear integral of the induced electric field. Hence, we have

$$\oint_{\mathrm{C}} \boldsymbol{E} \cdot \mathrm{d}\boldsymbol{s} = -\frac{\mathrm{d}}{\mathrm{d}t} \int_{\mathrm{S}} \boldsymbol{B} \cdot \mathrm{d}\boldsymbol{S}. \tag{2.47}$$

Using Stokes' theorem, the left side of this equation is rewritten as the left side of (2.17). Since the plane S does not change with time, the order of the time derivative and surface integral can be changed:

$$\int_{\mathrm{S}} (\nabla \times \boldsymbol{E}) \cdot \mathrm{d}\boldsymbol{S} = -\int_{\mathrm{S}} \frac{\partial \boldsymbol{B}}{\partial t} \cdot \mathrm{d}\boldsymbol{S}. \tag{2.48}$$

Since this holds for arbitrary S, we have

$$\nabla \times \boldsymbol{E} = -\frac{\partial \boldsymbol{B}}{\partial t}. \tag{2.49}$$

This is the differential form of Faraday's law. When there is no variation with time, this equation leads to (2.19), which describes the electrostatic field. Hence (2.49) holds generally, including the electrostatic field.

Assume that plane S moves with velocity $\boldsymbol{V}$ in a space with uniform magnetic flux density $\boldsymbol{B}$. We calculate the magnetic flux $\Delta\Phi$ that enters S during a short period Δt. Since the magnetic flux that enters through a small segment $\mathrm{d}\boldsymbol{s}$, which is the magnetic flux in the hatched region shown in Fig. 2.9, is $(\boldsymbol{V}\Delta t \times \mathrm{d}\boldsymbol{s}) \cdot \boldsymbol{B} = (\boldsymbol{B} \times \boldsymbol{V}) \cdot \mathrm{d}\boldsymbol{s}\Delta t$, $\Delta\Phi$ is obtained as

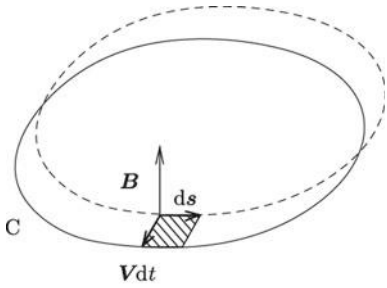

Fig. 2.9 Closed line C moving with velocity $\boldsymbol{V}$ and the region swept by d$\boldsymbol{s}$

$$\Delta\Phi = \Delta t \oint_{\mathrm{C}} (\boldsymbol{B} \times \boldsymbol{V}) \cdot \mathrm{d}\boldsymbol{s}. \tag{2.50}$$

This gives $\Delta\Phi/\Delta t$. In the limit $\Delta t \to 0$, this leads to the derivative with time, $\mathrm{d}\Phi/\mathrm{d}t$. Since the electromotive force is given by the left side of (2.47), we have

$$\oint_{\mathrm{C}} \boldsymbol{E} \cdot \mathrm{d}\boldsymbol{s} = -\oint_{\mathrm{C}} (\boldsymbol{B} \times \boldsymbol{V}) \cdot \mathrm{d}\boldsymbol{s}. \tag{2.51}$$

Thus, we can assume

$$\boldsymbol{E} = \boldsymbol{V} \times \boldsymbol{B}. \tag{2.52}$$

Although there is arbitrariness by an mount of a gradient of a scalar function f between both sides in (2.52), it is empirically known that this term is zero. Thus (2.52) holds generally.

One more equation that needs to be corrected is Ampere's law of (2.30), which does not satisfy the continuity equation of current. The left side of this equation is given by $\mu_0 \nabla \times \boldsymbol{H}$. The displacement current, $\partial \boldsymbol{D}/\partial t$, is added on the right side after the correction:

$$\nabla \times \boldsymbol{H} = \boldsymbol{i} + \frac{\partial \boldsymbol{D}}{\partial t}. \tag{2.53}$$

This is the generalized differential form of Ampere's law. This satisfies the continuity equation of current.

The electromagnetic energy density in conditions varying with time is given by

$$u = \frac{\epsilon}{2}\boldsymbol{E}^2 + \frac{1}{2\mu}\boldsymbol{B}^2 + \int \boldsymbol{i} \cdot \boldsymbol{E}\mathrm{d}t, \tag{2.54}$$

where the first and second terms are the electric and magnetic energy densities, and the third term is the kinetic energy given to a moving electric charge. In fact, if the current density is expressed as a movement of the charge particles of the electric

charge q, density n, and velocity $\boldsymbol{v}$, the current density is given by $\boldsymbol{i} = nq\boldsymbol{v}$. Hence, using the Coulomb force $\boldsymbol{F} = q\boldsymbol{E}$, the term $\boldsymbol{i} \cdot \boldsymbol{E}$ in the third term is rewritten as

$$\boldsymbol{i} \cdot \boldsymbol{E} = n\boldsymbol{F} \cdot \boldsymbol{v}. \tag{2.55}$$

Thus, the third term of (2.54) is the work done by the Coulomb force. The variation in the electromagnetic energy in space V with time is given by

$$\frac{\partial U}{\partial t} = \frac{\partial}{\partial t} \int_{\mathrm{V}} u \mathrm{d}V = \int_{\mathrm{V}} \left(\epsilon \boldsymbol{E} \cdot \frac{\partial \boldsymbol{E}}{\partial t} + \frac{\boldsymbol{B}}{\mu} \cdot \frac{\partial \boldsymbol{B}}{\partial t} + \boldsymbol{i} \cdot \boldsymbol{E} \right) \mathrm{d}V. \tag{2.56}$$

Using (2.42) and (2.53), the sum of the first and third terms in (2.56) leads to

$$\epsilon \boldsymbol{E} \cdot \frac{\partial \boldsymbol{E}}{\partial t} + \boldsymbol{i} \cdot \boldsymbol{E} = \boldsymbol{E} \cdot \left(\frac{\partial \boldsymbol{D}}{\partial t} + \boldsymbol{i} \right) = \boldsymbol{E} \cdot (\nabla \times \boldsymbol{H}). \tag{2.57}$$

Using (2.45) and (2.49), the second term becomes

$$\frac{\boldsymbol{B}}{\mu} \cdot \frac{\partial \boldsymbol{B}}{\partial t} = -\boldsymbol{H} \cdot (\nabla \times \boldsymbol{E}). \tag{2.58}$$

Thus, the right side of (2.56) is rewritten as

$$\int_{\mathrm{V}} [\boldsymbol{E} \cdot (\nabla \times \boldsymbol{H}) - \boldsymbol{H} \cdot (\nabla \times \boldsymbol{E})] \mathrm{d}V = -\int_{\mathrm{V}} \nabla \cdot (\boldsymbol{E} \times \boldsymbol{H}) \mathrm{d}V. \tag{2.59}$$

Here, Poynting's vector is defined as

$$\boldsymbol{S}_{\mathrm{P}} = \boldsymbol{E} \times \boldsymbol{H}. \tag{2.60}$$

Then, using Gauss' theorem (2.56) becomes

$$\frac{\partial}{\partial t} \int_{\mathrm{V}} u \mathrm{d}V + \int_{\mathrm{S}} \boldsymbol{S}_{\mathrm{P}} \cdot \mathrm{d}\boldsymbol{S} = 0, \tag{2.61}$$

where V is the surface of region S. This equation describes the flow of energy: the variation in energy with time is equal to the sum of Poynting's vector penetrating through the surface.

2.5 Maxwell's Equations and Breaking of Symmetry

Maxwell's equations that describe electromagnetic phenomena are:

$$\nabla \times \boldsymbol{E} = -\frac{\partial \boldsymbol{B}}{\partial t}, \tag{2.62}$$

$$\nabla \times \boldsymbol{H} = \boldsymbol{i} + \frac{\partial \boldsymbol{D}}{\partial t,} \tag{2.63}$$

$$\nabla \cdot \boldsymbol{D} = \rho, \tag{2.64}$$

$$\nabla \cdot \boldsymbol{B} = 0. \tag{2.65}$$

These are solved with the material relationships:

$$\boldsymbol{D} = \epsilon \boldsymbol{E}, \tag{2.66}$$

$$\boldsymbol{B} = \mu \boldsymbol{H}, \tag{2.67}$$

$$\boldsymbol{i} = \sigma_{\mathrm{c}} \boldsymbol{E}. \tag{2.68}$$

In the above, σ_{c} is the electric conductivity and (2.68) is the empirical Ohm's law. Comparing (2.62) with (2.63) and (2.64) with (2.65), it is clear that symmetry between electric and magnetic phenomena does not exist. What is the reason for the breaking of symmetry?

If we treat the condition in which there is no electric charge and current ($\rho = 0$ and $\boldsymbol{i} = 0$), however, we find that the symmetry appears among them (although note that the sign factor of the derivative with respect to time is different). This corresponds to electromagnetic waves. Here we look carefully at how the symmetry breaks by introducing sources that produce the fields. Since the electric charge is a scalar, the distortion of the vector field (electric field) is nothing else than the divergence. This means that the effect of the electric charge can appear only in (2.64). On the other hand, the current is a vector and the distortion of the vector field (magnetic flux density) is nothing else than the rotation. Hence, the effect of the current can appear only in (2.63). This discussion shows that the breaking of symmetry comes from the mathematical difference between the source being a scalar or vector. This difference also causes the different natures of the fields, as mentioned above.

Coffee break (2)

Does the Lorentz force do mechanical work?

It is stated in textbooks on electromagnetism that the Lorentz force does not do mechanical work, since it only changes the direction of motion of an electric charge in a magnetic field but does not influence the kinetic energy. On the other hand, when a current is applied to a conductor in a magnetic field, it can happen that the conductor is driven by the Lorentz force. In this case the mechanical work is done. How can we understand this phenomenon?

Suppose that there is an electron travelling in a conductor. The electron tends to move in the normal direction to the propagation direction in the conductor due to the Lorentz force. In practice, however, the electron moves along the conductor. This is caused by the Coulomb force of cations (and if the Hall effect is appreciable, the influence of the distributed Hall electrons is also included). That is, the transverse movement of the traveling electron is strongly suppressed by the cations. This means that a reaction, which is also the Coulomb force, is exerted on the cations. Hence, this reaction pushes the conductor in the direction of the Lorentz force. Thus, a Coulomb force of the same strength as the Lorentz force is exerted on the conductor. Hence, the statement that the Lorentz force moves the conductor is not correct.

In fact, the Coulomb force moves the conductor, and it is false to think that the Lorentz force moves it. The Coulomb force is not responsible for this, however, but the origin of this movement is electric power source. An electromotive force is induced when the conductor is forced to move, and the electromotive force works to stop the motion of the conductor. That is, if the work done by the electromotive force is realized, it cancels out the mechanical work that causes a loss energy. Nevertheless, the electric power source supplies additional energy to the circuit to keep the current constant. This causes the loss energy.

Someone is walking while revolving a ball by pulling a string connected to the ball. Assume that the ball approaches an object and the object falls down due to the wind produced by the moving ball and is damaged. The force that destroyed the object is the wind pressure, but it is not the centripetal force, i.e., the line tension of the string. The responsibility for the destruction lies with the person who revolved the ball and added a force to prevent the ball from slowing down by the reaction of the wind pressure. If he would not have added the force, the speed of the ball might have been reduced and the object might not have fallen down.

Then, what is the case of the Lorentz force that works on quantized flux lines when a current is applied to a superconductor in a magnetic field? It is assumed that the superconductor is fixed so as not to move.

Chapter 3
Effects of the Introduction of Superconductivity into Electromagnetism

Abstract If the ***E*-*B*** analogy, which is current in the present electromagnetism, is perfect, it seems to be natural that some magnetic material must exist that keeps the interior magnetic flux density $\boldsymbol{B}$ zero, corresponding to a conductor that keeps its interior electric field $\boldsymbol{E}$ zero. This is in fact a superconductor, which really exists. Hence, if someone would have assumed the existence of such a magnetic material based on this analogy in the 19th century, he would have predicted the superconductor, since it is possible to show that the electrical resistivity of this material must be zero by using Maxwell's theory. The magnetic phenomena exhibited by superconductors correspond to electric phenomena exhibited by conductors in various aspects, including this point. In this chapter it is shown that introduction of the magnetic phenomena of superconductors into electromagnetism is inevitable to make the ***E*-*B*** analogy more rigorous. Reference [1] covers the topical area in this chapter.

3.1 Electricity in a Conductor and Magnetism in a Superconductor

The internal electrostatic field is kept at zero in a conductor, even in an external electric field:

$$\boldsymbol{E} = 0. \tag{3.1}$$

The internal magnetic flux density is kept at zero in a superconductor, even in an external magnetic field, when the magnetic field is not strong:

$$\boldsymbol{B} = 0. \tag{3.2}$$

This property that shows the perfect diamagnetism is called the Meissner-Ochsenfeld effect. These phenomena are quite analogous and support the present ***E*-*B***analogy.

Here, electric phenomena in a conductor and magnetic phenomena in the perfect diamagnetic state in a superconductor are compared in more detail. Equations (2.7)

T. Matsushita, *Superconductivity and Electromagnetism*, Springer Series in Solid-State Sciences 195, https://doi.org/10.1007/978-3-030-67568-4_3

and (3.1) lead to

$$\rho = 0, \tag{3.3}$$

which requires that there is no electric charge inside the conductor. Hence, if electric charge exists in a conductor, it stays only on the surface of the conductor. From (3.1) the electric potential of a conductor is

$$\phi = \text{ const.} \tag{3.4}$$

That is, conductor has equi-electric potential. When electric charge is distributed with density σ on the surface of a conductor, the electric field in the vicinity of the surface is perpendicular to the surface and its value is given by

$$E = \frac{\sigma}{\varepsilon_0}. \tag{3.5}$$

On the other hand, (2.30) and (3.2) lead to

$$\boldsymbol{i} = 0, \tag{3.6}$$

which requires that there is no current inside the superconductor. Hence, if current flows in a superconductor, it flows only on the surface of the superconductor. From (3.2) the vector potential of superconductor is

$$\boldsymbol{A} = \text{ const.}, \tag{3.7}$$

except in the case where the superconductor is not simply connected and a magnetic flux penetrates a space surrounded by the superconductor such as with a solenoid coil. Thus, superconductor has equi-vector potential in most cases. When current flows on the surface of the superconductor with surface density τ, the magnetic flux density in the vicinity of the surface is parallel to the surface and its value is given by

$$B = \mu_0 \tau. \tag{3.8}$$

It will be easily understood from the above example that there is an analogy between the electric phenomena in a conductor and the magnetic phenomena in a superconductor. Figure 3.1 shows the electric field lines produced by the electric charge on the surface of a conductor and the magnetic flux lines produced by the current on the surface of a superconductor. The difference comes from the different features of the respective fields, i.e., the electric field with divergence and the magnetic flux density with rotation.

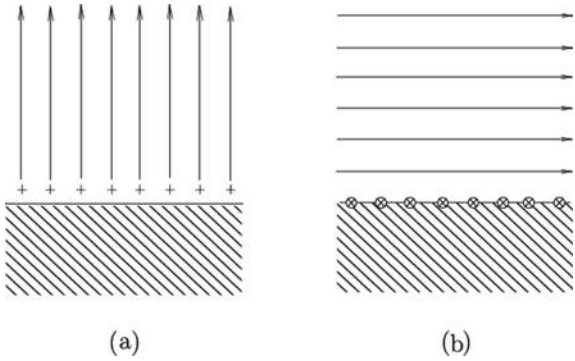

Fig. 3.1 **a** Electric field due to the electric charge on the conductor surface and **b** the magnetic flux density due to the current on the superconductor surface

Here we compare the electric phenomenon in a conductor and the magnetic phenomenon in a superconductor in more detail. We suppose that two wide slab conductors are parallel to each other, as shown in Fig. 3.2, and apply electric charge of surface density σ to the left conductor and that of $-\sigma$ to the right conductor. In this case the electric charges appear on the surfaces that face each other as in the case of a capacitor. Under these conditions, the electric field inside the conductors ($-b \le x \le -a$, $a \le x \le b$) is zero. The electric field is directed along the x axis, and its strength is

$$\begin{aligned} E_x &= \frac{\sigma}{\varepsilon_0}; \quad -a \le x \le a, \\ &= 0; \quad x < -a, x > a. \end{aligned} \tag{3.9}$$

The electric potential is

$$\phi = \frac{\sigma}{\varepsilon_0} a; \quad x < -a,$$

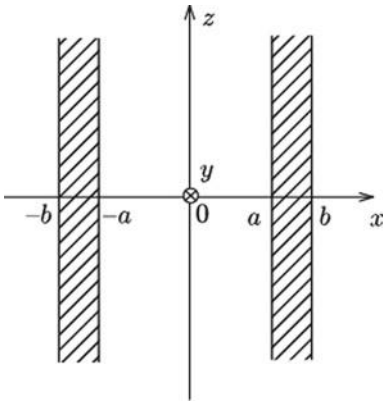

Fig. 3.2 Two wide parallel slab conductors

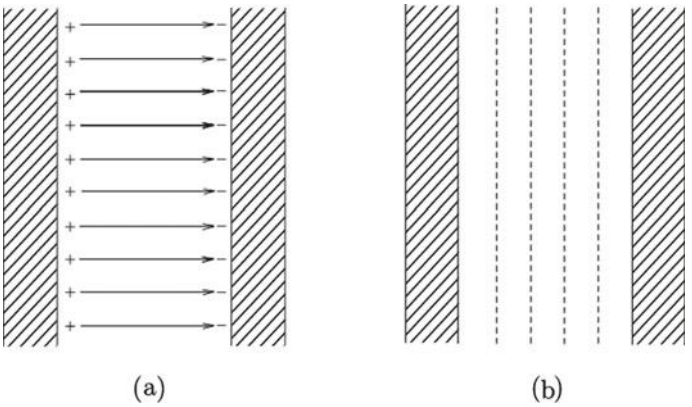

Fig. 3.3 **a** Electric field lines and **b** equi-electric potential surfaces between the two slab conductors

$$
\begin{aligned}
&= -\frac{\sigma}{\varepsilon_0} x; \quad -a \le x \le a, \\
&= -\frac{\sigma}{\varepsilon_0} a; \quad x > a.
\end{aligned} \tag{3.10}
$$

The electric field lines are directed from the left conductor to the right conductor, the equi-electric potential surfaces are parallel to the conductor surfaces, and the electric potential of the left conductor is higher than that of the right conductor (see Fig. 3.3).

Here, we assume two parallel superconducting slabs of the same shape and consider the case in which currents with surface densities τ and $-\tau$ are applied along the y-axis on the left and right slabs, respectively. The currents flow on the surfaces that face each other in this case also. This current distribution makes the magnetic flux density zero in the interior of the superconductor, $-b \le x \le -a$ and $a \le x \le b$. The magnetic flux density is directed along the z-axis and is given by

$$
\begin{aligned}
B_z &= -\mu_0 \tau; -a \le x \le a, \\
&= 0; \qquad x < -a, x > a.
\end{aligned} \tag{3.11}
$$

Since the current flows only along the y-axis, the vector potential has only the y component, A_y, as shown by (2.38). From the relationship $B_z = \partial A_y / \partial x$, we have

$$
\begin{aligned}
A_y &= \mu_0 \tau a; \qquad x < -a, \\
&= -\mu_0 \tau x; \quad -a \le x \le a, \\
&= -\mu_0 \tau a; \quad x > a.
\end{aligned} \tag{3.12}
$$

The magnetic flux lines are parallel to the superconductor surfaces, and the equi-vector potential surface is also parallel to the surfaces with a higher potential in the left superconductor (see Fig. 3.4). It is also possible to show this phenomenon

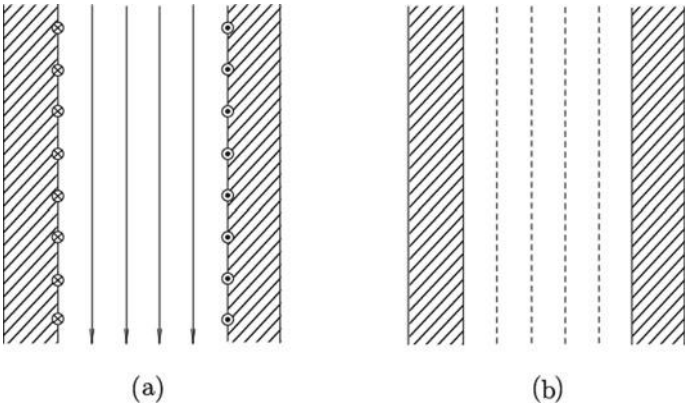

Fig. 3.4 **a** Magnetic flux lines and **b** equi-vector potential surfaces between the two superconducting slabs

with the magnetic potential. In this case the magnetic potential takes on a higher value at the upper position in the space between the two superconducting slabs. Hence, each superconductor surface is not equipotential. On the other hand, the magnetic potential is zero in the superconductors and the space outside them. Hence, the magnetic potential is not continuous on the inner surfaces. This shows that, although the problem can be solved using the magnetic potential, it does not help in understanding the magnetic phenomena.

Here, we show another similarity between the electric and magnetic phenomena. We assume that electric charge of uniform line density λ is put on a line at distance a from a flat infinite conductor surface. Electric charge appears on the conductor surface to make the electric field zero in the interior of the conductor. It may seem to be difficult to determine the electric charge distribution, the resultant electric field, and the electric potential. There is a useful method, however, to solve this problem. This method is called the image method, which utilizes the feature that the conductor surface is equipotential. Here, we define the coordinates; the x-y plane ($z = 0$) is defined on the conductor surface, and the y-axis is defined at the projection of the linear charge on the x-y plane (see Fig. 3.5a). It is virtually assumed that there is no conductor. In this case it is enough to put electric charge of linear density $-\lambda$ on the line at $z = -a$, which is symmetrical to the given linear charge with respect to the conductor surface, so as to make this surface equipotential ($\phi = 0$), as shown in Fig. 3.5b. This method of putting electric charge at a symmetric position with respect to the original conductor surface after virtually removing the conductor is the image method, and the virtual electric charge is called the image charge. The electric field and electric potential obtained using this method are useful only in the vacuum region ($z > 0$). The electric potential outside the conductor produced by the given and virtual electric charges is

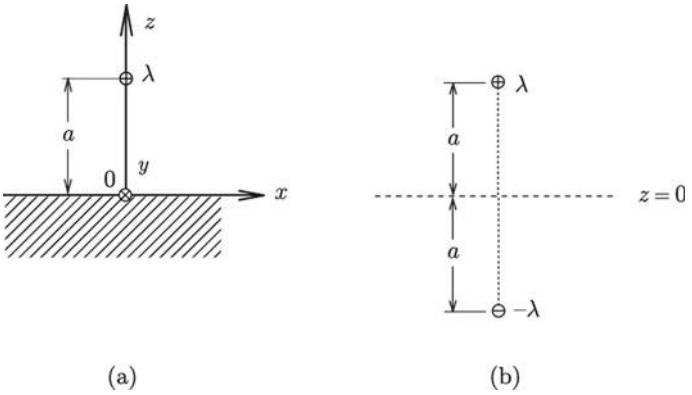

Fig. 3.5 **a** Linear charge of density λ placed above the flat conductor surface, and **b** linear charge of density −λ placed at the symmetric position with respect to the conductor surface after virtually removing the conductor

$$\phi = \frac{\lambda}{4\pi\epsilon_0}\log\frac{x^2+(z+a)^2}{x^2+(z-a)^2}. \tag{3.13}$$

In fact, this leads to $\phi(z=0) = 0$ and the condition of the electric potential is satisfied. Using this result, the electric field outside the conductor is

$$\begin{aligned} E_x &= -\frac{\partial\phi}{\partial x} = \frac{2a\lambda xz}{\pi\varepsilon_0\left[x^2+(z-a)^2\right]\left[x^2+(z+a)^2\right]}, \\ E_y &= -\frac{\partial\phi}{\partial y} = 0, \\ E_z &= -\frac{\partial\phi}{\partial z} = \frac{a\lambda\left(-x^2+z^2-a^2\right)}{\pi\varepsilon_0\left[x^2+(z-a)^2\right]\left[x^2+(z+a)^2\right]}. \end{aligned} \tag{3.14}$$

In particular, on the conductor surface ($z = 0$), this leads to

$$E_x = E_y = 0, E_z = -\frac{a\lambda}{\pi\epsilon_0\left(x^2+a^2\right)}, \tag{3.15}$$

showing that the electric field is perpendicular to the surface. From (3.5) the density of the surface electric charge is obtained as

$$\sigma = \epsilon_0 E_z(z=0) = -\frac{a\lambda}{\pi\left(x^2+a^2\right)}. \tag{3.16}$$

The total electric charge in a unit length along the y-axis on the conductor surface is

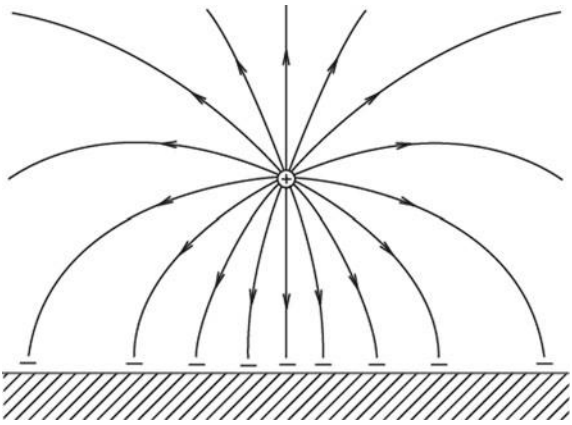

Fig. 3.6 Electric field outside the conductor

$$-\int_{-\infty}^{\infty} \frac{a\lambda \mathrm{d}x}{\pi\left(x^2+a^2\right)} = -\frac{\lambda}{\pi}\int_{-\pi/2}^{\pi/2} \mathrm{d}\theta = -\lambda, \tag{3.17}$$

which is equal to the image charge. In the above calculation, the transformation, $x = a\tan\theta$, was used. The electric field outside the conductor is schematically shown in Fig. 3.6.

In the above, only the region outside the conductor was treated. The fact that the inner region of the conductor ($z < 0$) is equipotential ($\phi = 0$) can be proved as follows: If there is no electric charge on the conductor surface, the given charge of linear density λ produces electric potential in the conductor region. From symmetry, this electric potential is equal to that produced by electric charge of linear density $-\lambda$ put on the original position where electric charge λ was put. As a result, the electric potential inside the conductor is the sum of two electric potentials produced by the electric charges of λ and $-\lambda$ placed at the same position. That is, this is the electric potential when there is no electric charge. Thus, it can be proved that the conductor is equipotential.

Now we assume that current I is applied to a line at distance a from a flat infinite superconductor surface. Current appears on the superconductor surface, so the magnetic flux density is zero in the interior of the superconductor. The image method can also be used to determine the vector potential and magnetic flux density on the outside of the superconductor. The coordinates are defined similarly. The image current $-I$ is put at the symmetric position, $z = -a$. The vector potential outside the superconductor has only the y compotent, A_y, which is given by

$$A_y = \frac{\mu_0 I}{4\pi}\log\frac{x^2+(z+a)^2}{x^2+(z-a)^2}. \tag{3.18}$$

This satisfies the requirement, $A_y(z=0) = 0$, which proves that the superconductor is equi-vector potential. The magnetic flux density is then given by

$$
\begin{aligned}
B_x &= -\frac{\partial A_y}{\partial z} = \frac{\mu_0 aI\left(-x^2+z^2-a^2\right)}{\pi\left[x^2+(z-a)^2\right]\left[x^2+(z+a)^2\right]},\\
B_y &= \frac{\partial A_x}{\partial z} - \frac{\partial A_z}{\partial x} = 0,\\
B_z &= \frac{\partial A_y}{\partial x} = -\frac{2\mu_0 aIxz}{\pi\left[x^2+(z-a)^2\right]\left[x^2+(z+a)^2\right]}.
\end{aligned}
\tag{3.19}
$$

In particular, the magnetic flux density on the superconductor surface ($z = 0$) is

$$
B_x = -\frac{\mu_0 aI}{\pi\left(x^2+a^2\right)},\ B_y = B_z = 0. \tag{3.20}
$$

Thus, it is shown shows that the magnetic flux density is parallel to the surface. Using (3.8), the current density on the superconductor surface is obtained as

$$
\tau = \frac{1}{\mu_0} B_x(z=0) = -\frac{aI}{\pi\left(x^2+a^2\right)}. \tag{3.21}
$$

The total current on the surface is

$$
-\int_{-\infty}^{\infty} \frac{aI\,\mathrm{d}x}{\pi\left(x^2+a^2\right)} = -\frac{I}{\pi}\int_{-\pi/2}^{\pi/2} \mathrm{d}\theta = -I, \tag{3.22}
$$

which is equal to the image current. Thus, this phenomenon is similar to the electric phenomenon of the conductor. The magnetic flux density outside the superconductor is schematically shown in Fig. 3.7. The difference from the electric field in Fig. 3.6 comes from the different nature of the field.

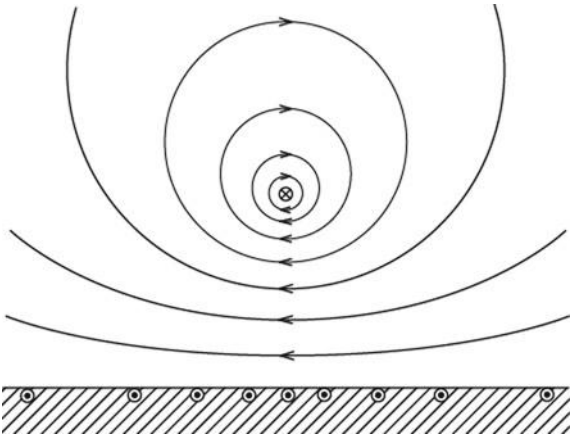

Fig. 3.7 Magnetic flux density outside the superconductor

In this case, the calculation of the magnetic flux density can also be done with the magnetic potential instead of the vector potential. It is found from Fig. 3.7 that the magnetic potential decreases monotonically with motion along the direction of the magnetic flux density. Since the magnetic flux lines are closed, however, the magnetic potential does not take the initial value when going back to the initial position. That is, the magnetic potential is a multi-valued function, the value of which changes by the same amount when circulating once. On the other hand, the vector potential takes a constant value on the closed flux lines in Fig. 3.7, and the equi-vector potential surfaces are of the same form as the equipotential surfaces in Fig. 3.6.

3.2 Prediction of Superconductivity

As is seen in the last section, the electric phenomena in a conductor showing $\boldsymbol{E} = 0$ and the magnetic phenomena in a superconductor showing $\boldsymbol{B} = 0$ are analogous to each other. This is an outstanding analogy in the present $\boldsymbol{E}$-$\boldsymbol{B}$analogy. If this analogy was believed, someone might have happened to predict the superconductor, a material showing perfect diamagnetism, even just after the formulation of Maxwell's theory in the 19th century. People know now that the resistivity of this material is zero. It could be easily shown that the resistivity of a material with perfect diamagnetism must be zero. That is, the prediction of a perfectly diamagnetic material is equivalent to the prediction of superconductivity.

Here, the proof of the zero-resistivity is treated. It may be supposed that the zero-resistivity can be easily proved, since the current must continue to flow to shield the magnetic field produced by the outer current, as in the case of Fig. 3.7. We have to consider the point, however, that such shielding can be accomplished by the diamagnetism of the material itself, as will be mentioned later. Since this type of material was not discovered in the 19th century, it was not possible to attribute the diamagnetic response to the shielding by the current or the intrinsic diamagnetism.

Hence, we have to consider the case in which a current is directly applied to a diamagnetic material. In this case the current must flow on the surface of the material, as shown in (3.6). As shown in Fig. 3.8, here, we suppose that rectangle C is located inside the material in such a way that one side is placed on the surface and parallel to the current. The current density is integrated on C. The integrated value is not zero on the side on the surface, while the contribution from other three sides is zero. That is, we have

$$\oint_{\mathrm{C}} \boldsymbol{i} \cdot \mathrm{d}\boldsymbol{s} \neq 0. \tag{3.23}$$

If Ohm's law $\boldsymbol{E} = \rho_{\mathrm{r}} \boldsymbol{i}$ holds, (3.23) leads to

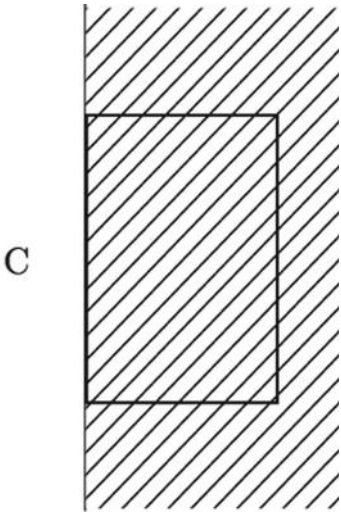

Fig. 3.8 Rectangular C with one side that stays on the surface of the diamagnetic material and is directed parallel to the current

$$\oint_{\mathrm{C}} \boldsymbol{E} \cdot \mathrm{d}\boldsymbol{s} \neq 0. \tag{3.24}$$

This contradicts (2.14), which must be satisfied under static conditions. Hence, the resistivity must be zero to be consistent with (2.14). The material that shows $\boldsymbol{B} = 0$ under any conditions is nothing else than a superconductor. Thus, the prediction of a diamagnetic material is equivalent to the prediction of a superconductor.

3.3 Merits of Introducing Superconductivity

Here, the merits of introducing the superconductor into electromagnetism as a member of the class of magnetic materials are discussed.

(1) **Example 1 of progress on the *E*-*B*analogy**

One of these merits is an improvement of the analogy between electric phenomena in electric materials and magnetic phenomena in magnetic materials. The upper panels in Fig. 3.9 show electric field lines when a uniform electric field is applied to a spherical conductor (left) and a dielectric sphere (right), and the lower panels show magnetic flux lines when a uniform magnetic flux density is applied to a spherical superconductor (left) and a magnetic sphere (right). It can be seen that the spherical conductor and the spherical superconductor completely shield the external electric field and the external magnetic flux density with electric charge and current that appear on the surface, respectively. The electric charge is the source of divergence,

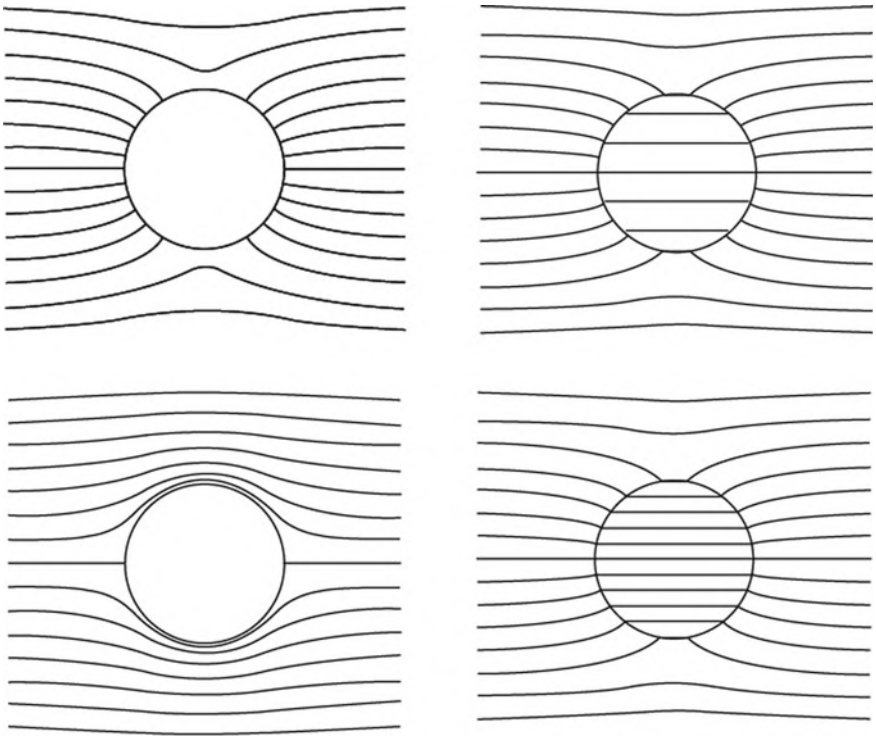

Fig. 3.9 The upper panels show the structure of electric field lines around a spherical conductor (left) and a dielectric sphere (right) in a uniform electric field, and the lower panels show the structure of magnetic flux lines around a spherical superconductor (left) and a magnetic sphere (right) in a uniform magnetic flux density

and hence, it shields by absorbing electric field lines. On the other hand, the current is a source of rotation, and hence, it shields by pushing magnetic flux lines and keeping them outside with vortices. Figure 3.9 shows that the density of the electric field lines is at a maximum at both poles, and the electric charge is mostly concentrated there. On the other hand, the density of the magnetic field lines is at a maximum on the equator, and the current is mostly concentrated there.

It may seem that the analogy is not so strong between the electric field lines around the dielectric sphere and the magnetic flux lines around the magnetic sphere in Fig. 3.9. If the magnetic field lines for $\boldsymbol{H}$ around the magnetic sphere are drawn, however, those are quite similar to the electric field lines (and if the relative dielectric constant and the relative magnetic permeability are the same, the two kinds of field lines exactly coincide each other). This comes from the fact that the both fields are irrotational, i.e., these are fields with no vorticity ($\nabla \times \boldsymbol{E} = \nabla \times \boldsymbol{H} = 0$). If the electric flux lines are drawn around the dielectric sphere in Fig. 3.9, they are similar to the magnetic flux lines around the magnetic sphere. The two kinds of flux lines are continuous on the surfaces. This comes from the fact that both kinds of flux lines are

solenoidal, i.e., these are flux lines with no divergence ($\nabla \cdot \boldsymbol{D} = \nabla \cdot \boldsymbol{B} = 0$). Thus, although there is no similarity between the most important variables, $\boldsymbol{E}$ and $\boldsymbol{B}$, in the $\boldsymbol{E}$-$\boldsymbol{B}$ analogy, these are quite analogous to the second most important variables, $\boldsymbol{H}$ and $\boldsymbol{D}$, respectively. The comparison between the electric and magnetic materials in Fig. 3.9 makes it clear that only the magnetic material does not shield the external field. In the case of a dielectric material, the polarization charge shields the inside imperfectly and the inner electric field is weaker than the external field.

The analogy between the electric and magnetic phenomena shown here may be more deeply understood with the statement in Sect. 3.1. Although there is a difference based on the different natures of the fields, this shows the validity of the $\boldsymbol{E}$-$\boldsymbol{B}$ analogy. If the superconductor is removed from the frame shown in Fig. 3.9, it will be understandable that the analogy becomes extremely weak.

(2) **Example 2 of progress on the $\boldsymbol{E}$-$\boldsymbol{B}$analogy**

Figure 3.10a shows the electric charge that appears on the surface of a hollow cylindrical conductor when a transverse external electric field E_0 is applied. The electric charge does not appear on the inner surface and the inner hollow region is completely shielded. On the other hand, Fig. 3.10b shows the polarization charge that appears on the surface of a hollow cylinder of a dielectric material when a transverse external electric field is similarly applied. In this case the polarization charge appears also on the inner surface because of relative displacement of the positive and negative electric charges. As a result the electric field appears in the hollow region.

Here we compare the difference between hollow cylinders of superconducting and magnetic materials when a longitudinal external magnetic flux density is applied, which is analogous to the above comparison. When the magnetic flux density B_0 is applied parallel to the superconducting hollow cylinder, the shielding current appears on the outer surface but not on the inner surface, as shown in Fig. 3.11, and the inner

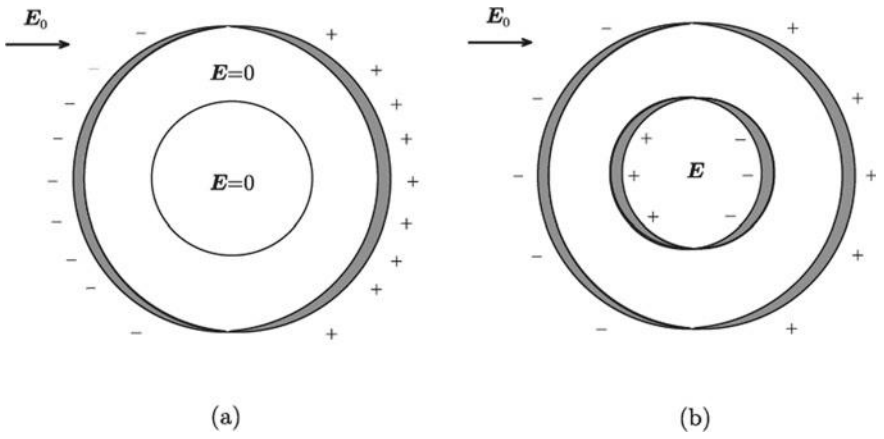

Fig. 3.10 Electric charge and internal electric field when a transverse electric field is applied to a hollow cylinder composed of **a** a conductor and **b** a dielectric material

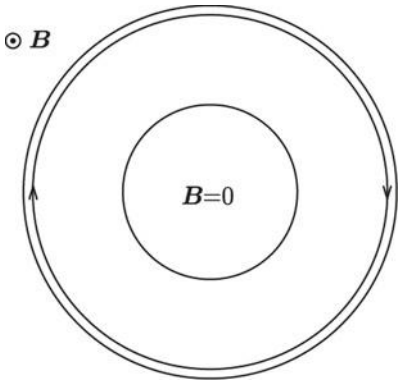

Fig. 3.11 Current and internal magnetic flux density when a longitudinal magnetic flux density is applied to a hollow cylindrical superconductor

hollow region is completely shielded. On the other hand, the magnetic moment inside the magnetic material is expressed as an assembly of small magnetizing current loops, as shown in Fig. 3.12a. Since these currents cancel out between adjacent loops, the magnetizing current remains also on the inner surface (see Fig. 3.10b). Thus, the magnetic flux density appears in the hollow region without being shielded.

The above comparisons clearly show the analogy between the electric and magnetic phenomena. That is, the difference between the electric charge and the polarization charge is analogous to that between the current and the magnetizing current. Hence, it can be said that the introduction of a superconductor is effective to show this example.

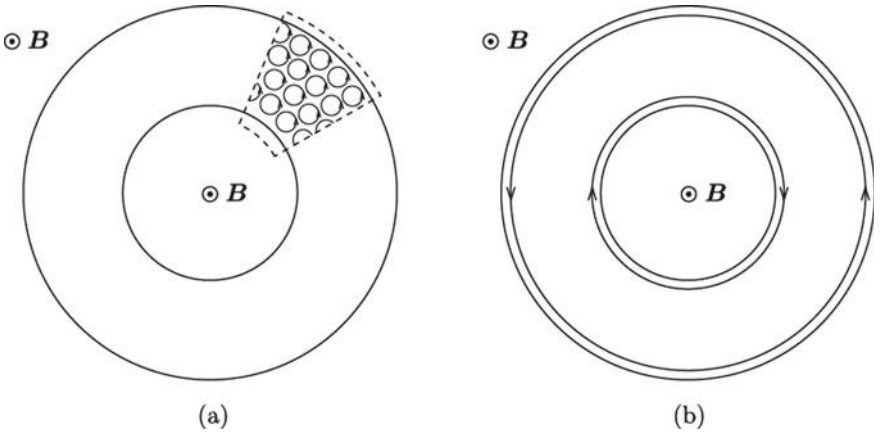

Fig. 3.12 **a** Internal magnetizing current loops and **b** the resultant magnetizing current remaining on the surfaces and the magnetic flux density in the hollow center when a longitudinal magnetic flux density is applied to a hollow cylinder of magnetic material

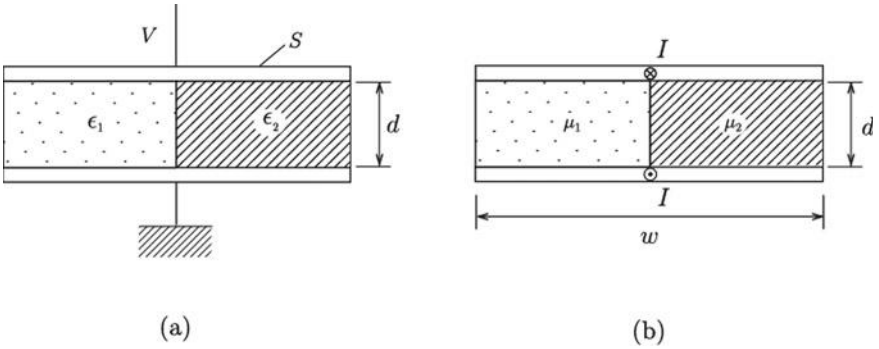

Fig. 3.13 **a** Capacitor filled with different dielectric materials and **b** superconducting transmission line filled with different magnetic materials

(3) Example 3 of progress on the *E*-*B*analogy

There is also another merit to the introduction of superconductivity. It is possible to learn the analogy through exercises on electromagnetism. Figure 3.13a shows a capacitor in which the space between the two electrodes is filled with two dielectric materials with different dielectric constants, ϵ_1 and ϵ_2, and we must determine the capacitance. When an electric potential difference V is applied to the capacitor, the electric charge density is different between the interfaces of the electrode with each dielectric material. The area of the electrodes and the distance between the two electrodes are denoted by S and d, respectively. Since the electric field in each dielectric material is $E = V/d$, the electric charge densities on the interface in each region are $\sigma_1 = \epsilon_1 V/d$ and $\sigma_2 = \epsilon_2 V/d$. Hence, the total electric charge is

$$Q = \frac{S}{2}(\sigma_1 + \sigma_2) = \frac{(\epsilon_1 + \epsilon_2)SV}{2d}, \tag{3.25}$$

and the capacitance, i.e., the electric charge stored by a unit electric potential difference, is

$$C = \frac{Q}{V} = \frac{(\epsilon_1 + \epsilon_2)S}{2d}. \tag{3.26}$$

It is possible to design an analogous exercise for a superconductor. Figure 3.13b shows a superconducting power transmission line with two magnetic materials with different magnetic permeabilities μ_1 and μ_2. We calculate the self-inductance in a unit length. It should be noted that the surface current density is different between the interfaces with each magnetic material, when current I is applied. If the usual

conductor for which Ohm's law holds is used, such a situation cannot be realized. The width, length, and thickness of the transmission line are denoted by w, l, and d, respectively. Since the magnetic flux density B is common to the two magnetic materials, the surface current densities are $\tau_1 = B/\mu_1$ and $\tau_2 = B/\mu_2$. Hence the total current is

$$I = \frac{w}{2}(\tau_1 + \tau_2) = \frac{(\mu_1 + \mu_2)wB}{2\mu_1\mu_2}. \tag{3.27}$$

Since the magnetic flux is $\Phi = dlB$, the self-inductance, i.e., the magnetic flux stored by a unit current, is

$$L = \frac{\Phi}{I} = \frac{2\mu_1\mu_2 dl}{(\mu_1 + \mu_2)w}. \tag{3.28}$$

From the viewpoint of impedance, $1/C$ corresponds to L. Since ϵ corresponds to $1/\mu$ from (2.2) and (2.22) (note that $\epsilon\mu$ has dimension of $(\mathrm{s/m})^2$), and S and dl are the areas of the planes normal to $\boldsymbol{E}$ and $\boldsymbol{B}$, respectively, it can be understood that (3.26) and (3.28) are analogous to each other. Such effectiveness in education is also one of the merits of introducing superconductivity.

(4) **Derivation of magnetic energy and prediction of the induction law**

One of other big merits of introducing superconductivity into electromagnetism is direct derivation of magnetic energy from mechanical work. The electric energy can be calculated from the mechanical work needed to carry small electric charges from infinity until the final desired distribution of electric charge is completed. If we similarly try to derive the magnetic energy, however, the attractive force works between currents, and the mechanical work to carry a current is negative. This is attributed to the electromotive induction. For this reason, it is common that students learn the magnetic energy, which is derived through equivalent electric energy, after learning about electromotive induction. That is, learning about dynamic phenomena is required to learn about the static magnetic phenomena.

On the other hand, it is possible to directly derive the magnetic energy from the mechanical work done by the Lorentz force in a circuit composed of superconductors. Suppose that there is a closed circuit made of superconducting slabs, as shown in Fig. 3.14. The superconducting circuit is composed of a fixed superconducting slab with three sides and a movable superconducting slab with superconducting contact between them. For simplicity, b is assumed to be much larger than a. It is assumed that the magnetic flux Φ is stored in the space surrounded by the circuit. This situation can be achieved by the following procedure: external magnetic field is first applied to the superconducting circuit at a temperature higher than the critical temperature, and then the temperature is lowered below the critical temperature, which makes the circuit superconducting. Finally, the external magnetic field is removed. This is called the field-cooled process. In this situation, a shielding current is induced in the circuit. This process is employed to realize a permanent current. The Lorentz

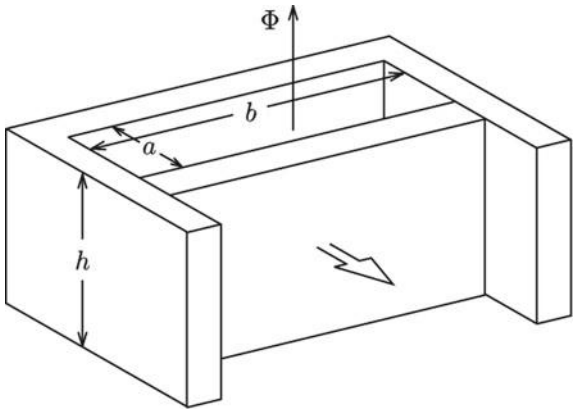

Fig. 3.14 Magnetic flux stored in closed circuit made of superconducting slabs

force is exerted on the movable superconducting slab that carries the current. Even if the distance between the slabs changes from a to $a + x$, the magnetic flux inside the circuit is preserved. This is because the magnetic flux cannot pass through the superconducting region to go outside. Hence, the magnetic flux density changes to

$$B = \frac{\Phi}{(a+x)b} \tag{3.29}$$

and the density of the current flowing on the inner surface of the superconductors changes to

$$\tau = \frac{B}{\mu_0} = \frac{\Phi}{\mu_0(a+x)b}. \tag{3.30}$$

Since the magnetic flux density produced by the fixed superconducting slab is half of the value given by (3.29), the force exerted on the movable slab is

$$F = \frac{1}{2}\tau Bbh = \frac{\Phi^2 h}{2\mu_0(a+x)^2 b}. \tag{3.31}$$

Since this circuit is isolated from its surroundings, this force originates from the variation in the magnetic energy U_m of this circuit. From the relationship,

$$F = -\frac{\partial U_\mathrm{m}}{\partial x}, \tag{3.32}$$

the magnetic energy is obtained as

$$U_\mathrm{m} = \frac{\Phi^2 h}{2\mu_0(a+x)b} = \frac{1}{2\mu_0}B^2(a+x)bh. \tag{3.33}$$

Since $(a + x)bh$ is the volume of the interior space with constant magnetic flux density, the magnetic energy density is given by

$$u_{\mathrm{m}} = \frac{1}{2\mu_0} B^2. \tag{3.34}$$

The total current is $I = \tau h$, the self-inductance is

$$L = \frac{\Phi}{I} = \frac{\mu_0 (a + x) b}{h}. \tag{3.35}$$

Using the self-inductance, the magnetic energy is also expressed as

$$U_{\mathrm{m}} = \frac{1}{2} L I^2 = \frac{1}{2} \Phi I = \frac{1}{2L} \Phi^2. \tag{3.36}$$

The obtained (3.34) is analogous to the facts that the electrostatic energy density of the space with electric field E is given by

$$u_{\mathrm{e}} = \frac{1}{2} \epsilon_0 E^2, \tag{3.37}$$

and (3.36) corresponds also to the electrostatic energy of a capacitor with capacitance C when electric charge of $\pm Q$ is given under electric potential difference V:

$$U_{\mathrm{e}} = \frac{1}{2C} Q^2 = \frac{1}{2} VQ = \frac{1}{2} CV^2. \tag{3.38}$$

As shown in above, isolated current systems are realized for superconducting electric circuits. In addition, magnetic flux cannot penetrate a superconductor, and hence, the magnetic flux inside the circuit is preserved. As a result, the electromotive force does not appear. This is the reason why the magnetic energy can be directly derived from the magnetic force.

For the usual electric circuits, the magnetic energy cannot be derived from the magnetic force because of the electromagnetic induction. Hence, it is even possible to derive the electromagnetic induction law from the difference between a superconducting circuit and a non-superconducting circuit. Here we suppose that current I_1 flows in a straight line and current I_2 flows along a rectangular circuit with two sides parallel to the straight line, as shown in Fig. 3.15. These are placed on a common plane. The force on the rectangular circuit is calculated as

$$F = -\frac{\mu_0 I_1 I_2}{2\pi x} b + \frac{\mu_0 I_1 I_2}{2\pi (x + a)} b = -\frac{\mu_0 a b I_1 I_2}{2\pi x (x + a)}. \tag{3.39}$$

The force is negative, indicating an attractive force. Here the magnetic energy of this system is calculated. The self-inductance of the straight line, that of the rectangular

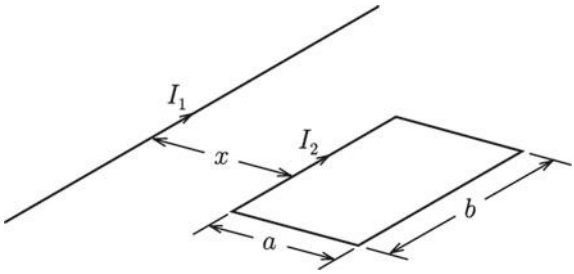

Fig. 3.15 Long straight line and rectangular circuit

circuit, and the mutual inductance between them are denoted by L_1, L_2 and M, respectively. Then, the magnetic energy of the system is given by

$$U_{\mathrm{m}} = \frac{1}{2}L_1{I_1}^2 + \frac{1}{2}L_2{I_2}^2 + MI_1I_2. \tag{3.40}$$

Since the first and second terms are independent of the distance between the two circuits, these can be disregarded. Only the third term depends on the distance x between them. Since the magnetic flux produced by current I_1 that penetrates the rectangular circuit is

$$\Phi = MI_1 = \frac{\mu_0 I_1 b}{2\pi}\int_x^{x+a}\frac{\mathrm{d}r}{r} = \frac{\mu_0 I_1 b}{2\pi}\log\frac{x+a}{x}, \tag{3.41}$$

the associated energy is

$$U_{\mathrm{m}} = \frac{\mu_0 b I_1 I_2}{2\pi}\log\frac{x+a}{x}. \tag{3.42}$$

Thus, the magnetic force seems to be

$$F = -\frac{\partial U_{\mathrm{m}}}{\partial x} = \frac{\mu_0 a b I_1 I_2}{2\pi x(x+a)}. \tag{3.43}$$

This disagrees with the force in (3.39) and means that the above procedure to calculate the magnetic force from the magnetic energy is problematic. The result of (3.43) indicates that the magnetic energy decreases by $-F\Delta x$ during the displacement of the rectangular circuit from x to $x + \Delta x$. The total magnetic energy, however, must additionally increase by $\Delta U_{\mathrm{m}} = 2F\Delta x$ to reach the correct result. From the reciprocity theorem, half of this energy increase is the increase in the magnetic energy of the rectangular circuit itself, which is expected to be caused by the induced electromotive force V in the circuit. If the circuit is displaced by Δx within time Δt, the work done by the induced electromotive force is $VI_2\Delta t$. This work can be rewritten as $-\Delta\Phi I_2$ in terms of the magnetic flux that penetrates the circuit,

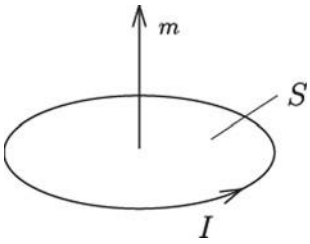

Fig. 3.16 Magnetic moment produced by closed current

$$\Delta\Phi = -\frac{\mu_0 abI_1}{2\pi x(x+a)}\Delta x. \tag{3.44}$$

Taking the limit of small Δt, we have

$$V = -\frac{\Delta\Phi}{\Delta t} \to -\frac{\mathrm{d}\Phi}{\mathrm{d}t}. \tag{3.45}$$

Thus, the principle of induced electromotive force can be derived.

(5) **Electric polarization and magnetic polarization**

One of the effects of the introduction of superconductivity is pointing out a problem for education in electromagnetism. This is associated with the magnetic moment. When closed current I flows as shown in Fig. 3.16, the magnetic moment is given by

$$m = IS, \tag{3.46}$$

where S is the area of the current loop. The closed current is equivalent to a virtual magnetic dipole and corresponds to an electric dipole in the electric phenomena. The magnetic moment in a unit volume is called the magnetization, which is used for superconductors and magnetic materials. In electromagnetism, however, the magnetization is defined by (2.44):

$$\boldsymbol{M} = \frac{\boldsymbol{B}}{\mu_0} - \boldsymbol{H}, \tag{3.47}$$

which describes the local relationship. This is not problematic for magnetic materials. On the other hand, the relationship,

$$\boldsymbol{B} = \mu_0 \boldsymbol{H}, \tag{3.48}$$

holds for the usual superconductors. Hence, if we use (3.47), $\boldsymbol{M} = 0$ is the result, and superconductors are classified as non-magnetic materials but not as diamagnetic

materials. This is caused by the fact that the magnetic moment is not produced by $\boldsymbol{M}$ but by $\boldsymbol{H}$. The magnetization of a superconductor is given by

$$M = \frac{\langle B \rangle}{\mu_0} - H_0, \tag{3.49}$$

when there is no influence of demagnetization caused by the shape, where $\langle B \rangle$ is the mean value of the magnetic flux density inside the superconductor and H_0 is the external magnetic field. The magnetization defined by (3.49) is not a local quantity, as defined in (3.47), but is a macroscopic quantity for each superconductor. This is also different from the mean value of (3.47). This description for the superconductor is attributed to the treatment by thermodynamics for long period, beginning after the discovery of superconductivity, in which the inner magnetic flux density $\langle B \rangle$ was discussed as an internal variable against the external variable H_0. This also means that the superconductor has not been treated in electromagnetism.

The analogous comparison in the electric phenomena is electrostatic shielding in a conductor and electric polarization in a dielectric material. These are similar shielding phenomena, although the shielding is imperfect in the dielectric material, while the shielding is perfect in the conductor. Both of these shielding phenomena are explained as due to relative movement of positive and negative electric charges under the applied electric field, although these phenomena have not been compared. The terms are also different, i.e., electrostatic shielding and electric polarization. For this reason, there was no confusion as in the magnetic phenomena. If we discuss these phenomena as in the magnetization, however, we have $\boldsymbol{P} = 0$ in a conductor, assuming the relationship of $\boldsymbol{D} = \epsilon_0 \boldsymbol{E}$. On the other hand, it is true that the electric dipole moment in the conductor is not zero under the condition of electrostatic shielding. Thus, a similar contradiction appears in electric phenomena.

When we look back at the magnetization, it makes a difference whether the source of the magnetic moment is a real current that produces $\boldsymbol{H}$ or a virtual magnetization current that produces $\boldsymbol{M}$. In addition, the magnetization in a superconductor and that in a magnetic material are also different from the viewpoint of shielding. Nevertheless, the same term is used for these phenomena. For this reason, some scientists have believed that the magnetization in a superconductor can be described either by $\boldsymbol{H}$ or by $\boldsymbol{M}$. From the consideration of a hollow superconductor, as in Fig. 3.11, however, it is clear which is correct.

As shown above, the scientific description of magnetization is not complete. The introduction of superconductivity has clarified this lack of completeness. The complete description cannot be implemented by the author alone, since the agreement of society is required. Here, the author wishes to propose the following: Since the term "magnetization" has been used for magnetic materials for long time, this term may continue to be used for these materials. Then, we need to use another term for superconductors. The first proposal is to use "magnetic moment density", which follows from the original definition of magnetization, i.e., the magnetic moment in a unit volume. In addition, from the basic viewpoint of the $\boldsymbol{E}$-$\boldsymbol{B}$ analogy, it is desirable

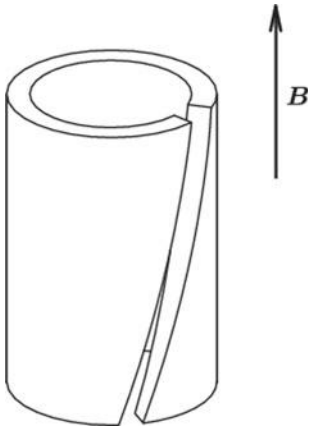

Fig. 3.17 Long superconducting hollow cylinder with tilted slit

to define a new term for the electric polarization in a conductor, which is analogous to the electric polarization in a dielectric material. The second proposal is to use "electric dipole moment density" for this term.

We have shown that the introduction of superconductivity into electromagnetism brings about a deep correspondence between electric and magnetic phenomena in the present ***E*-*B*** analogy, which will be effective for education. In other words, if superconductivity is not introduced, the ***E*-*B*** analogy seems to be quite insufficient.

Coffee break (3)

Penetration of magnetic flux into a superconducting hollow cylinder with a tilted slit

Magnetic flux cannot penetrate a superconductor. Suppose that a magnetic field is applied to a superconducting hollow cylinder with a tilted slot, as shown in Fig. 3.17. Does the magnetic flux, which is not parallel to the slit, penetrate into the interior of the hollow superconductor?

If the magnetic flux tends to penetrate straight into the interior, it may cross the superconductor. This suggests that the magnetic flux cannot penetrate the superconductor. Is this true?

Remember here that a superposition holds for the magnetic flux density. When the magnetic field is applied, a shielding current flows on the superconductor surface to stop the magnetic flux penetration, as shown in Fig. 3.18b. This current is realized by the sum of the shielding current on the inner and outer surfaces of a virtual hollow superconductor with no slit, as shown in Fig. 3.18b, and the current flowing in the opposite direction only in the region of the slit, as shown in Fig. 3.18c. The external magnetic field and the current in Fig. 3.18b shields the virtual hollow superconductor completely but produces a magnetic field of the same strength as the external field in the interior. In the region of the slit, these currents do not produce the magnetic field, but the current in Fig. 3.18c produces the magnetic field. The resultant magnetic flux

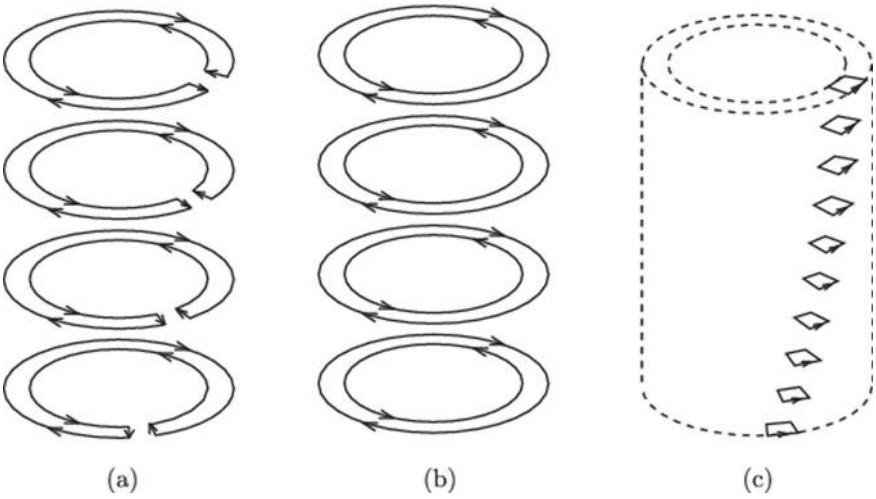

Fig. 3.18 **a** Current on the superconductor surface, **b** current on the surface of a virtual superconductor with no slit, and **c** current in the opposite direction in the slit region. The current in **a** is obtained by superimposing those in **b** and **c**

is tilted to fit the slit. This means that the magnetic flux is tilted when it penetrates into the interior.

Reference

1. T. Matsushita, *Electricity and Magnetism—New Formulation by Introduction of Superconductivity* (Springer, 2014, Tokyo)

Chapter 4
Fundamental Electromagnetic Properties of Superconductors

Abstract In this chapter fundamental properties such as quantization of magnetic flux, the normal core in the central region in each packet of quantized magnetic flux, and the induced electric field under the motion of quantized magnetic flux driven by the Lorentz force are described by using the Ginzburg–Landau theory. These are important for understanding the electromagnetic characteristics of superconductors that will be introduced in Chap. 5. Reference [1] covers a wide area of the material in this chapter.

4.1 Type II Superconductor

Superconductors used as materials for magnets are type II superconductors. Magnetic properties of type I and type II superconductors are compared in Fig. 4.1. A type I superconductor shows perfect diamagnetism until the external magnetic field H_0 reaches a certain value, H_c, as shown in Fig. 4.1a, and the magnetization (magnetic moment density) defined by (3.49) is

$$M = -H_0. \tag{4.1}$$

This state is called the Meissner state. At a higher field the superconductor changes to the normal state and the magnetization is $M = 0$. The magnetic field H_c at which the transition takes place is called the critical field. On the other hand, a type II superconductor shows the Meissner state until the external magnetic field reaches H_{c1} and changes to a partially diamagnetic state with penetration of the magnetic flux above this field. This state is called the mixed state. When the external field exceeds H_{c2}, the superconductor goes into the normal state, and $M = 0$. These characteristic fields, H_{c1} and H_{c2}, are called the lower and upper critical fields, respectively. The magnetic flux in the superconductor is quantized as shown in Fig. 4.2 in the mixed state. The quantized packet of magnetic flux is called the magnetic flux line. When the magnetization is expresses as a property of the equivalent type I superconductor with the same area, as shown in Fig. 4.1b, H_c is called the thermodynamic critical field. The phase diagrams on the temperature vs magnetic field plane for type I and type II superconductors are shown in Fig. 4.3a, b, respectively.

T. Matsushita, *Superconductivity and Electromagnetism*, Springer Series in Solid-State Sciences 195, https://doi.org/10.1007/978-3-030-67568-4_4

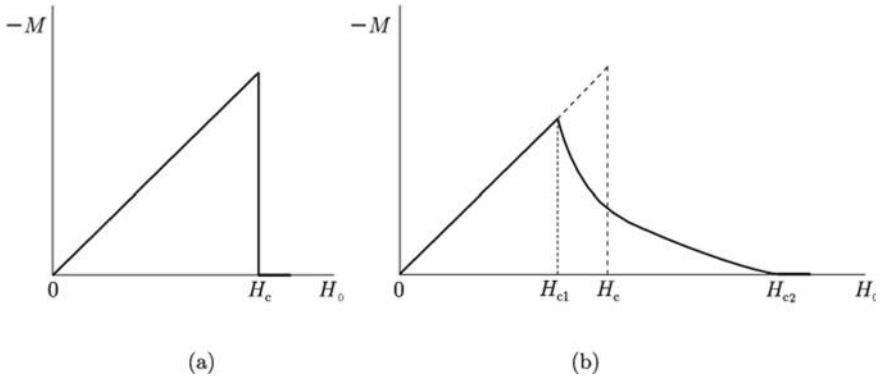

Fig. 4.1 Magnetization of **a** type I and **b** type II superconductors. The broken line in **b** shows the behavior of an equivalent type I superconductor, and H_c is the thermodynamic critical field

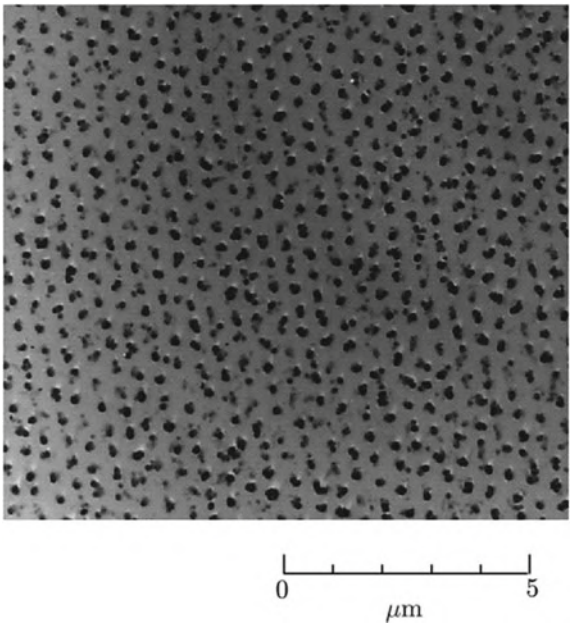

Fig. 4.2 Magnetic flux line lattice in Pb-1.6wt%Tl formed by applying 35 mT above the critical temperature and then cooling down to 1.2 K (Courtesy of Dr. B. Obst)

The magnitude of H_c is roughly proportional to the critical temperature T_c for all superconductors, and hence, it does not change very widely. On the other hand, H_{c2} of a type II superconductor can take on a large value. In particular, H_{c2} of practical superconductors is very large, and this is an advantageous property for applications. The critical temperature and critical fields of various superconductors are listed in Table 4.1.

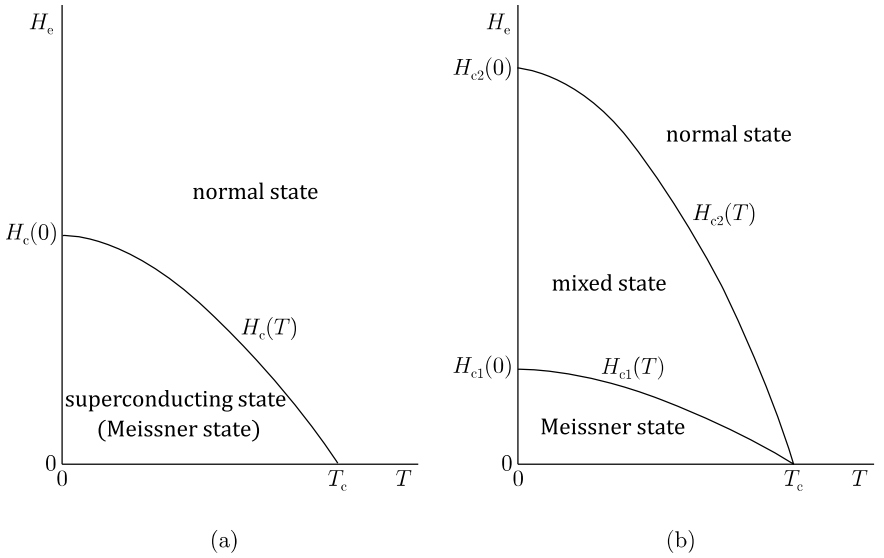

Fig. 4.3 Phase diagrams of **a** type I and **b** type II superconductors

4.2 Ginzburg–Landau Theory

(1) Ginzburg–Landau equations

The magnetic properties of type II superconductors are well described by the Ginzburg-Landau theory. The main points are introduced here. In the beginning, the density of superconducting electrons is defined and assumed to be given by $|\Psi|^2$, where Ψ is a complex quantity called the order parameter. Since the free energy in the superconductor depends on the density of superconducting electrons, the free energy is assumed to be given by a function of a power series of $|\Psi|^2$. The momentum is given by a spatial variation of Ψ in a similar manner to the wave function in quantum mechanics, and the kinetic energy is proportional to the square of the momentum. With this energy and the magnetic energy, the Helmholtz free energy density is given by

$$\mathcal{F}_s(B) = \mathcal{F}_n(0) + \alpha|\Psi|^2 + \frac{1}{2}\beta|\Psi|^4 + \frac{1}{2\mu_0}(\nabla \times \boldsymbol{A})^2 + \frac{1}{2m^*}|(-i\hbar\nabla + 2e\boldsymbol{A})\Psi|^2, \tag{4.2}$$

which is called the Ginzburg-Landau free energy density, where α and β are parameters, $\boldsymbol{A}$ is the vector potential, m^* and $-2e$ are the mass and electric charge of a superconducting electron, respectively, and $\hbar$ is Planck's constant, h_P, divided by 2π. $\mathcal{F}_n(0)$ is the free energy density in the normal state in zero field ($B = 0$) and the

Table. 4.1 Critical temperatures and critical fields at 0 K for various superconductors. In some superconductors $H_{c1}(0)$ cannot be measured because of the influence of flux pinning, and/or the value of $H_{c2}(0)$ is different depending on the direction of the magnetic field due to anisotropy

Type	Superconductor	T_c (K)	$\mu_0 H_c(0)$ (mT)	$\mu_0 H_{c1}(0)$ (mT)	$\mu_0 H_{c2}(0)$ (T)
I	Hg(α)	4.15	41		
	In	3.41	28		
	Pb	7.20	80		
	Ta	4.47	83		
II	Nb	9.25	199	174	0.404
	$Nb_{37}Ti_{63}$	9.08	253		15
	Nb_3Sn	18.3	530		29
	Nb_3Al	18.6			33
	$PbMo_6S_8$	15.3			60
	MgB_2	39			
	$SmFeAsO_{1-x}F_x$	57.5			
	$YBa_2Cu_3O_{7-\delta}$	93			
	$(Bi,Pb)_2Sr_2Ca_2Cu_3O_x$	115			
	$HgBa_2Ca_2Cu_3O_x$	138	820		

fourth and fifth terms are the magnetic and kinetic energies, respectively. The order parameter, Ψ, and the vector potential, $\boldsymbol{A}$, are determined in such conditions that the energy density is minimized with respect to these quantities. These conditions are respectively given by

$$\frac{1}{2m^*}(-\mathrm{i}\hbar\nabla + 2e\boldsymbol{A})^2\Psi + \alpha\Psi + \beta|\Psi|^2\Psi = 0, \tag{4.3}$$

$$\boldsymbol{i} = \frac{1}{\mu_0}\nabla \times \nabla \times \boldsymbol{A} = \frac{i\hbar e}{m^*}\left(\Psi^*\nabla\Psi - \Psi\nabla\Psi^*\right) - \frac{4e^2}{m^*}|\Psi|^2\boldsymbol{A}, \tag{4.4}$$

where $\boldsymbol{i}$ is the superconducting current density (see Appendix A.1). These equations are called the Ginzburg-Landau (GL) equations.

(2) **Transition at $\boldsymbol{T = T_c}$**

Here, we treat the transition at $T = T_c$ in the absence of magnetic field. We can assume that $\boldsymbol{A} = 0$. Spatial variation in Ψ can be disregarded, and (4.2) leads to

$$\mathcal{F}_s(0) = \mathcal{F}_n(0) + \alpha|\Psi|^2 + \frac{1}{2}\beta|\Psi|^4. \tag{4.5}$$

When this is minimized with respect to Ψ, the condition $\partial\mathcal{F}_s/\partial|\Psi|^2 = 0$ leads to

$$|\Psi|^2 = -\frac{\alpha}{\beta} \equiv |\Psi_\infty|^2, \tag{4.6}$$

where Ψ_∞ is the equilibrium value of Ψ. The parameter α should depend on the temperature as

$$\alpha \propto T_c - T, \tag{4.7}$$

and the condition $\partial^2\mathcal{F}_s(0)/\partial\left(|\Psi|^2\right)^2 = \beta > 0$ should be satisfied, so that the superconducting state is stable at temperatures below T_c. The free energy density in this case is:

$$\mathcal{F}_s(0) = \mathcal{F}_n(0) - \frac{\alpha^2}{2\beta}, \tag{4.8}$$

which indicates that the free energy is lower in the superconducting state. At temperatures above T_c, the state of (4.6) can no longer be realized, but the normal state of $\Psi = 0$ with a lower energy is the result. Thus, the transition to the normal state at $T = T_c$ is explained, as shown in Fig. 4.4.

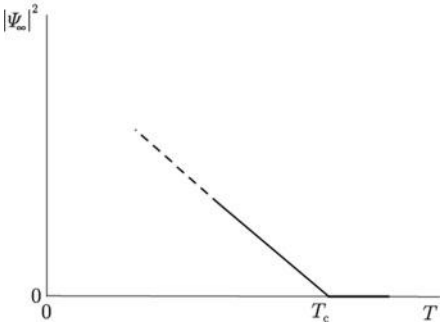

Fig. 4.4 Temperature dependence of the superconducting electron density in the equilibrium state. It changes from the value given by (4.6) to the value $|\Psi_\infty|^2 = 0$ in the normal state at $T = T_c$

(3) **Transition in magnetic field**

Here, we discuss the transition in magnetic field. It is necessary to treat the Gibbs free energy density for this purpose. The magnetic flux density in the superconductor in the external magnetic field H_0 is denoted by B. Using the Helmholtz free energy density, the Gibbs free energy density is given by

$$\mathcal{G}_s(H_0) = \mathcal{F}_s(B) - BH_0. \tag{4.9}$$

In the superconducting state the magnetic flux density is zero ($B = 0$) and the first term is given by (4.8). Thus, we have

$$\mathcal{G}_s(H_0) = \mathcal{F}_n(0) - \frac{\alpha^2}{2\beta}. \tag{4.10}$$

In the normal state, substitution of $|\Psi|^2 = 0$ and $B = \mu_0 H_0$ leads to

$$\mathcal{G}_n(H_0) = \mathcal{F}_n(0) + \frac{B^2}{2\mu_0} - BH_0 = \mathcal{F}_n(0) - \frac{1}{2}\mu_0 {H_0}^2. \tag{4.11}$$

Since $\mathcal{G}_s$ and $\mathcal{G}_n$ are equal to each other at the transition field $H_0 = H_c$, we have

$$\frac{\alpha^2}{\beta} = \mu_0 {H_c}^2. \tag{4.12}$$

From (4.10)—(4.12) the Gibbs free energy density is given by

$$\mathcal{G}_s(H_0) = \mathcal{G}_n(H_0) - \frac{1}{2}\mu_0\left({H_c}^2 - {H_0}^2\right). \tag{4.13}$$

Equation (4.13) explains that the superconducting and normal states are derived at $H_0 < H_c$ and $H_0 > H_c$, respectively. In particular (4.14) leads to

$$\mathcal{G}_s(0) = \mathcal{G}_n(0) - \frac{1}{2}\mu_0 {H_c}^2. \tag{4.14}$$

The maximum difference in the energy density $(1/2)\mu_0 {H_c}^2$ is called the condensation energy density.

(4) **Meissner state**

Here, the Meissner state is treated. The magnetic field penetrates only in the vicinity of the surface, while the magnetic flux density is zero and the order parameter has the equilibrium value Ψ_∞ in most regions of the superconductor. Thus, the spatial variation in the order parameter can be safely neglected, and (4.4) leads to

$$\boldsymbol{i} = -\frac{4e^2}{m^*}|\Psi_\infty|^2 \boldsymbol{A}. \tag{4.15}$$

The rotation of this equation leads to

$$\nabla \times \nabla \times \boldsymbol{B} = -\frac{1}{\lambda^2}\boldsymbol{B}, \tag{4.16}$$

where λ is the penetration depth given by

$$\lambda = \left(\frac{m^*}{4\mu_0 e^2 |\Psi_\infty|^2}\right)^{1/2}. \tag{4.17}$$

Equation (4.16) is called the London equation. Here, it is shown that this equation describes the Meissner state. Assume that we apply external magnetic field H_0 along the z–axis to a semi-infinite superconductor that occupies $x \geq 0$. The inner magnetic flux density also has the z–component and depends only on x, the distance from the surface. Then, we have $\nabla \times \boldsymbol{B} = -(\partial B_z/\partial x)\boldsymbol{i}_y$, and (4.16) leads to

$$\frac{\partial^2 B_z}{\partial x^2} = \frac{1}{\lambda^2} B_z. \tag{4.18}$$

This equation can be easily solved. Under the conditions of $B_z(0) = \mu_0 H_0$ and a finite value at $x \to \infty$, we have

$$B_z(x) = \mu_0 H_0 \exp\left(-\frac{x}{\lambda}\right). \tag{4.19}$$

Thus, the magnetic flux penetrates only up to the distance λ from the surface, as shown in Fig. 4.5. This is the reason why λ is called the penetration depth. Since λ is usually smaller than 100 nm, the inner magnetic flux can be neglected for a superconductor of usual size, and hence, the Meissner state can be explained.

(5) **Quantization of magnetic flux**

It is shown here that the magnetic flux inside the superconductor is quantized. It is expected that the magnetic flux has a high density at the center and is extended up

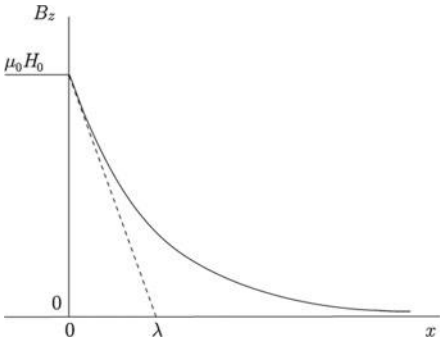

Fig. 4.5 The magnetic flux density in the superconductor given by (4.19)

to the distance of about λ from the center. Here we assume an isolated flux line and suppose circle C of a sufficiently large radius with the center at the flux line on a plane perpendicular to the flux line. The order parameter is expressed as $\Psi = |\Psi|\exp(\mathrm{i}\varphi)$. Then, (4.4) is rewritten as

$$\boldsymbol{i} = -\frac{2\hbar e}{m^*}|\Psi|^2\nabla\varphi - \frac{4e^2}{m^*}|\Psi|^2\boldsymbol{A}. \tag{4.20}$$

We can safely assume $\boldsymbol{i} = 0$ on C, because $\boldsymbol{B} = 0$ there. Since $|\Psi|^2$ is not zero on C, we have

$$\boldsymbol{A} = -\frac{\hbar}{2e}\nabla\varphi. \tag{4.21}$$

Integrating this on C leads to the magnetic flux surrounded by C:

$$\Phi = \int_{\mathrm{S}} \nabla\times\boldsymbol{A}\cdot\mathrm{d}\boldsymbol{S} = \oint_{\mathrm{C}} \boldsymbol{A}\cdot\mathrm{d}\boldsymbol{s} = -\frac{\hbar}{2e}\oint_{\mathrm{C}} \nabla\varphi\cdot\mathrm{d}\boldsymbol{s} = -\frac{\hbar}{2e}\Delta\varphi, \tag{4.22}$$

where S is the region surrounded by C and $\Delta\varphi$ is the increase in the phase after one circulation, based on Stokes' theorem. We should note that the curvilinear integral of a gradient of a scalar function on a closed loop is usually zero. There are two exceptions: One of them is the case where space S is not simply connected. That is, some closed loop cannot shrink to a point inside the space. A superconducting ring is an example of this case. The other is the case where singular points exist inside loop C. The present situation belongs to the latter case. The singular point will be discussed later and we will proceed to discuss the quantization of magnetic flux. From the requirement that the order parameter is a single-valued function, $\Delta\varphi$ in (4.22) must be an integral multiple of 2π. In the present case this value is -2π. That is,

$$\Phi = \phi_0, \tag{4.23}$$

where ϕ_0 is the magnetic flux quantum, i.e., the unit of the magnetic flux given by

$$\phi_0 = \frac{h_\mathrm{P}}{2e} = 2.0678 \times 10^{-15}\ \mathrm{Wb}. \tag{4.24}$$

When n flux lines exist inside C, the total magnetic flux is $n\phi_0$. Thus, it can be shown that the magnetic flux is quantized inside superconductor.

Here, we investigate the structure of the central area of a quantized magnetic flux line. Using cylindrical coordinates, the curvilinear integral of $\nabla\varphi$ in (4.22) on loop C is

$$\oint_\mathrm{C} \nabla\varphi \cdot \mathrm{d}\boldsymbol{s} = \oint_\mathrm{C} \frac{\partial\varphi}{\partial\theta}\mathrm{d}\theta, \tag{4.25}$$

where θ is the azimuthal angle. The solution for φ that results in the integral being equal to -2π is

$$\varphi = -\theta. \tag{4.26}$$

Hence, we have

$$\nabla\varphi = -\frac{1}{r}\boldsymbol{i}_\theta, \tag{4.27}$$

with $\boldsymbol{i}_\theta$ denoting the azimuthal unit vector. The magnitude of this quantity diverges at the center of the quantized magnetic flux ($r = 0$). Thus, the center is a singular point. This is the reason why the curvilinear integral of this quantity on a closed loop is not zero.

Another important feature is derived from this singularity. The first term of the superconducting current density in (4.20) is proportional to $\nabla\varphi$. Therefore, $|\Psi|$ must be zero at the center of the flux line, so as to prevent the current density from diverging to infinity. It is indeed derived from a detailed analysis that $|\Psi| \propto r$ around the center. Thus, the central area in each quantized magnetic flux packet is in the normal state.

(6) **Coherence length**

The characteristic length of the spatial variation in the magnetic field is the penetration depth given by (4.17). Here we discuss the characteristic length of the spatial variation in the order parameter. For simplicity, we treat the case where magnetic field is not applied. Hence, we can assume $\boldsymbol{A} = 0$. In addition, we assume that Ψ varies only along the x-axis. Using the normalized order parameter $\psi = \Psi/|\Psi_\infty|$, (4.3) is written as

$$\xi^2 \frac{\mathrm{d}^2\psi}{\mathrm{d}x^2} + \psi - |\psi|^2\psi = 0, \tag{4.28}$$

where ξ is the coherence length given by

$$\xi = \frac{\hbar}{(2m^*|\alpha|)^{1/2}} = \frac{\hbar}{2\sqrt{2}e\mu_0 H_c \lambda}. \tag{4.29}$$

We can chose a real number for ψ. Since the magnetic field is not applied, ψ is close to 1. Hence, if we put as $\psi = 1 - f$, f is much smaller than 1. Thus, (4.28) is reduced to

$$\xi^2 \frac{\mathrm{d}^2 f}{\mathrm{d}x^2} - 2f = 0. \tag{4.30}$$

The solution of this equation is given by

$$f = f_0 \exp\left(-\frac{\sqrt{2}|x|}{\xi}\right). \tag{4.31}$$

This shows that ξ is the characteristic length of the spatial variation in the order parameter.

The spatial variation in the order parameter around the center of a quantized magnetic flux packet is also given by ξ. The structure of the central region of the quantized magnetic flux in type II superconductors is shown in Fig. 4.6. The region of radius ξ around the center of the quantized magnetic flux is called the normal core. The coherence length in the Ginzburg–Landau theory given by (4.29) increases with increasing temperature, because $|\alpha|$ varies in proportion to $1 - T/T_c$. This is different from the coherence length ξ_0 in the Bardeen-Cooper-Schrieffer (BCS) theory, which

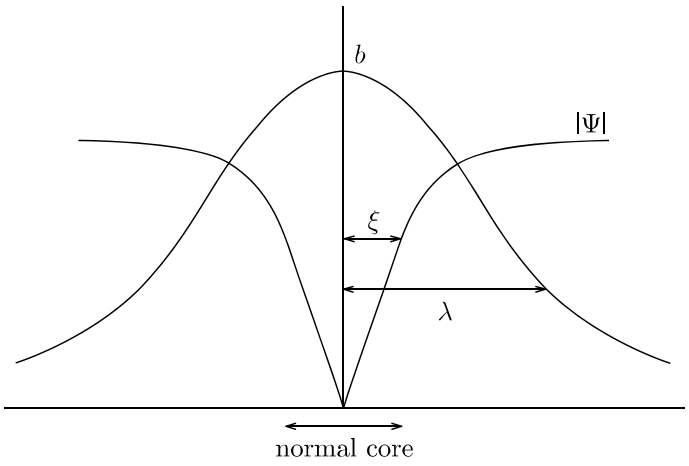

Fig. 4.6 Spatial structure of the order parameter and magnetic flux density in the central region of an isolated quantized magnetic flux packet

is independent of the temperature. For clean superconductors, however, ξ and ξ_0 are roughly the same at low temperatures. If the number density of scattering centers for electrons such as impurities increases, the electron mean free path, l, decreases, which results in a decrease in the coherence length as $(\xi_0 l)^{1/2}$. ξ_0 does not change with l in this case either.

(7) **Upper critical field and type II superconductor**

In the vicinity of the upper critical field the distance between flux lines decreases, and hence, the magnetic flux overlaps, resulting in an almost uniform magnetic flux density. Hence, we can assume that $B \cong \mu_0 H_0$ around the transition to the normal state. The order parameter has a small value and the term proportional to $|\Psi|^4$ can be safely neglected in the free energy density given by (4.2). Rewriting the kinetic energy density, the Ginzburg–Landau free energy density is expressed as (see Appendix A.2)

$$\langle \mathcal{F}_s(B) \rangle = \mathcal{F}_n(0) + \mu_0 {H_c}^2 \langle -|\psi|^2 + 2\xi^2 (\nabla |\psi|)^2 \rangle + \frac{1}{2} \mu_0 {H_0}^2. \tag{4.32}$$

Here, $\langle\rangle$ represents a spatial average. The Gibbs free energy density in the superconducting state is given by

$$\langle \mathcal{G}_s(B) \rangle = \mathcal{F}_n(0) + \mu_0 {H_c}^2 \langle -|\psi|^2 + 2\xi^2 (\nabla |\psi|)^2 \rangle - \frac{1}{2} \mu_0 {H_0}^2. \tag{4.33}$$

On the other hand, the Gibbs free energy density in the normal state is

$$\langle \mathcal{G}_n(B) \rangle = \mathcal{F}_n(0) - \frac{1}{2} \mu_0 {H_0}^2. \tag{4.34}$$

Hence, the transition to the normal state occurs at the magnetic field at which the spatial variation in the second term in (4.33) is zero. That is, the upper critical field is the magnetic field at which the increase in the kinetic energy consumes the condensation energy. Abrikosov determined the upper critical field as the maximum value of the magnetic field at which (4.3), with neglect of the higher order term of Ψ, has a solution. This theoretical treatment leads to the same result as the above treatment using the Gibbs free energy density, although the latter process is essential from the viewpoint of thermodynamics. According to the result Abrikosov obtained, the upper critical field is given by

$$H_{c2} = \frac{4e\mu_0 {H_c}^2 \lambda^2}{\hbar}. \tag{4.35}$$

The ratio of the two characteristic lengths

$$\kappa = \frac{\lambda}{\xi} \tag{4.36}$$

is called the Ginzburg-Landau parameter. κ is almost independent of temperature. We have $|\Psi_\infty|^2 = \mu_0 {H_c}^2/|\alpha|$ using (4.6) and (4.12). Then, (4.17) is rewritten as $\lambda = (m^*|\alpha|)^{1/2}/(2e\mu_0 H_c)$. Eliminating $(m^*|\alpha|)^{1/2}$ in the expression of ξ in terms of λ, we have

$$\kappa = \frac{2\sqrt{2}e\mu_0 H_c \lambda^2}{\hbar}. \tag{4.37}$$

Then, (4.35) is reduced to

$$H_{c2} = \sqrt{2}\kappa H_c. \tag{4.38}$$

A type II superconductor is a superconductor with H_{c2} higher than H_c, i.e., with κ higher than $1/\sqrt{2}$. It is required that superconducting current can flow around the center in a region of about λ from the center so as to keep the structure of the quantized magnetic flux stable, as shown in Fig. 4.5. That is, superconducting electrons of sufficient density must exist in this region. This also shows that the condition that λ is larger than ξ is needed for type II superconductors.

Eliminating $(m^*|\alpha|)^{1/2}$ in λ by using ξ, (4.35) is written as

$$H_{c2} = \frac{\hbar}{2e\mu_0 \xi^2} = \frac{\phi_0}{2\pi\mu_0 \xi^2}. \tag{4.39}$$

This formula is used to estimate the coherence length using the observed upper critical field.

The lower critical field of a type II superconductor is also expressed using H_c and κ as

$$H_{c1} = \frac{H_c}{\sqrt{2}\kappa}(\log\kappa + 0.081). \tag{4.40}$$

4.3 Flux Flow State

In this section the case is treated where the flux lines with density $\boldsymbol{B}$ flow with velocity $\boldsymbol{v}$ under the Lorentz force. In this situation a macroscopic electric field of strength

$$\boldsymbol{E} = \boldsymbol{B} \times \boldsymbol{v} \tag{4.41}$$

is induced. This equation is called Josephson's formula. This can be expected from (2.52) for the general case. That is, when a substance moves with velocity $\boldsymbol{V}$ in a space of uniform magnetic flux density, it is equivalent to the situation where flux

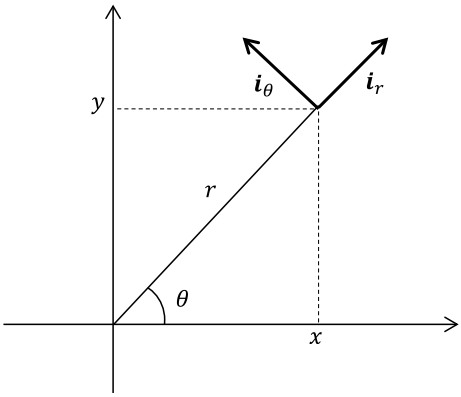

Fig. 4.7 Cylindrical coordinates with the origin on the center of the moving magnetic flux line

lines move with velocity $-\boldsymbol{V}$ in the substance. On substituting $\boldsymbol{V} = -\boldsymbol{v}$ into (2.52), we have (4.41).

Here we investigate the phenomenon microscopically. The essential point is roughly explained following the Bardeen-Stephen model [2]. It is assumed that the spacing between flux lines is sufficiently large that overlap of the magnetic flux of each flux line can be neglected. Thus, we treat an isolated flux line. The local model is applied that assumes a simplified structure of the flux line with the core of radius ξ in the fully normal state. The two dimensional cylindrical coordinates are defined with the origin on the center of the flux line and the azimuthal angle θ is defined measured from the x-axis along which the flux line is driven. When a screw is rotated to increase θ, it points along the direction of the magnetic flux (see Fig. 4.7). From the equation of motion of a superconducting electron on the outside of the normal core ($r > \xi$), the local electric field on the electron can be derived as (see Appendix A.3)

$$\boldsymbol{e} = \frac{\phi_0 v}{2\pi r^2}(\boldsymbol{i}_\theta \cos\theta - \boldsymbol{i}_r \sin\theta) + \frac{1}{2}(\boldsymbol{B} \times \boldsymbol{v}), \tag{4.42}$$

where $\boldsymbol{i}_\theta$ and $\boldsymbol{i}_r$ are azimuthal and radial unit vectors, respectively. On the other hand, the local electric field inside the normal core ($r < \xi$) is obtained as

$$\boldsymbol{e} = \frac{\phi_0 v}{2\pi \xi^2}\boldsymbol{i}_y + \frac{1}{2}(\boldsymbol{B} \times \boldsymbol{v}) \tag{4.43}$$

from the condition that the tangential component of the electric field should be continuous on the boundary $r = \xi$. Here $\boldsymbol{i}_y$ is the unit vector along the y-axis. The spatial average of the electric field gives (4.41). Hence, there is no contradiction with the macroscopic description. Exactly speaking, the first term is reduced to 0, and the sum of the second terms of (4.42) and (4.43) results in $(1/2)(\boldsymbol{B} \times \boldsymbol{v})$. We used the condition that the area for the average is equal to B/ϕ_0. The condition of

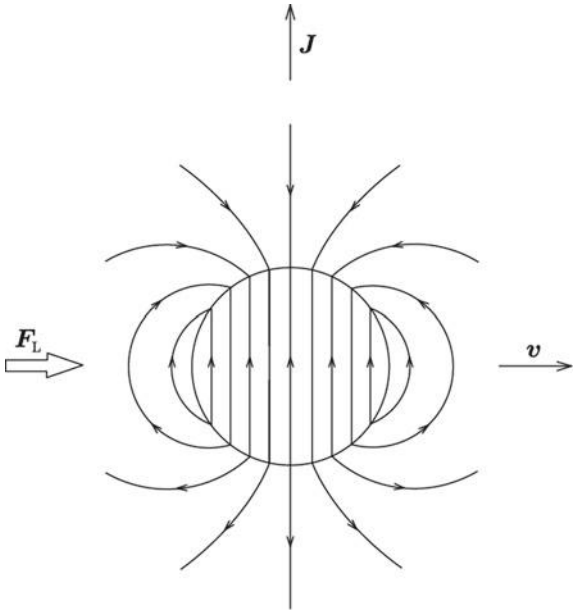

Fig. 4.8 Nonuniform component of the electric field inside and outside the normal core

the nonuniform component of the electric field, which is given by the first terms of (4.42) and (4.43), is shown in Fig. 4.8.

Here we estimate the macroscopic power loss density due to the obtained electric field. The power loss density is averaged over a space sufficiently larger than λ or the flux line spacing and can be regarded as a quantity that varies gradually in space. Most of the power loss is caused by the intensified electric field inside the normal core, i.e., the first term in (4.43). The power loss in a unit length of flux line is given by

$$P' = \pi\xi^2 \frac{\boldsymbol{e}^2}{\rho_\mathrm{n}} = \frac{\phi_0^2 v^2}{4\pi\xi^2\rho_\mathrm{n}}, \tag{4.44}$$

where ρ_n is the normal resistivity. Equation (4.44) gives the power loss under the macroscopic electric field of (4.41). Since the power loss is expressed as

$$P' = \frac{\phi_0}{B} \cdot \frac{E^2}{\rho_\mathrm{f}} \tag{4.45}$$

in terms of the effective resistivity ρ_f in the flux flow state, we have

$$\rho_\mathrm{f} = \frac{B}{\mu_0 H_{c2}} \rho_\mathrm{n}, \tag{4.46}$$

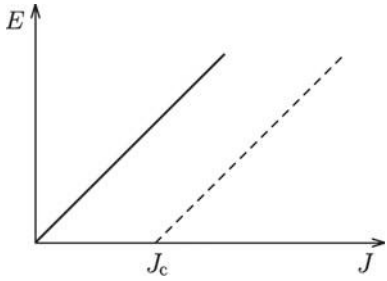

Fig. 4.9 *E-J* characteristics in the flux flow state. The solid and broken lines correspond to the cases without and with the pinning interaction

where (4.39) is used. This is called the flux flow resistivity. This relationship shows that energy dissipation similar to that in the normal state takes place in the normal cores, which occupy approximately the area fraction $(B/\mu_0 H_{c2})$.

Here, we treat the macroscopic current–voltage characteristics in the flux flow state. The macroscopic current density is denoted by J. The corresponding *E-J* characteristics are expressed as

$$E = \rho_f J, \tag{4.47}$$

which is similar to Ohm's law, as shown in Fig. 4.9. The flux lines are driven into motion when the Lorentz force exceeds the pinning force in practical cases. That is, the flux flow occurs when a current with a density higher than the critical current density, J_c, is applied. The *E-J* characteristics are given by

$$E = \rho_f (J - J_c), \tag{4.48}$$

as shown by the broken line in Fig. 4.9.

Coffee break (4).

Quantization of magnetic flux

Assume that an isolated flux line exists inside a superconductor. We estimate the magnetic flux inside the area shown in Fig. 4.10a. The surface integral of the magnetic flux density is given by the curvilinear integral of the vector potential as shown by (4.22). In the present case this is written as

$$\Phi = \int_R \boldsymbol{A} \cdot \mathrm{d}\boldsymbol{s} + \int_L \boldsymbol{A} \cdot \mathrm{d}\boldsymbol{s},$$

where R is the half circle and L is the straight line through the center of the flux line. The radius of the half circle is assumed to be sufficiently large and we can consider that the magnetic flux density and current density are zero on the half circle. Thus, the first term is the curvilinear integral of $-(\hbar/2e)\nabla\varphi$. The second term is given by the sum of the curvilinear integrals of $-(\hbar/2e)\nabla\varphi$ and $-(m^*/4e^2|\Psi|^2)\boldsymbol{i}$. From the

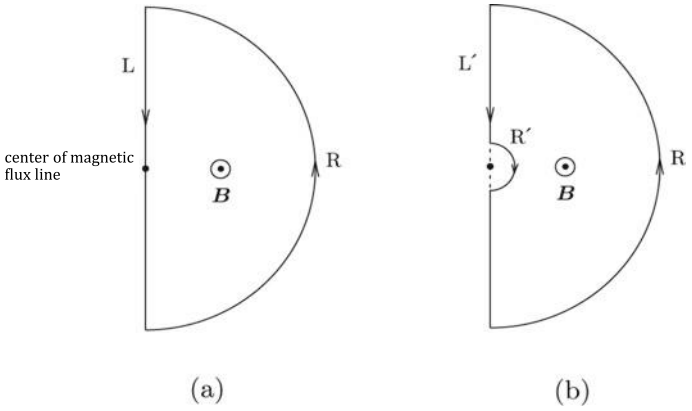

Fig. 4.10 **a** Closed loop composed of straight line L and half circle R sufficiently far from the center of the magnetic flux line, and **b** closed loop that does not pass through the center. The radius of the half circle R′ is r

cylindrical symmetry, $\boldsymbol{i}$ and d$\boldsymbol{s}$ are perpendicular to each other, and the curvilinear integral of the latter quantity is zero. Thus, the magnetic flux is given by the curvilinear integral of $-(\hbar/2e)\nabla\varphi$ on the closed loop. As a consequence, it is concluded that the total magnetic flux in this area is equal to ϕ_0, because of the requirement of a single-value function for the order parameter Ψ. This conclusion is wrong. What is the problem?

The wrong result is brought about by neglect of the fact that $\nabla\varphi$ is singular at the center of the quantized magnetic flux on the integral path. Here, we change slightly the integral path for the second integral to deviate from the singular point, as illustrated in Fig. 4.10b. Assume a half circle R′ with sufficiently small radius r. The second curvilinear integral on the new closed loop is the sum of the curvilinear integral of $-(\hbar/2e)\nabla\varphi$ and that of $-(m^*/4e^2|\Psi|^2)\boldsymbol{i}$. The former integral is zero since there is no singular point inside the closed loop. The second integral is zero on the loop except for the half circle R′, since $\boldsymbol{i} = 0$ on the half circle R, and $\boldsymbol{i}$ and d$\boldsymbol{s}$ are perpendicular to each other on the straight part of the path L′. The remaining integral on R′ is rewritten as the sum of the integral of $(\hbar/2e)\nabla\varphi$ and that of $\boldsymbol{A}$. The latter integral is equal to the magnetic flux of negative value in the area surrounded by R′ and the straight section. This magnetic flux can be neglected by reducing r to an infinitesimal. From (4.27) the latter integral leads to

$$-\frac{\hbar}{2e}\int_{\pi}^{0}\frac{1}{r}r\mathrm{d}\theta = \frac{h}{4e} = \frac{\phi_0}{2}.$$

Hence, the magnetic flux in the closed loop in Fig. 4.10a is given by $\Phi = \phi_0/2$. This agrees with the intuitive answer.

The same result should be obtained, if we choose an integral path so that the singular point is included inside the closed loop. Derive the correct result in this case.

References

1. T. Matsushita, *Flux Pinning in Superconductors*, 2 edn. (Springer, 2014), p. 26 (Chaps. 1 and 2).
2. J. Bardeen, M.J. Stephen, Phys. Rev. **140**, A1197 (1965).

Chapter 5
Flux Pinning Phenomena

Abstract The main advantage of superconductors, that these materials can transport electric current without energy dissipation, is achieved by the mechanism of flux pinning. Quantized flux lines that contain superconducting structure inside do not move under interaction with defects in the superconductor, even when the Lorentz force is present due to the current. As a consequence, no electromotive force appears, resulting in no energy dissipation. The mechanism of flux pinning is, in principle, reversible with respect to the motion of flux lines. The observed results are commonly irreversible, however, as described by the critical state model, which assumes that there is a balance between the Lorentz force and the irreversible pinning force. In this Chapter, the summation theory is introduced, which is used to analytically determine the critical current density, i.e., the maximum non-dissipative current density. The reason why the resultant electromagnetic phenomena become irreversible is clarified, even though the fundamental flux pinning mechanism is reversible. The irreversibility in flux pinning phenomena does not originate from the breaking of time reversal symmetry, but is of another type, such as friction, that is non-dissipative in stationary condition, although it causes energy dissipation in motion due to the applied force.

5.1 Flux Pinning Mechanism

The resistivity of superconductors takes on a smaller value in the superconducting state than in the normal state, as shown by (4.46). This property cannot be utilized, however, since the normal resistivity ρ_n is very much higher than those of conductive materials such as copper. The only possibility for application is prevention of the appearance of induced voltage by stopping the flux motion.

The useful mechanism for this purpose is flux pinning. The superconducting structure of flux lines, as shown in Fig. 4.5, is associated with this mechanism. The essential point is that the central region is almost in the normal state ($\Psi = 0$). Equation (4.2) shows us that the energy in this region is higher than that in the surrounding superconducting region. If the normal core of a flux line meets a normal precipitate in the superconductor, as illustrated in Fig. 5.1a, it is energetically favorable because of the smaller volume in which the superconductivity is destroyed than when the

T. Matsushita, *Superconductivity and Electromagnetism*, Springer Series in Solid-State Sciences 195, https://doi.org/10.1007/978-3-030-67568-4_5

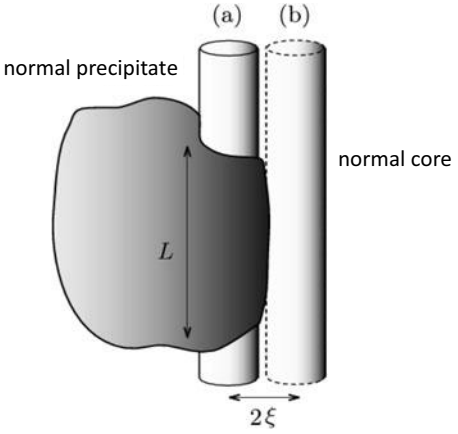

Fig. 5.1 Arrangement of the normal core of a flux line around a normal precipitate: **a** overlapping case and **b** separated case

normal core is apart from the precipitate, as shown in Fig. 5.1b. Hence, normal precipitates work as attractive pinning centers. The interaction energy in this case is given by the condensation energy density $(1/2)\mu_0 H_c^2$, the energy difference between the superconducting and normal states, multiplied by the overlapping volume.

In the case where the size of the precipitate L is larger than the diameter of the normal core 2ξ, the overlapping volume is approximately equal to $\pi\xi^2 L$. Hence, the interaction energy is given by

$$U_p = \frac{\pi}{2}\mu_0 H_c^2 \xi^2 L. \tag{5.1}$$

Since the change in the energy of this amount occurs during the displacement of the flux line by 2ξ, as shown by Fig. 5.1, the elementary pinning force, i.e., the maximum pinning force that this precipitate can exert is estimated as

$$f_p = \frac{U_p}{2\xi} = \frac{\pi}{4}\mu_0 H_c^2 \xi L. \tag{5.2}$$

α-Ti phase contained in the most widely used Nb-Ti alloy superconductor is an example of normal precipitates working as pinning centers.

Secondly, we will focus on the flux pinning by grain boundaries. These are pinning centers in Nb_3Sn superconductor, which is the second most widely used superconductor in the world. The effective thickness of grain boundaries is very small in comparison with normal precipitates. Hence, it may be considered that the elementary pinning force of a grain boundary is very small due to the very small overlapping volume. Electron scattering is associated with the flux pinning mechanism in this case. When electrons are scattered by defects, the electron mean free path is shortened, which causes a reduction in the coherence length, as stated in Sect. 4.1f. Hence, the coherence length, which is the radius of the normal core, becomes shorter when

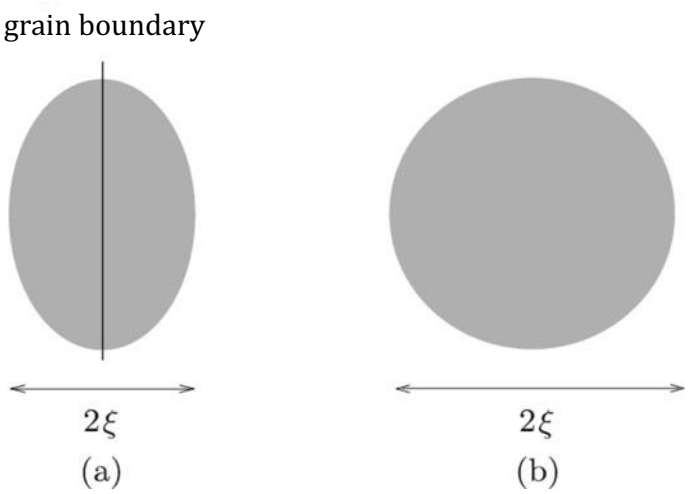

Fig. 5.2 Arrangement of the normal core of a flux line around a grain boundary: **a** overlapping case and **b** separated case

the normal core meets a grain boundary, as illustrated in Fig. 5.2a. Since the cross-sectional area of the normal core with the higher energy decreases, the grain boundary also works as an attractive pinning center. For the calculation of the elementary pinning force of a grain boundary, we need certain information, such as the degree of reduction in the electron mean free path due to scattering and the dependence of the coherence length on the electron mean free path. Hence, the details are not discussed here. It is evident, however, that the elementary pinning force of a grain boundary is weaker than that of a normal precipitate, since only the cross-sectional area changes slightly during the interaction.

The flux pinning mechanisms involving normal precipitates and grain boundaries have been treated as examples in above. Since the condensation energy is involved in both cases, these pinning mechanisms are classified under the condensation energy interaction. The critical temperature T_c is different between the superconducting matrix and normal precipitates in which T_c is zero, and the pinning mechanism caused by this difference is called the δT_c interaction. On the other hand, the electron mean free path l is different between the superconducting matrix and grain boundaries. The pinning mechanism due to this difference is called the δl interaction.

In general, the superconducting layer grows in a spiral direction on the substrate during the process of deposition of high-temperature superconducting films. As a consequence, a screw dislocation is formed at the center of the spiral. Since the mechanical strain is very high on the center of the screw dislocation, the carrier density around this region will be appreciably different from the optimal one. It is speculated that the superconductivity is broken there. Fairly strong flux pinning

by screw dislocations in high-temperature superconductors is also explained by the condensation energy interaction.

Niobium was introduced into Nb-Ti as a material for pinning centers. Since Nb itself is a superconductor with almost the same T_c as the superconducting matrix, the condensation energy is not involved in the pinning mechanism. On the other hand, the upper critical field and hence, the coherence length of Nb is significantly different from those of the matrix. For this reason, the free energy associated with the flux pinning is the kinetic energy given by the second term in the brackets of (4.32).

The elementary pinning mechanism is explained for various cases above. The pinning force density observed in practice is given by the sum of individual pinning forces contained in a macroscopic scale volume. Assume a superconductor that contains pinning centers with the number density N_p and the elementary pinning force f_p. The mathematical problem of estimating the pinning force density F_p as a function of N_p and f_p is called the summation problem. Most simply, we can assume the relationship

$$F_p = N_p f_p. \tag{5.3}$$

This is called the direct summation. The pinning force density is usually smaller than this prediction, however, since the inning forces originate from interaction with pinning potentials. In many cases pinning centers act as attractive potentials. Thus, the direction of each pinning force depends on the relative position of the flux line with respect to the interacting pinning center, and hence, some part of the pinning forces, which are directed randomly, are cancelled, as illustrated in Fig. 5.3, resulting

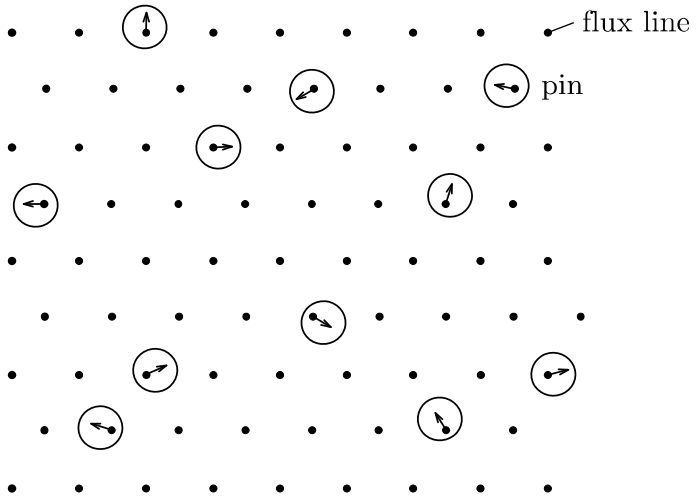

Fig. 5.3 Randomly distributed pinning centers and flux lines forming a lattice due to magnetic interaction. Individual pinning forces are directed randomly, depending on the relative position of each flux line with respect to the interacting pinning center

in a smaller value than that in (5.3). For this reason, it is not easy to estimate the pinning force density.

Figure 5.4 shows the observed relationship between the elementary pinning force and the contribution of one pinning center to the pinning force density for Nb at 4.2 K and at reduced magnetic field $B/\mu_0 H_{c2} = 0.55$ [1]. The straight line with a slope of unity is the direct summation given by (5.3). This result shows that the pinning force density obeys the relationship called the linear summation:

$$F_p = \eta_p N_p f_p \tag{5.4}$$

in the case of strong pinning. Here, η_p is a constant smaller than 1 and is called the pinning efficiency. When the pinning is weak, the pinning force density obeys the relationship

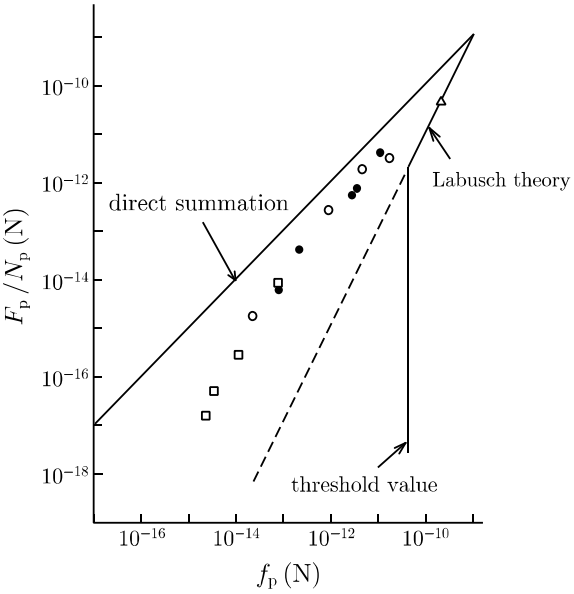

Fig. 5.4 Relationship between the elementary pinning force (f_p) and the contribution of one pinning center to the pinning force density (F_p/N_p) for Nb at 4.2 K and at reduced magnetic field $B/\mu_0 H_{c2} = 0.55$ [1]. The threshold value of the elementary pinning force will be discussed in Sect. 5.4

$$F_p \propto N_p f_p^2. \tag{5.5}$$

This is called the statistical summation, since the functional form is the same as the prediction of the statistical theory.

5.2 Critical State Model

Before going to the summation theory, the critical state model is introduced, which correctly describes irreversible electromagnetic phenomena in superconductors, since it is necessary to understand the irreversibility.

It is assumed in the static critical state model that the magnetic flux distribution is determined by the balance between the Lorentz force and the pinning force [2]:

$$\boldsymbol{F}_L + \boldsymbol{F}_p = 0. \tag{5.6}$$

The Lorentz force obeys Fleming's left-hand rule, as illustrated in Fig. 5.5, and is given by

$$\boldsymbol{F}_L = \boldsymbol{J} \times \boldsymbol{B}. \tag{5.7}$$

Hence, the pinning force density is related to the critical current density as

$$F_p = J_c B. \tag{5.8}$$

When a transverse magnetic field is applied parallel to a superconducting slab, as shown in Fig. 5.6a, the magnetic flux density has a gradient, and the restoring force acts to reduce the gradient, as shown in Fig. 5.6b. This is called the magnetic pressure. When a current is applied to a superconducting slab in a normal magnetic field, as shown in Fig. 5.7a, the magnetic flux lines are curved, as illustrated in Fig. 5.7b, and the restoring force acts to straighten the flux lines. This is called the line tension. Both

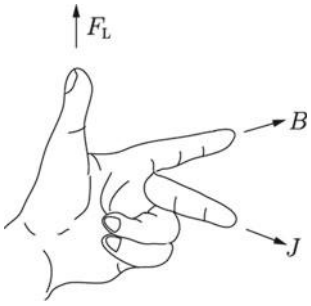

Fig. 5.5 Fleming's left-hand rule

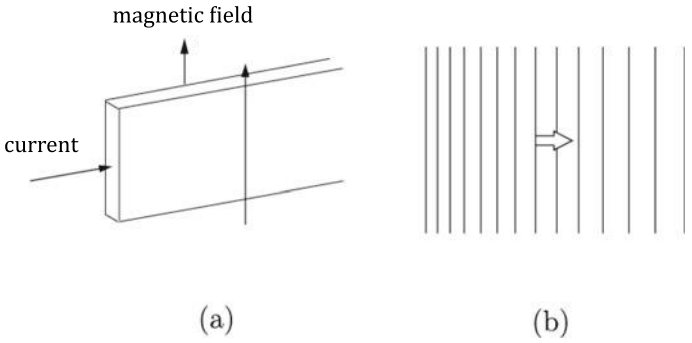

Fig. 5.6 **a** Superconducting slab carrying a current in a parallel magnetic field, and **b** the condition of the magnetic flux. There is a gradient in the magnetic flux density, and the magnetic pressure works to reduce the gradient, as shown by the arrow

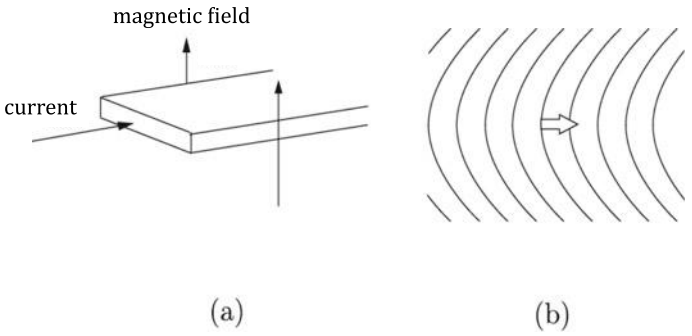

Fig. 5.7 **a** Superconducting slab carrying a current in a normal magnetic field, and **b** the condition of the magnetic flux. A curved deformation of the magnetic flux occurs, and the line tension works to make the magnetic flux straight, as shown by the arrow

of these forces are the Lorentz force given by (5.7), as will be shown in Sect. 5.7. This force is a restoring force to reduce strains in the magnetic flux structure caused by the current. Equation (5.6) means that

$$\boldsymbol{F}_{\mathrm{p}} = -\boldsymbol{\delta} F_{\mathrm{p}}, \tag{5.9}$$

where $\boldsymbol{\delta}$ represents a unit vector in the direction of the Lorentz force. That is, the pinning force is assumed to work in the opposite direction to the Lorentz force. The electromagnetic phenomena in superconductors will be described using the critical state model.

(1) **Magnetic flux distribution**

First, we treat the magnetic flux distribution. Assume that an external magnetic field H_0 is applied to a wide superconducting slab of thickness $2d$ ($0 \leq x \leq 2d$) along the z-axis. From symmetry, we need only to consider the half region, $0 \leq x \leq d$. Magnetic

flux invades the superconductor from both surfaces. The magnetic flux density inside the superconductor is also the z-component. It can also be assumed that no quantity varies along the y- or z-axes. Hence, the current density has a y-component only:

$$\boldsymbol{J} = -\frac{1}{\mu_0} \cdot \frac{\partial B}{\partial x} \boldsymbol{i}_y. \tag{5.10}$$

The Lorentz force is of the y-component, and (5.6) is reduced to

$$B\frac{\partial B}{\partial x} + \delta \mu_0 F_\mathrm{p} = 0, \tag{5.11}$$

where δ is a sign factor and takes the values $+1$ and -1, when the Lorentz force is directed along the positive or negative x-axis, respectively. In the present initial condition, since the flux lines are driven in the positive direction by the Lorentz force, $\delta = 1$. Here, we assume the simple B-dependence of F_p as

$$F_\mathrm{p} = \alpha_\mathrm{p} B. \tag{5.12}$$

This is called Bean's model [2]. In this case we have

$$J_\mathrm{c} = \alpha_\mathrm{p}(\text{const.}). \tag{5.13}$$

Under the boundary condition $B(0) = \mu_0 H_0$, (5.11) can be solved easily as

$$B(x) = \mu_0(H_0 - J_\mathrm{c} x). \tag{5.14}$$

For $H_0 < J_\mathrm{c} d$, the magnetic flux does not reach the center of the superconducting slab, as shown in Fig. 5.8, and (5.14) holds for $0 \leq x \leq H_0/J_\mathrm{c}$. The magnetic flux density is zero in the region $H_0/J_\mathrm{c} < x \leq d$. The penetration of the magnetic flux induces the current, and its distribution is given by

$$\begin{aligned} J &= J_\mathrm{c}; \quad 0 \leq x \leq H_0/J_\mathrm{c}, \\ &= 0; \quad H_0/J_\mathrm{c} < x \leq d. \end{aligned} \tag{5.15}$$

This current distribution is shown in the lower panel in Fig. 5.8.

For $H_0 > J_\mathrm{c} d$, the magnetic flux penetrates the entire region of the superconducting slab, and the current with density J_c flows throughout the whole area. The distributions of the magnetic flux and current in this case are shown in Fig. 5.9. The external magnetic field at which the magnetic flux reaches the center of the superconductor is given by

$$H_0 = J_\mathrm{c} d \equiv H_\mathrm{p}. \tag{5.16}$$

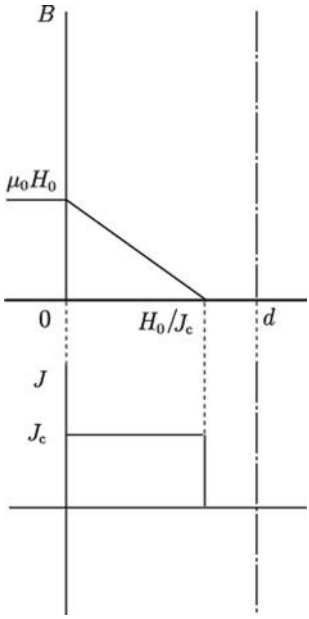

Fig. 5.8 Distributions of magnetic flux (upper panel) and current (lower panel) under an increasing external magnetic field

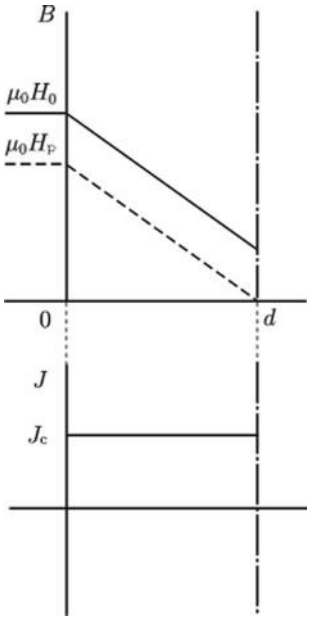

Fig. 5.9 Distributions of magnetic flux (upper panel) and current (lower panel) when the external magnetic field is increased above the penetration field

This is called the penetration field. The distributions of the magnetic flux and current in the region of $d < x < 2d$ are symmetric and antisymmetric to those shown in above with respect to $x = d$, respectively.

We assume that the external magnetic field is increased to H_m and then, decreased. The magnetic flux tends to pass out of the superconductor. Hence, in the region near the surface, $\delta = -1$, and the magnetic flux distribution is given by

$$B(x) = \mu_0(H_0 + J_c x). \tag{5.17}$$

In the inner region, the former magnetic flux distribution remains (see Fig. 5.10):

$$B(x) = \mu_0(H_m - J_c x). \tag{5.18}$$

The branching point of the two magnetic flux distributions of (5.17) and (5.18) is

$$x = \frac{H_m - H_0}{2J_c} \equiv x_b. \tag{5.19}$$

The direction of the current differs between the two regions separated by this point. Hence, even when the external magnetic field is the same, the inner magnetic flux distribution is different between the increasing and decreasing magnetic field processes. Thus, the irreversibility in the magnetic behavior can be understood.

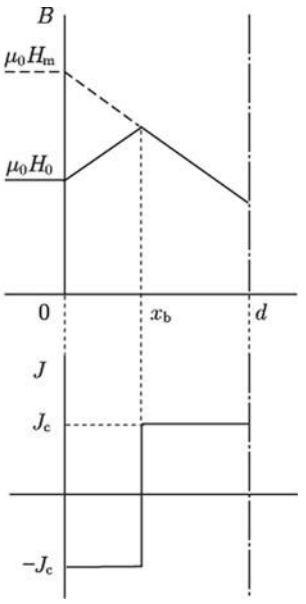

Fig. 5.10 Distributions of magnetic flux (upper panel) and current (lower panel) when the external magnetic field is increased to H_m and then, decreased

(2) **Magnetization**

Here, we will estimate the magnetization for the processes of increasing and decreasing magnetic field that were treated in the last subsection. Since there is no effect of demagnetization, the magnetization can be simply calculated using (3.49). In the initial process ($0 \leq H_0 \leq H_p$), a simple calculation leads to

$$M = \frac{H_0^2}{2J_c d} - H_0 = \frac{H_0^2}{2H_p} - H_0. \tag{5.20}$$

For $H_0 > H_p$, we have

$$M = -\frac{1}{2}J_c d = -\frac{1}{2}H_p. \tag{5.21}$$

Equation (5.21) represents the magnetization on the major magnetization curve. When the external magnetic field is decreased from H_m, the situation depends on the value of H_m. There are three cases; $H_m < H_p$, $H_p < H_m < 2H_p$ and $H_m > 2H_p$. We treat the case of $H_m > 2H_p$. In the range of $H_m > H_0 > H_m - 2H_p$, the magnetization is given by

$$M = -\frac{(2H_p - H_m + H_0)^2}{4H_p} + \frac{1}{2}H_p. \tag{5.22}$$

For $H_0 < H_m - 2H_p$, the magnetization is on the opposite major magnetization curve and is given by

$$M = \frac{1}{2}H_p. \tag{5.23}$$

The calculated results are shown in Fig. 5.11. The minor magnetization reaches the major curve before H_0 is reduced to 0 under the present condition for H_m. For $H_m < 2H_p$, the minor magnetization reaches the major curve after H_0 is reduced to 0.

The critical current density is often estimated from the magnetization measurement. In the present analysis, the hysteresis width of the major magnetization curve is calculated as

$$\Delta M = H_p = J_c d \tag{5.24}$$

using (5.21) and (5.23) (see Fig. 5.11). Hence, we have

$$J_c = \frac{\Delta M}{d}. \tag{5.25}$$

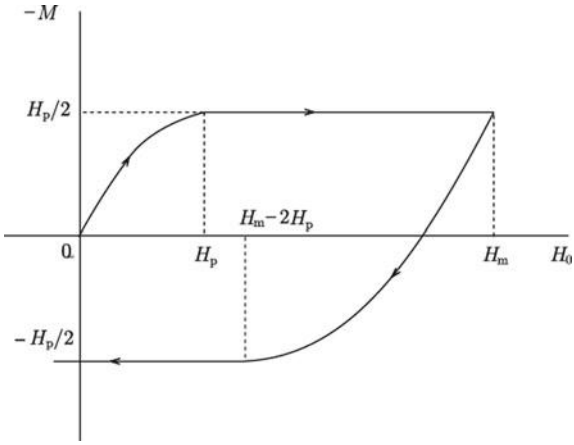

Fig. 5.11 Magnetization curve while the external magnetic field is increased from 0 to $H_m(> 2H_p)$ and then, decreased

The critical current density is in general a function of the magnetic field, and many models have been proposed for the magnetic field dependence of the critical current density. In many cases, except for bulk superconductors, etc., the variation in the critical current density due to distribution of the magnetic flux density inside the superconductor can be safely neglected, since the size of the superconductor is not large. Thus, there is no problem in using (5.25) to estimate the critical current density from the magnetization hysteresis.

(3) **Case of current flow**

The critical current density is usually measured under the condition of applying a transport current to a superconductor in a magnetic field. The magnetic flux distribution in this condition is treated here. Assume that a DC magnetic field H_0 along the z-axis is applied to a superconducting slab of thickness $2d\,(0 \le x \le 2d)$, and then, a transport current I is applied along the z-axis. In this case the magnetic flux distribution in not symmetrical with respect to the center of the slab $(x = d)$. So, the magnetic flux distribution is estimated in the whole region of the superconductor. First, the magnetic flux distribution is shown in Fig. 5.12a when the DC magnetic field is increased from 0 to H_0. After applying the transport current, the boundary conditions to be satisfied are

$$\begin{aligned} B(0) &= \mu_0(H_0 + H_I), \\ B(2d) &= \mu_0(H_0 - H_I), \end{aligned} \tag{5.26}$$

where w is the width of the superconductor along the z-axis and H_I is the self field due to the current given by

$$H_I = \frac{I}{2w}. \tag{5.27}$$

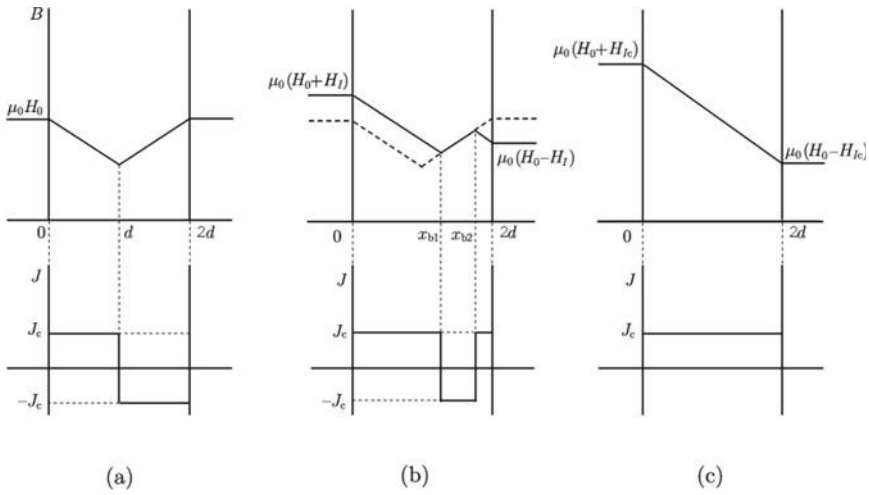

Fig. 5.12 Distributions of magnetic flux density (upper panels) and current (lower panels) **a** before application of the current, **b** in the intermediate condition, and **c** at the critical current

The motion of the magnetic flux occurs in the direction of the positive x-axis near the two surfaces, but the magnetic flux in the middle area does not move. The magnetic flux distribution is given by (see Fig. 5.12b)

$$\begin{aligned} B &= \mu_0(H_0 + H_I - J_c x); && 0 \le x < x_{b1}, \\ &= \mu_0[H_0 - J_c(2d - x)]; && x_{b1} < x < x_{b2}, \\ &= \mu_0[H_0 - H_I + J_c(2d - x)]; && x_{b2} < x \le 2d. \end{aligned} \tag{5.28}$$

The branching points are

$$\begin{aligned} x_{b1} &= d + \frac{H_I}{2J_c}, \\ x_{b2} &= 2d - \frac{H_I}{2J_c}. \end{aligned} \tag{5.29}$$

The two branching points grow close during the increase in current and collapse when the current reaches

$$I = 2J_c d \quad w = I_c, \tag{5.30}$$

and a magnetic distribution with a uniform slope is attained, as shown in Fig. 5.12c. The current given by (5.30) is the critical current, and the corresponding self-field is

$$H_{Ic} = J_c d = H_p. \tag{5.31}$$

When the current exceeds the critical current (I_c), the force balance given by (5.6) no longer holds, and the flux flow state sets in.

(4) **Pinning loss energy**

Next, we will estimate the loss energy in the superconductor. Sometimes the loss energy is calculated from the area of the closed magnetization curve in the case of AC loss energy. This method cannot be used, however, in the case of the loss energy in a superconducting magnet during the energizing process or that in a superconducting power transmission line during the process of increasing the current. On the other hand, the loss energy in any case can be estimated using the critical state model. The total loss power density is [3]

$$P = \boldsymbol{J} \cdot \boldsymbol{E} = \boldsymbol{J} \cdot (\boldsymbol{B} \times \boldsymbol{v}) = (\boldsymbol{J} \times \boldsymbol{B}) \cdot \boldsymbol{v}. \tag{5.32}$$

The reason why the loss power can be estimated is guaranteed by the assumption of irreversibility in the critical state model. The loss power density given by (5.32) can be regarded as the power generated by the Lorentz force when it drives flux lines with velocity $\boldsymbol{v}$. This agrees with a model of dynamics. From (5.6)–(5.9) the pinning loss power density is given by

$$P_p = |J_c B v|, \tag{5.33}$$

where we used the fact that $\boldsymbol{\delta}$ and $\boldsymbol{v}$ point in the same direction. Hence, it is necessary to estimate the velocity $\boldsymbol{v}$ to calculate the loss power. The electromotive induction is caused by a time variation in the magnetic flux density, and such a variation comes from the motion of flux lines. Substitution of (4.41) into (2.49) leads to

$$\nabla \times (\boldsymbol{B} \times \boldsymbol{v}) = -\frac{\partial \boldsymbol{B}}{\partial t}, \tag{5.34}$$

which is called the continuity equation for flux lines [3]. This equation is useful to determine $\boldsymbol{v}$.

Here, we treat the AC loss energy density when an AC magnetic field of amplitude H_m is applied parallel to a superconducting slab of thickness $2d (0 \leq x \leq 2d)$. From symmetry, we have only to treat the half region $0 \leq x \leq d$. We needed the classification of the value of H_m for the calculation of the magnetization in (2). The same thing occurs again. We treat the case of $H_m < H_p$ here.

Since the AC loss energy density is the same between the process of changing the external magnetic field from H_m to $-H_m$ and that from $-H_m$ to H_m, it is enough to double the loss energy density in the former process. The magnetic flux distribution when the external magnetic field is decreased from $H_0 = H_m$ is shown in Fig. 5.13. The branching point of the magnetic flux distribution is

$$x_b = \frac{H_m - H_0}{2J_c}. \tag{5.35}$$

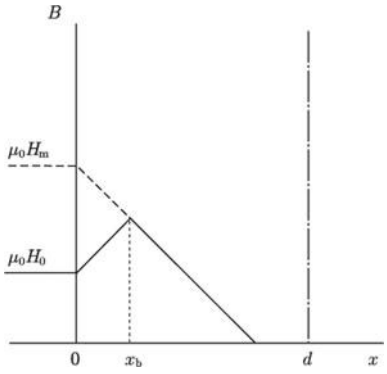

Fig. 5.13 Magnetic flux distribution in the superconductor in the process of decreasing the external magnetic field from the initial state

Here, we estimate the velocity v from (5.34). Since $\boldsymbol{v}$ and $\boldsymbol{B}$ are directed along the x- and z-axes, respectively, (5.34) is reduced to

$$\frac{\partial}{\partial x} Bv = -\frac{\partial B}{\partial t}. \tag{5.36}$$

Since magnetic flux lines move in the direction of the negative x-axis from the branching point $x = x_b$, v is zero at $x = x_b$. The variation with time on the right-hand side is given by $-\mu_0 \partial H_0/\partial t$ from the magnetic flux distribution given by (5.17). Hence, we have

$$Bv(x) = -\int_{x_b}^{x} \mu_0 \frac{\partial H_0}{\partial t} \mathrm{d}x = -\mu_0 \frac{\partial H_0}{\partial t}(x - x_b). \tag{5.37}$$

Note that $Bv(x)$ is negative, independently of the sign of B. That is, $v > 0$ in the region where $B < 0$ and $v < 0$ in the region where $B > 0$. Since the loss occurs in the region $0 \le x \le x_b$ in which magnetic flux lines move, the pinning loss power density is written as

$$\begin{aligned} P_p &= \frac{1}{d} \int_0^{x_b} |J_c Bv| \mathrm{d}x = \frac{\mu_0 J_c}{d} \cdot \frac{\partial H_0}{\partial t} \int_0^{x_b} (x - x_b) \mathrm{d}x \\ &= -\frac{\mu_0 (H_m - H_0)^2}{8 H_p} \cdot \frac{\partial H_0}{\partial t}. \end{aligned} \tag{5.38}$$

Note that $\partial H_0/\partial t < 0$. Then, the AC loss energy density is calculated as

$$W = \int P_{\mathrm{p}} \mathrm{d}t = -\frac{\mu_0}{8H_{\mathrm{p}}} \int_{H_{\mathrm{m}}}^{-H_{\mathrm{m}}} (H_{\mathrm{m}} - H_0)^2 \mathrm{d}H_0 \times 2 = \frac{2\mu_0 H_{\mathrm{m}}^3}{3H_{\mathrm{p}}}. \tag{5.39}$$

This result shows that the pinning loss energy in a unit cycle is constant. This is a characteristic property of hysteresis loss. The same result can be obtained from the area of a closed magnetization loop.

For $H_{\mathrm{m}} > H_{\mathrm{p}}$, a similar calculation is derived:

$$W = 2\mu_0 H_{\mathrm{p}} H_{\mathrm{m}} \left(1 - \frac{2H_{\mathrm{p}}}{3H_{\mathrm{m}}}\right). \tag{5.40}$$

The obtained AC loss energy density is shown in Fig. 5.14.

(5) **Extension to dynamic state**

When a current higher than the critical current is applied, the flux flow state described in Sect. 4.3 sets in. The force balance equation in this case is not given by (5.6) but by

$$\boldsymbol{F}_{\mathrm{L}} + \boldsymbol{F}_{\mathrm{p}} + \boldsymbol{F}_{\mathrm{v}} = 0, \tag{5.41}$$

where $\boldsymbol{F}_{\mathrm{v}}$ is the phenomenological viscous force density. This is called the dynamic critical state model [3]. The magnitude of the viscous force density is proportional to the velocity of magnetic flux lines and it is directed opposite to the flux motion. Hence, the viscous force density is expressed as

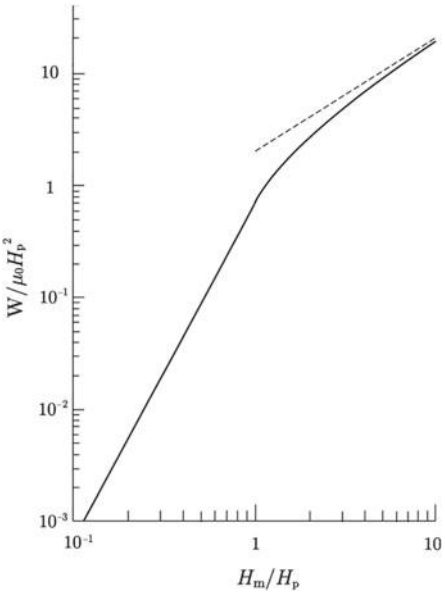

Fig. 5.14 Dependence of AC loss energy density on the magnetic field amplitude. The dashed line shows the approximate formula $W = 2\mu_0 H_{\mathrm{p}} H_{\mathrm{m}}$ of (5.40) in the limit of large field amplitude

$$\boldsymbol{F}_{\mathrm{v}} = -\eta \frac{B}{\phi_0} \boldsymbol{v}, \tag{5.42}$$

where η is the viscous coefficient. When (5.41) is divided by the magnetic flux density B and v is eliminated using (4.41), we have

$$J - J_{\mathrm{c}} - \frac{\eta}{\phi_0 B} E = 0. \tag{5.43}$$

This can be rewritten to the E-J characteristics of (4.48). Hence, the viscosity is related to the flow resistivity as

$$\eta = \frac{\phi_0 B}{\rho_{\mathrm{f}}}. \tag{5.44}$$

As discussed above, the critical state model forms the analytic system in which $\boldsymbol{B}$ and $\boldsymbol{v}$ are used as variables, and the force balance equation and the continuity equation for flux lines are used for analysis. It is also possible to use the electric field $\boldsymbol{E}$ and Maxwell's (2.49) instead of $\boldsymbol{v}$ and the continuity equation for flux lines. The present method using $\boldsymbol{v}$ is beneficial, however, because of the analogy with mechanical systems.

5.3 Reversible Flux Motion

The critical state model correctly describes irreversible electromagnetic phenomena in superconductors, as shown in the last section, although the flux pinning phenomena originate from energetic interaction between flux lines and defects, and such individual interactions are in principle reversible. In fact, detailed observations reveal some reversible phenomena. Such reversible phenomena, i.e., electromagnetic phenomena associated with reversible flux motion, are introduced in this section. This seems to be contradictory to the principle of the critical state model. The reason why the irreversibility occurs will be discussed in Sect. 5.4.

When the external magnetic field is decreased after increasing to some strength, the critical state model assumes that the current keeps its critical current density J_{c}, but sharply changes its direction across the branching point of the magnetic flux distribution, as shown in Fig. 5.10. This is a rough approximation. If we look at the magnetic flux distribution in more detail, however, the distribution is found to be slightly different from the description by the model. Since magnetic flux lines elastically repel each other through their magnetic interaction, the magnetic flux distribution does not change sharply at the branching point but changes gradually in space. The current also gradually changes its density from J_{c} to $-J_{\mathrm{c}}$ around the branching point. The characteristic length of this spatial variation is typically on the order of 1 μm, and if this length is negligible in comparison with the size of the superconductor, the macroscopic description by the critical state model is sufficient.

When the size of the superconductor is comparable to or only slightly larger than the characteristic length, the reversible phenomena become prominent.

It is assumed that a superconductor in the normal state is cooled down in a magnetic field. In this condition, the magnetic flux density in the superconductor is expected to be constant on a macroscopic scale and is denoted by B. There is no macroscopic current inside the superconductor. In this case, a group of flux lines, which will move collectively if necessary, are considered to stay at the bottom of the pinning potential. It is assumed that these flux lines are displaced by distance u by an increase in the external magnetic field or by an applied current. Then, the force that the flux lines receive from the pinning potential will be given by

$$F = -\alpha_{\mathrm{L}} u \tag{5.45}$$

in a unit volume, where α_{L} is the Labusch parameter that represents the strength of the flux pinning. The variation in the magnetic flux density caused by the displacement of flux lines is denoted by $\boldsymbol{b}$. Integrating the continuity equation for flux lines, (5.34), with time, we obtain

$$\nabla \times (\boldsymbol{B} \times \boldsymbol{u}) = -\boldsymbol{b}. \tag{5.46}$$

For simplicity, we assume that the magnetic field is applied along the z-axis and the displacement is along the x-axis. Then, the spatial variation occurs only along the x-axis, and (5.46) is reduced to

$$B\frac{\partial u}{\partial x} = -b, \tag{5.47}$$

where b is the z-component of $\boldsymbol{b}$. The restoring force, i.e., the Lorentz force, acts to reduce the strain that appears in the flux line system. This acts along the x-axis as

$$F_{\mathrm{L}} = -\frac{(B+b)}{\mu_0}\frac{\partial}{\partial x}(B+b) \cong -\frac{B}{\mu_0}\frac{\partial b}{\partial x}. \tag{5.48}$$

Since this is balanced with the pinning force given by (5.45), we have

$$\frac{B}{\mu_0}\frac{\partial b}{\partial x} = -\alpha_{\mathrm{L}} u. \tag{5.49}$$

Elimination of u using (5.47) leads to

$$\frac{B^2}{\mu_0}\frac{\partial^2 b}{\partial x^2} = \alpha_{\mathrm{L}} b. \tag{5.50}$$

Under the boundary condition that $b = 0$ on the surface $x = 0$ and the condition that b is finite at infinity ($x \to \infty$), (5.50) is solved as

$$b(x) = \mu_0 h_0 \exp\left(-\frac{x}{\lambda_0'}\right), \tag{5.51}$$

where λ_0' is Campbell's AC penetration depth [4], given by

$$\lambda_0' = \left(\frac{B^2}{\mu_0 \alpha_L}\right)^{1/2}. \tag{5.52}$$

This length is the characteristic length of the above-mentioned spatial variation in the current density from J_c to $-J_c$. If the pinning strength is increased, i.e., α_L is increased, λ_0' becomes shorter. The displacement of flux lines u also has a functional form similar to (5.51).

Just after the change in the external magnetic field from the increasing process to the decreasing one, a similar thing happens. Spatial variation in the magnetic flux distribution near the surface is expected, as shown in Fig. 5.15. The penetration depth of the variation in the magnetic flux distribution is not proportional to the variation in the external magnetic field, but is given by λ_0', so long as the variation in the external magnetic field is small.

When the displacement of flux lines is enhanced, the pinning force density increases according to (5.45). Some flux lines are depinned from pinning centers, and new flux lines are captured by pinning centers when the displacement exceeds some level. Thus, it is expected that the pinning force density is saturated to the bulk value. This relationship is schematically shown in Fig. 5.16 [5]. The displacement d_i at which the pinning force density reaches $F_p = J_c B$ at the critical point A is called the interaction distance and satisfies

$$\alpha_L d_i = J_c B. \tag{5.53}$$

The field-cooled process is not adopted frequently, but the process of sweeping the external magnetic field is mostly changed from increasing to decreasing or vice versa in an isothermal condition. When the direction of the displacement of flux lines changes, the pinning force density also changes. For example, when flux lines

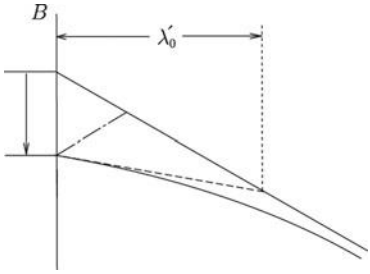

Fig. 5.15 Variation in the magnetic flux distribution near the surface when the external magnetic field is decreased after the increasing process. The dot-dashed line shows the prediction of the critical state model

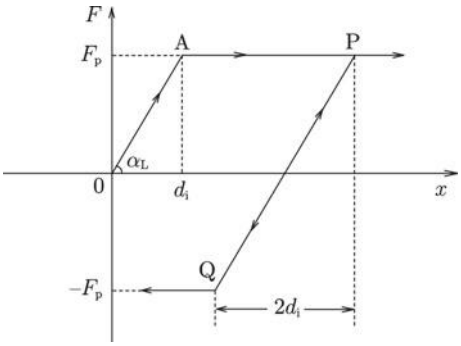

Fig. 5.16 Relationship between the pinning force density and the displacement of flux lines [5]. The origin shows the condition achieved by the field-cooled process

are displaced back from condition P in the critical state in Fig. 5.16, the pinning force density does not keep the critical value but changes, following the line to condition Q in the opposite critical state. When the flux lines go back again to P before reaching Q, the phenomenon is reversible. The loss energy density in the AC condition is equal to the area of the closed loop in the force density versus displacement characteristic, similarly to friction. For this reason, the energy is not dissipated in the reversible case. This means that the energy dissipation occurs when the flux lines are depinned or when new flux lines are captured by pinning centers.

The relationship in Fig. 5.16 can be checked experimentally using Campbell's method [6]. Assume that a small AC magnetic field is applied to a superconductor in a DC magnetic field. If we measure the AC magnetic flux penetrating the superconductor, the penetration depth of the AC magnetic flux can be estimated. The relationship between the AC field amplitude and the penetration depth of the AC magnetic flux is shown in Fig. 5.17 [7]. When the AC field amplitude becomes large, the penetration depth increases linearly. This region corresponds to the linear magnetic flux distribution in Fig. 5.9 and shows that Bean's model holds. On the other hand, the penetration depth is almost constant for small AC field amplitudes, as expected from Fig. 5.15. This constant value is λ_0'. The displacement of flux lines

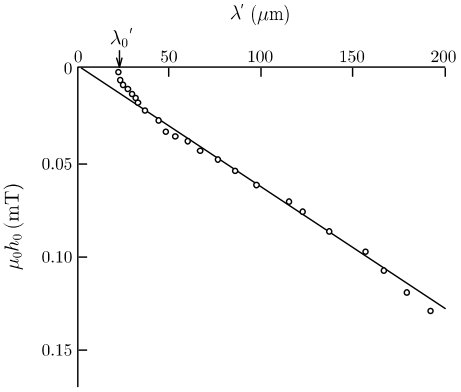

Fig. 5.17 Relationship between the AC field amplitude and the penetration depth of the AC magnetic flux observed for Nb-50 at.%Ta at 0.336 T [7]. The solid line shows the magnetic flux distribution predicted by Bean's model

is estimated from the penetrating AC magnetic flux and (5.47), and the pinning force density is obtained from the slope of the magnetic flux distribution in Fig. 5.17. The obtained pinning force vs. displacement characteristic obtained in such a way is shown in Fig. 5.18 [7]. In the figure, the initial state is the critical state, and hence, the origin corresponds to point P in Fig. 5.16. Thus, the deviation from the prediction of the critical state model is correctly described by the reversible motion of flux lines.

As mentioned above, the effect of reversible flux motion is significant for small superconductors with dimensions comparable to or smaller than λ_0' along the direction of penetration of flux lines. Assume the case of an applied AC magnetic field, for example. Flux lines penetrate from both sides of the superconductor. From the symmetry, the flux lines at the center cannot move, and these flux lines stay at the bottom of the pinning potential. Note that the displacement of flux lines is different from the distance over which the change in the magnetic flux distribution occurs. The displacement is usually much smaller than the latter distance. For this reason, it can happen that the displacement is smaller than the interaction distance, i.e., the effective size of the pinning potential, even at both surfaces at which the displacement is at its maximum. In this case almost all flux motion is reversible inside the pinning potential, resulting in a quite small AC loss energy. In Fig. 5.17, λ_0' is about 20 μm, while d_i is only about 2 nm.

The AC loss energy density predicted by the critical state model shown in Fig. 5.14 has different dependences on the AC field amplitude, based on whether it is higher or lower than the penetration field H_p. That is, the loss energy density is proportional to H_m^3/H_p for $H_m < H_p$ and approximately proportional to $H_p H_m$ for $H_m > H_p$. Since H_p is proportional to the size of the superconductor, the AC loss energy density is predicted to change with the size, as shown in Fig. 5.19. The observed loss energy density in a transverse AC magnetic field for a superconducting composite with very fine filaments changes with the filament diameter (d_f), however, as shown in Fig. 5.20 [8]. This shows that the prediction of the critical state model cannot explain the

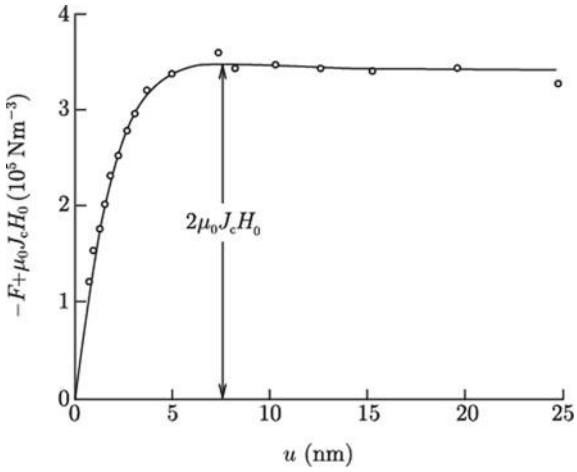

Fig. 5.18 Pinning force versus displacement characteristic for Nb-50 at.%Ta, previously shown in Fig. 5.17 [7]. This figure corresponds to displacement in the opposite direction from point P in Fig. 5.16

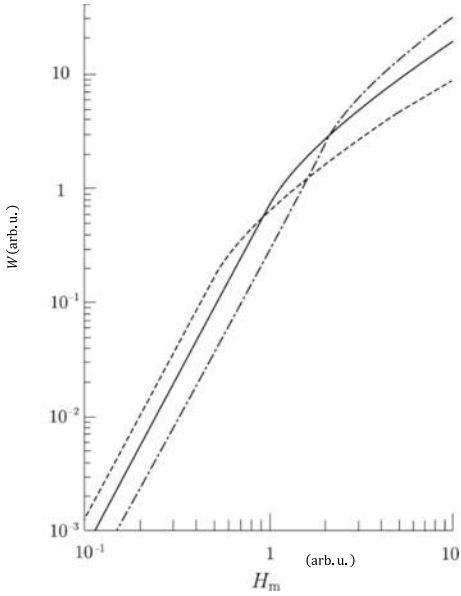

Fig. 5.19 Change in the AC loss energy density predicted by the critical state model when the diameter of the superconductor is changed. The dashed and dot-dashed lines are the losses when the diameter is halved and doubled, respectively

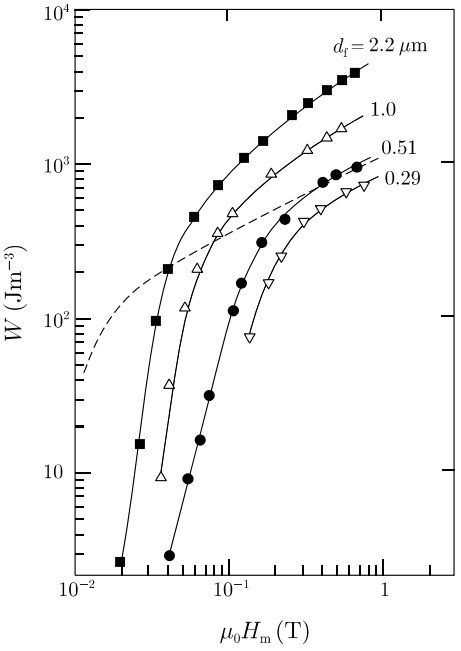

Fig. 5.20 Change in the loss energy density in a transverse AC magnetic field with change in the filament diameter for Nb-Ti composite superconductor [8]. The dashed line is the prediction of the critical state model for $d_f = 0.51\ \mu$m

observed results. In particular, the AC loss energy density for the filament diameter of 0.51 μm is much smaller than the theoretical prediction, as shown by the dashed line for small AC field amplitudes. This is caused by the reversible flux motion. Taking the effect of reversible flux motion into consideration, the AC loss energy density is theoretically predicted to be

$$W = \frac{\mu_0 H_m^3}{3 J_c d_f} \left(\frac{d_f}{\lambda_0'} \right)^4 = \frac{1}{4} \left(\frac{d_f}{\lambda_0'} \right)^4 W_{cs} \tag{5.54}$$

for superconductors of filament diameter d_f smaller than $2\lambda_0'$ [9]. Here W_{cs} is the AC loss energy density of (5.39) that is predicted by the critical state model, where $H_p = J_c d_f/2$.

Here we discuss the magnetization curve under reversible flux motion. The magnetization width, i.e., the difference between the two major magnetization curves ΔM, is equal to H_p in the critical state model. When the magnetization curve during the field decreasing process from the upper major curve to the lower one is approximated by the tangential line at the starting point, the variation in the external magnetic field necessary to reach the lower curve ($\hat{H}_p$) is equal to H_p in the critical state model. This is because the slope of the tangential line is 1. Then, the question is how $\hat{H}_p$ behaves under the reversible flux motion. The slope is expected to be much smaller than 1 from the change in the magnetic flux distribution in Fig. 5.15. Under the flux penetration from both surfaces ($x = \pm d_f/2$), from (5.51), the variation in the magnetic flux density is given by

$$b(x) = \mu_0 h_0 \frac{\cosh\left(x/\lambda_0'\right)}{\cosh\left(d_f/2\lambda_0'\right)}. \tag{5.55}$$

Thus, the magnetization is calculated as

$$M = \frac{1}{\mu_0 d_f} \int_{-d_f/2}^{d_f/2} b(x) \mathrm{d}x - h_0 = h_0 \left[\frac{2\lambda_0'}{d_f} \tanh\left(\frac{d_f}{2\lambda_0'} \right) - 1 \right]. \tag{5.56}$$

In the above, the value in the square brackets is the slope of the minor magnetization curve, and we have

$$\hat{H}_p = H_p \left[1 - \frac{2\lambda_0'}{d_f} \tanh\left(\frac{d_f}{2\lambda_0'} \right) \right]^{-1}. \tag{5.57}$$

The characteristic magnetic field strength $\hat{H}_p$ is called the apparent penetration field. Observations of H_p and $\hat{H}_p$ for multi-filamentary superconductors are compared with the theoretical predictions in Fig. 5.21. A good agreement is found over a wide range of filament diameters [8]. Especially for $d_f \ll 2\lambda_0'$, (5.57) is reduced

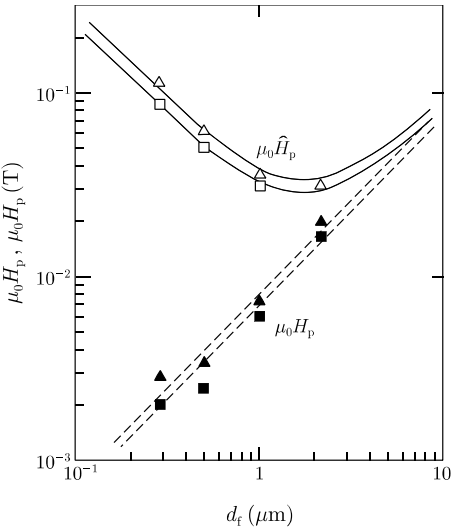

Fig. 5.21 The penetration field (H_p) and the apparent penetration field ($\hat{H}_p$) observed for two series of multi-filamentary Nb-Ti superconductors [8]. The solid lines show (5.57), and the dashed lines are the relationship $H_p = J_c d_f/2$

to $\hat{H}_p = 3\left(2\lambda_0'/d_f\right)^2 H_p$, and $\hat{H}_p$ increases in proportion to $1/d_f$, when the filament diameter decreases. The characteristic field $\hat{H}_p$ corresponds to the magnetic field amplitude H_m at which the H_m dependence of the AC loss energy density changes in Fig. 5.20. Thus, the filament diameter dependence of the AC loss energy density can be seen in the behavior of $\hat{H}_p$ in Fig. 5.21. The magnetization curve for H_m in the intermediate region between H_p and $\hat{H}_p$ is schematically shown in Fig. 5.22. It can be seen that the magnetization width is very thin in comparison with the prediction by the critical state mode, which explains the appreciable reduction in the AC loss energy density. When H_m further decreases, the magnetization at the peak field does not reach the major magnetization curve, resulting in a much smaller AC loss energy density.

The reversible flux motion surely occurs near the surface, independently of the size of the superconductor, as shown in Fig. 5.15, when the field sweep direction is changed. Nevertheless, the AC loss energy density in thick superconductors does not take a small value but obeys (5.39), derived using the critical state model, when an AC field of sufficiently small amplitude is applied. This may seem strange. In

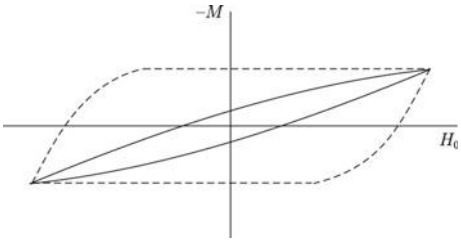

Fig. 5.22 Closed magnetization loop for $H_p < H_m < \hat{H}_p$. The dashed line shows the prediction of the critical state model

reality, the area in which the energy dissipation occurs is fairly extended, as shown in Fig. 5.15, and this factor approximately cancels the reduction in the loss energy density. You will find much more details in Ref. [10]. The reason why the loss energy density is kept small in very thin superconductors is that there is no extension of the energy dissipating area.

5.4 Summation Problem and Irreversibility

In this section the theoretical treatment needed to solve the summation problem explained in Sect. 5.1 is briefly introduced. Magnetic flux lines form a lattice under the repulsive magnetic interaction that exists among them, and each flux line interacts with pinning centers distributed randomly in the superconductor. Because of the randomness of the distribution of pinning centers, the statistical calculation method is employed. Namely, an interaction between one pinning center and a flux line near it is treated representatively, and the pinning force density is estimated from an average for similar N_p interactions in a unit volume. For simplicity, we use a one-dimensional approximation system along the direction of the Lorentz force. For the representative interaction, we assume a pinning center with its center at $x = 0$. The position of the flux line near the pinning center is denoted by x. The flux line spacing is denoted by a_f. Since the area of a unit cell of the triangular flux line lattice is $\left(\sqrt{3}/2\right)a_f^2$, under the magnetic flux density B, using the flux quantum ϕ_0, we have

$$a_f = \left(\frac{2\phi_0}{\sqrt{3}B}\right)^{1/2}. \tag{5.58}$$

The pinning force given by the pinning center is periodic with respect to the displacement of flux lines by a_f. This is because the next flux line interacts with the pinning center, even if one flux line is depinned. It is assumed that flux lines are driven in the direction of the positive x-axis. Campbell's model [5] that assumes a simple one-dimensional pinning is employed, in which the pinning force is given by (see Fig. 5.23)

$$\begin{aligned} f(x) &= \frac{4f_p}{a_f}\left(x + \frac{a_f}{2}\right); -\frac{a_f}{2} \le x < -\frac{a_f}{4}, \\ &= -\frac{4f_p}{a_f}x; -\frac{a_f}{4} \le x < \frac{a_f}{4}, \\ &= \frac{4f_p}{a_f}\left(x - \frac{a_f}{2}\right); \frac{a_f}{4} \le x < \frac{a_f}{2}, \end{aligned} \tag{5.59}$$

where f_p is the elementary pinning force. The force in the direction of the positive x-axis is defined to be positive. The force balance on observed flux line is given by

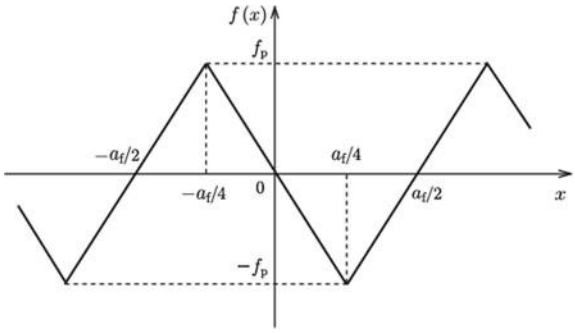

Fig. 5.23 One-dimensional periodic pinning model of Campbell [5]

$$k'_{\mathrm{f}}(\Delta - x) + f(x) = 0, \tag{5.60}$$

where Δ is the virtual position of the flux line if the pinning interaction does not occur and k'_{f} is the spring constant for the deformation of the flux line lattice. The first term in (5.60) is the restoring force against the displacement of the flux line by $x - \Delta$. This force balance holds under a given global driving force. The sum of the first term over N_{p} pinning centers gives the Lorentz force, and that of the second term gives the pinning force density.

The summation used here is carried out on all of the individual pinning centers in the superconductor. This is usually replaced by the statistical average multiplied by the number density of pinning centers N_{p}. This calculation method is called the statistical summation. The important point in this theoretical treatment is how to take into account the randomness of the spatial distribution of pinning centers. If we assume a perfect flux line lattice, it can be said that the relative position between each pinning center and its nearest flux line is random. It may be assumed that the positions of real flux lines can be approximately used instead of the lattice points of the perfect flux line lattice. Since flux lines are displaced due to the interaction with their corresponding pinning centers, however, the relative position between pinning center and flux line is not random, but there is a precise correlation between them. In the case of attractive pinning centers, for example, the probability of finding flux lines around pinning centers is high. Hence, the above-mentioned Δ that represents the position of the flux line when the pinning effect is virtually switched off is suitable for the statistical summation.

Here, we calculate the pinning force density. We assume the initial condition attained by the field-cooled process. It can be assumed that the virtual position Δ of the representative flux line is within the region $-a_{\mathrm{f}}/2 \leq \Delta < a_{\mathrm{f}}/2$. When Δ is given, the position of the flux line x can be determined graphically. When a straight line with slope k'_{f} is drawn from position Δ, as shown in Fig. 5.24, the dot-dashed line represents the first term in (5.60) with the opposite sign, and the point at which this line meets the pinning force $f(x)$ gives the solution for x. Note that the solution is different depending on the value of k'_{f} relative to $4f_{\mathrm{p}}/a_{\mathrm{f}}$.

For $k'_{\mathrm{f}} > 4f_{\mathrm{p}}/a_{\mathrm{f}}$ the position of the flux line in the initial condition is

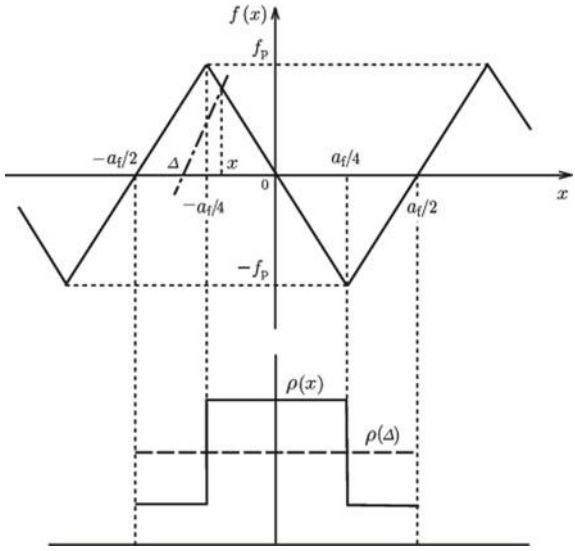

Fig. 5.24 Pinning force (upper panel) and statistical distribution of flux lines (lower panel) for $k_f' > 4f_p/a_f$

$$x = \frac{f_{pt}\Delta + (f_p a_f/2)}{f_{pt} - f_p};\ -\frac{a_f}{4}\left(3 - \frac{f_p}{f_{pt}}\right) \le \Delta < -\frac{a_f}{4}\left(1 + \frac{f_p}{f_{pt}}\right),$$
$$= \frac{f_{pt}\Delta}{f_{pt} + f_p};\ -\frac{a_f}{4}\left(1 + \frac{f_p}{f_{pt}}\right) \le \Delta < \frac{a_f}{4}\left(1 + \frac{f_p}{f_{pt}}\right), \tag{5.61}$$

where f_{pt} is given by

$$f_{pt} = \frac{k_f' a_f}{4}. \tag{5.62}$$

The above condition is written as $f_p < f_{pt}$. The statistical distribution of x, $\rho(x)$, is represented in the lower panel of Fig. 5.24. Flux lines are likely to stay around the center of the pinning center ($x = 0$), while the statistical distribution $\rho(\Delta)$ for the lattice point Δ of the perfect flux line is uniform. When flux lines are displaced in the direction of the positive x-axis, new flux lines come into the treated region from the left side, and the same number of flux lines go out of the region. As a consequence, the statistical distribution in Fig. 5.24 is unchanged. The pinning force density is calculated as

$$F_p = -\frac{N_p}{a_f}\int_{-a_f/2}^{a_f/2} f(x)\mathrm{d}\Delta = 0. \tag{5.63}$$

For $f_p > f_{pt}$, the position x is obtained as

$$x = \frac{f_{\mathrm{pt}}\Delta}{f_{\mathrm{pt}} + f_{\mathrm{p}}}; -\frac{a_{\mathrm{f}}}{2} \leq \Delta < \frac{a_{\mathrm{f}}}{2} \tag{5.64}$$

independently of Δ. The statistical distribution in the initial condition is shown in the middle panel of Fig. 5.25. There are unstable regions where flux lines do not stay. In the initial state, the distribution is symmetric with respect to $x = 0$, and the pinning force density is zero. When the flux lines are displaced in the direction of the positive x-axis, there is no change in the number of flux lines. The left unstable region becomes wider, while the right one becomes narrower. The critical state is attained when the flux front reaches $x = a_{\mathrm{f}}/4$. The corresponding distribution is shown in the lowest figure in Fig. 5.25. For further displacement, new flux lines come in from the left side, and the same number of flux lines go out on the right side. Thus, the distribution is in the steady state. The pinning force density in the critical state is [5]

$$F_{\mathrm{p}} = -\frac{N_{\mathrm{p}}}{a_{\mathrm{f}}} \int_{x_0}^{a_{\mathrm{f}}/4} \left(-\frac{4f_{\mathrm{p}}}{a_{\mathrm{f}}}x\right) \frac{\mathrm{d}\Delta}{\mathrm{d}x} \mathrm{d}x = N_{\mathrm{p}} f_{\mathrm{p}} \frac{f_{\mathrm{p}} - f_{\mathrm{pt}}}{f_{\mathrm{p}} + f_{\mathrm{pt}}}. \tag{5.65}$$

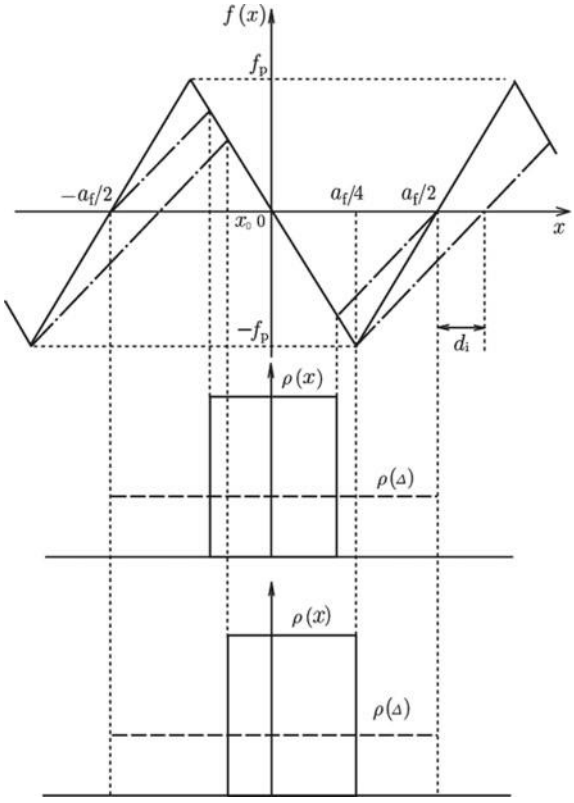

Fig. 5.25 Pinning force (upper panel), statistical distribution of flux lines in the initial state (middle panel), and that in the critical state (lower panel) for $k_{\mathrm{f}}' < 4f_{\mathrm{p}}/a_{\mathrm{f}}$

Here, we have used the relationship $\mathrm{d}\Delta/\mathrm{d}x = \left(f_{\mathrm{pt}} + f_{\mathrm{p}}\right)/f_{\mathrm{pt}}$ from (5.64), and x_0 represents the position of the flux line at the left edge given by

$$x_0 = \frac{a_{\mathrm{f}}}{4} \cdot \frac{f_{\mathrm{p}} - 3f_{\mathrm{pt}}}{f_{\mathrm{p}} + f_{\mathrm{pt}}}. \tag{5.66}$$

To obtain a nonzero pinning force density the elementary pinning force f_{p} should be larger than f_{pt}, which is called the threshold value of elementary pinning force.

The statistical calculation method was employed by Labusch [11] and Campbell [5]. Later, Kramer [1] found, however, that there was a significant discrepancy between the results of theoretical calculations and those of experiments on the threshold value. This raised doubt about the reliability of the statistical calculation method. As shown in Fig. 5.4, even defects with an elementary pinning force smaller by a factor of 10^4 than the threshold value can effectively work as pinning centers. This result may indicate that there is no threshold value.

The problem with the threshold value will be discussed later, but we will now discuss the situation in which the flux lines are displaced back in the direction of the negative x-axis from the condition shown in the lower panel of Fig. 5.25. The distribution changes through that in the middle panel of Fig. 5.25 to the symmetric distribution with respect to $x = 0$ in the lower panel. In the final state, the pinning force density is $-F_{\mathrm{p}}$. For a further displacement, the critical state is kept. This shows that the macroscopic irreversibility originates from the biased distribution of flux lines inside the pinning potential, which is associated with the instability of flux lines. That is, the unstable region appears on the opposite side to the direction of the Lorentz force, and the resultant pinning force works opposite to the Lorentz force. Such an instability is an assumption at this moment, but it will be proved theoretically in Sect. 5.6. The difference between the general irreversibility and the irreversibility inherent to the flux pinning will be discussed in Sect. 5.7. Zero pinning force density, i.e., reversibility, for flux pinning strength below f_{pt} is a consequence of the fact that the local pinning interaction is reversible. This indicates also that the irreversibility comes from the above point, which is another mechanism. Thus, both reversibility and irreversibility are explained by Campbell [5]. Note that the displacement of flux lines measured by experiments is estimated from that of Δ.

5.5 Pinning Loss Energy Density

In this section the pinning loss energy density is treated. All the loss energy is ohmic and caused by motion of normal electrons in the normal core, as mentioned in Sect. 4.3. Hence, it has been speculated that the loss energy depends on the flow resistivity ρ_{f} or viscous coefficient η. As shown in (5.39), however, the AC loss energy density does not depend on ρ_{f}. The material parameter that affects the loss energy is the critical current density J_{c} or the pinning force density F_{p}. How can we understand this result?

According to the explanation in Fig. 5.25, the phenomena are reversible when the flux lines move continuously within the pinning potential. In this situation there is no energy dissipation. It is suggested, therefore, that the energy is dissipated when the flux lines move very fast across the unstable region in which those cannot remain statically. Here, we analyze the unstable flux motion. It is assumed that the elementary pinning force is larger than the threshold value, so that the pinning is effective. We have to treat the dynamic force balance instead of the static one given by (5.60). The equation that describes the flux motion is

$$\eta^* v + k_{\mathrm{f}}'(\Delta - x) + f(x) - \eta^* \frac{\mathrm{d}x}{\mathrm{d}t} = 0, \tag{5.67}$$

where v is the mean velocity of flux lines and satisfies

$$v = \frac{\mathrm{d}\Delta}{\mathrm{d}t} \tag{5.68}$$

and η^* is the effective viscous coefficient for the flux lines in the volume N_{p}^{-1} given by

$$\eta^* = \frac{B\eta}{\phi_0 N_{\mathrm{p}}}. \tag{5.69}$$

The first term in (5.67) is the driving force needed to drive the flux lines in the representative region with the mean velocity v, and the second term is the restoring force against the distortion. The sum of these two terms gives the driving force. The third and fourth terms are the viscous force and the pinning force, respectively. Campbell's model is used again for the pinning force.

It is assumed that the flux line initially located at $-a_{\mathrm{f}}/4$ in Fig. 5.23 starts to move to the right side at time $t = 0$. The virtual position of the flux line Δ is defined as

$$\Delta = vt + \delta, \tag{5.70}$$

where δ is an unknown constant. The time at which the flux line reaches $a_{\mathrm{f}}/4$ is denoted by $t = t_1$. Equation (5.67) is easily solved and we have [12]:

$$x(t) = -\frac{a_{\mathrm{f}}}{4} + \frac{f_{\mathrm{pt}}}{f_{\mathrm{p}} + f_{\mathrm{pt}}}\left\{vt + K_1\left[1 - \exp\left(-\frac{t}{\tau_1}\right)\right]\right\};$$
$$0 \le t < t_1\left(-\frac{a_{\mathrm{f}}}{4} \le x < \frac{a_{\mathrm{f}}}{4}\right), \tag{5.71}$$

$$x(t) = \frac{a_{\mathrm{f}}}{4} - \frac{f_{\mathrm{pt}}}{f_{\mathrm{p}} - f_{\mathrm{pt}}}\left\{v(t - t_1) - K_2\left[\exp\left(\frac{t - t_1}{\tau_2}\right) - 1\right]\right\};$$
$$t_1 \le t < T\left(\frac{a_{\mathrm{f}}}{4} \le x < \frac{3a_{\mathrm{f}}}{4}\right), \tag{5.72}$$

where $T = a_f/v$ is the period and the other constants are given by

$$K_1 = \delta + \frac{a_f(f_p + f_{pt})}{4f_{pt}} + \frac{\eta^* v a_f f_p}{4f_{pt}(f_p + f_{pt})}, \tau_1 = \frac{\eta^* a_f}{4(f_p + f_{pt})}, \tag{5.73}$$

$$K_2 = \delta + vt_1 - \frac{a_f(f_p + f_{pt})}{4f_{pt}} + \frac{\eta^* v a_f f_p}{4f_{pt}(f_p - f_{pt})}, \tau_2 = \frac{\eta^* a_f}{4(f_p - f_{pt})}. \tag{5.74}$$

The conditions at $t = t_1$ and $t = T$ are respectively given by

$$vt_1 + K_1\left[1 - \exp\left(-\frac{t_1}{\tau_1}\right)\right] = \frac{a_f(f_p + f_{pt})}{2f_{pt}}, \tag{5.75}$$

$$vt_1 + K_2\left[\exp\left(\frac{a_f - vt_1}{v\tau_2}\right) - 1\right] = \frac{a_f(f_p + f_{pt})}{2f_{pt}}. \tag{5.76}$$

The movement of the position of the flux line (x) and that of its virtual position (Δ) are shown in Fig. 5.26 [13].

According to Yamafuji and Irie [14], the pinning loss power density is given by

$$P_p = \frac{B\eta}{\phi_0}\left(\langle \dot{x}_t \rangle^2 - v^2\right), \tag{5.77}$$

where $\dot{x} = dx/dt$ and $\langle\rangle_t$ represents the time average. The first term is the total loss power density EJ, and the second term is the apparent viscous loss power density given by E^2/ρ_f. That is, the pinning loss is an additional loss associated with the

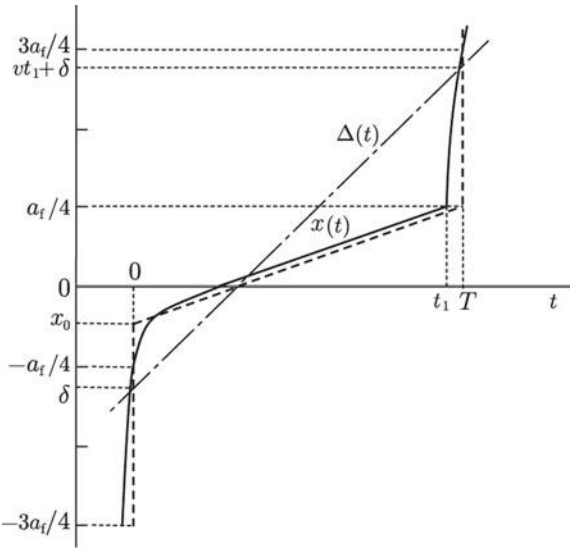

Fig. 5.26 Change in the position of the flux line (x) and in its virtual position (Δ) [13]. The dashed line shows the quasi-static motion of the flux line. The details are described in Appendix A.4

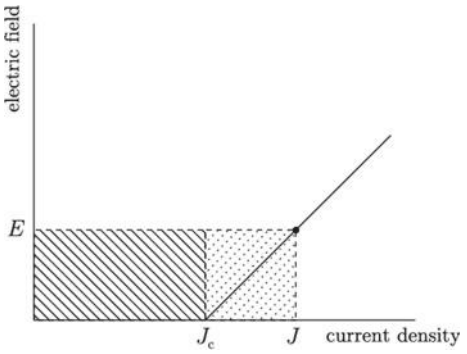

Fig. 5.27 The total loss power density is given by EJ. The dotted area is the apparent viscous loss power density, and the hatched area is the pinning loss power density

velocity fluctuation of the flowing flux line caused by the pinning interaction (see Fig. 5.27). In the condition of low flux velocity, small terms on the order of v^2 can be neglected and we have [13]

$$P_{\mathrm{p}} = \frac{N_{\mathrm{p}} f_{\mathrm{p}} \left(f_{\mathrm{p}} - f_{\mathrm{pt}}\right) v}{f_{\mathrm{p}} + f_{\mathrm{pt}}}. \tag{5.78}$$

The derivation of this result is shown in Appendix A.4. Using (5.65), the pinning loss power density is given by

$$P_{\mathrm{p}} = F_{\mathrm{p}} v, \tag{5.79}$$

which agrees with (5.33), as predicted by the critical state model. Campbell's model is used here. It is proved, however, that (5.79) holds in general, independently of the pinning model [15]. As shown here, the resultant pinning loss is not proportional to the viscous coefficient η but to the pinning force density, although the mechanism of the loss is the viscosity. In addition, it is independent of the mean velocity v. This clearly shows that the pinning loss is a hysteresis loss. The pinning loss power density is derived to be zero for $f_{\mathrm{p}} < f_{\mathrm{pt}}$. In this case all the loss is the viscous loss. Thus, the condition of effective pinning for the elementary pinning force, $f_{\mathrm{p}} > f_{\mathrm{pt}}$, is the same as the condition that the loss is a hysteresis loss.

In the Yamafuji-Irie model [14], a different pinning model than (5.59) was assumed and the pinning force density was derived from (5.77) and (5.79). The obtained pinning force density is proportional to $N_{\mathrm{p}} f_{\mathrm{p}}^2$, similar to the prediction of the statistical theory of Labusch. Nevertheless, the important feature that the pinning loss is independent of the viscous coefficient, but depends only on the pinning force density, is essentially the same as the present result.

On the other hand, very small loss energies owing to reversible flux motion are known. This indicates that the usual loss energy described by the critical state model is caused by the unstable flux motion inside and outside of the pinning potential. For the assumed continuous periodic pinning potential, the flux line velocity takes on a much larger value than v in the regions of $-a_{\mathrm{f}}/4 < x < x_0$ and $a_{\mathrm{f}}/4 < x < 3a_{\mathrm{f}}/4$,

i.e., in the continuous region of $-3a_f/4 < x < x_0$, and this leads to an appreciable loss, where x_0 is given by (5.66).

As shown above, the description of the summation theory for flux pinning and that of the loss energy caused by unstable flux motion are formally valid, and the essential problem is summarized as the determination of the threshold value of the elementary pinning force. In the next section, the summation theory is treated again to explore the threshold value problem.

5.6 Coherent Potential Approximation Theory

Larkin and Onchinnikov [16] proposed a new summation theory after the threshold value problem in the statistical theory of Labusch [11] was pointed out. The main point of this theory was that, since the pinning correlation lengths are finite, individual pinning forces in each correlated region are not perfectly cancelled out, resulting in a nonzero macroscopic pinning force density. One of the correlated lengths is Campbell's AC penetration depth, given by (5.52). This length gives the distance over which a perturbation such as displacement of flux lines extends and becomes shorter for stronger pinning. It was assumed in Labusch's theory that a perfect flux line lattice with long-range order, which gives the lattice point Δ, can be achieved by virtually switching off the interaction force of the representative pinning center alone. Since strains remain in the flux line lattice due to the many surrounding pinning centers, as pointed out by Larkin and Onchinnikov, the assumption in Labusch's theory is not correct. There are also points, however, in the Larkin-Onchinnikov theory. Although the pinning forces remain without being perfectly cancelled out in each correlated region, there is no theoretical proof of the assumption that these forces must be directed opposite to the Lorentz force. That is, it is impossible to explain the assumption in terms of the randomness alone. If individual pinning forces obey a Gaussian distribution with standard deviation σ, the pinning force in each correlated region can be approximated by a sum of pinning forces sampled randomly from the Gaussian distribution. If the number of samples is N, the pinning forces in each correlated region are known to obey another Gaussian distribution with standard deviation $\sqrt{N}\sigma$. The expected pinning force density, which is proportional to the average of this distribution, is zero. Since there is no interaction among correlated regions, the speculation by Larkin and Ovchinnikov might be allowed. This is, however, only a hope, and it is not possible to prove it. In addition, the correlation extends over the whole superconductor in the critical state. The unstable flux motion is inevitable for a finite pinning force density, which is also effective in the critical state. In addition, the distinction between the reversible and irreversible phenomena is not clear. In particular, the mechanism causing the irreversibility is not clearly given.

For this reason, we have to employ the statistical summation theory that can describe the irreversibility. Here, we will examine the problems in Labusch's theory. One of them is the point made by Larkin and Ovchinnikov on the pinning correlation lengths. In order to achieve long- range order in the flux line lattice, all pinning

interactions must be virtually switched off. In fact, if all pinning forces are zero, the pinning correlation length diverges, and perfect long-range order is achieved. Another problem is that Labusch's theory is not a mean field theory, although the Labusch parameter α_L is used to represent the mean strength of the pinning interactions. Here, a simple discrepancy is shown. Assume that the flux pinning is not effective because the pinning force is lower than the threshold. Thus, flux lines can move to any place, even with an infinitesimal driving force. Hence, they can move to places effective for pinning, resulting in a nonzero pinning force. In practice, flux lines cannot freely move under the interaction field of the surrounding pinning centers. It is expected, however, that there is a compatible situation between the statistically summed pinning force density and the interaction field. This is the essential standpoint of the mean field theory. In Labusch's theory, the spring constant in (5.60) is determined under the fixed condition of the flux line lattice at infinity. This may be based on the idea that the elastic interaction does not extend to infinity when only one pinning interaction is switched on. The elastic constant takes on a large value due to this condition, resulting in the large threshold value. The boundary condition at infinity must be free, however, if the pinning is not effective. In order to realize long-range order in the flux line lattice, all other pinning forces must also be virtually switched off. It is important to clarify how this virtual step contributes to deriving the spring constant.

Here, the coherent potential approximation theory [17] is introduced. This theory is a kind of mean field theory used for random systems. The mean interaction field of surrounding pinning centers is assumed first, and then, the pinning force density is formally determined under the influence of the mean field strength using a statistical method. Finally, the pinning force density and mean field strength are determined self-consistently. In the case of flux pinning phenomena in superconductors, the Labusch parameter α_L is used as a parameter representing the mean field strength of flux pinning. The mean spacing of pinning centers is denoted by d_p. Then, we have $N_p = d_p^{-3}$. The easiest way to perform the statistical summation is to employ a model in which each elementary region of flux lines includes a single pinning center. In this case, all elementary regions are equivalent to each other, and it is not necessary to consider the interaction among pinning centers in each elementary region. Hence, the volume of each elementary region is $V = d_p^3$. The details of the shape of the elementary region will be shown later.

If all the pinning interactions are virtually switched off at the same time to realize the long-range order in the flux line lattice, no information can be obtained. Hence, we first switch off the pinning force in a representative elementary region, as done by Labusch. We assume that the flux line interacting with the pinning center at x moves to x_0. The force balance in this case is

$$k_f(x_0 - x) + f(x) = 0, \tag{5.80}$$

where k_f is the spring constant. The first term is the restoring force against the displacement by $x_0 - x$. The result of Labusch's theory can be used for k_f. Next, we assume that all remaining pinning interactions are switched off. In this case the flux line lattice is perfect, and the observed flux line is assumed to move to Δ. This means

that the remaining pinning interactions exert an elastic restoring force proportional to the displacement $\Delta - x_0$. The corresponding spring constant is denoted by K. This is related to the Labusch parameter representing the strength of the pinning field. It should be noted that the elastic force caused by the surrounding pinning centers, $K(\Delta - x_0)$, is an internal force that is conveyed from one to another. Hence, it is nothing else than the elastic restoring force on the observed flux line given by the first term in (5.80). This force is balanced by the pinning force on the observed flux line:

$$K(\Delta - x_0) + f(x) = 0. \tag{5.81}$$

From (5.80) and (5.81), we obtain the force balance of (5.60) with

$$k_{\mathrm{f}}'^{-1} = k_{\mathrm{f}}^{-1} + K^{-1}. \tag{5.82}$$

Figure 5.28 schematically illustrates the elastic condition around the pinning center. The observed flux line interacting with the pinning center is also interacting elastically with other flux lines within the correlation length. This elastic interaction is due to the short-range distortion, and the corresponding spring constant is given by k_{f}. On the other hand, the flux lines in the elementary region are interacting with the surrounding pinning centers through the elasticity of the flux line lattice, the spring constant of which is K. The force balance treated here can be expressed as an elastic interaction connected in series. Based on the present argument, each size of the three-dimensional elementary region of flux lines is determined in proportion to the pinning correlation length in the corresponding direction (see Appendix A.5).

If we use k_{f}' given by (5.82), all the results in Sect. 5.4 can be used. Another important point is shown here. This is a relationship with (5.53). The interaction distance is generally in proportion to the flux line spacing as

$$d_i = \frac{a_{\mathrm{f}}}{\zeta}, \tag{5.83}$$

where ζ is a constant depending on the shape of the pinning centers, and we have $\zeta = 2\pi$ for point pins. Hence, the pinning force density is given by

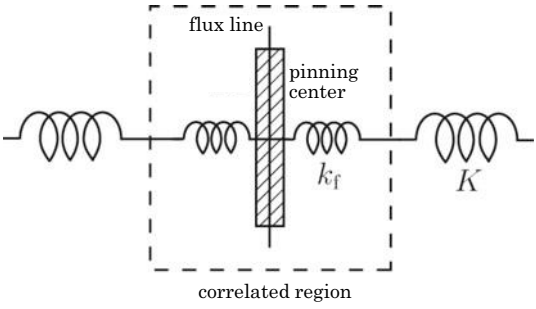

Fig. 5.28 Elastic interaction connected in series between the pinning center and its surroundings

$$F_{\mathrm{p}} = N_{\mathrm{p}} f_{\mathrm{p}} \frac{f_{\mathrm{p}} - f_{\mathrm{pt}}}{f_{\mathrm{p}} + f_{\mathrm{pt}}} = \alpha_{\mathrm{L}} \frac{a_{\mathrm{f}}}{\zeta}. \tag{5.84}$$

As mentioned above K is proportional to the Labusch parameter α_{L}, and hence, the right-hand side of (5.84) is proportional to the threshold value f_{pt}. It should be noted that f_{pt} is a quantity proportional to the strength of the mean pinning field, and (5.84) is the condition to obtain f_{pt} self-consistently. The details of the analysis are shown in Appendix A.5. If we set

$$f_{\mathrm{pt}} = t f_{\mathrm{p}}, \tag{5.85}$$

the equation to determine t is

$$\beta \cdot \frac{4 f_{\mathrm{p}}}{k_{\mathrm{f}} a_{\mathrm{f}}} \cdot \frac{1 - t}{1 + t} = \frac{t^2}{\left[\left(k_{\mathrm{f}} a_{\mathrm{f}} / 4 f_{\mathrm{p}} \right) - t \right]^2}, \tag{5.86}$$

where β is a constant given by

$$\beta = \frac{1}{16} \left(\frac{2}{\sqrt{3}\pi} \right)^{1/2} \left(\frac{C_{44}}{C_{66}} \right)^{5/6} \frac{\zeta d_{\mathrm{p}}}{a_{\mathrm{f}}}, \tag{5.87}$$

where C_{44} and C_{66} are the elastic moduli of flux line lattice for bending deformation and shear, respectively (see Appendix A.5). Usually, $C_{44} \gg C_{66}$, and β is sufficiently larger than unity.

Here the solution of t in (5.86) is simply investigated. The left-hand side takes on a positive finite value at $t = 0$, decreases monotonically with increasing t, and reaches 0 at $t = 1$. The right-hand side is 0 at $t = 0$, increases monotonically with increasing t, and diverges at $t = k_{\mathrm{f}} a_{\mathrm{f}} / 4 f_{\mathrm{p}}$. Hence, t surely has a solution smaller than 1, independently of the value of $k_{\mathrm{f}} a_{\mathrm{f}} / 4 f_{\mathrm{p}}$. Namely, the threshold value is a function of the elementary pinning force and never exceeds the elementary pinning force. Thus, a consistent solution is obtained, as is known from the mean field theory.

Here, we investigate the solution of t in (5.86), depending on the value of $k_{\mathrm{f}} a_{\mathrm{f}} / 4 f_{\mathrm{p}}$. If $k_{\mathrm{f}} a_{\mathrm{f}} / 4 f_{\mathrm{p}}$ is sufficiently large, as in the case of strong pinning, the left-hand side of (5.86) is very large. Hence, there is a solution in the vicinity of

$$t = \frac{k_{\mathrm{f}} a_{\mathrm{f}}}{4 f_{\mathrm{p}}} \tag{5.88}$$

at which the right-hand side diverges. Thus, from (5.65) we have

$$F_{\mathrm{p}} = N_{\mathrm{p}} f_{\mathrm{p}} \frac{1 - k_{\mathrm{f}} a_{\mathrm{f}} / 4 f_{\mathrm{p}}}{1 + k_{\mathrm{f}} a_{\mathrm{f}} / 4 f_{\mathrm{p}}}. \tag{5.89}$$

The obtained result obeys the linear summation of (5.4), and the pinning efficiency is given by [17]

$$\eta_{\mathrm{p}} = \frac{1 - k_{\mathrm{f}} a_{\mathrm{f}}/4f_{\mathrm{p}}}{1 + k_{\mathrm{f}} a_{\mathrm{f}}/4f_{\mathrm{p}}}. \tag{5.90}$$

The value of η_{p} is almost constant, and the linear summation holds over a relatively wide range of f_{p}.

In the case of weak pinning, in which $4f_{\mathrm{p}}/k_{\mathrm{f}}a_{\mathrm{f}}$ is very small, the right-hand side of (5.86) is small. This suggests that there is a solution in the vicinity of $t = 1$ around which the left-hand side is small. We replace t by one except in the numerator on the left-hand side and neglect t in the denominator on the right-hand side. Thus, we have

$$t \cong 1 - \frac{8f_{\mathrm{p}}}{\beta k_{\mathrm{f}} a_{\mathrm{f}}}, \tag{5.91}$$

and the pinning force density is given by

$$F_{\mathrm{p}} \cong \frac{4N_{\mathrm{p}} f_{\mathrm{p}}^2}{\beta k_{\mathrm{f}} a_{\mathrm{f}}}. \tag{5.92}$$

The obtained pinning force density obeys the statistical summation given by (5.5) [17]. As shown here, the coherent potential approximation theory explains the experimental results over a wide range of the elementary pinning force in Fig. 5.4.

The most important result obtained in this section is that the threshold value of the elementary pinning force exists formally, but it is always smaller than the elementary pinning force. That is, no substantial threshold value exists. Hence, the pinning loss in an AC magnetic field of sufficiently large amplitude is hysteresis loss, which depends only on the pinning force density, but not on the flow resistivity, as described by the critical state model.

The theoretical result obtained in this section can be extended to the flux flow state above the critical current density. This is supported by the fact that the time average and statistical average agree as

$$\frac{1}{T}\int_0^T f(x)\mathrm{d}t = \frac{1}{a_{\mathrm{f}}}\int_0^{a_{\mathrm{f}}} f(x)\mathrm{d}\Delta, \tag{5.93}$$

in the range of small v, where (5.68) and the relationship $T = a_{\mathrm{f}}/v$ are used. In fact, the agreement has been shown theoretically for various pinning models [12, 18]. This supports the dynamic critical state model of (5.41).

5.7 Critical State Theory

The irreversibility was derived using the statistical mean field approximation in Sect. 5.4. On the other hand, individual elementary energetic interactions with defects are reversible in nature, and this theoretical method also describes reversible behavior in the flux pinning phenomena, which can be observed experimentally. It is expected, therefore, that the flux pinning phenomena can be explained by first principles to minimize the relevant free energy, similarly to superconductivity, which is explained by minimizing the Ginzburg-Landau free energy.

In the critical state model, the balance between the Lorentz force and the pinning force is essential, and the energies related to the force balance are only the magnetic energy and the pinning energy. Practical superconductors to which the critical state model is applicable are type II superconductors with high κ values, and the condensation energy and the kinetic energy are relatively small enough to disregard. Thus, the free energy density to be treated is

$$\mathcal{F} = \frac{1}{2\mu_0}\boldsymbol{B}^2 + U_\mathrm{p}, \tag{5.94}$$

where U_p is the pinning energy density.

We assume that the flux line system is isolated and that there is no energy flow across the boundary to the surroundings. This situation corresponds to that in the field-cooled process, which is attained by cooling down the superconductor after applying a magnetic field. This situation also corresponds to the statistical distribution of magnetic flux lines in the middle panel of Fig. 5.25 and to the origin of Fig. 5.16. The flux line lattice is distorted by pinning interactions activated by cooling down, and current flows locally. The total current within the superconductor is zero, and the mean magnetic flux density is unchanged from the initial value, $\boldsymbol{B}_0$. It is assumed that the magnetic flux density varies slightly as $\boldsymbol{B} = \boldsymbol{B}_0 + \boldsymbol{b}$. Then, the magnetic energy density changes as

$$\mathcal{F}_\mathrm{m} = \frac{1}{2\mu_0}(\boldsymbol{B}_0 + \boldsymbol{b})^2 = \frac{1}{2\mu_0}\left(\boldsymbol{B}_0^2 + 2\boldsymbol{B}_0 \cdot \boldsymbol{b} + \boldsymbol{b}^2\right). \tag{5.95}$$

The displacement of flux lines that causes this change in the magnetic flux density is denoted by $\boldsymbol{u}$. Since the displacement of flux lines along their length is meaningless, $\boldsymbol{u}$ is perpendicular to $\boldsymbol{B}_0$. Using the continuity equation for flux lines, we have

$$\boldsymbol{b} = \nabla \times (\boldsymbol{u} \times \boldsymbol{B}_0) = (\boldsymbol{B}_0 \cdot \nabla)\boldsymbol{u} - \boldsymbol{B}_0 \nabla \cdot \boldsymbol{u} = B_0 \frac{\partial \boldsymbol{u}}{\partial \zeta} - \boldsymbol{B}_0 \frac{\partial u}{\partial \xi}, \tag{5.96}$$

where $\partial/\partial\zeta$ and $\partial/\partial\xi$ are derivatives along the directions of $\boldsymbol{B}_0$ and $\boldsymbol{u}$, respectively. The unit vectors along the respective directions are denoted by $\boldsymbol{i}_\zeta$ and $\boldsymbol{i}_\xi$. Then, the magnetic energy density, apart from the first constant term, is written as

$$\mathcal{F}_{\mathrm{m}} = \frac{B_0^2}{2\mu_0}\left[-2\frac{\partial u}{\partial \xi} + \left(\frac{\partial u}{\partial \zeta}\right)^2 + \left(\frac{\partial u}{\partial \xi}\right)^2\right]. \tag{5.97}$$

The condition needed to minimize the free energy density is given by Euler's equation (see Appendix A.6):

$$\frac{\partial \mathcal{F}}{\partial \boldsymbol{u}} - \boldsymbol{i}_\xi\left[\frac{\partial}{\partial \zeta}\frac{\partial \mathcal{F}}{\partial(\partial u/\partial \zeta)} + \frac{\partial}{\partial \xi}\frac{\partial \mathcal{F}}{\partial(\partial u/\partial \xi)}\right] = 0. \tag{5.98}$$

The first term is written as

$$\frac{\partial U_{\mathrm{p}}}{\partial \boldsymbol{u}} = -\boldsymbol{F}, \tag{5.99}$$

where $\boldsymbol{F}$ is the pinning force density. The second term is reduced to

$$-\boldsymbol{i}_\xi \frac{B_0^2}{\mu_0}\left(\frac{\partial^2 u}{\partial \zeta^2} + \frac{\partial^2 u}{\partial \xi^2}\right). \tag{5.100}$$

The current density is given by

$$\begin{aligned}\boldsymbol{J} &= \frac{1}{\mu_0}\nabla \times \boldsymbol{b} = \frac{1}{\mu_0}\left(B_0 \nabla \times \frac{\partial \boldsymbol{u}}{\partial \zeta} - \nabla \times \boldsymbol{B}_0 \frac{\partial u}{\partial \xi}\right) \\ &= \boldsymbol{i}_\eta \frac{B_0}{\mu_0}\left(\frac{\partial^2 u}{\partial \zeta^2} + \frac{\partial^2 u}{\partial \xi^2}\right),\end{aligned} \tag{5.101}$$

where $\boldsymbol{i}_\eta$ is a unit vector given by

$$\boldsymbol{i}_\eta = \boldsymbol{i}_\zeta \times \boldsymbol{i}_\xi. \tag{5.102}$$

The Lorentz force is written as

$$\boldsymbol{F}_{\mathrm{L}} = \boldsymbol{J} \times \boldsymbol{B}_0 = \boldsymbol{i}_\xi \frac{B_0^2}{\mu_0}\left(\frac{\partial^2 u}{\partial \zeta^2} + \frac{\partial^2 u}{\partial \xi^2}\right), \tag{5.103}$$

which is equal to (5.100) with the opposite sign. Hence, we obtain the force balance equation [19]:

$$\boldsymbol{F}_{\mathrm{L}} + \boldsymbol{F} = 0. \tag{5.104}$$

The Lorentz force is rewritten as

$$\boldsymbol{F}_{\mathrm{L}} = \boldsymbol{i}_\xi\left(C_{11}\frac{\partial^2 u}{\partial \xi^2} + C_{44}\frac{\partial^2 u}{\partial \zeta^2}\right), \tag{5.105}$$

where C_{11} is the elastic moduli of flux line lattice for uniaxial compression (see Appendix A.5). The first and second terms correspond to the magnetic pressure (Fig. 5.6) and the line tension (Fig. 5.7), respectively. Equation (A5.1) for elastic moduli of the flux line in Appendix A.5 is derived from this equation.

Before proceeding to the next step, we will discuss the magnetic energy density given by (5.97) in more detail. On averaging the magnetic energy density, the first term is zero and the second and third terms remain. In this equation the bending and uniaxial compressional strains are respectively given by

$$\frac{\partial u}{\partial \zeta} = \epsilon_\zeta, \frac{\partial u}{\partial \xi} = \epsilon_\xi. \tag{5.106}$$

Hence, (5.97) represents the strain energy density and can be described as

$$\mathcal{F}_\mathrm{m} = \frac{1}{2} C_{11} \epsilon_\xi^2 + \frac{1}{2} C_{44} \epsilon_\zeta^2. \tag{5.107}$$

The first and second terms are caused by the compressional and bending strains, respectively. The Lorentz force is an elastic restoring force against such strains of the flux lines. The increase in energy caused by such strains in the isolated flux line system is absorbed by the negative pinning energy, and the condition of force balance expressed by (5.104) is obtained. If there are no pinning interactions, such strains are not produced.

As shown above, the force balance (5.104) on the isolated flux line system can be derived from first principles. Then, this will be extended to non-isolated flux line systems. This is the process in which the statistical distribution of flux lines changes from the middle panel to the lower panel in Fig. 5.25 and corresponds to the variation from the origin to point A in Fig. 5.16. There is a slight difference in the calculations between the case of magnetic pressure in Fig. 5.6 and that of the line tension in Fig. 5.7. Here, we treat the case of the line tension. Please refer to [19] for the magnetic pressure.

Assume a wide superconducting slab that occupies $-d \leq z \leq d$. When a uniform magnetic field with the magnetic flux density B_0 is applied along the direction of the z-axis, the magnetic flux penetrates the slab uniformly due to the demagnetization factor. Then, a current of density J is applied along the y-axis. The magnetic flux density inside the slab is

$$\boldsymbol{B} = (B_x(z), 0, B_0), B_x(z) = \mu_0 J z. \tag{5.108}$$

Hence, the electric field induced along the y-axis while applying the current is obtained from (2.49) as

$$E_y(z) = \int_0^z \frac{\partial B_x}{\partial t} \mathrm{dz} = \frac{\mu_0 z^2}{2} \cdot \frac{\partial J}{\partial t}. \tag{5.109}$$

In the above we used the condition that the electric field is zero at the center $z = 0$, where the magnetic flux density does not change from symmetry. We assume that the current density is increased from J to $J + \delta J$ in a short period δt. The power that penetrates into the region between z and $z + \delta z$ through a unit area in the x-y plane in this period is calculated using Poynting's vector as

$$\begin{aligned}\delta P =& \frac{1}{\mu_0}\left[E_y(z+\delta z)B_x(z+\delta z) - E_y(z)B_x(z)\right] \\ =& \frac{3\mu_0 z^2 \delta z}{2} \cdot J\frac{\partial J}{\partial t}.\end{aligned} \tag{5.110}$$

Thus, the energy that comes into this region during this period is determined as

$$\delta \mathcal{F} = \frac{3\mu_0 z^2 \delta z}{2}\int_0^{\delta t} J\frac{\partial J}{\partial t}\mathrm{d}t = \frac{3\mu_0 z^2 \delta z}{2} J\delta J. \tag{5.111}$$

It should be noted that the internal magnetic energy changes during this period, since the internal magnetic flux density changes. When the current density is J, the magnetic energy at position z is

$$\frac{1}{2\mu_0}\left[B_0^2 + B_x^2(z)\right] = \frac{1}{2\mu_0}\left(B_0^2 + \mu_0^2 J^2 z^2\right). \tag{5.112}$$

When the current density is increased by δJ, the increase in the magnetic energy in a unit area of the x–y plane in the region between z and $z + \delta z$ is given by

$$\delta \mathcal{F}_\mathrm{m} = \frac{\mu_0}{2}\int_z^{z+\delta z}\left[(J+\delta J)^2 - J^2\right]z^2 \mathrm{d}z = \mu_0 J\delta J z^2 \delta z. \tag{5.113}$$

The difference in the energy is given by

$$\delta W = \delta \mathcal{F} - \delta \mathcal{F}_\mathrm{m} = \frac{\mu_0}{2} J\delta J z^2 \delta z, \tag{5.114}$$

which is the work done by the elastic restoring force when the magnetic structure changes. The displacement of flux lines δu along the x-axis due to the restoring force is obtained from the continuity equation for flux lines:

$$\frac{\partial \delta u(z)}{\partial z} = \frac{\delta B_x(z)}{B_0}, \tag{5.115}$$

which leads to

$$\delta u(z) = \frac{\mu_0 z^2}{2B_0}\delta J, \tag{5.116}$$

where $\delta B_x(z) = \mu_0 \delta J z$ is the increment of the x component of the magnetic flux density when the current is slightly increased. We have used the boundary condition $\delta u(0) = 0$. If we denote the elastic restoring force density by f, we have

$$f = \frac{1}{\delta z}\lim_{\delta J \to 0}\frac{\delta W}{\delta u} = JB_0. \tag{5.117}$$

Thus, the driving force density f is the Lorentz force, i.e., the line tension. On the other hand, the pinning force density is derived from the pinning energy density U_p and is formally the same as that for the isolated flux line system. Hence, the force balance (5.104) is obtained also for non-isolated systems [19].

As shown above, the energy penetrating the superconductor during the virtual displacement, which is obtained using Poynting's vector, is larger than the increase in the magnetic energy, and the additional energy density δW is independent of the magnetic flux distribution and cannot be seen in it. This will be discussed in more detail in Appendix A.7. In the above case the additional energy is absorbed as an increase in the pinning energy to realize the assumed magnetic flux distribution, i.e., the increase from the initial isolated state to the new equilibrium state after the displacement driven by the restoring force. Since the pinning energy is a kind of thermodynamic energy, it cannot be seen from the viewpoint of electromagnetism. The same result is obtained for the case of magnetic pressure.

As shown above, the driving force is proved to be the Lorentz force, and the Gibbs free energy density is generally described as

$$\mathcal{G} = \mathcal{F} - (\boldsymbol{J} \times \boldsymbol{B}) \cdot \boldsymbol{u}. \tag{5.118}$$

The force balance equation in the critical state model is derived from the condition of the minimum Gibbs free energy, $\partial \mathcal{G} / \partial \boldsymbol{u} = 0$ (see Appendix A.8).

The pinning force discussed up to now is reversible in nature and derived from the pinning energy. Finally, it is necessary to extend such a reversible pinning force to the irreversible one under practical conditions. This is done by the summation theory for flux pinning in Sect. 5.4. In the final state, the pinning force density $\boldsymbol{F}$ changes to the irreversible pinning force density with the maximum value $\boldsymbol{F}_\mathrm{p}$, and the force balance (5.104) changes to (5.6) in the critical state model.

As shown here, the critical state model that can explain various experimental results is no longer a phenomenological model but a rigorous theory. In particular, the summation theory used in the proof is regarded as a useful theory that can statistically derive a macroscopic irreversibility from the random interactions of many bodies among pinning potentials. The resultant irreversibility is caused by the biased flux distribution due to unstable flux motion inside pinning potentials. Hence, the origin of the irreversibility in this case is independent of the usual breaking of time reversal symmetry. Namely, the irreversibility in the flux pinning results from the difference

in the equation of motion before and after the instability. When flux lines move even slightly along the positive direction from the position at $x = -(3a_f/4)$ in Fig. 5.25, these flux lines move discontinuously to $x = x_0$ in the pinning potential. After that, even if the flux lines move in the opposite direction, they must go back continuously until they reach $x = -a_f/4$. That is, the situation is different from that before the instability. It is also shown that the first law of thermodynamics is not satisfied, if there is no energy dissipation. For the two kinds of irreversibility, refer to Appendix A.9.

Here, we consider the irreversibility in superconductors microscopically. The derivation of irreversibility is difficult, for example, for the motion of molecules, because of the time reversal symmetry of the equation of motion. On the other hand, the mechanism of the irreversibility is different in superconductors. Whereas molecules move freely in various directions, atoms, including those in defects that can pin flux lines, which are responsible for energy dissipation, are restrained and thermally vibrating around their equilibrium positions in a solid superconductor. When a current is applied to the superconductor in a magnetic field, the Lorentz force acts on it. It is assumed that the superconductor is fixed, so as not to move under the Lorentz force. Each atom around the defects is slightly displaced by the flux pinning interaction. In fact, distortion can be observed in superconductors, when the Lorentz force is present. In the condition where voltage appears, the Lorentz force causes motion of the flux lines. When flux lines are depinned, the atoms around defects that have pinned flux lines become free and start to oscillate. That is, the atoms acquire energy through interaction with flux lines from the source that supplies the current. As discussed in the summation theory, pinning centers are distributed randomly without any correlation with non-distorted lattice points (Δ) with long-range order. Each flux line is depinned when it reaches $\Delta = \delta(x = -3a_f/4)$ and the corresponding time t_0 is also random among the depinned flux lines for the above reason. If we denote the amplitude and angular frequency of oscillation of each atom by A and ω, respectively, the moment of each atom of weight m is represented as $Am\omega\cos[\omega(t - t_0)]$. Hence, if n is the number of atoms that oscillate around one pinning center, the moment that the superconductor of unit volume acquires during one cycle is given by

$$\frac{N_p nAm\omega}{2\pi} \int_0^{2\pi} \cos[\omega(t - t_0)]\mathrm{d}(\omega t_0) = 0, \tag{5.119}$$

where fluctuation is disregarded. Thus, it is not possible to take out kinetic energy from such motions of atoms. As a consequence, the oscillation energy becomes thermal energy, and the phenomenon is irreversible. If the motion of atoms is synchronized throughout the superconductor, the oscillation energy can be taken out as an ultrasonic energy.

Here, it is shown that flux lines driven by the Lorentz force transfer their energies irreversibly to the regions around pinning centers through pinning interactions. We do not discuss the consequent diffusion of the energy inside the superconductor,

however, since this process essentially contains the problem of the breaking of time reversal symmetry.

Coffee break (5)

Principle of minimum energy dissipation

It is assumed in the critical state model that the flux pinning interaction minimizes the change in the magnetic flux distribution caused by a change in the external magnetic field, etc. Here, we discuss the relationship between this assumption and the principle of minimum energy dissipation in irreversible thermodynamics. Assume that the magnetic field H_0, which is applied along the z-axis of a very wide superconductor ($x \geq 0$), is increased from 0 to H_m. We assume that the current density is given by $\lambda J_\mathrm{c} (0 < \lambda \leq 1)$. Note that the condition of λ smaller than 1 is realized for the reversible flux motion. In this case, the magnetic flux density near the surface is given by

$$B(x) = \mu_0 (H_0 - \lambda J_\mathrm{c} x)$$

in the region of $0 \leq x \leq H_0/\lambda J_\mathrm{c} \equiv x_0$. The velocity of magnetic flux lines in the vicinity of the surface is obtained from (5.34) as

$$Bv(x) = -\int_{x_0}^{x} \mu_0 \frac{\partial H_0}{\partial t} \mathrm{d}x = \mu_0 \frac{\partial H_0}{\partial t}(x_0 - x).$$

Hence, the loss power density in a unit area of the y-z plane is

$$\begin{aligned} P &= \int_0^{x_0} \lambda J_\mathrm{c} B v \mathrm{d}x = \mu_0 \lambda J_\mathrm{c} \frac{\partial H_0}{\partial t} \int_0^{x_0} (x_0 - x) \mathrm{d}x \\ &= \frac{\mu_0 \lambda J_\mathrm{c}}{2} \cdot \frac{\partial H_0}{\partial t} x_0^2 = \frac{\mu_0}{2\lambda J_\mathrm{c}} H_0^2 \frac{\partial H_0}{\partial t}. \end{aligned}$$

Thus, the loss energy in a unit surface area during the increase in the external magnetic field from 0 to H_m is given by

$$W = \int P \mathrm{d}t = \int_0^{H_\mathrm{m}} \frac{\mu_0}{2\lambda J_\mathrm{c}} H_0^2 \mathrm{d}H_0 = \frac{\mu_0}{6\lambda J_\mathrm{c}} H_\mathrm{m}^3.$$

The loss energy is at a minimum at $\lambda = 1$, i.e., the condition of maximum pinning, as assumed in the critical state model. In the above, $\lambda = 0$ corresponds to a special case, and the divergence of energy dissipation comes from the divergence of x_0. Since practical superconductors have finite sizes, the loss energy density is zero.

It should be noted that the result of the summation theory shown in Sects. 5.4 and 5.6 automatically satisfies this condition. Since the summation theory leads to the same result as the critical state model, it is also consistent with first principles. The state described by these theories in the quasi-static process is just in contact with the state derived by the principle of minimum energy dissipation (see Appendix A.10).

References

1. E.J. Kramer, J. Nucl. Mater. **72**, 5 (1978)
2. C.P. Bean, Phys. Rev. Lett. **8**, 250 (1962)
3. F. Irie, K. Yamafuji, J. Phys. Soc. Jpn. **23**, 255 (1967)
4. A.M. Campbell, J. Phys. C **2**, 1492 (1969)
5. A.M. Campbell, Philos. Mag. **37**, 149 (1978)
6. A.M. Campbell, J. Phys. C **4**, 3186 (1971)
7. T. Matsushita, T. Honda, K. Yamafuji, Mem. Fac. Eng., Kyushu Univ. **43**, 233 (1983)
8. F. Sumiyoshi, M. Matsuyama, M. Noda, T. Matsushita, K. Funaki, M. Iwakuma, K. Yamafuji, Jpn. J. Appl. Phys. **25**, L148 (1986)
9. S. Takács, A.M. Campbell, Supercond. Sci. Technol. **1**, 53 (1988)
10. T. Matsushita, N. Harada, K. Yamafuji, M. Noda, Jpn. J. Appl. Phys. **28**, 356 (1989)
11. R. Labusch, Cryst. Lattice Defects **1**, 1 (1969)
12. T. Matsushita, J. Phys. Soc. Jpn. **46**, 1109 (1979)
13. T. Matsushita, J. Phys. Soc. Jpn. **84**, 034705 (2015)
14. K. Yamafuji, F. Irie, Phys. Lett. A **25**, 387 (1967)
15. T. Matsushita, Teionkougaku **43**, 382, 468 (2008) (in Japanese)
16. A.I. Larkin, Yu.N. Ovchinnikov, J. Low Temp. Phys. **34**, 409 (1979)
17. T. Matsushita, Physica C **243**, 312 (1995)
18. T. Matsushita, E. Kusayanagi, K. Yamafuji, J. Phys. Soc. Jpn. **46**, 1101 (1979)
19. T. Matsushita, Jpn. J. Appl. Phys. **51**, 010109 (2012)

Chapter 6
Longitudinal Magnetic Field Effect

Abstract Under the usual electromagnetic conditions, magnetic flux lines and current are perpendicular to each other, and electromagnetic phenomena are determined by the balance between the Lorentz force and the pinning force. On the other hand, various peculiar phenomena are observed when a current is applied to a superconductor in a parallel magnetic field. These phenomena are introduced in this chapter. These phenomena are also determined by a general driving force on flux lines and the pinning force to maintain the distorted structure of the flux lines. The Lorentz force is zero, however, because the current and magnetic flux lines are parallel to each other. Hence, another force is driving the flux lines. Following the general idea that the driving force is a restoring force to release the distortion, it is easy to suppose that it is a torque to rotate the flux lines. In fact, this torque can be derived similarly from the principle of virtual displacement as was done in the derivation of the Lorentz force in Chap. 5. Various peculiar phenomena associated with the longitudinal magnetic field effect are generally explained by the rotational flux motion caused by the torque. These phenomena can occur only in superconductors with the pinning effect, and new phenomena that have not been considered in electromagnetism can be seen.

6.1 Experimental Results

The magnetic field produced by a current is usually normal to the current, and electromagnetic phenomena in superconductors are determined by the balance between the Lorentz force on flux lines and the pinning force, as described by the critical state model. Such a magnetic field is called a transverse magnetic field.

When a magnetic field is applied along the length of a superconducting wire or slab, and then, a current is applied, as shown in Fig. 6.1, electromagnetic phenomena completely different from those in transverse magnetic fields are observed. Since such a magnetic field is called a longitudinal magnetic field, these phenomena are classed together as the longitudinal magnetic field effect. The main phenomena are introduced here.

T. Matsushita, *Superconductivity and Electromagnetism*, Springer Series in Solid-State Sciences 195, https://doi.org/10.1007/978-3-030-67568-4_6

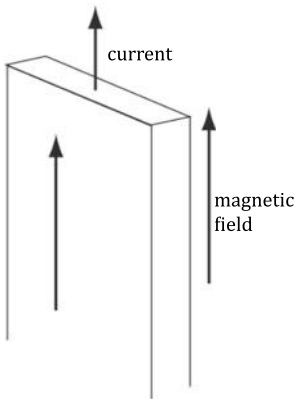

Fig. 6.1 Conditions for the longitudinal magnetic field

(1) **Increase in critical current density**

The critical current density decreases monotonically with increasing transverse magnetic field, except for the peak effect.[1] This is caused by the decrease in the condensation energy density with increasing magnetic field. In the longitudinal magnetic field, however, the critical current density increases with increasing magnetic field and takes on a much larger value than that in the transverse magnetic field, as shown in Fig. 6.2 [1]. This increase cannot be explained by a simple superposition of the magnetic field components. That is, the transverse magnetic field component is produced by the current, and if the Lorentz force caused by this field component determines the critical state, the critical current density cannot exceed the value in the self-field, i.e., the condition of zero external magnetic field. It is speculated, therefore, that some interaction between the applied longitudinal magnetic field and the transverse magnetic field caused by the current determines the distributions of the magnetic field and the current, i.e., the critical state in the whole superconductor.

[1] Peak effect: Phenomenon in the critical current density that shows a peak at some magnetic field caused by a suitable matching between flux lines and distributed pinning centers. Such a matching is realized by softened elasticity of flux lines due to a phase transition. In this case the critical current density starts to increase at some magnetic field and never starts at zero magnetic field, as shown in Fig. 6.2.

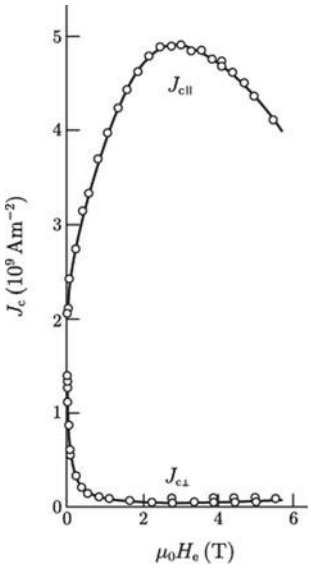

Fig. 6.2 Critical current density in the transverse magnetic field ($J_{c\perp}$) and that in the longitudinal magnetic field ($J_{c\parallel}$) in a Nb-Ti wire [1]

(2) **Paramagnetic effect**

Usually, superconductors show diamagnetism when an external magnetic field is applied. When a current is applied to a superconducting wire or slab in the diamagnetic state in a longitudinal magnetic field, magnetic flux penetrates the superconductor, resulting in a paramagnetic state. Figure 6.3 shows variations in the magnetization (upper panel) and the voltage (lower panel) when a current is applied to a superconducting cylinder in a longitudinal magnetic field [2]. It can be seen that the magnetization changes from diamagnetic to paramagnetic when the current is increased. The dashed line in the magnetization is the theoretical prediction of the force-free model that will be described later.

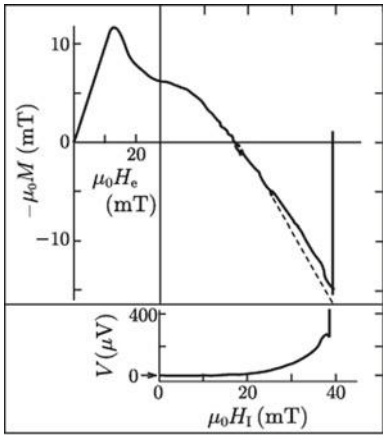

Fig. 6.3 Variations in the magnetization (upper panel) and the voltage (lower panel) when a transport current is applied to a Pb-Tl cylinder in a longitudinal magnetic field (H_e) [2]. H_I is the self-field due to the current, and the dashed line is the theoretical prediction of the force-free model

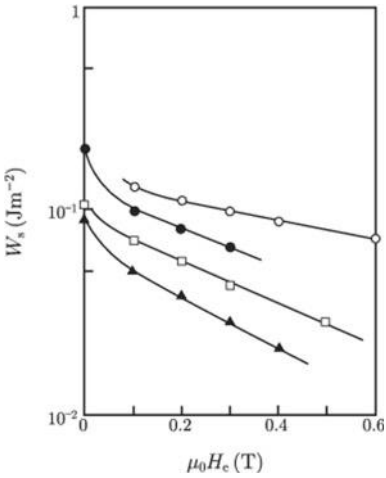

Fig. 6.4 Dependence of the AC current loss energy density in Nb-Ti wires on the DC longitudinal magnetic field [3]

(3) **Reduction in loss energy due to AC current**

The AC current loss energy is the loss energy produced by the self-field of the current. The loss energy is decreased by applying a longitudinal magnetic field. Figure 6.4 shows the observed loss energy density in Nb-Ti wires that carry AC current of a fixed amplitude as a function of the longitudinal DC magnetic field [3]. The loss energy density decreases with increasing longitudinal magnetic field. This can be attributed to the increase in the critical current density with the longitudinal magnetic field.

(4) **Breaking of Josephson's formula for induced electric field**

When the longitudinal and azimuthal electric field components were measured for a superconducting wire carrying a DC and superposed small AC current in a parallel magnetic field by the four-probe method and the pick-up coil method, respectively, the total electric field was found to be directed almost parallel to the DC magnetic field [4]. Since the magnetic field due to the current was sufficiently smaller than the applied DC magnetic field, this observation shows that Josephson's formula (4.41) does not hold. If this formula holds, the observed electric field must be normal to the DC magnetic field. Since both (2.49) and (5.34) hold, we have

$$\boldsymbol{E} = \boldsymbol{B} \times \boldsymbol{v} - \nabla\phi. \tag{6.1}$$

This relationship is of the same form as the electric field in materials that are not superconductors. Note that ϕ is not an electrostatic potential, since the electric field including the second term is an electric field induced by the AC magnetic field.

(5) **Resistive state**

The phenomenon described in (4) applies for a DC current that is lower than the critical current in a superconductor, and hence, that in a resistive state is not included. In

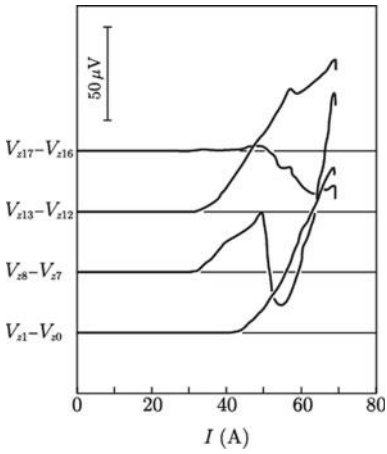

Fig. 6.5 Current versus longitudinal voltage characteristic at various positions in a Pb-Tl superconducting rod [5]. There is a region where the voltage takes on a negative value

the resistive state where the current is higher than the critical current, a surface electric field structure including a negative electric field region is observed. Figure 6.5 shows examples of the observed current versus the longitudinal voltage characteristics: It can be found that the observed voltage is negative with respect to the current direction at some position [5]. The surface electric field structure specified by the observed results is shown in Fig. 6.6 [5]. It can be seen that the cylindrical symmetry is broken and that regions with positive and negative electric fields with respect to the current direction form a helical structure. As will be shown later, Josephson's formula does not hold in this case either, and the electric field has the form of (6.1) again. This electric field is an induced electric field similar to that in the usual flux flow state.

The interpretation of the above experimental results reported in the 1970s is as follows:

(a) The force-free model that assumes that the magnetic flux density $\boldsymbol{B}$ and the current density $\boldsymbol{J}$ are locally parallel to each other was expected to hold [6]. This model explains the experimental results such as the paramagnetic magnetization, etc. This model can be described as

$$\boldsymbol{J} \times \boldsymbol{B} = 0. \tag{6.2}$$

This means that the Lorentz force on the flux lines is zero.

(b) Josephson derived (6.2) as an equation representing the equilibrium state in pin-free superconductors [7]. The result of Josephson's theory was considered to hold in the longitudinal magnetic field configuration. The equilibrium state in superconductors with pinning centers is given by (5.6).

(c) It was believed that flux lines that have penetrated the superconductor move translationally while keeping their angles [8]. If flux lines rotate, the induced

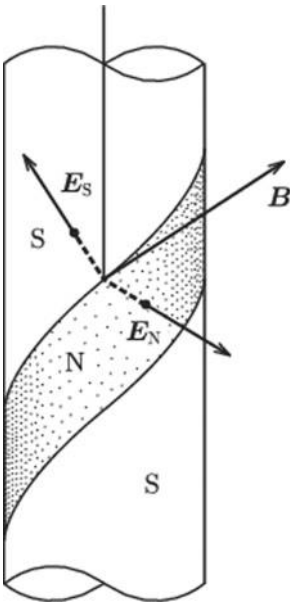

Fig. 6.6 Surface electric field structure specified by the observed results shown in Fig. 6.5 [5]. The region with the negative voltage is denoted by N

electric field and energy loss change, depending on the distance from the rotation center, as expected from (4.41) and (5.32), which contradicts the observed uniformity in these quantities. Namely, it was believed that the correspondence with mechanical systems holds, similarly to the phenomena in the usual transverse magnetic field as described by the critical state model.

(d) Flux cutting models were proposed to explain various electromagnetic phenomena [2, 4, 9, 10]. For example, the longitudinal electric field in the resistive state in Fig. 6.3 was attributed to the continuous penetration of the azimuthal component of the magnetic flux into the cylindrical superconductor with elimination at the center. On the other hand, this was considered to be contradictory to the observed constant longitudinal magnetization with time, if flux lines penetrate continuously. It was assumed that only the azimuthal flux component penetrates so as to be compatible with the constant longitudinal magnetization [2]. The situation is similar to the case of an induced longitudinal electric field explained in (4), which showed a deviation from Josephson's formula $\boldsymbol{E} = \boldsymbol{B} \times \boldsymbol{v}$ [4]. The authors proposed a flux cutting model assuming that the small azimuthal flux component goes in and out of the cylindrical specimen while the longitudinal component is stationary, as shown in Fig. 6.7, to explain the observed induced electric field roughly parallel to the magnetic flux.

(e) If the force-free state is stable, there is no mechanism to determine the critical current density in the longitudinal magnetic field configuration. Thus, it was

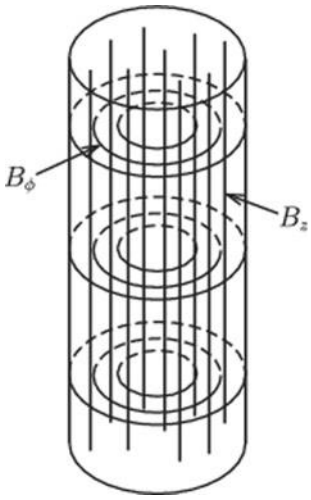

Fig. 6.7 Flux cutting between the longitudinal magnetic flux component (B_z) and the azimuthal component (B_ϕ) [4]

assumed that the threshold value of the flux cutting event determines the critical current density [11].

(f) There was no essential argument on the reason for the negative electric field observed in the resistive state.

In the above, it is considered that the force-free model explains the experimental results, although the reason why it holds is not clear. Other ideas are doubtful. Although the theory of Josephson may be expected to be the basis of the validity of the force-free model, this theory deals with pin-free superconductors. In superconductors in which the longitudinal magnetic field effect is observed, the effect of flux pinning is found to be as shown in Fig. 6.2. In addition, the critical current density in the longitudinal magnetic field also depends directly on the flux pinning strength, similarly to that in the transverse magnetic field. Figure 6.8a shows the variation in the critical current density in the transverse and longitudinal magnetic fields through the introduction of pinning centers by neutron irradiation [12]. The critical current density in the longitudinal magnetic field increases with introduction of pinning centers as does that in the transverse magnetic field. Figure 6.8b shows the correlation between the critical current densities in the transverse and longitudinal magnetic fields in Nb-50at.%Ta, in which the sizes and concentrations of Nb_2N normal precipitates working as pinning centers were changed [13]. A strong correlation can be seen between them. These results indicate that the critical current density in the longitudinal magnetic field goes to zero when there are no pinning centers in the superconductor, similarly to what occurs in the transverse magnetic field. In addition, the irreversibility in the observed magnetic phenomena also shows that flux pinning is involved in them. Hence, the theory of Josephson, which insists

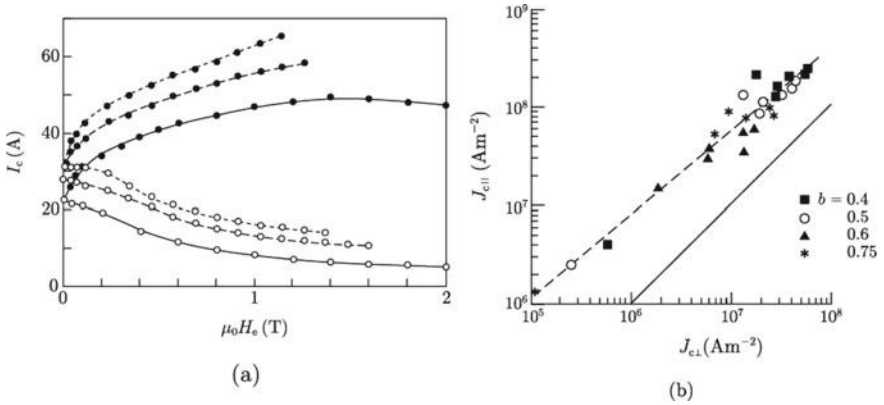

Fig. 6.8 **a** Critical current of Nb_3Sn tape in the transverse (○) and longitudinal (●) magnetic fields [12]. Both of them are increased through the introduction of defects by neutron irradiation. **b** Correlation between the critical current density in the transverse magnetic field ($J_{c\perp}$) and that in the longitudinal one ($J_{c\parallel}$) for Nb-50at.%Ta with Nb_2N normal precipitates [13]

that a force-free current parallel to flux lines can stably flow without flux pinning seems to be incorrect.

The author investigated personally an experimental result concerned with (c) as follows. It was based only on the information that the critical current was 30 A for a superconducting rod 0.8 mm in diameter in a longitudinal magnetic field of 14 mT. The self-field at the critical current is 7.5 mT. How much magnetic flux invades the superconductor during an increase in the self-field? Since the mean spacing of flux lines just before applying the current is 380 nm, when the flux lines near the surface move inward by this distance, the first row of flux lines penetrate the superconductor. This situation is realized when the current reaches 1.72 A. As shown in Appendix A.11, it was expected that flux lines did not penetrate translationally while maintaining their angle, but penetrated rotationally while changing their angle to result in a continuous variation in the magnetization under the boundary condition of the surface field. In addition, if the first row of flux lines penetrates translationally, the area of the transport current flow is restricted only in the region of the flux line penetration, resulting in a current density very much higher than the critical current density. When the current reaches the critical value, the current flows only in the region down to the depth of 0.12 mm from the surface, which is far different from the usual concept of the critical state. It cannot be explained why the superconductor goes into the resistive state when the current is increasesd more. That is, the flux lines must have a structure so that the current flows in the whole area. Hence, the axial flux lines that are already inside the superconductor must also rotate. This will be discussed again in Sect. 6.4. It is possible to try to explain this phenomenon by the mechanism of flux cutting. This will be discussed in the next paragraph.

If the flux cutting event occurs as assumed in (d), the flux lines that cut each other must grow close, as shown in Fig. 6.9, and it is considered that a significantly strong Lorentz force works locally on the flux lines to maintain their distance. There is no theoretical proof of the existence of a force that makes the flux lines grow closer to each other, overcoming the repulsive Lorentz force. Hence, it seems to be impossible for the flux cutting event to actually take place. The assumption was made that, when there are three flux lines A, B and C as illustrated in Fig. 6.10, the strong repulsive force from A to B helps the flux cutting between B and C. This is not realistic, however. When B approaches C, the force that pushes B to C is weakened. This force never exceeds the repulsive force between B and C. Even if the flux cutting event occurs based on this process, the needed current density exceeds the depairing current density. This means that the superconductivity is surely broken before the flux cutting occurs. Reconnection of magnetic flux lines in plasma may be imagined as a similar phenomenon. Such a phenomenon occurs when an extremely large energy dissipation event takes place. On the other hand, there is almost no energy dissipation during quasi-static variations in the superconductor. Hence, it is difficult or impossible for flux cutting similar to the reconnection to take place. Nevertheless, there are many young researchers who think that the flux cutting must explain the experimental results. It should be noted that there is a theoretical contradiction in this understanding. Josephson's theory that describes the relationship between the velocity of flux lines and the electric field does not hold. Hence, there is no reason to directly relate the electric field to the velocity of flux lines. In other words, the virtual process of flux cutting is meaningless, since it is based on Josephson's theory.

As to (e), the threshold value of the current density needed for the flux cutting is too high, and it exceeds the depairing current density. Hence, the idea of attributing the critical current density to the flux cutting is not realistic. In addition, the observed

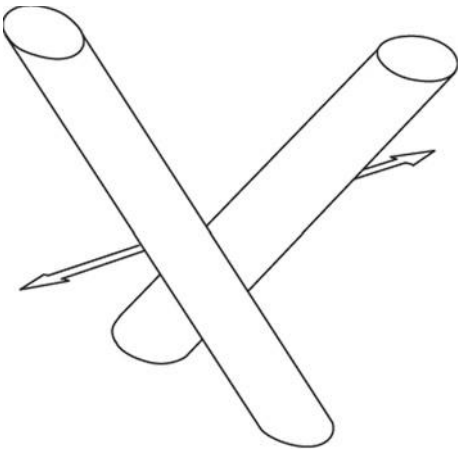

Fig. 6.9 Two flux lines growing closer to each other. The strong repulsive Lorentz force works to maintain the distance between the flux lines

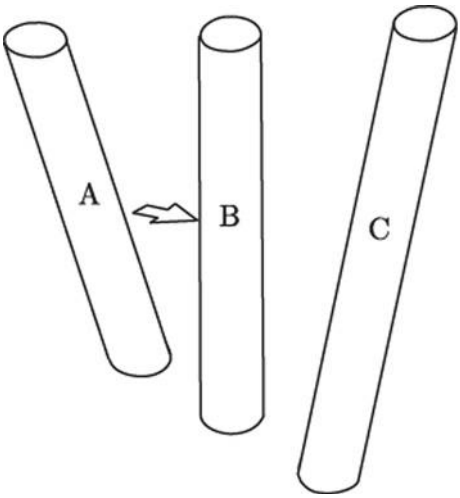

Fig. 6.10 Three flux lines repelling each other

critical current densities depend on the flux pinning strength. This indicates that some flux pinning mechanism determines the critical current density.

As to (f), there was an argument that the negative electric field might be introduced by the flux cutting, even though the negative electric field could not be explained by the flux cutting. In particular, the reason for the breaking of cylindrical symmetry associated with the surface electric field structure shown in Fig. 6.6 was not explained.

Various problems related to the flux cutting are generally discussed in Appendix A.12.

6.2 Clue to the Solution

Since the essential mechanism of the longitudinal magnetic field effects was not clarified, it is necessary to find a clue to the solution. The key point is the experimental result that the critical current density depends on the flux pinning strength, similarly to that in the usual transverse magnetic field, as shown in Fig. 6.8. This fact suggests that the flux pinning interaction stabilizes the distorted structure of flux lines introduced by the current. Under the usual transverse magnetic field, the distortion of flux lines caused by the current is a density gradient or bending deformation, as shown in Figs. 5.6b or 5.7b, respectively. The Lorentz force works to reduce these distortions. Even in the longitudinal magnetic field, a non-dissipative current can be carried in a stable manner, since the distorted structure of flux lines is expected to be stabilized by flux pinning interactions against the restoring force to release the distortion. Then, what kind of distortion exists in the flux lines in the force-free state?

Here we describe the magnetic flux density as

$$\boldsymbol{B} = B\boldsymbol{i}_B, \tag{6.3}$$

where $\boldsymbol{i}_B$ is a unit vector directed along $\boldsymbol{B}$. Then, the current density is

$$\boldsymbol{J} = \frac{1}{\mu_0}\nabla \times \boldsymbol{B} = -\frac{1}{\mu_0}(\boldsymbol{i}_B \times \nabla)B + \frac{1}{\mu_0}B\nabla \times \boldsymbol{i}_B. \tag{6.4}$$

Since the first term is normal to $\boldsymbol{B}$, it is not a force-free component. The second term is important. It is assumed for simplicity that the vector $\boldsymbol{B}$ stays in the x-z plane. Its angle from the z-axis is denoted by θ. Using the unit vectors $\boldsymbol{i}_x$ and $\boldsymbol{i}_z$ along the x- and z-axis, $\boldsymbol{i}_B$ is written as

$$\boldsymbol{i}_B = \boldsymbol{i}_x \sin\theta + \boldsymbol{i}_z \cos\theta. \tag{6.5}$$

If we assume that the angle θ varies only along the y-axis, the second term in (6.4) is reduced to

$$\boldsymbol{J} = \frac{1}{\mu_0} \cdot \frac{\partial B}{\partial y}\boldsymbol{i}_{\mathrm{L}} - \frac{B}{\mu_0} \cdot \frac{\partial \theta}{\partial y}\boldsymbol{i}_B, \tag{6.6}$$

where

$$\boldsymbol{i}_{\mathrm{L}} = \boldsymbol{i}_x \cos\theta - \boldsymbol{i}_z \sin\theta. \tag{6.7}$$

The first term in (6.6) is the current caused by the Lorentz force, i.e., the magnetic pressure, as expected. The second current is parallel to the magnetic flux density, i.e., the force-free current. This shows that, when the force-free current flows, the magnetic flux structure has distortion as shown in Fig. 6.11. That is, the angle of the flux lines staying on a plane changes along the direction perpendicular to the plane. This distortion is different from the density gradient and bending deformation shown in Figs. 5.6b and 5.7b, respectively.

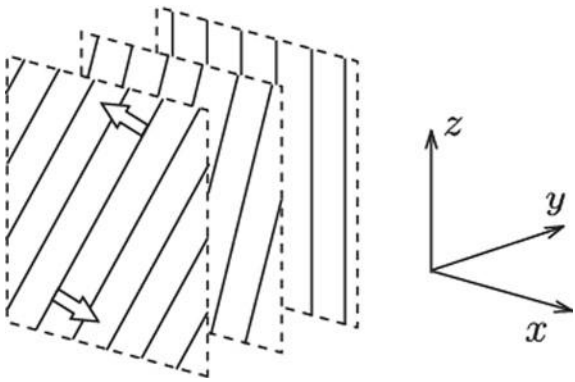

Fig. 6.11 Distorted structure of flux lines in the force-free state. It is expected that a torque works to release the distortion as shown by the arrows

Here, we realize the force-free state in a superconducting slab occupying $0 \leq y \leq 2d$. It is assumed that we apply the external magnetic field H_e along the z-axis, and then, the current I is applied in the same direction. The self-field along the x-axis due to the current is denoted by H_I. From symmetry we focus on half of the slab, $0 \leq y \leq d$. The magnetic flux density inside the slab has no y-component, and we can assume

$$\boldsymbol{B} = (B\sin\theta, 0, B\cos\theta), \tag{6.8}$$

where θ is the angle of the magnetic flux density measured from the z-axis. It can be assumed that the spatial variation occurs only along the y-axis. Then, the current densities along the x and z-axes are

$$J_x = \frac{1}{\mu_0} \cdot \frac{\partial}{\partial y} B\cos\theta = \frac{1}{\mu_0}\left(\frac{\partial B}{\partial y}\cos\theta - B\sin\theta\frac{\partial\theta}{\partial y}\right), \tag{6.9a}$$

$$J_z = -\frac{1}{\mu_0} \cdot \frac{\partial}{\partial y} B\sin\theta = -\frac{1}{\mu_0}\left(\frac{\partial B}{\partial y}\sin\theta + B\cos\theta\frac{\partial\theta}{\partial y}\right). \tag{6.9b}$$

If the current density is described as

$$\boldsymbol{J} = (J\sin\theta, 0, J\cos\theta), \tag{6.10}$$

it is parallel to $\boldsymbol{B}$ in (6.8). In this case the current components in (6.9a) and (6.9b) are

$$J\sin\theta = \frac{1}{\mu_0}\left(\frac{\partial B}{\partial y}\cos\theta - B\sin\theta\frac{\partial\theta}{\partial y}\right), \tag{6.11a}$$

$$J\cos\theta = -\frac{1}{\mu_0}\left(\frac{\partial B}{\partial y}\sin\theta + B\cos\theta\frac{\partial\theta}{\partial y}\right). \tag{6.11b}$$

Eliminating J, we have

$$\frac{\partial B}{\partial y} = 0. \tag{6.12}$$

This shows that the magnetic flux density is constant in the superconductor. This value is equal to that on the superconductor surface

$$B = \mu_0\left(H_\mathrm{e}^2 + H_I^2\right)^{1/2}. \tag{6.13}$$

This leads to the outcome that the current density depending on the magnetic flux density is also constant inside the superconductor. Substituting (6.12) into (6.11a) and (6.11b), we have

$$J = -\frac{B}{\mu_0} \cdot \frac{\partial \theta}{\partial y}. \tag{6.14}$$

Hence, the angle of flux lines is expressed as

$$\theta(y) = \theta_0 - \alpha_{\mathrm{f}} y, \tag{6.15}$$

where θ_0 is given by the boundary condition as

$$\theta_0 = \tan^{-1} \frac{H_I}{H_{\mathrm{e}}}. \tag{6.16}$$

From (6.14) and (6.15), α_{f} is expressed as

$$\alpha_{\mathrm{f}} = \frac{\mu_0 J}{B}. \tag{6.17}$$

Hence, the variation rate of the angle α_{f} is large, when the current density J is large. The variation in the angle and the distributions of the components of the magnetic flux density are shown in Figs. 6.12 and 6.13, respectively. In these figures, y_0 given by

$$y_0 = \frac{\theta_0}{\alpha_{\mathrm{f}}} \tag{6.18}$$

is the depth down to which the force-free state penetrates.

The transport current along the z-axis flowing in a unit length of the x-axis is H_I, and hence, it is self-consistent. The critical state is the state at which the current reaches the center, $y = d$. In this condition we have

$$\theta_0 = \alpha_{\mathrm{f}} d \equiv \theta_{\mathrm{c}}. \tag{6.19}$$

The self-field in this condition is

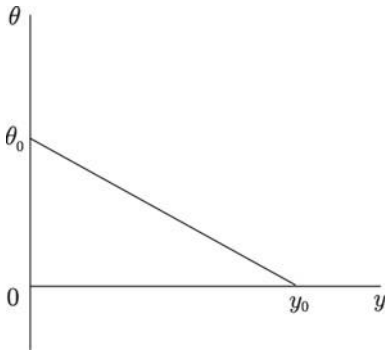

Fig. 6.12 Variation in the angle of flux lines in the superconductor

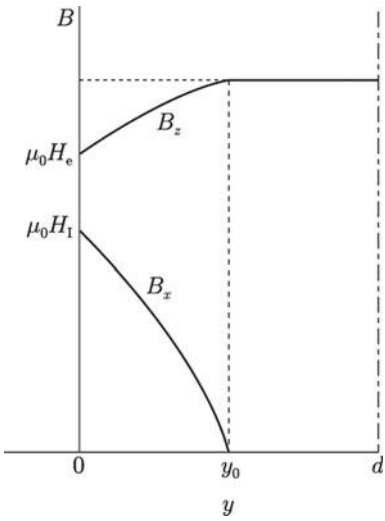

Fig. 6.13 Distribution of the components of the magnetic flux density

$$H_{Ic} = \frac{B}{\mu_0}\sin\theta_c. \tag{6.20}$$

In the force-free state the magnetic flux density given by (6.8) and the current density given by (6.10) have the same structure. In addition, the vector potential also has the same structure. As a result, we have

$$\boldsymbol{A} = \frac{1}{\alpha_f}\boldsymbol{B} = \frac{\mu_0}{\alpha_f^2}\boldsymbol{J}. \tag{6.21}$$

In the region where the force-free current flows, the magnetic energy density $(1/2\mu_0)\boldsymbol{B}^2$ is equal to $(1/2)\boldsymbol{A}\cdot\boldsymbol{J}$, and the quantity given by

$$\boldsymbol{A}\cdot\boldsymbol{B} = \frac{1}{\alpha_f}B^2 \tag{6.22}$$

has a non-zero value. Hence, in this state the magnetic helicity[2] is not zero. In normal conductors or superconductors under the transverse magnetic field discussed in Chap. 5, $\boldsymbol{A}$ and $\boldsymbol{B}$ are perpendicular to each other, and the quantity given by (6.22) is zero. Nonzero magnetic helicity in the static condition is only realized in superconductors in a longitudinal magnetic field. We can easily show that $\nabla\times\boldsymbol{J} = \alpha_f\boldsymbol{J} \neq 0$ for the force-free current. If Ohm's law holds as in normal materials, we have $\nabla\times\boldsymbol{E} \neq 0$ by multiplying the normal state resistivity, which contradicts the principle of the electrostatic field given by (2.19). Hence, it can be said that the

[2]Magnetic helicity: The volume integral of the scalar product of the vector potential and the magnetic flux density $\boldsymbol{A}\cdot\boldsymbol{B}$ is called the magnetic helicity. This quantity is commonly discussed in the case of a plasma in which the electromagnetic fields change with time.

longitudinal field effect is realized only in superconductors. The magnetic helicity is discussed in Appendix A.13.

Here, we show that the paramagnetic effect can be obtained in the force-free state. From the magnetic flux distribution given by (6.8), the longitudinal component of the magnetic flux density is

$$\begin{aligned}\langle B_z \rangle &= \frac{1}{d}\int_0^{y_0} B\cos\theta \mathrm{d}y + B\left(1 - \frac{y_0}{d}\right) \\ &= \frac{\mu_0 H_I}{\alpha_\mathrm{f} d} + \mu_0\left(H_\mathrm{e}^2 + H_I^2\right)^{1/2}\left(1 - \frac{\theta_0}{\alpha_\mathrm{f} d}\right). \end{aligned} \tag{6.23}$$

Hence, from (3.49) the magnetization is given by

$$M = \frac{H_I}{\alpha_\mathrm{f} d} + \left(H_\mathrm{e}^2 + H_I^2\right)^{1/2}\left(1 - \frac{\theta_0}{\alpha_\mathrm{f} d}\right) - H_\mathrm{e}. \tag{6.24}$$

The longitudinal component of the magnetic flux density is larger than the magnetic flux density of the external magnetic field $\mu_0 H_\mathrm{e}$, as can be seen from Fig. 6.13. Hence, the paramagnetic effect can be shown. In case of $H_\mathrm{e} \gg H_I$, we have $M \cong H_I^2/2H_\mathrm{e}$.

It is shown above that the force-free state explains the paramagnetic effect shown in Fig. 6.2. In this state, the flux lines are distorted, as shown in Fig. 6.11. From the analogy with the Lorentz force, therefore, a restoring reaction to release the distortion is expected. Since the condition $\theta(y) = 0$ is the state in which there is no current, the reaction is not a simple force, but rather is a torque that acts to rotate the flux lines, as indicated by arrows. This torque is expected to be derived from the energy increase when the distortion is virtually introduced, similarly to the derivation of the Lorentz force in Sect. 5.7. It is also expected that such a rotation of flux lines is able to solve the contradiction stated in (c) in Sect. 6.1. In addition, if we assume that the flux lines are rotated by a small angle $\Delta\theta$ from the z-axis to the x-axis, the variation in the z component of the magnetic flux is of the order of $(\Delta\theta)^2$, which is negligible, while the variation in the x component is of the order of $\Delta\theta$. Hence, the induced electric field is almost directed along the z-axis. Thus, the explanation of the breaking of Josephson's formula is also expected.

As shown in this section, various unique properties that cannot be found in the transverse magnetic field are observed in the longitudinal magnetic field.

6.3 Derivation of the Force Free Torque

In this section the force-free torque is derived from the principle of virtual displacement, similarly to the derivation of the Lorentz force in Sect. 5.7. Since the derivation of the pure torque is our aim, we assume a virtual displacement to directly achieve the

structure shown in Fig. 6.11, which is different from the common process of applying a magnetic field and then applying a transport current. This can be achieved by rotating the applied magnetic field. In the usual process the penetration of magnetic flux driven by the Lorentz force also occurs due to the self-field, resulting in a complex situation. Some experiments corresponding to the assumed process have been done. In this case, a uniform rotation of the magnetic flux is not easy, and hence, the superconductor is rotated in a uniform magnetic field, since the condition is relativistically the same.

Thus, we assume that an external magnetic field H_e is applied along the z-axis parallel to a superconducting slab, and then, the magnetic field is rotated to achieve the magnetic structure given by (6.8) and (6.15). In the case $B = \mu_0 H_e$. It is assumed that the penetration depth of the rotation y_0 does not change and that only α_f increases for the purpose of using a simple process to introduce the rotational strain. Under these conditions, it is better to rewrite (6.15) as

$$\theta = \alpha_f(y_0 - y). \tag{6.25}$$

The rotation of flux lines induces an electric field:

$$\boldsymbol{E} = (E_x, 0, E_z), \tag{6.26}$$

$$\begin{aligned} E_x(y) &= -B\frac{\partial \alpha_f}{\partial t}\int_{y_0}^{y}(y_0 - y)\sin\theta \mathrm{d}y = \frac{B}{\alpha_f^2}\cdot\frac{\partial \alpha_f}{\partial t}(\sin\theta - \theta\cos\theta), \\ E_z(y) &= -B\frac{\partial \alpha_f}{\partial t}\int_{y_0}^{y}(y_0 - y)\cos\theta \mathrm{d}y = \frac{B}{\alpha_f^2}\cdot\frac{\partial \alpha_f}{\partial t}(\theta\sin\theta + \cos\theta - 1). \end{aligned} \tag{6.27}$$

Poynting's vector on the superconducting surface ($y = 0$) is given by

$$\boldsymbol{S}_P = \frac{1}{\mu_0}(\boldsymbol{E}\times\boldsymbol{B})_{y=0} = \frac{B^2}{\mu_0\alpha_f^2}\cdot\frac{\partial \alpha_f}{\partial t}\left[\alpha_f y_0 - \sin(\alpha_f y_0)\right]\boldsymbol{i}_y, \tag{6.28}$$

which is directed towards the interior of the superconductor (along the positive y-axis). Hence, the power density that penetrates into the region of distorted area of the magnetic structure ($0 \le y \le y_0$) is

$$p = \frac{B^2}{\mu_0\alpha_f^2 y_0}\cdot\frac{\partial \alpha_f}{\partial t}\left[\alpha_f y_0 - \sin(\alpha_f y_0)\right] = \frac{B^2}{\mu_0\theta_0^2}\cdot\frac{\partial \theta_0}{\partial t}(\theta_0 - \sin\theta_0). \tag{6.29}$$

When the angle θ_0 is sufficiently small, expansion as $\sin\theta_0 \cong \theta_0 - \theta_0^3/6$ of $\sin\theta_0$ in the brackets in the above equation leads to

$$p = \frac{B^2}{6\mu_0}\theta_0\frac{\partial\theta_0}{\partial t}. \tag{6.30}$$

Thus, the energy density that penetrates the superconductor during the increase in the angle of the external magnetic field from 0 to θ_m is given by

$$w = \int p\mathrm{d}t = \frac{B^2}{6\mu_0}\int_0^{\theta_\mathrm{m}} \theta_0\mathrm{d}\theta_0 = \frac{B^2}{12\mu_0}\theta_\mathrm{m}^2. \tag{6.31}$$

The force-free torque density that works to release the introduced distortion is [14]

$$\Omega = \frac{\partial w}{\partial\theta_\mathrm{m}} = \frac{B^2}{6\mu_0}\theta_\mathrm{m} = \frac{1}{6}JBy_0. \tag{6.32}$$

Thus, the force-free torque density is proportional to the magnetic flux density and the current density, both of which correspond to the strength of the distortion. This is similar to the Lorentz force.

When the force-free current flows, the magnetic energy does not change, since the magnetic flux density does not change. The energy associated with the force-free distortion shown in Fig. 6.11 penetrates the superconductor, however. This must be the work done by the torque, which is similar to the work done by the Lorentz force in the usual transverse magnetic field (see Appendix A.7). Under practical conditions, this additional energy is absorbed as an increase in the pinning energy, i.e., a kind of thermodynamic energy. As a consequence, the distorted flux line structure is stabilized by the pinning interaction. If there is no pinning interaction, the distorted structure cannot be stabilized, resulting in a resistive state. Thus, the static critical state is determined by the torque balance between the force-free torque density and the pinning torque density $\boldsymbol{\Omega}_\mathrm{p}$ [14]

$$\boldsymbol{\Omega} + \boldsymbol{\Omega}_\mathrm{p} = 0. \tag{6.33}$$

This result is derived by minimizing the Gibbs free energy and is similar to the derivation of the force-balance (5.6) (see Appendix A.8). Equation (6.33) is consistent with the experimental results showing that the critical current density depends on the flux pinning strength. On the other hand, the above theoretical treatment essentially denies the mechanism of flux cutting [15]. That is, flux cutting is a mechanism of magnetic interaction between flux lines, and hence, it is independent of the flux pinning. In addition, the energy that was introduced as work done by the driving torque cannot be stored as a pinning energy. Thus, the principle of energy conservation is not fulfilled. See the details in (2) in Appendix A.12.

Note the fact that the magnetic torque appears in spite of the lack of any magnetic force, i.e., the Lorentz force. Such a situation cannot be found in dynamics, in which the torque is a moment of a force. Namely, no torque exists, if there is no force. The force-free torque density is independent of the size of the superconductor, whereas the mechanical torque density becomes large as the distorted body becomes large. This is because the relative displacement becomes large between two points in adjacent planes as the distance from the rotation center becomes large. This is essentially different from the correspondence between the electromagnetic phenomena in the transverse magnetic field and mechanical phenomena in dynamics. This will be discussed in more detail in Sect. 6.6.

Here, we show the experimental result that directly demonstrates that the critical current density in the longitudinal magnetic field is determined by the torque balance. One of the main factors in the summation in the longitudinal magnetic field is the elementary pinning torque, while its counterpart in the transverse magnetic field is the elementary pinning force f_p. The elementary pinning torque is given by the product of the elementary pinning force and the spacing of two adjacent pinning centers, $d_p = N_p^{-1/3}$, i.e., the moment of the pinning force $f_p d_p$. In Fig. 6.14, the critical current density in the longitudinal magnetic field is compared with the product of the elementary pinning torque $f_p d_p$ and the number density of pinning centers N_p, i.e., the prediction of the direct summation of the pinning torque density for Pb–Bi superconductor with normal Bi precipitates as pinning centers [16]. Since the observed critical current density is proportional to this product, we can say that a linear summation holds for the pinning torque density. As a result, the critical current density in the longitudinal magnetic field is proportional to $N_p^{2/3} f_p$. On the other hand, the critical current density of this superconductor in the transverse magnetic field is proportional to $N_p f_p$ and obeys the linear summation of (5.4). Hence, when the pinning becomes stronger due to an increase in N_p, the difference in the critical current density between the two magnetic fields becomes smaller, as shown in Fig. 6.8b. Thus, the result in Fig. 6.14 also explains such a trend.

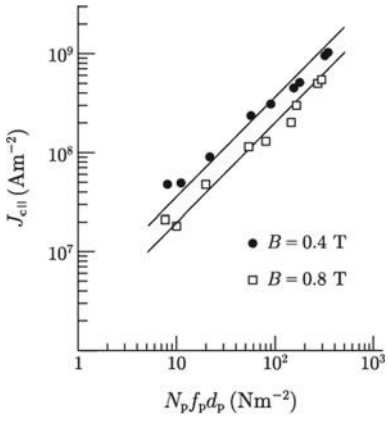

Fig. 6.14 Relationship between the critical current density in the longitudinal magnetic field and the direct summation of the pinning torque density for Pb-Bi superconductor with normal Bi precipitates as pinning centers [16]. The solid lines show the theoretical predictions of the linear summation

6.4 Electromagnetic Phenomena Caused by Rotation of Flux Lines

The flux pinning interactions determine the critical current density, as discussed above. This is supported by the experimental result that observed electromagnetic phenomena are irreversible. When an alternating transport current or a small alternating transverse magnetic field is applied to a long superconducting slab in a longitudinal direct magnetic field, an alternating magnetic flux penetrates, as shown in Fig. 6.15. This is a linear distribution similarly to the description by the critical state model shown in Fig. 5.9 and suggests that the force-free state given by (6.8) and (6.15) is attained throughout the superconductor (note that the angle θ is sufficiently small because of the longitudinal magnetic field of 0.290 T) [17].

Although such experiments show that the force-free state is realized, this state does not suddenly appear only by application of the longitudinal magnetic field. From the concept of the critical state model, it seems to be natural to assume that the area in which the force-free state is attained gradually penetrates the superconductor with increasing applied current. Here, we investigate the flux motion during the process in which the force-free state is established.

We assume that the magnetic field H_e is applied along the z-axis to a sufficiently wide superconducting slab that occupies $0 \leq y \leq 2d$. For simplicity it is assumed that the magnetic flux density is uniform and given by $\mu_0 H_e$ in the superconductor. Then, the transport current I is applied along the z-axis. We can assume that there is no spatial variation along the x- and z-axes because of the width of the superconductor. From symmetry it is enough to consider half of the slab, $0 \leq y \leq d$. If the width is denoted by w, the self-field of the current is $H_I = I/2w$, and the magnetic flux density on the superconductor surface ($y = 0$) is given by

$$B = \mu_0 \left(H_e^2 + H_I^2\right)^{1/2}. \tag{6.34}$$

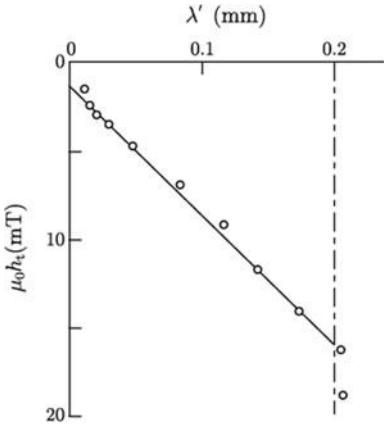

Fig. 6.15 Distribution of the transverse magnetic flux density observed by the similar method to that shown in Fig. 5.17 for a Na-Ta slab specimen in the force-free state in a longitudinal magnetic field of 0.290 T [17]. The gradient of the slope is proportional to the critical current density

The practical magnetic flux distribution is formally given by (6.8) and (6.15), as discussed before, whereas the variation rate of the angle α_f is not given by (6.17) but is a constant given by

$$\alpha_f = \frac{\mu_0 J_c}{B}. \tag{6.35}$$

In this case the angle of the magnetic flux density is

$$\begin{aligned} \theta &= \theta_0 - \alpha_f y; \ 0 \le y < \theta_0/\alpha_f, \\ &= 0; \qquad\quad \theta_0/\alpha_f \le y \le d, \end{aligned} \tag{6.36}$$

where θ_0 is given by

$$\theta_0 = \tan^{-1}\left(\frac{H_I}{H_e}\right). \tag{6.37}$$

The area from the surface ($y = 0$) to the depth θ_0/α_f is in the force-free state.

Here we denote the velocity of the flux lines as

$$\boldsymbol{v} = \left(v_x, v_y, v_z\right). \tag{6.38}$$

In the above, only v_y represents the penetration of magnetic flux contributing to the variation in the magnetic flux density. From symmetry, we can assume that this component does not depend on x and z. Since the flux motion in x-z planes does not bring about any variation in the magnetic flux density, the divergence of $\boldsymbol{v}$ must be zero in these planes. Thus, the condition

$$\frac{\partial v_x}{\partial x} + \frac{\partial v_z}{\partial z} = 0 \tag{6.39}$$

must be satisfied. Since the velocity $\boldsymbol{v}$ is defined to be normal to the magnetic flux density $\boldsymbol{B}$, the condition of (6.39) is written as

$$v_x \sin\theta + v_z \cos\theta = 0. \tag{6.40}$$

Using (6.39) and (6.40), the continuity equation for flux lines (5.34) is written as (see Appendix A.14)

$$\frac{\partial B}{\partial t} = -B\frac{\partial v_y}{\partial y} \tag{6.41}$$

and

$$\frac{\partial\theta}{\partial t} = \alpha_{\mathrm{f}} v_y + \frac{1}{\sin\theta\cos\theta} \cdot \frac{\partial v_x}{\partial x}. \tag{6.42}$$

Here we assume a quasi-static process. That is, the variation with time comes only through the variation in the self-field H_I of the current. Then, the left-hand sides of (6.41) and (6.42) are respectively given by

$$\frac{\partial B}{\partial t} = \mu_0 \sin\theta_0 \frac{\partial H_I}{\partial t} \tag{6.43}$$

and

$$\frac{\partial\theta}{\partial t} = \frac{\partial\theta_0}{\partial t} = \frac{\mu_0\cos\theta_0}{B} \cdot \frac{\partial H_I}{\partial t}. \tag{6.44}$$

Using (6.41) and (6.42), we have the solutions of each component of the flux line velocity in the region $0 \le y < \theta_0/\alpha_{\mathrm{f}}$ [18]

$$\begin{aligned} v_x &= \frac{\partial\theta_0}{\partial t}\cos\theta\left[1 - \frac{H_I}{H_{\mathrm{e}}}\alpha_{\mathrm{f}}(d-y)\right]\left[x\sin\theta + z\cos\theta + g_{\mathrm{r}}\left(y - \frac{\theta_0}{\alpha_{\mathrm{f}}}\right)\right], \\ v_y &= \frac{\partial H_I}{\partial t} \cdot \frac{\mu_0^2 H_I}{B^2}(d-y), \\ v_z &= -\frac{\partial\theta_0}{\partial t}\sin\theta\left[1 - \frac{H_I}{H_{\mathrm{e}}}\alpha_{\mathrm{f}}(d-y)\right]\left[x\sin\theta + z\cos\theta + g_{\mathrm{r}}\left(y - \frac{\theta_0}{\alpha_{\mathrm{f}}}\right)\right], \end{aligned} \tag{6.45}$$

where g_{r} is a function that satisfies

$$g_{\mathrm{r}}(0) = 0. \tag{6.46}$$

In a plane of $y = \text{const.}$, v_x and v_z take on the value of zero on the line given by

$$x\sin\theta + z\cos\theta + g_{\mathrm{r}}\left(y - \frac{\theta_0}{\alpha_{\mathrm{f}}}\right) = 0. \tag{6.47}$$

Here we watch one flux line and its intersection point P, with the line expressed by (6.47), i.e., the point at which the velocity components are zero is denoted by (x_0, y, z_0). Then, the velocity components are expressed as

$$\begin{aligned} v_x &= r\frac{\partial\theta_0}{\partial t}\cos\theta\left[1 - \frac{H_I}{H_{\mathrm{e}}}\alpha_{\mathrm{f}}(d-y)\right], \\ v_z &= -r\frac{\partial\theta_0}{\partial t}\sin\theta\left[1 - \frac{H_I}{H_{\mathrm{e}}}\alpha_{\mathrm{f}}(d-y)\right], \end{aligned} \tag{6.48}$$

where

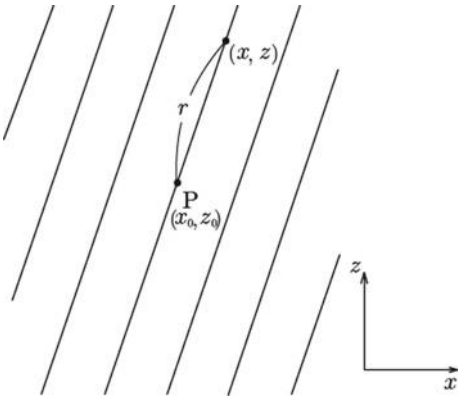

Fig. 6.16 Relationship between the rotation center P of a flux line and an arbitrary point on it

$$r = (x - x_0)\sin\theta + (z - z_0)\cos\theta \tag{6.49}$$

is the distance of a point on the flux line measured from the static point P, i.e., the rotation radius (see Fig. 6.16). Thus, the obtained solution of (6.45) supports the expectation that the rotational motion of flux lines really takes place. The fact that this solution satisfies the continuity equation for flux lines is easily proved (see Appendix A.15). This rotational motion of flux lines is caused by the force-free torque. If the flux pinning effect is disregarded for simplicity, the solution of $\boldsymbol{v}$ in the region of $\theta_0/\alpha_\mathrm{f} < y < d$ is given by

$$\begin{aligned} v_x &= 0, \\ v_y &= \frac{\partial H_I}{\partial t} \cdot \frac{\mu_0^2 H_I}{B^2}(d - y), \\ v_z &= 0. \end{aligned} \tag{6.50}$$

In this region the rotation of flux lines does not occur, and (4.41) holds for the electric field. In reality v_y changes slightly due to the force balance condition. If you are interested in it, the derivation of the solution is recommended.

Here we derive the induced electric field in the area $0 \le y < \theta_0/\alpha_\mathrm{f}$. From (2.49) the electric field is estimated as

$$E_x(y) = \int_d^y \frac{\partial}{\partial t}(B\cos\theta)\mathrm{d}y, \quad E_z(y) = -\int_d^y \frac{\partial}{\partial t}(B\sin\theta)\mathrm{d}y, \tag{6.51}$$

where we used the condition $\boldsymbol{E} = 0$ at the center $y = d$. A simple calculation derives

$$\begin{aligned} E_x &= -\frac{\mu_0}{\alpha_\mathrm{f}} \cdot \frac{\partial H_I}{\partial t}[\cos(\theta_0 - \theta) - \cos\theta_0 + (\alpha_\mathrm{f} d - \theta_0)\sin\theta_0]; && 0 \le y < \frac{\theta_0}{\alpha_\mathrm{f}}, \\ &= -\mu_0 \frac{\partial H_I}{\partial t}(d - y)\sin\theta_0; && \frac{\theta_0}{\alpha_\mathrm{f}} \le y \le d, \end{aligned}$$

$$\begin{aligned} E_z &= \frac{\mu_0}{\alpha_\mathrm{f}} \cdot \frac{\partial H_I}{\partial t}[\sin\theta_0 - \sin(\theta_0 - \theta)]; \quad 0 \le y < \frac{\theta_0}{\alpha_\mathrm{f}}, \\ &= 0; \qquad\qquad\qquad\qquad\qquad\qquad \frac{\theta_0}{\alpha_\mathrm{f}} \le y \le d. \end{aligned} \tag{6.52}$$

This result shows that the electric field takes on a uniform value on the x-z plane, whereas the rotational motion occurs on it. Thus, it can be shown that Josephson's formula does not hold; the electric field obeys (6.1) [18]. It should be noted that the electric field is always an induced one, and the scalar function ϕ is not an electrostatic potential. In particular, the dissipated power density is given by

$$P = \boldsymbol{E} \cdot \boldsymbol{J} = -\boldsymbol{J} \cdot \nabla\phi \tag{6.53}$$

and the term $\boldsymbol{B} \times \boldsymbol{v}$ does not contribute to the energy dissipation. Thus, the term $-\nabla\phi$ is more important.

It has been clarified that the axial magnetic flux lines inside the superconductor must also rotate when the current is applied, as discussed in Sect. 6.1. This can also be shown as follows: The increase in the magnetic flux density on the surface due to the self-field H_I of an applied current in the longitudinal magnetic field of H_e is $b_0 = \mu_0 H_I^2/2H_\mathrm{e}$. When H_I is small, this value is very small, and the penetration depth of new flux lines is very small. On the other hand, the penetration depth of the force-free structure, i.e., that of the rotational motion of flux lines, is proportional to H_I and is much deeper than the estimated penetration depth of new flux lines. This supports the above speculation. Such a rotation of inner flux lines is considered to be caused by the interaction with new tilted flux lines to reduce the angular difference between them.

This result shows that the motion of flux lines in the longitudinal magnetic field is not similar to that in mechanics, since it is different from the situation in the transverse magnetic field, as mentioned in Sect. 6.1. Thus, the idea that the observed phenomena cannot be explained without assuming the flux cutting event is not correct. In particular, it can be shown from (6.52) that the angle of the induced electric field on the surface is

$$\frac{E_x(0)}{E_z(0)} = -\frac{1 - \cos\theta_0}{\sin\theta_0} = -\tan\frac{\theta_0}{2}, \tag{6.54}$$

even when the force-free area reaches the center ($\theta_0 = \alpha_\mathrm{f} d$). Usually $\theta_0 \ll 1 (H_I \ll H_\mathrm{e})$, and the electric field is directed almost parallel to the longitudinal magnetic field, as observed in experiments. All the mistakes start from the attempt to understand the electromagnetic phenomena in the longitudinal magnetic field similarly to the phenomena in dynamics, which was successful for those in the transverse magnetic field. On the other hand, the continuity equation for flux lines is consistent with Maxwell's equations, and its solution shows the rotation of flux lines. The essential point is that we should correctly understand the matter that such an equation describes. In comparison, meaningless biased intuition leads us on a wrong path that hides the truth.

Finally, we discuss the phenomena in the resistive state. In the transverse magnetic field, the Lorentz force exceeds the pinning force, and flux flow occurs. By analogy, it is speculated that flux lines become unstable under a force-free torque that exceeds the pinning torque. The expected motion of flux lines in this case is rotation driven by the excess force-free torque. In this section an example of such a rotation was shown in the quasi-static condition. This is the rotation illustrated in Fig. 6.11. In the usual resistive state, however, if only such a rotation occurs, the steady condition does not hold. To keep the steady state, when the flux lines in the former plane rotate as shown by the arrows, those must move to the next plane, i.e., to the place of the flux lines of the adjacent plane in the former instance. The steady state can be kept under the rotational motion accompanied by such a translational motion. Since the Lorentz force on the flux lines is zero, no energy dissipation occurs due to the induced translational motion.

We try to realize such a motion in a cylindrical superconductor. The expected flux motion is illustrated in Fig. 6.17 [19]. The movement of a flux line that passes through the center is shown in (a), and the direction of the motion at each position along the length of the superconductor is shown in (b). This flux flow is called helical flux flow. This flux motion can be simply realized: we have only to twist the structure of flux lines that move along one direction with a constant velocity $\boldsymbol{v}_2$, as shown in Fig. 6.18. The induced electric field is given by (6.1). Here we discuss each term in this equation. Since $\boldsymbol{B}$ and $\boldsymbol{v}$ are known based on the motion illustrated in Fig. 6.17, we can directly calculate the first term, $\boldsymbol{B} \times \boldsymbol{v}$. Here we measure the potential difference between two points "a" and "b" on the surface of the cylindrical superconductor shown in Fig. 6.19. It is assumed that these two points are on a flux line that stays on the surface at some instant, and the distance between them is just the pitch of the

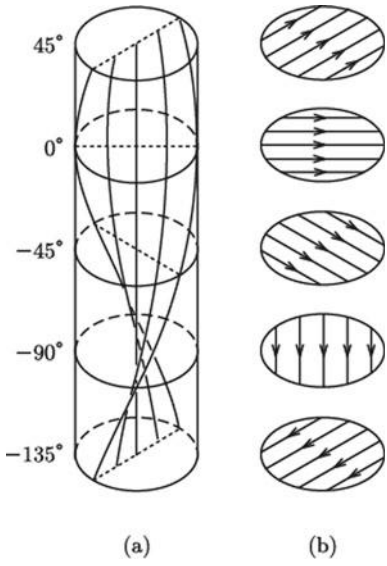

Fig. 6.17 Helical flux flow in a cylindrical superconductor [19]. **a** shows the motion of a flux line that passes through the center, and **b** shows the direction of the motion at each position along the length

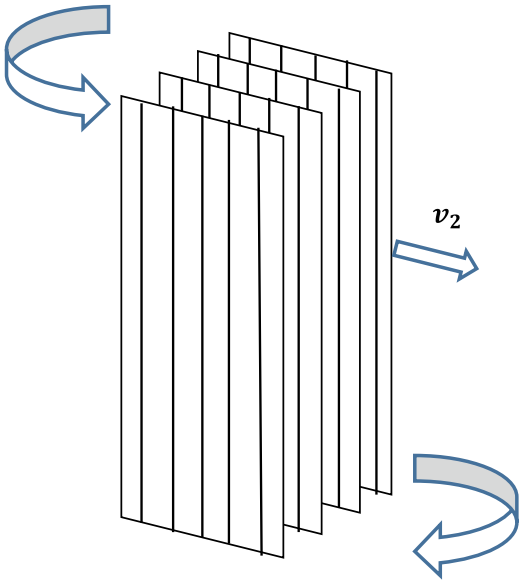

Fig. 6.18 Helical flux flow realized by twisting flux lines that are flowing with translational velocity $\boldsymbol{v}_2$

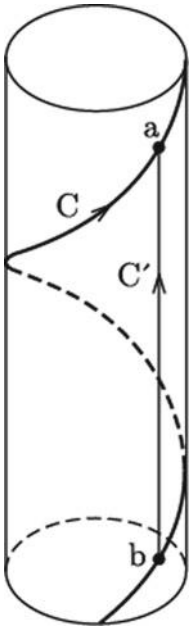

Fig. 6.19 A flux line on the surface of the cylindrical superconductor and paths for the curvilinear integral

helical form. The potential difference is given by a curvilinear integral of the electric field and is independent of the integral path C. Hence, the same potential difference results either from the integral path C along the flux line or from the straight integral path C′. Here we note that $(\boldsymbol{B} \times \boldsymbol{v}) \cdot \mathrm{d}\boldsymbol{s} = (\mathrm{d}\boldsymbol{s} \times \boldsymbol{B}) \cdot \boldsymbol{v}$. Since d$\boldsymbol{s}$ is parallel to $\boldsymbol{B}$ on the integral path C, the curvilinear integral along it is zero. As a result, we have

$$\int_{\mathrm{C}'} (\boldsymbol{B} \times \boldsymbol{v}) \cdot \mathrm{d}\boldsymbol{s} = 0. \tag{6.55}$$

Hence, the term $\boldsymbol{B} \times \boldsymbol{v}$ does not contribute to the potential difference between two points separated by a sufficiently longer distance than the helical pitch. The loss component is contained again in the second term in (6.1), similarly to the case of the non-steady state. Hence, the second term $-\nabla\phi$ can be estimated from the work done by the force-free torque in a unit time:

$$P = \Omega \frac{\mathrm{d}\theta_0}{\mathrm{d}t}. \tag{6.56}$$

Although the details of the analysis are omitted, the electric potential at z (longitudinal position) and φ (azimuthal angle) on the surface is given by [19]

$$\begin{aligned} \Delta V &= V(z, \varphi) - V(0, 0) \\ &= Bv_2 \left[\frac{z}{2} \sin\theta_R - R\cos\theta_R \sin\left(\varphi - \frac{z}{R} \tan\theta_R \right) \right], \end{aligned} \tag{6.57}$$

where θ_R is the angle of the magnetic field on the surface measured from the z-axis. The second term is the contribution from $\boldsymbol{B} \times \boldsymbol{v}$. The observed electric potential at three positions along the length of a Pb–Tl cylindrical superconductor [5] and the corresponding prediction of (6.57) are shown in Fig. 6.20a and b, respectively. The qualitative agreement is good, and it supports the helical flux flow. In particular, it is found that the electric field is negative around the area where the variation in the electric potential along the length of the sample is reversed. In this area the velocity of flux lines is directed outward from the superconductor, and the term $\boldsymbol{B} \times \boldsymbol{v}$ gives a negative longitudinal component for helical flux lines (see Fig. 6.21). It was shown in another experiment that Poynting's vector is directed outward from the superconductor where the electric field is negative, directly indicating that flux lines flow out of the superconductor there [20]. Thus, the negative electric field comes from the unimportant term $\boldsymbol{B} \times \boldsymbol{v}$, and it does not mean a nucleation of energy. The current flows helically along flux lines and it should be noted that $\boldsymbol{i} \cdot \boldsymbol{E} > 0$.

Another characteristic point of the helical flux flow is the appearance of a radial electric field from the second term of (6.57). On the medium line of the theoretical prediction in Fig. 6.20b, it can be found that the maximum transverse electric field,

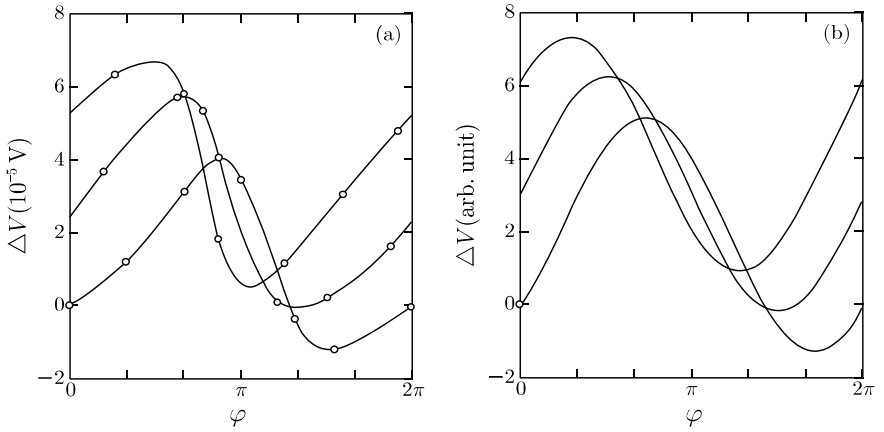

Fig. 6.20 **a** Electric potential observed at three positions along the specimen length on the surface of a cylindrical Pb-Tl superconductor [5] and **b** the corresponding theoretical prediction based on helical flux flow [19]

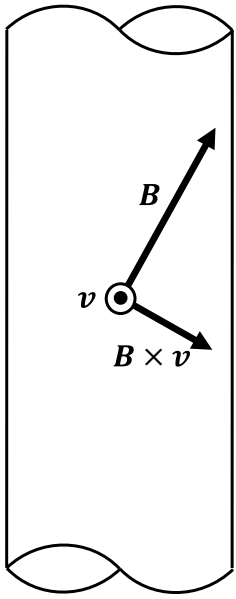

Fig. 6.21 Electric field component due to $\boldsymbol{B} \times \boldsymbol{v}$ in a region where flux lines go out of the superconductor

i.e., the radial electric field, occurs along the direction from $\varphi = \pi/2$ to $\varphi = 3\pi/2$. This electric field is caused by the translational motion of the longitudinal flux component along the direction from $\varphi = 0$ to $\varphi = \pi$. This is consistent with the appearance of the longitudinal negative electric field at around $\varphi = \pi$. Such a radial electric field was really observed [21], and this observation gives a proof of the helical flux flow.

Finally, we discuss the velocity component v_2 in (6.57). The first term that contains v_2 is transformed to $\rho_{\mathrm{ff}}(J - J_{\mathrm{c}})z$. The resistivity ρ_{ff} in this case has been experimentally confirmed to be same as the value ρ_{f} in the transverse magnetic field [20]. Thus, v_2 can be estimated with this relationship.

6.5 Completion of Theory

It can be said that the framework of this theory of electromagnetic phenomena in the longitudinal magnetic field is almost complete except for two points. One of them is the problem of Josephson's theory [7], which predicts that the force-free state is stable without stabilization by flux pinning interactions. The other is that the pinning force does not appear in the force-balance equation resulting in the force-free condition, as shown by (6.2), whereas the flux pinning strength plays an important role in the determination of the critical current density.

Here, we discuss the first point. Josephson assumed that the work done by the external power source is equal to the variation in the inner free energy in the equilibrium state in a pin-free superconductor. We assume that the magnetic flux density and current density in the superconductor are $\boldsymbol{B}$ and $\boldsymbol{J}$, respectively. This situation is described as

$$-\int_{\mathrm{V}} \boldsymbol{J} \cdot \delta \boldsymbol{A} \mathrm{d}V = 0, \tag{6.58}$$

where $\delta \boldsymbol{A}$ is a variation in the vector potential and V represents the region occupied by the superconductor. Josephson assumed that relation given by

$$\delta \boldsymbol{A} = \delta \boldsymbol{u} \times \boldsymbol{B} \tag{6.59}$$

holds by choosing a suitable gauge. In the above $\delta \boldsymbol{u}$ is the displacement of flux lines corresponding to the variation. If this holds, the left-hand side of (6.58) is written as

$$-\int_{\mathrm{V}} \boldsymbol{J} \cdot (\delta \boldsymbol{u} \times \boldsymbol{B}) \mathrm{d}V = \int_{\mathrm{V}} \delta \boldsymbol{u} \cdot (\boldsymbol{J} \times \boldsymbol{B}) \mathrm{d}V. \tag{6.60}$$

The condition given by

$$\boldsymbol{J} \times \boldsymbol{B} = 0 \tag{6.61}$$

is required so that (6.58) is fulfilled for arbitrary $\delta \boldsymbol{u}$. Thus, the force-free state is derived. This is the result of Josephson's theory. Yet, the assumption of (6.59) is

a problem. Equation (4.41) is derived from its variation with respect to time. It is proved, however, both experimentally and theoretically that (4.41) does not hold.

Here, we examine the phenomenon in the force-free state treated in Sect. 6.4. Firstly, the x components on the both sides are compared in (6.59). The left-hand side is

$$\delta A_x = \frac{\mu_0^2}{\alpha_f B}(H_I \sin\theta + H_e \cos\theta)\delta H_I \tag{6.62}$$

and the right-hand side is

$$\delta u_y B_z = \frac{\mu_0^2}{B} H_I (d - y)\cos\theta \delta H_I. \tag{6.63}$$

The derivation on each side is described in Appendix A.16. Thus, the x components on the two sides are different. Next, the y component on the left-hand side is 0, while that on the right-side is $\delta u_z B_x - \delta u_x B_z$, which is not zero. In addition, this quantity is not a constant depending on the distance r from the rotation center. Thus, it is clear that (6.59) does not hold. The blind spot in Josephson's theory is that the rotational motion of flux lines is not considered.

The other point is that the pinning force does not appear in the force-balance equation, resulting in the force-free condition, even though the flux pinning governs the associated phenomena. It has been shown that the critical state in the longitudinal magnetic field is determined by the balance between the force-free torque that works to release the distortion of flux lines caused by the parallel current and the pinning torque that works to stabilize the distortion. On the other hand, it is speculated that the balance between the Lorentz force and the pinning force determines the state in the region where the current flow is normal to flux lines. These two kinds of balance may coexist in general.

Here, we consider the general case where flux lines penetrate the superconductor parallel to the x-z plane, which was treated in Sect. 6.4. The superconducting current can flow freely inside the superconductor, and components normal and parallel to the flux lines may co-exist. The former component produces the Lorentz force, and the latter produces the force-free torque. The pinning force and pinning torque are necessary to maintain the corresponding distortions in the flux line structure. These reactions originate from the common interaction energy, i.e., the pinning energy, and hence, these cannot be independent of each other. Namely, the pinning energy must be shared between the two reactions. Thus, the respective balances are written as

$$\frac{\partial B}{\partial y} = \mu_0 \delta_\perp J_{c\perp} f, \tag{6.64}$$

$$B\frac{\partial \theta}{\partial y} = \mu_0 \delta_\parallel J_{c\parallel} g, \tag{6.65}$$

where $J_{c\perp}$ and $J_{c\parallel}$ are the critical current densities along the normal and parallel directions of flux lines, $\delta_\perp$ and $\delta_\parallel$ are the sign factors of the directions of the corresponding currents, respectively, and f and g are the sharing factors of the pinning energy that satisfy [22]

$$f^2 + g^2 = 1. \tag{6.66}$$

In the case of a superconductor, the dissipated energy in irreversible processes is much smaller than the total energy, i.e., mostly the magnetic energy. From various examples, the pinning energy is expected to be shared under the principle of minimum energy dissipation. The critical state model that explains electromagnetic phenomena in the transverse magnetic field is based on the assumption that the pinning interaction works to minimize the variation in the magnetic flux distribution. As a result, the AC loss energy density given by (5.39) takes on its minimum value by maximizing the critical current density, and the critical state model follows this principle. The critical current density in the longitudinal magnetic field, $J_{c\parallel}$, is much larger than that in the transverse magnetic field, $J_{c\perp}$, and hence, it is convenient to distribute the pinning energy not to the force-balance but to the torque-balance to reduce the energy dissipation. In fact, the loss energy density due to alternating current is appreciably reduced in the transverse magnetic field (see Fig. 6.4). Thus, we have

$$f \cong 0, g \cong 1. \tag{6.67}$$

Here, we show some experimental results that support the principle of minimum energy dissipation. Figure 6.22 shows the results of longitudinal magnetization when

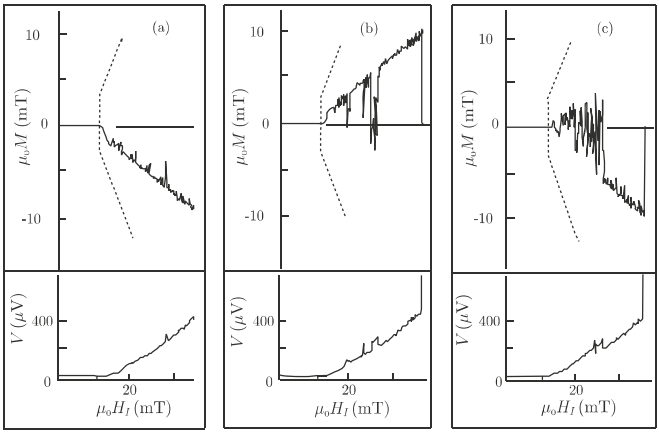

Fig. 6.22 Longitudinal magnetization (upper panel) and voltage (lower panel) when current is applied to a cylindrical Pb-40at.%Tl superconductor 4.0 mm in diameter in the absence of an external magnetic field [2]

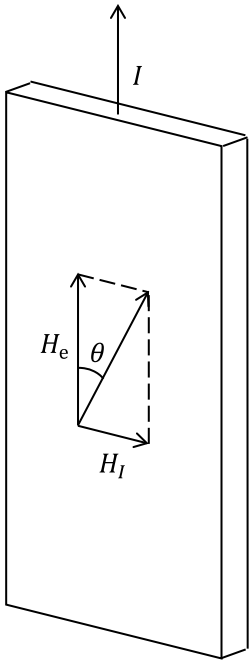

Fig. 6.23 Conditions of an experiment to keep the angle θ of the resultant magnetic field constant by simultaneously increasing the longitudinal magnetic field H_e and the self-field H_I of the current I [23]

only the current is applied to a cylindrical superconductor without an applied longitudinal magnetic field, and three typical states are observed [2]. The longitudinal magnetization appears in the resistive state, as can be seen in (a) and (b). This indicates that the current does not flow parallel to the cylindrical axis but flows helically, so it produces a parallel or anti-parallel magnetic field, as shown in Fig. 6.22b and a, respectively. Although the current flows on the shortest path parallel to the axis in the non-resistive state, as described by the critical state model ($f = 1$), it is shown that the current flows helically along a longer path in the resistive state to reduce the loss energy by enhancing the critical current density under the longitudinal magnetic field produced by the current. The dashed lines in the figure show the predicted magnetizations when the force-free state ($g = 1$) is established. The observed magnetization is smaller than this prediction. This is because the current must flow in the azimuthal direction on the surface under the force-free condition, which result in bad efficiency for the transport current. Thus, the current flows helically. This is an intermediate state between the transverse and longitudinal magnetic field configurations. Since an external longitudinal magnetic field is not applied, a transition between the two stable states is sometimes observed, as shown in Fig. 6.22c.

Another experimental result is a measurement of the critical current density in a superconducting slab specimen when the longitudinal magnetic field H_e and the current I are simultaneously increased, while keeping the angle of the surface magnetic field θ constant, as shown in Fig. 6.23 [23]. Hence, only the magnitude of

the surface magnetic field changes, and it may be expected that flux lines are driven by the Lorentz force as the critical state model assumes. In this case the critical state may be reached when the surface magnetic field matches the penetration field and the flux lines penetrating from the two surfaces meet at the center of the slab. The observed critical current density was much larger than that in the transverse magnetic field, however, and was equal to that in the usual longitudinal magnetic field. This shows that the current is free to flow along the direction that minimizes the loss energy.

Thus, the effect of flux pinning does not appear in the force-balance, whereas it actually determines the critical state. The force-balance equation in the force-free condition represents the characteristic feature of the longitudinal field effects. It is not an essential equation, however, but is a shadow like a "cast-off skin" of the pinning effect.

As is shown above, it can be empirically demonstrated that the principle of minimum energy dissipation is applicable to various examples of flux pinning phenomena. This principle is also deeply associated with the determination of the flux bundle size in flux creep[3] [24], as well as the critical state in the transverse magnetic field and the sharing of pinning energy in the longitudinal magnetic field. This principle is known to hold for a linear dissipation system. On the other hand, the flux pinning phenomena belong to nonlinear case. The critical state model holds, however, in the quasi-static process accompanied by pinning loss. Hence, this principle may be applicable to nonlinear systems so long as the energy dissipation is small, and further discussion is desirable (see Appendix A.10).

Based on the above discussion on the remaining two points, we can say that the theoretical framework to explain the electromagnetic phenomena in the longitudinal magnetic field is completed.

6.6 Comparison with Electromagnetic Phenomena in the Transverse Magnetic Field

As shown in this chapter, the electromagnetic phenomena in the longitudinal magnetic field are dramatically different from those in the transverse magnetic field. In this section the differences between them are compared.

The explanation of each of the peculiar longitudinal magnetic field effects is listed in Table 6.1. Understanding them is essentially different from understanding the electromagnetic phenomena in the transverse magnetic field. The existence of the force-free torque was unknown even in traditional electromagnetism, since the

[3]Flux creep: The state in which flux lines are captured by pinning centers is a non-equilibrium state, and hence, it can happen that flux lines are depinned by thermal agitation. This phenomenon is flux creep and is remarkable in high-temperature superconductors. A group of flux lines that are simultaneously depinned is called a flux bundle. The superconducting current density determined by flux pinning interactions sometimes decreases with time due to flux creep. When the effect of the flux creep is significant, the critical current density sometimes is reduced to zero.

Table 6.1 Explanation of each electromagnetic phenomenon in the longitudinal magnetic field

Phenomenon	Explanation
Existence of force-free torque	Principle of virtual displacement
Enhancement of critical current density	Torque balance
Paramagnetic phenomena	Force-free model (The principle of minimum energy dissipation)
Deviation from $\boldsymbol{E} = \boldsymbol{B} \times \boldsymbol{v}$	Rotational motion of flux lines (Solution of the continuity equation for flux lines)
Electric field structure in the resistive state (Breaking of cylindrical symmetry)	Helical flux flow initiated by rotational motion
Contradiction in Josephson's theory	Deviation from the gauge under rotational motion of flux lines

longitudinal magnetic field effects can occur only in superconductors, as shown in Sect. 6.2, and the flux pinning effect is needed to realize the torque. This torque is the essential factor that causes the longitudinal magnetic field effects. The condition to determine the critical current density is not the force balance but the torque balance. The fact that the theoretical background of this model was given by Josephson's theory for pin-free superconductors was quite unlucky, since it significantly delayed the solution to the longitudinal magnetic field effects. In practice, most pinning energy is distributed to the torque balance, based on the principle of irreversible thermodynamics, resulting in almost no influence of the flux pinning on the force balance. Thus, our understanding of the force-free state is completely different. The deviation of the induced electric field from Josephson's formula is caused by the rotational motion of flux lines driven by the excess of the force-free torque over the pinning torque. This understanding is supported by the solution to the rotational motion derived from the continuity equation for flux lines. On the other hand, the flux cutting model was proposed to explain the deviation from Josephson's formula by traditional ways of thinking. Various phenomena can be explained by the rotational motion of flux lines without such a mechanism. There seem to be many researchers who still believe in the flux cutting, and hence, the problem of the flux cutting model is discussed in Appendix A.12.

The electric structure on the superconductor surface in the resistive state is also explained by the rotational motion of flux lines driven by the force-free torque. During the rotational motion, translational motion is induced to fulfill the steady state condition, and a negative electric field appears in the region where flux lines go out of the superconductor. The flux cutting event was also assumed in this case to make the steady longitudinal magnetization and continuous voltage compatible with each other. The flux cutting is not necessary to explain them, however, as shown in above. In particular, the negative electric field cannot be explained by the flux cutting.

Finally, the rotational motion of flux lines was not considered in Josephson's theory that provided the theoretical foundation for the force-free model. This is

Table 6.2 General comparison of electromagnetic phenomena between the transverse and longitudinal magnetic fields

	Transverse magnetic field	Longitudinal magnetic field
Distortion of flux lines	Magnetic pressure strain (gradient of density) and tilt distortion	Rotational shearing distortion
Balance equation	$\boldsymbol{F}_{\mathrm{L}} + \boldsymbol{F}_{\mathrm{p}} = 0$	$\boldsymbol{\Omega} + \boldsymbol{\Omega}_{\mathrm{p}} = 0$
Principle of minimum energy dissipation	Holds	Holds
Flux motion for $I < I_{\mathrm{c}}$ and $I > I_{\mathrm{c}}$	Translational motion	Rotational motion + translational motion
Induced electric field	$\boldsymbol{E} = \boldsymbol{B} \times \boldsymbol{v}$	$\boldsymbol{E} = \boldsymbol{B} \times \boldsymbol{v} - \nabla\phi$
Magnetic helicity	$\boldsymbol{A} \cdot \boldsymbol{B} = 0$	$\boldsymbol{A} \cdot \boldsymbol{B} \neq 0$

natural, however, since the electromagnetic phenomena arising from the longitudinal magnetic field effects exceed the traditional framework of electromagnetism.

The electromagnetic phenomena in the transverse and longitudinal magnetic fields are generally compared in Table 6.2. The distortion in the flux line structure caused by the current is the magnetic pressure distortion (gradient of density) or tilt distortion that gives rise to the Lorentz force to release these distortions in the transverse magnetic field. The corresponding distortion is the rotational shearing distortion and produces the force-free torque in the longitudinal magnetic field. The mechanism that determines the quasi-static stable condition in the transverse magnetic field is the force balance. On the other hand, there are two mechanisms, i.e., the torque balance and the force balance, in the longitudinal magnetic field. The pinning energy is mostly distributed to the former balance, resulting in the force-free condition in the latter balance. The energy dissipation is minimized under a given condition in each magnetic field. While the flux motion in the dynamic state in the transverse magnetic field is a translational motion, that in the longitudinal magnetic field is mainly a rotational motion with an accompanying translational motion. The latter component is given by v_y in (6.45) for currents smaller than I_{c} and by v_2 for currents larger than I_{c}. It happens that only the rotational motion occurs when the external magnetic field is rotated. The induced electric field in the transverse magnetic field is expressed as $\boldsymbol{E} = \boldsymbol{B} \times \boldsymbol{v}$ and that in the longitudinal magnetic field is in the form of $\boldsymbol{E} = \boldsymbol{B} \times \boldsymbol{v} - \nabla\phi$ in both the steady and non-steady states. In the future, it will be required to clarify the relationship between such peculiar phenomena and the magnetic helicity.

In Sect. 5.2 the advantage of choosing $\boldsymbol{B}$ and $\boldsymbol{v}$ as independent variables in the critical state model was proposed to analyze the electromagnetic phenomena in the transverse magnetic field, since the analogy to dynamics helps us to understand the phenomena. On the other hand, since such an analogy does not hold in the longitudinal magnetic field, there is no advantage to doing so. It is better to choose $\boldsymbol{B}$ and $\boldsymbol{E}$ to

avoid any confusion. It is sometimes useful, however, to clarify $\boldsymbol{v}$ to find essential points such as the rotational motion.

In this section we treated only the simple process of applying a longitudinal magnetic field and then applying a current, or changing the direction of the field to realize the phenomena arising from the longitudinal magnetic field effects. There are various cases where the longitudinal magnetic field is changed later, or the longitudinal magnetic field and current are simultaneously changed, etc. It is necessary to clarify the distribution of the pinning energy to the force balance and torque balance in each case. It is also necessary to clarify if the energy dissipation really takes on its minimum value.

6.7 New Electromagnetism

Traditional electromagnetism was systematized by Maxwell, and its framework was shown in Chap. 2. The fundamental principles are the Coulomb force (including Coulomb's law), the Lorentz force (including the Biot-Savart law), the displacement current, and Faraday's law for induction. The empirical Ohm's law for the resistivity is included to describe practical phenomena. Thus, the magnetic force is only the Lorentz force. The quasi-static electromagnetic phenomena in superconductors in the transverse magnetic field can be described by replacing Ohm's law by the relationship between $\boldsymbol{E}$ and $\boldsymbol{J}$ in the critical state theory, which is no longer a phenomenological model. In the resistive state, the phenomenological dynamic critical state model that assumes the flux flow resistivity is used.

In the superconductor in the longitudinal magnetic field, another magnetic general force, the force-free torque, appears in addition to the Lorentz force. This torque was not known in the traditional framework of Maxwell's theory, although the existence of this torque is not denied by Maxwell's theory. In practice, the force-free torque is derived using Maxwell's theory. This is similar to the point that the electromagnetic phenomena in superconductors can be described by Maxwell's theory, although superconductivity was not discovered when Maxwell's theory was completed. The state in which the force-free torque appears is the state with a finite static magnetic helicity. This state can be realized only in superconductors with the flux pinning effect. For this reason, the discovery of the force-free torque was delayed. The new framework of Maxwell's theory is shown in Fig. 6.24. The current flow in the static condition is determined by the critical state theory, taking into account the distribution of the pinning energy, and that in the dynamic condition is determined by the phenomenological model extended to the resistive state.

The force-free torque appears only in superconductors and under the special condition of a longitudinal magnetic field. This is the reason why the discovery of the force-free torque was delayed. There is another big reason. This can be understood from the fact that this torque is an internal torque, as can be seen in Fig. 6.11. That is, its value is zero when averaged inside the superconductor. The flux lines in the former plane receive the torque shown by the arrows, while those in the next plane receive

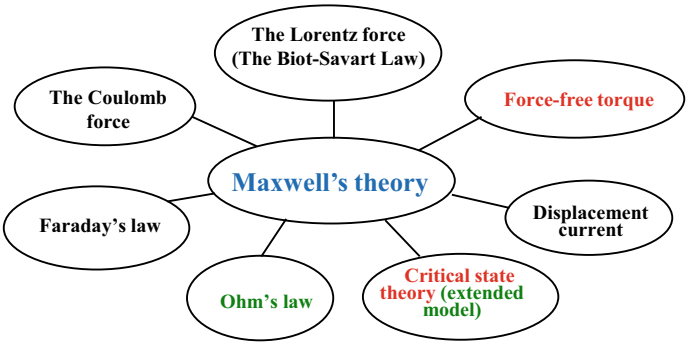

Fig. 6.24 New framework for Maxwell's theory including electromagnetic phenomena in superconductors. Ohm's law is an empirical law and has not been proved theoretically. The current flow in superconductors is determined by the critical state theory in the static case and by the extended model with the assumption of energy dissipation in the dynamic case

the torque in the opposite direction. When people enjoy a rope pulling game, they may feel that the rope is pulling them. The rope does not assist both sides, however, and the total tension is zero. The same thing happens in the case of the Lorentz force in the magnetization process. The Lorentz force completely cancels out in the superconductor, as illustrated in Fig. 6.25. On the other hand, when a current is applied to a superconductor in an external magnetic field, the Lorentz force appears and is directly observed.

From this analogy, we note that the torque is observed when the magnetic field applied to a superconductor is rotated, as illustrated in Fig. 6.26. It may be expected that the force-free torque can be easily proved, but there is a problem. Since the current flowing inside the superconductor is closed, the current flowing in the edge region is perpendicular to the external magnetic field, and the torque due to the Lorentz force is surely included in the observed torque. Thus, the correct quantitative comparison with the theoretical prediction is complicated.

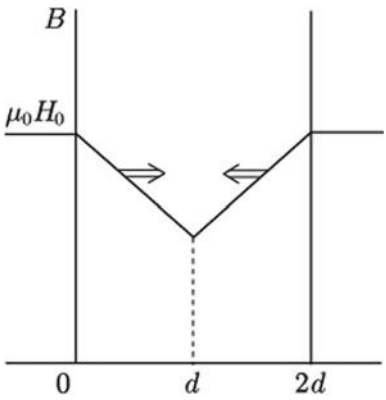

Fig. 6.25 The Lorentz force that appears in the magnetization process

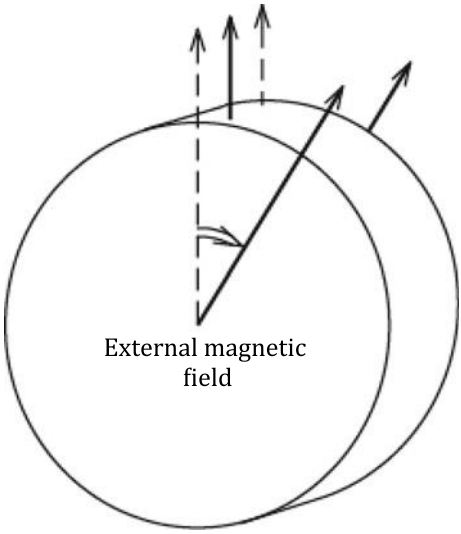

Fig. 6.26 Superconducting disk in a parallel rotating magnetic field

The force-free torque is a new phenomenon discovered in the 20th century after the completion of Maxwell's theory. This discovery is similar to the theory of relativity by Einstein in various points as follows:

(a) Both of them are expected ideologically. That is, the relativistic theory was based on the principle of relativity, i.e., equivalence among the different coordinate systems moving with different velocities and the principle of the constancy of light velocity. The force-free torque is based on the fundamental idea that, when a distortion exists, some restoring force should work to release the distortion.
(b) Both of them are quite different from traditional concepts. The prediction of the theory of relativity was contradictory with respect to Newtonian mechanics. The prediction of the force-free torque was contradictory to the fixed idea of electromagnetism that the magnetic force is only the Lorentz force.
(c) Both of them appear only under special conditions. The theory of relativity predicts that characteristic phenomena occur only when the velocity is close to the velocity of light or under the influence of a huge mass. The force-free torque appears only in superconductors in a longitudinal magnetic field.
(d) Both of them are indirectly proved by experiments. The theory of relativity was proved by the elongated life-time of muons and by the refraction of light by the strong field of gravity. The force-free torque is proved by a comprehensive explanation of the longitudinal magnetic field effects.
On the other hand, these theories are different in the following points:
(e) The difficulty of the required mathematics is quite different. To understand the theory of relativity, advanced mathematics is required. In the case of the force-free torque, mathematics on the level of undergraduate students in the scientific faculties is sufficient.

(f) People's interest is completely different. When the theory of relativity appeared at the beginning of the 20th century, people in various fields were very interested in physics. When the force-free torque was discovered at the end of the 20th century, each research field was subdivided and deeply developed, so that interest from another research field was significantly reduced. Although the explanation of the longitudinal magnetic field effect represented by the force-free torque was a proposal of an essential problem in electromagnetism, there was no research field of electromagnetism in the existing main journals, and the submission of a paper was possible only in the field of superconductivity. Thus, the opportunity to attract the attention of researchers in various fields is quite small now. In addition, the discovery of high-temperature superconductivity in 1986 attracted great interest from people and this had a bad effect on the research on the longitudinal magnetic field effects, which were mostly done on metallic superconductors. Even in the field of superconductivity, most young researchers do not know about the longitudinal magnetic field effect. Now, many professional people in this field have passed away or retired from research.

The author is a member of the last generation who experienced research on the longitudinal magnetic field effect. Hence, he believes that the arrangement of the essential points of important features of the longitudinal magnetic field effect is his task for researchers in the next generations. It is hoped that publication of this book will be useful for the purpose. The longitudinal magnetic field effect may be completely forgotten in the future, however, with the rapid development of science and technology. It is necessary, therefore, to apply this effect in useful technologies to prevent the effect from being forgotten. Such a duty may be required of the author. In the next chapter, the electromagnetic phenomena in superconductors are summarized, and the technologies that superconductivity supports are introduced, including an example of an application of the longitudinal magnetic field effect.

Coffee break (6)

Continuity equation for flux lines

The continuity equation for flux lines (5.34) describes the variation in the magnetic flux distribution with time in a superconductor, based on using the velocity $\boldsymbol{v}$ of flux lines. Josephson's formula (4.41) can be derived under a certain condition from this equation and from (2.49) for induction. Equation (5.34) is used for calculation of the AC loss energy, as shown in Sect. 5.2. In addition, this equation is also used for estimation of the displacement of flux lines, analysis of the reversible flux motion in Sect. 5.3, performance of the virtual displacement, and the derivation of the Lorentz force in Sect. 5.7. Equation (5.34) also plays an important role in the derivation of the rotational motion of flux lines in the longitudinal magnetic field treated in this chapter.

Equation (5.34) was originally derived expecting the situation where flux lines move translationally. It is worth noting, however, that this equation can describe general flux motion, including the rotation. Such an evolution in a theoretical approach can be found in other cases. For example, the derivation of the law of

motion (2.52) from the magnetic flux law (2.48) for the variation in the magnetic flux with time is also one such evolution.

References

1. Y.F. Bychkov, V.G. Vereshchagin, M.T. Zuev, V.R. Karasik, G.B. Kurganov, V.A. Mal'tsev, JTEP Lett. **9**, 404 (1969)
2. D.G. Walmsley, J. Phys. F **2**, 510 (1972)
3. Y. Nakayama, O. Horigami, Teion Kogaku **6**, 95 (1971). [in Japanese]
4. J.R. Cave, J.E. Evetts, A.M. Campbell, J. Phys. (Paris) **39**, C6–614 (1978)
5. T. Ezaki, F. Irie, J. Phys. Soc. Jpn. **40**, 382 (1976)
6. C.J. Bergeron, Appl. Phys. Lett. **3**, 63 (1963)
7. B.D. Josephson, Phys. Rev. **152**, 211 (1966)
8. A.M. Campbell, J.E. Evetts, Adv. Phys. **21**, 199 (1972) (See p. 252)
9. J.R. Clem, J. Low Temp. Phys. **38**, 353 (1980)
10. E.H. Brandt, J. Low Temp. Phys. **39**, 41 (1980)
11. E.H. Brandt, J.R. Clem, D.G. Walmsley, J. Low Temp. Phys. **37**, 43 (1979)
12. G.W. Kullen, R.L. Novak, Appl. Phys. Lett. **4**, 147 (1964)
13. F. Irie, T. Matsushita, S. Otabe T. Matsuno, K. Yamafuji, Cryogenics **29**, 317 (1989)
14. T. Matsushita, J. Phys. Soc. Jpn. **54**, 1054 (1985)
15. T. Matsushita, M. Kiuchi, Jpn. J. Appl. Phys. **57**, 103101 (2018)
16. T. Matsushita, Y. Miyamoto, A. Kikitsu, K. Yamafuji, Jpn. J. Appl. Phys. **25**, L725 (1986)
17. A. Kikitsu, Y. Hasegawa, T. Matsushita, Jpn. J. Appl. Phys. **25**, 32 (1986)
18. T. Matsushita, Y. Hasegawa, J. Miyake, J. Appl. Phys. **54**, 5277 (1983)
19. T. Matsushita, F. Irie, J. Phys. Soc. Jpn. **54**, 1066 (1885)
20. T. Matsushita, A. Shimogawa, M. Asano, Phys. C **298**, 115 (1998)
21. B. Makiej, A. Sikora, S. Golab, W. Zacharko, in *Proceedings of the International Disc. Meet. Flux Pinning in Supercondctors, Soonenberg* (1974), p. 305
22. T. Matsushita, *Flux Pinning in Superconducors*, 2nd edn. (Springer, 2014), p. 171
23. T. Matsushita, S. Ozaki, E. Nijimori, K. Yamafuji, J. Phys. Soc. Jpn. **54**, 1060 (1985)
24. T. Matsushita, Phy. C **217**, 461 (1993)

The following references are also generally recommended:

25. T. Matsushita, *Flux Pinning in Superconducors*, 2nd edn. (Springer, 2014)
26. T. Matsushita, Jpn. J. Appl. Phys. **51**, 010111 (2012)

Chapter 7
Concluding Remarks

Abstract In this chapter the contents from Chaps. 2–6 are briefly summarized, and the status of electromagnetic phenomena in superconductors is overviewed in the context of the current electromagnetic theory. Superconductors also have high potential for applications in various fields because of their characteristic features such as non-dissipative current and non-linear quantum phenomena. We focus on their applications in the medical, environmental, and energy fields. Finally, it should be emphasized that various electromagnetic phenomena in superconductors, whether reversible or irreversible, are concerned with the flux pinning. The possibilities and direction of progress of this science, which will extend over electromagnetism and irreversible thermodynamics in the future, are discussed.

7.1 Summary

Electromagnetism is a science that describes only the electromagnetic properties of substances without knowledge of the fundamental mechanisms of solid state physics that play dominant roles. For example, a conductor is defined as a substance in which the electric field is zero when an external electric field is applied, independently of our knowledge of the free electron theory in solids. Superconductors can also be defined as a substance in which the magnetic flux density is zero when an external magnetic field is applied. In this case there is no problem in such a definition. It makes even the present ***E*-*B*** analogy more perfect. Although superconductivity was not yet discovered when Maxwell's theory was completed, it is included in the comprehensive theory as if it was known. As was shown in Sect. 3.2, it can be proved by Maxwell's theory that the electrical resistivity of a material that shows $\boldsymbol{B} = 0$ must be zero. Thus, it was, in principle, possible to predict the superconductor in the 19th century, even though it might be an imaginary substance.

The phenomenon that adds a new page to electromagnetism is the longitudinal magnetic field effect. In this phenomenon the force-free state with non-zero magnetic helicity ($\boldsymbol{A} \cdot \boldsymbol{B} \neq 0$) is realized. The static state with non-zero magnetic helicity appears only in superconductors. The magnetic structure has a characteristic distortion called the force-free distortion in this state, and a general driving force is expected

T. Matsushita, *Superconductivity and Electromagnetism*, Springer Series
in Solid-State Sciences 195, https://doi.org/10.1007/978-3-030-67568-4_7

to release the distortion. In fact, the force-free torque, independent of the Lorentz force, is derived as the general driving force from the penetration of energy during the virtual displacement to introduce the distortion. This is quite similar to the derivation of the Lorentz force that corresponds to the distortions of the magnetic structure in the usual transverse magnetic field (see Appendix A.8). Since the observed critical current density depends on the flux pinning strength, similarly to that in the transverse magnetic field, it is considered that the minimization of the total free energy density, including the pinning energy, is essential. Thus, it is reasonable that the equation of torque balance to determine the critical current density is derived from first principles. As a result, if the increase in energy by introducing the force-free distortion cannot be stored as the pinning energy, the distorted state cannot be stabilized. The solution of rotational motion of flux lines driven by the excess of the force-free torque over the pinning torque is derived from the continuity equation for flux lines, and the electric field structure on the surface in the resistive state is explained. Thus, the longitudinal magnetic field effect, which is quite different from the electromagnetic phenomena in the transverse magnetic field, is generally explained. As shown above, the essential mechanism that causes the longitudinal magnetic field effect is the flux pinning that stabilizes the force-free distortion. It has been believed that the theory of electromagnetism was completed in the 19th century, but a new door has been opened now by the introduction of the longitudinal magnetic field effect.

Zero electrical resistivity is a specific character of superconductors, and application of this property to various devices is expected. In many cases superconductors are used in a high transverse magnetic field, and flux lines penetrate the superconductor in the form of quantized magnetic flux. The central area of each quantized magnetic flux line must be in the normal state, however, so as to prevent the superconducting current density from diverging due to the singularity in the phase of the order parameter. As a result, if flux lines are driven by the Lorentz force when a current is applied to the superconductor, energy dissipation takes place, and electrical resistance appears. If the flux motion can be stopped by introducing defects, we can apply a transport current without appearance of the electrical resistance. This is the principle of flux pinning and is the origin for various applications of superconductivity.

In the static state, there is no energy dissipation caused by flux pinning interactions. Under varying conditions, however, energy dissipation occurs, and electromagnetic phenomena in the superconductor become irreversible. This irreversibility can be explained by the critical state model, which assumes that the flux pinning interactions minimize the variation in the magnetic flux distribution inside the superconductor. The energy dissipation in this case is of the hysteretic type, such as iron loss, and its value does not depend on the resistivity, but rather on the critical current density, although the mechanism of energy dissipation is the same as for copper loss. Its dependence on the frequency in the case of alternating variation is also different: It is proportional to the frequency, while the copper loss is proportional to the second power of the frequency. The irreversibility and hysteretic nature of the pinning loss can be explained by the theory of the flux pinning mechanism that assumes that there is a many body interaction between flux lines and randomly

distributed pinning potentials. In particular, it should be emphasized that the irreversibility can be directly derived from this theory using a statistical method for the energetic interaction, i.e., independently of the breaking of time reversal symmetry. As a result, the irreversibility in which pinning loss becomes thermal energy is also obtained. On the other hand, this theory also explains reversible phenomena that are experimentally confirmed, since the interaction is caused by the pinning energy. Based on this aspect it was realized that the force-balance equation in the critical state model could be derived by minimizing the free energy, taking account of the work done by the Lorentz force in the pinning potential field, and by extending it to the irreversible case. As a result, the critical state model, i.e., a phenomenological model, could be improved as a general theory. In the irreversible state, including the resistive state, in which energy is dissipated, the first principles of minimizing the energy cannot be used. For example, this point is clear in the process from point A to point P in Fig. 5.16. At each instance in this process, the state is, however, almost close to the state derived from first principles, and the associated energy dissipation is at a minimum. Even for non-isolated systems, the state with minimum free energy is attained in the reversible region, such as those in the process from point P to point Q (see Appendix A.8).

Looking over a series of phenomena in superconductors, the idea that the superconductivity is a peculiar phenomenon may be said to be biased. No resistivity seems to be strange. The resistivity is, however, a phenomenological property that cannot be theoretically proved. On the other hand, the phenomena in superconductors, including the flux pinning can be explained by first principles to minimize the free energy. That is, superconductors are pure materials in physics. In addition, superconducting substances are not minor, since many elements or compounds show superconductivity, when conditions such as high pressure or thin film geometry are included. Only the transition temperature to the superconducting state is low. If room temperature superconductors are found in the future, the concept that superconductors are peculiar may fade away.

The high-temperature superconductors discovered in 1986 that showed a rapid development in their quality are not discussed in this book. This is because the critical current density caused by flux pinning can be defined, the electromagnetic phenomena are explainable using the irreversible critical state model, and the pinning loss has a hysteretic nature, as in metallic low temperature superconductors. That is, the main properties are essentially the same as the description in this book, although there are still some points that need to be considered. These are described in Appendix A.17.

7.2 Superconductor Technology in the Future

Superconductivity has significantly contributed to the progress in solid state physics in the 20th century. As described in this book, superconductors are common materials and are classified as one of the fundamental magnetic materials in electromagnetism. These are typical materials that show irreversibility in magnetic hysteresis from the viewpoint of thermodynamics. Some new physics may also be based on superconductors. Thus, superconductors are attractive substances.

The property of superconductors that the resistivity is zero under static conditions is not only interesting from the viewpoint of physics, but also attractive from that of application. The area of application that the superconductor technology using zero resistivity can cover is widely spread over various fields, including power applications, energy saving, the environment, transportation systems, industrial technology, medicine, etc. In addition, it extends even to the field of electronics, using its inherent nonlinear properties (see Fig. 7.1). Information technology was a part of electronics in former times, although it deeply penetrates all fields of technology now, and research and industry in each field can no longer exists without it. Even an important wide area in people's daily life, such as telecommunications, distribution, and medical services, is supported by information technology. Superconductor technology is also a similar but slightly different technology that supports society, and it is expected to support even high-level information technology.

In this section the application of superconductor technology in the fields of medical treatment, environment, transportation, and energy will be briefly introduced.

(1) **Medical treatment**

The application of superconductors to medical treatments is roughly classified into two categories from the viewpoint of technology. One of them is the application of flux pinning phenomena, which is similar to other applications in the fields of energy and environment, and the other is the application of the Josephson effect, which has not been introduced in this book.

The most widely used type of equipment in the first category comprises the magnetic resonance imaging (MRI) systems mentioned in Chap. 1. Very strong and stable magnetic fields can be produced by superconducting magnets operated in persistent current mode, which makes it possible to visualize clear cross-sections of human body using the nuclear magnetic resonance technique. Open-type MRI systems that reduce the anxiety of subjects are likely to become popular in the near future.

Another system using superconducting magnets is heavy ion therapy for cancer treatment. This is similar to a technique used in particle physics, where heavy ions accelerated by a strong magnetic field are used to directly irradiate tumor cells with high precision. In particular, a rotating gantry can irradiate the tumor while directing the beam from an arbitrary direction, and hence, the subject's body can remain in a fixed position, which helps to prevent his or her internal organs from moving due to gravity and contributes to a precise irradiation. If normal magnets are used for this

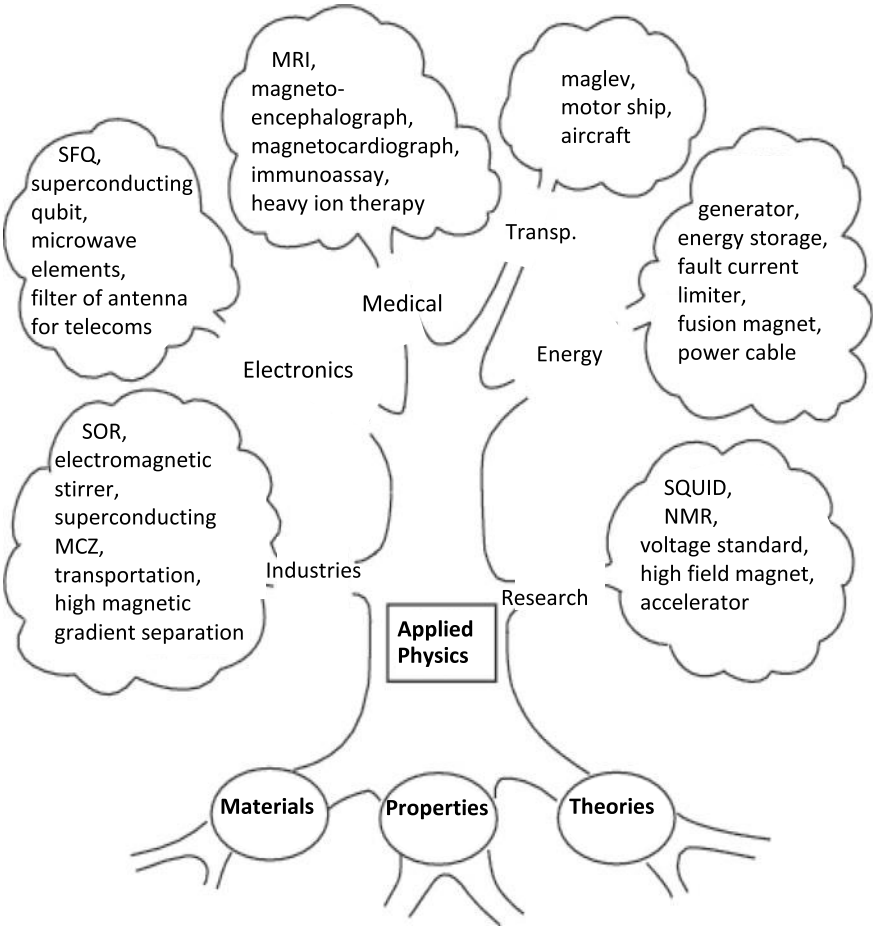

Fig. 7.1 Various applications of superconductor technology

system, their size must be very large, and a huge amount of electric power is needed for operation. If we introduce superconducting magnets, the size can be significantly reduced, and the operation cost can also be dramatically reduced. Figure 7.2 shows a superconducting magnet that is to be installed in a rotating gantry system.

Drug delivery systems represent another type of application of superconductor technology in the field of medical treatment. First, a magnetic seeding technique is used for the needed medicine, i.e., a small amount of fine magnetic particles is added to the medicine, and the medicine is delivered to the desired location in the diseased part of the subject by using a strong magnetic field from a magnetized bulk superconductor. The treatment is carried out by keeping the medicine at the diseased part for the desired period.

Fig. 7.2 Superconducting magnet installed in a rotating gantry system (Courtesy of Dr. Koji Nomura of the National Institute of Radiological Sciences)

Another type of medical treatment is based on the Josephson effect. A Superconducting Quantum Interference Device (SQUID) composed of two Josephson junctions[1] and a superconducting loop is used. A SQUID is quite sensitive to magnetic field, as can be understood from (4.20), and various types of information can be obtained from magnetic measurements. One such medical system is the magnetic cardiograph used for examination of the heart, similarly to the usual cardiograph. One of the merits of the new system is that there is no need to attach electrodes to the body for the usual cardiograph, and the examination can be conducted with the patient in a clothed condition. The information obtained is increased significantly, because the magnetic field can be measured as a vector. It is possible even to inspect the heart of a baby in its mother. The magnetoencephalograph is a similar medical system used for inspection of the brain by measuring very weak magnetic fields produced by a current flowing in the brain. This is used for locating diseased regions in the brain.

The SQUID is also used for investigation of antigen-antibody interactions. It is used to measure the rate at which antigens, which cause allergic reactions, combine with antibodies in a subject. Antibodies mixed with magnetic nanoparticles called magnetic markers are used as the reagent. First, antibodies in the reagent are combined with antigens of the subject, and then, free antibodies are washed away. Finally, the magnetic moment of the remaining antibodies combined with magnetic nanoparticles is sensitively measured using a SQUID magnetometer. Thus, the density of antigens combined with antibodies can be found. If the magnetic marker tends to concentrate in a diseased region, it is also possible to diagnose the location and degree of disease by searching for the location and the amount of magnetic marker. Since the amount of magnetic substances that can be dosed safely is limited, highly sensitive magnetic measurements are needed, and the SQUID magnetometer is used.

[1] Josephson junction: Device consisting of two superconductors separated by a very thin insulating layer. When a phase difference φ is introduced between the order parameters in each superconductor, a superconducting tunneling current can flow through the layer, as given by the first term of (4.20).

(2) **Applications for environment**

One superconductor technology that contributes to environmental issues is high-gradient magnetic separation (HGMS). Much higher magnetic field can be produced by magnetized high-temperature superconducting bulks than permanent magnets in the Nd system. The combination of this strong magnetic field with a filter made of a magnetic material with high permeability makes it possible to separate magnetic particles from other materials by attracting them strongly at places where the strength of the magnetic field varies greatly in space. In many cases the magnetic seeding process is employed to attach magnetic nanoparticles to the substance to be removed. Then, the substance is removed using HGMS. Examples are found in the purification of water used for paper manufacturing, removal of harmful chemicals that cause environmental pollution from liquids, improvement of the water quality of lakes or ponds in which large amounts of blue-green algae grow, etc. It is also expected to be applicable for purification of sea water from red tides. Figure 7.3 shows the composition of a fine magnetic separator, in which a high-temperature superconducting bulk magnet is installed in a high-gradient magnetic separator for water purification. Water processed by magnetic-seeding comes from the left side, and substances to be removed are attracted to the magnetic filter near the bulk magnet, so purified water only flows to the right side. This technology is also used for purification of

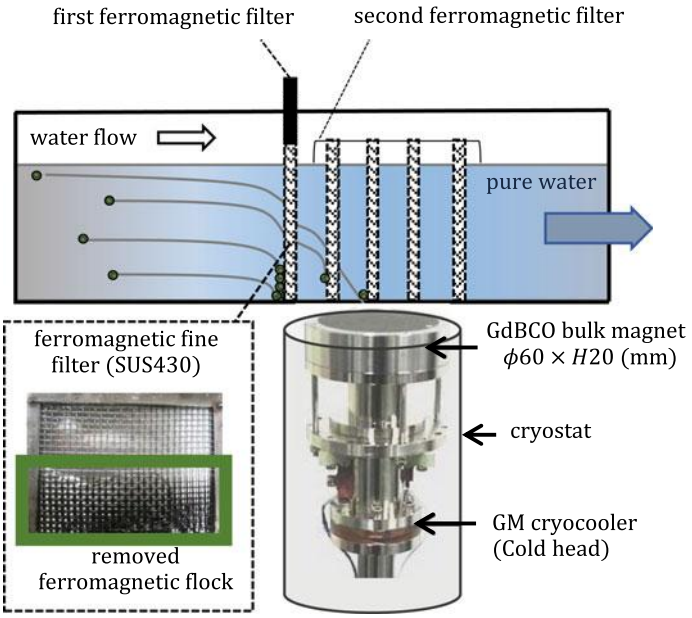

Fig. 7.3 Fine magnetic separator in a high-gradient magnetic separator for water purification. The high-temperature superconducting bulk magnet and cryocooler for cooling it are placed in the lower part (Courtesy of Prof. Shigehiro Nishijima of Osaka University)

water in the field of electric power generation. Water must be circulated for cooling in thermal power plants. If impure substances contained in the water adhere to the inner walls of heat exchangers, they degrade the heat exchange performance. Thus, it is necessary to purify the water. In geothermal power generation, this technology is also expected to prevent impurities contained in the hot spring water from adhering to the inner walls of pipes or rotating fans, which will cause clogging or reduction in the efficiency, respectively.

(3) **Transportation**

One of applications for transportation systems is the superconducting magnetic levitated (SCMAGLEV) train. It is planned that these trains will run between Tokyo and Nagoya, and the line will be extended to Osaka in the future. Superconducting magnets in the train are operated in the persistent current mode, and the train is levitated by the repulsive interaction between the magnetic field produced by the superconducting magnets and the magnetic field that is induced in closed coils or conducting plates arranged on the ground when the train gets close. Acceleration or deacceleration is done by controlling the current applied to the driving coils that produce attractive or repulsive forces. Since the levitation is realized by using repulsive forces, the train does not touch the walls due to the strong repulsive force, even when there is a big earthquake. The operating speed of the trains will be 500 km/h. This is limited to prevent the power efficiency from being reduced by air resistance and to keep the noise level low when the train goes into or out of a tunnel. In principle, however, there is no limit to the speed. It would be possible to increase the speed even up to 3500 km/h, if the train runs in an evacuated tube.

Ships usually move by means of engine that directly rotate their screws, which are placed at the stern. Mostly, ships do not sail at the maximum speed but with about half that value. In this case, the efficiency of the engine is not high. It is better to drive the screw with an electric motor to improve the efficiency. Then, an electric generator is necessary to drive the motor. It seems to be inefficient to generate electricity and rotate the screw using generated electric power instead of the direct drive by the engine. The efficiency mostly increases, however, since the efficiencies of electric generators and motors are high. An additional merit of this system is the increase in the efficiency brought about by a smart shape for the stern, which reduces the water resistance, since the engine can be replaced by a small, powerful electric motor. In addition, the generator can be placed in a free space in the ship, and this may give the ship a structure of high utility. It is possible to install a superconducting generator and motor to further increase the efficiency. This is expected for large ships and also contributes to a reduction in CO_2 emission.

The aerospace industry intends to reduce the amount of its CO_2 emissions around the world in 2050 to the half of the present amount as a measure against global warming. On the other hand, the need for air flights is estimated to be doubled. Hence, we have to develop a new technology to reduce the CO_2 emissions to one quarter in the present stage. Electrification is inevitable for the propulsion system, and the superconductor technology is expected to play a role in this achievement.

The principle is the same as that for the ship propulsion, and the superconducting generator and motor will contribute to the reduction of CO_2 emissions. In this case an effective and environmentally friendly system, in which the liquid hydrogen used for cooling superconducting devices is used as fuel for superconducting generators, will be examined. Various types of aircraft are now being designed, and it is imagined that aircraft with much different shapes will fly in the sky around the world in the future.

(4) **Applications for energy problems**

Recently, the global warming of the earth by CO_2 has been recognized as a serious problem. On the other hand, although nuclear electricity generation does not emit CO_2, people are quite sensitive to radioactive contamination caused by an accident at a nuclear electric power plant after the Great East Japan Earthquake. In addition, uncertainty about the safety of radioactive waste that has to be managed for over a long period of time that human beings have never experienced makes people anxious. Hence, nuclear electricity generation will diminish without public support. Thus, the use of renewable energy that does not emit CO_2 will advance. Solar power generation, the cost of which is expected to be dramatically reduced, is particularly promising. The problems in progressing the use of renewable energy are the installation of power transmission cables to the regions in which the electric power is used and devices to store the excess electrical energy. In particular, the energy storage devices that can store energy instantaneously are quite expensive now. This prevents local governments that intend to consume generated energy from ever starting solar power generation. If we look at Europe, they solve this problem by delivering excess energy to regions of power shortage instead of storing energy. Electric power may not be generated because there is no wind in some regions, while excess electric power is generated by strong wind in other regions. It is important to send excess electrical energy to regions of shortage over a wide area, which averages the demand for electrical energy. A similar situation occurs for solar power generation when it is diminished by cloud. This is the same principle as the improvement of signal to noise ratio by overlapping small signals buried in noise many times. If the area connected with the power line becomes wider, averaging becomes more effective. This reduces the necessity for installing expensive energy storage systems. In this case, the cost of the power line is an important factor.

When the power line becomes long, superconducting power transmission with small energy dissipation is advantageous. Direct current (DC) is advisable instead of alternating current (AC) for the power transmission. This is because the solar power generation is DC. DC electric power transmission is also better for wind power generation. Although the power generation takes place under AC conditions, the frequency and phase of the induced voltage are random among many generators. DC power transmission is also beneficial from the viewpoint of superconductor technology; there is no AC loss in the superconductor, and the structure of the superconducting cable becomes simple. In addition, the demand for DC electricity in society is larger than that for AC electricity. In modern homes, most of the electrical

appliances, such as televisions, are driven by DC electricity. In the case of refrigerators, washing machines, and air conditioners, commercial AC electricity is converted to high-frequency AC via DC. Hence, if DC electricity could be supplied to each home, the conversion from commercial AC to DC would not be necessary.

For superconducting power transmission, we need to cool the superconducting cable to a sufficiently low temperature such as liquid nitrogen temperature (77.3 K). The heat that invades the transmission line from the surface is about 1 W per unit length, and we need electric power of 15 W/m to remove this heat power from the region at 77.3 K. If this power is smaller than the electric power consumed in the usual copper transmission line, the superconducting power transmission is advantageous from the viewpoint of operation cost. If we assume an electric power transmission of 3 kA through a copper cable, the cross-sectional area of the copper wire is 3,000 mm^2, and the electrical resistance per unit length at room temperature is 5.7 $\mu\Omega$, which results in electric power consumption of 51 W/m. Hence, even if we take the rate of operation into account, the superconducting power transmission is economical. When the current is increased, the advantage of introducing superconducting power transmission increases, since the cost for cooling does not change. We now have the problem of the fabrication cost of superconducting cable. This will be solved, however, by reduction of the cost of superconducting tapes through improvement of the fabrication technology, with mass production based on the necessity of introducing superconductivity to reduce CO_2 emissions. The fairly high cost of copper brought about by global economic growth also supports the introduction of superconductivity. The above comparison has been made for the case where the power transmission voltage is kept the same as for the present system. If we increase the current, which increases the advantage of superconductivity, we can reduce the voltage. This is another advantageous point.

When a network of power transmission lines over a wide area is constructed, large fault currents caused by short circuits may happen. It is necessary to prevent such fault currents from propagating. The fault current limiter is the instrument used for this purpose, and application of superconductors is also expected. There are two types of superconducting fault current limiter, the resistive type and the magnetic shield type. The large impedance when the superconductor goes into the normal state is used to reduce the fault current for both types. The large electrical resistance in the normal state is directly used in the former type. In the latter type, a transformer is designed so that the magnetic flux in its iron core produced by the primary and secondary windings is usually cancelled. When the transport current exceeds the critical value in one winding, the resistance that appears in this winding reduces the current, and magnetic flux appears in the iron core, resulting in dramatic increase in the inductance. Thus, the magnetic shield type is used only for alternating currents, but the resistive type is used for direct and alternating currents. Rare earth barium copper oxide (REBCO) thin films are used for the resistive fault current limiter. Since high resistance is needed when the superconducting thin films go into the normal state, the use of copper for protection of the thin films is limited, and the possibility that the limiter will be damaged is fairly high. On the other hand, since the superconducting cable is very long, it is fairly easy to obtain high resistance. For

this reason, research on superconducting cable with a fault-current limiting function has been carried out in the USA, and such a long cable was practically fabricated in Korea recently.

The author has proposed a high-performance DC superconducting power cable in which the longitudinal magnetic field effect described in Chap. 6 is applied [1]. The longitudinal magnetic field effect was discovered more than 50 years ago. Although it is a fantastic phenomenon from the viewpoint of technology that the critical current density increases, no application of this effect has been proposed. It is especially strange that this effect has not been applied in superconducting power cables, where it offers the direct benefit of an increase in the critical current density. The essential point is to apply a magnetic field parallel to the cable itself, and hence, the superconducting tapes in the outer shielding conductor are wound in one direction so that the return current flowing in this conductor produces a longitudinal magnetic field. Then, the superconducting tapes in the inner conductor are wound so that the force-free structure is achieved (see Fig. 7.4). The magnetic field is almost directed parallel to the cable axis on the innermost layer and its angle tends to increase on the outer layers. Thus, the winding angle of the superconducting tapes is monotonically increased for the outer layers. Although a detailed analysis is needed to design an optimal structure, the principle is very simple. It may be anticipated that an appreciable effect will not be obtained, since the resultant longitudinal magnetic field is not very strong. A relatively strong longitudinal magnetic field can be achieved, however, since a longitudinal magnetic field is also produced by the inner conductor. Only

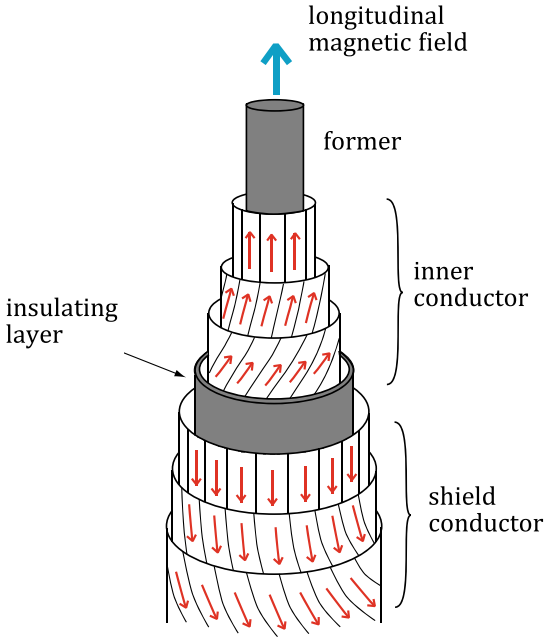

Fig. 7.4 Structure of superconducting DC power cable in which the longitudinal magnetic field effect is utilized. The arrows show the directions of the currents flowing in the superconducting tapes

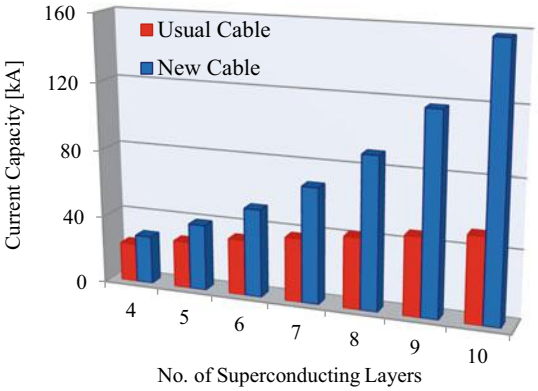

Fig. 7.5 Change in the current-carrying capacity when the number of superconducting tape layers is changed for usual and longitudinal-field cables

flat tapes can be fabricated from high-temperature superconductors, and these are considered to be disadvantageous in comparison with round wires made of metallic superconductors. This is true as a material for superconducting magnets, but tape superconductors are more advantageous to achieve the force-free structure in the cable. Hence, high-temperature superconductors are suitable for superconducting cables. Since the longitudinal magnetic field effect becomes more prominent under a stronger magnetic field, as shown in Figs. 6.2 and 6.8, this structure is more effective for power transmission of larger currents. When the number of superconducting layers is increased, the current-carrying capacity increases monotonically for both the usual and the new longitudinal-field cables. But the enhancement of the current-carrying capacity is stronger for the longitudinal-field cable, as shown in Fig. 7.5. This simply results from the difference in the magnetic field dependence of the critical current density between the transverse and longitudinal magnetic fields (see Fig. 6.8a).

It was mentioned that the introduction of fault current limiters is necessary to achieve an electric power network using superconducting DC power cable over a wide area to promote the use of renewable energy. It is possible to add a fault-current limiting function to the superconducting cable, and such a trial has been carried out in the USA and Korea, as mentioned above. The principle is the same as for the longitudinal-field cable. In the usual superconducting cable, the resistive transition of superconductors is simply used. On the other hand, the longitudinal magnetic field effect used for the enhancement of the critical current density is effectively used also for the limiting of fault current in the longitudinal-field cable. That is, the longitudinal magnetic field used to increase the critical current density in normal operation is designed to be decreased when a large fault current starts to flow. The resultant decrease in the critical current density accelerates the resistive transition, and the fault current limiting function is strengthened. The structure of superconducting cable with fault current limiting function is shown in Fig. 7.6 [2]. The copper wires for stabilization is twisted in the opposite direction to the superconducting tapes in

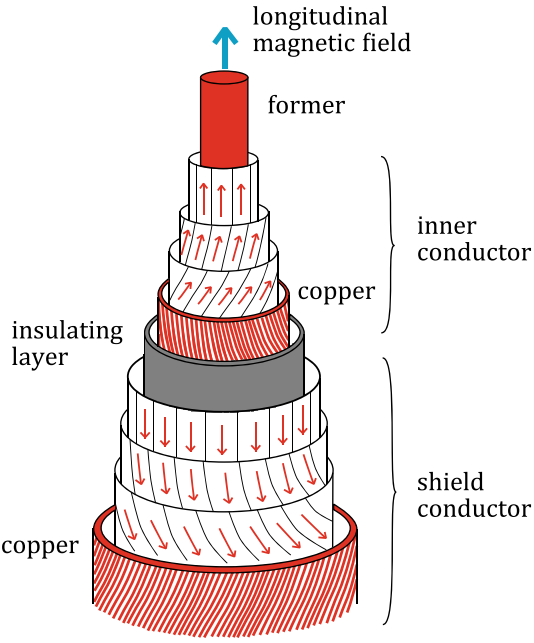

Fig. 7.6 Structure of a superconducting power cable in which the excess current flowing in copper layers decreases the longitudinal magnetic field to decrease the critical current density in the superconducting layers

each conductor to decrease the longitudinal magnetic field when the excess current flows in the copper layer.

A critical current density that increases with increasing longitudinal magnetic field, as shown in Fig. 6.8a, has been obtained for short samples of REBCO tapes. Its value for long commercial REBCO tapes is, however, almost flat or slightly decreasing with increasing longitudinal magnetic field. Hence, the improvement of the current-carrying capacity of a new-type cable is not so dramatic, as shown in Fig. 7.5, although it is appreciably higher than that in the usual cables [3]. This is probably caused by defects that disturb uniform current transportation in commercial tapes. Improvement of the current-carrying property of commercial tapes, which will realize a dramatic improvement in the cable performance, is expected in the future.

Superconducting instruments, such as generators, transformers, magnetic energy storage devices, fault current limiters, etc., that compose the electric power grid with generation using renewable energy are being developed now. Especially for the case of high power generation using wind turbines, reduction in size of generators is strongly required, and the application of superconducting generators is expected.

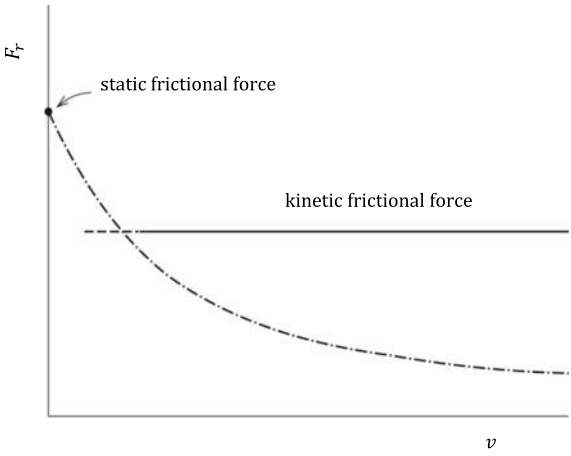

Fig. 7.7 Dependence of the frictional force F_r on the velocity v. The chained line shows the theoretical prediction of the frictional force on a perfectly rigid body moving in a periodic potential

7.3 Scientific Significance of Flux Pinning Phenomena

Even under applied current, energy dissipation does not occur in a superconductor, if flux lines are not driven to move. The loss due to the motion of flux lines is not of the copper-loss type similar to that in a usual current-carrying resistive material, but is a hysteresis loss of the iron-loss type. The details of this mechanism were explained in Chap. 5. The hysteresis loss is caused by the large velocity of flux lines when they fall into or jump out of the pinning potential well.

In other fields than flux pinning in superconductors, similar phenomena are found in the motion of magnetic domain walls[2] in ferromagnetic materials or in friction in mechanical systems. In particular, it is well known that a magnetic domain wall captured by a crystalline defect moves suddenly to a stable position when it is driven by a magnetic force. This is quite similar to the motion of a depinned flux line in a superconductor. The friction is speculated to be caused by Coulomb interaction between the unevenness of the adjacent frictional surfaces of the material and the floor, if we neglect complicated cases with microscopic destruction, and the oscillation of local parts driven by the added force causes the loss. Figure 7.7 shows the dependence of the frictional force on the macroscopic velocity of a material, and the dynamic frictional force is generally weaker than the static frictional force. Since a driven material moves suddenly for this reason, the frictional force cannot be measured in the region of low velocity. It is possible to reduce the velocity after the material has started to move. If the material moving on the floor is perfectly rigid,

[2]Magnetic domain wall: A region in which the magnetization is aligned parallel is called a magnetic domain in a ferromagnetic material and a ferromagnetic single crystal on a macroscopic scale is usually composed of many magnetic domains with magnetization in various directions. The boundary between two adjacent magnetic domains is the magnetic domain wall. Its thickness is about 50 nm for iron. The direction of the magnetization changes gradually along the direction across the wall. When the magnetic field is changed within a relatively weak range, the change in the magnetization of a ferromagnetic material is caused by displacement of magnetic domain walls.

the dynamic frictional force caused by its motion in the potential field is expected to approach zero asymptotically, as shown by the chained line in Fig. 7.7.[3] In practice, energy dissipation occurs due to the elastic damped oscillations of the projections on each rough surface. These two factors result in the dynamic frictional force, which diminishes but approaches a finite value, as illustrated in Fig. 7.7. In the case of flux pinning in a superconductor, the flux line lattice behaves elastically, and the resultant dynamic pinning force is similar to the static pinning force. This is assumed to be the same in the dynamic critical state model.

The common point in these phenomena is random interactions between a moving body and the matter that restricts the motion, which can be described as a potential. These interactions are reversible when the displacement of a flux line, magnetic domain wall, or body is small enough. In particular, such reversible phenomena can be measured when a variation in magnetization is observed due to a small AC magnetic field on a major magnetization curve. The play of a body when it is displaced slightly by a force corresponds to this in a mechanical system. The reversibility shows that such interactions are caused by potential, and this is the essence of those phenomena that show hysteresis under large displacements.

In the case of electromagnetic phenomena in a superconductor, the irreversibility was proved by the summation theory of flux pinning. The irreversibility does not come from the breaking of time reversal symmetry of the equation of motion but from the change in the force balance equation before and after the change in the direction of motion due to unstable flux motion. The unstable flux motion is also responsible for the hysteresis loss through the mechanism of viscous loss. A similar theoretical system can be constructed for the motion of magnetic domain walls in ferromagnetic materials or for friction in mechanical systems. The irreversibility in these systems is also derived from the change in the governing equation due to the instability. Hence, this kind of theory can be generalized to describe irreversibility of this nature, although some correction is necessary. In the case of the motion of magnetic domain walls, the spacing between magnetic domain walls is wide, and there is no periodicity among them, so a model of isolated pinning centers seems to be adequate instead of the periodic pinning model used in this book. It seems to be necessary to assume irregular pinning centers with high density for friction.

The longitudinal magnetic field effect was introduced as a new electromagnetic phenomenon in this book. The force-free state that appears in the longitudinal magnetic field effect is a special state with finite magnetic helicity in the static state, and hence, it can be achieved only in superconductors. The current and magnetic flux lines are locally parallel to each other, and the resultant Lorentz force is zero in this state. There is a characteristic torsion, however, i.e., a rotational shearing torsion, in the flux line system in this state, and a torque works on flux lines to reduce the torsion. This is the force-free torque. The pinning energy is shared between the force-balance and the torque balance. The flux line system is self-organized to

[3] See J. E. Evetts and J. R. Appleyard: Proc. Int. Disc. Meeting on Flux Pinning in Supercond., Göttingen, 1974, p. 69, or T. Matsushita, "Flux Pinning in Superconductors, Ed. 2," (Springer, 2014) p. 336 (Exercise 7.4).

minimize the energy dissipation, and most pinning energy is allotted for the torque balance. This explains why the pinning force does not appear in the force balance, resulting in the force-free state, whereas the critical current density is determined by the flux pinning strength. All the electromagnetic phenomena of the longitudinal magnetic field effect, including the negative electric field, can be generally explained by the rotational flux motion driven by the force-free torque. The magnetic helicity is retained, even in the situation of rotational flux motion. It is interesting to compare the behavior of flux lines in the superconductor in a longitudinal magnetic field with that of flux lines in a plasma that also has magnetic helicity. The electromagnetic phenomena in the longitudinal magnetic field are essentially different from those in the superconductor in the transverse magnetic field. The magnetic helicity in the latter case is zero. Although the force-free torque appears only in the superconductor in the longitudinal magnetic field, it surely adds a new page to Maxwell's theory.

In addition, the characteristic force-free state appears only under the influence of flux pinning. In other words, the longitudinal magnetic field effect is an effect in which the flux pinning plays a dominant role and it is essentially irreversible. The flux pinning effect has attracted attention in vortex physics as one of the factors that determine the phase of the flux line system. This is the first case where the flux pinning effect is dominant in the field of fundamental science.

The electromagnetic phenomena in the transverse magnetic field are described by the phenomenological critical state model. It was shown that the assumption in this model that the pinning force makes the maximum effort to prevent a variation in the magnetic flux distribution does not contradict the principle of irreversible thermodynamics of minimum energy dissipation. There are two kinds of balance in determining the current direction with two degrees of freedom under a longitudinal magnetic field, and it was shown again that the pinning energy is distributed so as to minimize the energy dissipation, as assumed in the principle. It is an important topic to prove theoretically that this principle holds generally, even in a nonlinear dissipation system, as discussed in Appendix A.10. Detailed analyses of various electromagnetic phenomena in the longitudinal magnetic field are not sufficient as yet, and research by many scientists is needed in the future. Thus, the physics of the longitudinal magnetic field effect is a new science, in which electromagnetism and irreversible thermodynamics merge together. Efforts to deepen this field are expected.

Coffee break (7)

Poynting's vector

One of most useful concepts besides the continuity equation of flux lines in this book is Poynting's vector. The energy that penetrates the superconductor while the external magnetic field is changing can be estimated using Poynting's vector. As shown in this book, the variation in the internal magnetic energy is different from this energy, indicating the possibility of the appearance or disappearance of energy. This is the work done by the driving force. The force-free torque in the longitudinal magnetic field effect is also derived using Poynting's vector.

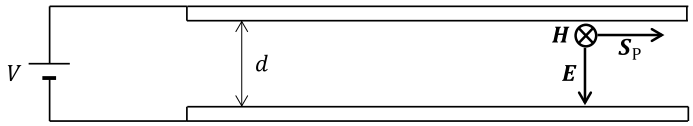

Fig. 7.8 Poynting's vector produced by electric and magnetic fields applied in the space between two parallel plate conductors

Although Poynting's vector is quite useful, as mentioned above, there is a case where we have to carefully understand the meaning of this quantity. We assume that voltage V is applied between two parallel long plate conductors separated by distance d. A magnetic field H is applied in the space between the two plates in the direction normal to the sheet using a permanent magnet, as shown in Fig. 7.8. Poynting's vector in the space is $S_P = VH/d$ and directed horizontally. This suggests an energetic flow in this situation, although no electric power is supplied by the source. How can we understand this?

Equation (2.61) holds. This result does not change, however, when Poynting's vector $\boldsymbol{S}_P$ is replaced by $\boldsymbol{S}_P + \nabla \times \boldsymbol{K}$. That is, there is a difference by an amount of the curl of an arbitrary vector $\boldsymbol{K}$ between Poynting's vector and the true energy flow [4]. Hence, it is necessary to check if Poynting's vector represents the true energy flow in each case. This is analogous to the arbitrariness when we derive the electric field from Maxwell's (2.49) and the continuity equation of flux lines (5.34). It does not result necessarily in (4.41) but in (6.1) in the longitudinal magnetic field. It is not possible to prove this theoretically, but we have to judge by comparing with experimental results.

References

1. T. Matsushita, Masaru Kiuchi and Edmund Soji Otabe: supercond. Sci. Technol. **25**, 125009 (2012)
2. T. Matsushita, M. Kiuchi, E.S. Otabe, V.S. Vyatkin, IEEE Trans. Appl. Supercond. **25**, 5401704 (2015)
3. V.S. Vyatkin, M. Kiuchi, E.S. Otabe, T. Matsushita, IEEE Trans. Appl. Supercond. **25**, 6606207 (2015)
4. T. Matsushita, K. Funaki, Teionkougaku **39**, 2 (2004). [in Japanese]

Afterword

In electromagnetism, the fundamental electromagnetic properties of substances are only described based on simple rules, without regards to the detailed mechanisms in each substance. It is astonishing, however, that this principle holds over a wide range, from the quantum scale to the astronomical scale. In addition, it won the argument against mechanics, which had been believed to be perfectly rigorous for hundreds of years, and opened the way to the principle of relativity. As shown in this book, the superconductor, which had not yet been discovered when Maxwell's theory was completed, has its own position in the present theory of electromagnetism, based on the $\boldsymbol{E}$-$\boldsymbol{B}$ analogy. The fact that zero electrical resistivity in diamagnetic superconductors can be derived by Maxwell's theory itself represents the profound rigor of this theory. In other words, the superconductor could have been predicted in the 19th century. This means that superconductors are not special, but one type of the common materials. In fact, many kinds of materials show superconductivity.

The electromagnetic phenomena associated with flux pinning in the superconductor, especially irreversibility and the longitudinal magnetic field effect, have been explained in this book. The physical properties of superconductors have attracted attention, and clarification of the mechanism of high temperature superconductivity in cuprates and further searching for room temperature superconductors are expected in the future. On the other hand, if we look at the electromagnetic phenomena in the superconductor, we can also find interesting subjects associated with irreversible thermodynamics and classic electromagnetism, as shown in this book. Further scientific development in these fields is expected in the future. For this reason, enrichment of the education of young scientists on primary electromagnetism is desirable as a first step.

The contents in this book are based on the research and education conducted by the author. Looking back at these, the sequence is not simple. The author started the study of applied superconductivity in 1969 for his graduate thesis in the group of Profs. Irie and Yamafuji of the Department of Electronics in the Faculty of Engineering in Kyushu University. This is the year in which the human being reached the moon.

T. Matsushita, *Superconductivity and Electromagnetism*, Springer Series in Solid-State Sciences 195, https://doi.org/10.1007/978-3-030-67568-4

This group was the first group worldwide to complete the theoretical framework of electromagnetic phenomena based on the critical state model and investigate the flux pinning mechanism in 1967. In addition, they designed the superconducting magnetic energy storage (SMES) system and classified such systems based on their stored energy and power in the early 1970s. In such a situation, his research was naturally directed to the electromagnetic properties and flux pinning phenomena relevant to applied superconductivity. Thus, the author received a doctoral degree for his research on the flux pinning mechanism.

In the course of the research in this group, the longitudinal magnetic field effect was investigated by other scientists, and the author was attracted to this peculiar phenomenon. The first analysis by the author on this effect was on the flux invasion into a superconducting cylinder, as shown in Appendix A.10. The author recognized the fundamental points on this effect, and then, he read many associated papers. Finally, he found that the misunderstanding of this effect in the 1970s was essentially based on a wrong interpretation of the theory by Josephson on general electromagnetic features. Then, each problem was solved step by step.

High temperature superconductivity was discovered in 1986. Soon after, almost all of the research on superconductivity was concentrated on the new materials. The author moved from Kyushu University to Kyushu Institute of Technology in 1990. Although the research on flux pinning phenomena and the longitudinal magnetic field effect in metallic superconductors was still interesting, the author also mainly investigated the electromagnetic phenomena, especially the flux creep, of high temperature superconductors and established the theory of collective flux creep and flow. In this theory the flux bundle size is assumed to be determined by the principle of minimum energy dissipation. This was based on his experience in studying the longitudinal magnetic field effect.

In the meantime, the author was asked to publish "Flux Pinning and Electromagnetic Phenomena in Superconductors" by Sangyo Tosho Co. in Japan. Then, the coherent potential approximation theory on the flux pinning mechanism was completed, since it was the main point in this book. Thus, the threshold problem in the summation theory that had been argued for a long time was solved. The complicated theory of the longitudinal magnetic field effect was also arranged in order for easy understanding.

The author was occasionally occupied by the administrative work of Kyushu Institute of Technology from the end of the 20th century to the beginning of the 21st century, so it was quite difficult to continue research in this period. There was a time to think over the difficult problem, however, of spreading the acquired knowledge on the longitudinal magnetic field effect to scientists around the world. Unfortunately, the electromagnetic phenomena in superconductors are familiar to only a small fraction of scientists, and almost no scientists in other fields will know about the longitudinal magnetic field effect. In addition, whereas this is a fundamental effect of electromagnetism, the section on electromagnetism has disappeared from the main journals on physics. Thus, there is no way to directly send a message to scientists around the world. The author then felt the necessity to familiarize young people with superconductivity. Fortunately, the author had taught the fundamental magnetic

properties of superconductors in lectures on electromagnetism and decided to publish a textbook in which superconductivity was introduced. This was quite successful, especially in terms of strengthening the present ***E*-*B*** analogy in electromagnetism. When the administrative work was over, the author engaged in writing this textbook. The textbook was then published, and the English edition entitled "Flux Pinning in Superconductors" was also published.

Later, the author published the main points of the longitudinal magnetic field effect through a newspaper. A newspaper reporter asked about the possibility of application of this effect. The author answered that the superconducting power cable would be a candidate. Several days later, an officer of the incubation center of the Institute asked the author about the possibility of this application, followed by a practical investigation of the new superconducting power cable. The principle of the cable is explained in Chap. 7. It was quite lucky for the author, who studied in the group of Profs. Irie and Yamafuji, to be engaged in a practical application of superconductivity.

Just before his retirement from Kyushu Institute of Technology, the author felt that it was necessary to unify the theories of flux pinning by Prof. Fujio Irie and Prof. Kaoru Yamafuji into a comprehensive structure. The flux pinning theory of Prof. Yamafuji was already proved many years ago, including the threshold problem by using the statistical method. Then, the critical state model was derived theoretically using first principles. Although each flux pinning theory was separately proved, the statistical summation theory and the critical state theory were still not yet unified. Then, the pinning loss power density was calculated, using the time average equivalent to the statistical average in the former theory, and it was shown that the obtained relationship between the pinning loss power density and the pinning force density was the same as that assumed in the critical state model. Thus, the theories published in 1967 by two professors ([3] and [13] in Chap. 5) could be completely unified, and the author could repay them.

Finally the author would like to thank Ms. Kaori Ono for drawing electronic figures and Dr. Tania M. Silver at Wollongong University for correction of the English in the book.

Appendix

A.1 Derivation of Ginzburg-Landau Equations

The equilibrium state in a superconductor is given by the condition in which the volume integral of the free energy density $\mathcal{F}_\mathrm{s}$ in (4.2) takes on a minimum value with respect to the order parameter Ψ and the vector potential $\boldsymbol{A}$.

It is assumed that Ψ changes by a small amount $\delta\Psi$. (Ψ^* also changes by $\delta\Psi^*$.) This leads to the variation in the total free energy:

$$\int_\mathrm{V}\left(\frac{\partial\mathcal{F}_\mathrm{s}}{\partial\Psi}\delta\Psi+\frac{\partial\mathcal{F}_\mathrm{s}}{\partial\nabla\Psi}\cdot\nabla\delta\Psi+\frac{\partial\mathcal{F}_\mathrm{s}}{\partial\Psi^*}\delta\Psi^*+\frac{\partial\mathcal{F}_\mathrm{s}}{\partial\nabla\Psi^*}\cdot\nabla\delta\Psi^*\right)\mathrm{d}V, \tag{A.1.1}$$

where V is the region occupied by the superconductor. Note that $\mathcal{F}_\mathrm{s}$ is also a function of $\nabla\Psi$. The above variation should be zero when $\mathcal{F}_\mathrm{s}$ takes on a minimum value with respect to Ψ. When partial integration is carried out for the second and third terms, we have

$$\begin{aligned}&\int_\mathrm{S}\left(\frac{\partial\mathcal{F}_\mathrm{s}}{\partial\nabla\Psi}\delta\Psi+\frac{\partial\mathcal{F}_\mathrm{s}}{\partial\nabla\Psi^*}\delta\Psi^*\right)\cdot\mathrm{d}\boldsymbol{S}\\&\quad+\int_\mathrm{V}\left[\left(\frac{\partial\mathcal{F}_\mathrm{s}}{\partial\Psi}-\nabla\cdot\frac{\partial\mathcal{F}_\mathrm{s}}{\partial\nabla\Psi}\right)\delta\Psi+\left(\frac{\partial\mathcal{F}_\mathrm{s}}{\partial\Psi^*}-\nabla\cdot\frac{\partial\mathcal{F}_\mathrm{s}}{\partial\nabla\Psi^*}\right)\delta\Psi^*\right]\mathrm{d}V=0,\end{aligned} \tag{A.1.2}$$

where S is the surface of V and Gauss' theorem was used. We can set the surface integral to zero by selecting a suitable condition, as will be shown later. So that the volume integral of the second term is zero for arbitrary $\delta\Psi^*$, Euler's equation should be satisfied:

T. Matsushita, *Superconductivity and Electromagnetism*, Springer Series in Solid-State Sciences 195, https://doi.org/10.1007/978-3-030-67568-4

$$\frac{\partial \mathcal{F}_s}{\partial \Psi^*} - \nabla \cdot \frac{\partial \mathcal{F}_s}{\partial \nabla \Psi^*} = 0. \tag{A.1.3}$$

The condition that the other volume integral is zero is complex conjugate with (A.1.3). Since the kinetic energy density of the fifth term in (4.2) is written as

$$|(-\mathrm{i}\hbar\nabla + 2e\boldsymbol{A})\Psi|^2 = \hbar^2 \nabla\Psi \cdot \nabla\Psi^* + 2\mathrm{i}\hbar e\boldsymbol{A} \cdot \left(\Psi\nabla\Psi^* - \Psi^*\nabla\Psi\right) + 4e^2\boldsymbol{A}^2\Psi\Psi^*, \tag{A.1.4}$$

we have

$$\frac{\partial \mathcal{F}_\mathrm{s}}{\partial \Psi^*} = \alpha\Psi + \beta|\Psi|^2\Psi + \frac{1}{m^*}\left(-\mathrm{i}\hbar e\boldsymbol{A} \cdot \nabla\Psi + 2e^2\boldsymbol{A}^2\Psi\right), \tag{A.1.5}$$

$$\frac{\partial \mathcal{F}_s}{\partial \nabla \Psi^*} = \frac{1}{2m^*}\left(\hbar^2\nabla\Psi + 2\mathrm{i}\hbar e\Psi\boldsymbol{A}\right). \tag{A.1.6}$$

Using the condition of $\nabla \cdot \boldsymbol{A} = 0$, (4.3) leads to

$$\frac{1}{2m^*}(-\mathrm{i}\hbar\nabla + 2e\boldsymbol{A})^2\Psi + \alpha\Psi + \beta|\Psi|^2\Psi = 0. \tag{A.1.7}$$

On substituting (A.1.7) into (A.1.2), it is found that the following condition should be fulfilled so that the surface integral of this equation is zero:

$$\boldsymbol{n} \cdot (-\mathrm{i}\hbar\nabla + 2e\boldsymbol{A})\Psi = 0, \tag{A.1.8}$$

where $\boldsymbol{n}$ is a unit vector normal to the surface of the superconductor. The meaning of this condition will be explained later.

Next, it is assumed that the vector potential $\boldsymbol{A}$ changes by a small amount $\delta\boldsymbol{A}$. This leads to a variation in the total free energy:

$$\int_\mathrm{V}\left[\frac{1}{\mu_0}(\nabla \times \boldsymbol{A}) \cdot (\nabla \times \delta\boldsymbol{A}) - \frac{\mathrm{i}\hbar e}{m^*}\delta\boldsymbol{A} \cdot \left(\Psi^*\nabla\Psi - \Psi\nabla\Psi^*\right) + \frac{4e^2}{m^*}|\Psi|^2\boldsymbol{A} \cdot \delta\boldsymbol{A}\right]\mathrm{d}V. \tag{A.1.9}$$

This should be zero in the equilibrium condition. By partially integrating the first term, we have

$$\int_\mathrm{S}\frac{1}{\mu_0}[\delta\boldsymbol{A} \times (\nabla \times \boldsymbol{A})] \cdot \mathrm{d}\boldsymbol{S} + \int_\mathrm{V}\delta\boldsymbol{A} \cdot \left[\frac{1}{\mu_0}\nabla \times \nabla \times \boldsymbol{A} - \frac{\mathrm{i}\hbar e}{m^*}\left(\Psi^*\nabla\Psi - \Psi\nabla\Psi^*\right) + \frac{4e^2}{m^*}|\Psi|^2\boldsymbol{A}\right]\mathrm{d}V = 0. \tag{A.1.10}$$

Under the condition of zero surface integral the content in the brackets is zero:

$$\boldsymbol{i} = \frac{1}{\mu_0}\nabla \times \nabla \times \boldsymbol{A} = \frac{\mathrm{i}\hbar e}{m^*}\left(\Psi^*\nabla\Psi - \Psi\nabla\Psi^*\right) - \frac{4e^2}{m^*}|\Psi|^2\boldsymbol{A}. \tag{A.1.11}$$

Thus, (4.4) is derived.

If the left-hand side of (A.1.8) is expressed as $\boldsymbol{n}\cdot\boldsymbol{K}$, the current density in (A.1.11) is written as

$$\boldsymbol{i} = -\frac{e}{m^*}\left(\Psi^*\boldsymbol{K} + \Psi\boldsymbol{K}^*\right). \tag{A.1.12}$$

Hence, the condition of (A.1.8) is that the current does not flow across the superconductor, i.e., $\boldsymbol{n}\cdot\boldsymbol{i} = 0$.

So that the surface integral of (A.1.10) is zero, the following condition should be fulfilled:

$$[\delta\boldsymbol{A} \times (\nabla \times \boldsymbol{A})]\cdot\boldsymbol{n} = 0. \tag{A.1.13}$$

Under the condition of the usual transverse magnetic field, (4.41) for the induced electric field holds. In this case, if the displacement of flux lines that causes $\delta\boldsymbol{A}$ is denoted by $\delta\boldsymbol{u}$, we have the relationship $\delta\boldsymbol{A} = \delta\boldsymbol{u} \times \boldsymbol{B}$. (Note that its time derivative leads to (4.41).) Hence, the content in the brackets in (A.1.13) is written as

$$(\delta\boldsymbol{u} \times \boldsymbol{B}) \times \boldsymbol{B} = (\boldsymbol{B}\cdot\delta\boldsymbol{u})\boldsymbol{B} - B^2\delta\boldsymbol{u}. \tag{A.1.14}$$

Since the displacement of flux lines along their length is meaningless, the displacement is defined so that it is perpendicular to the flux lines ($\boldsymbol{B}\cdot\delta\boldsymbol{u} = 0$). Thus, the condition of (A.1.13) is written as

$$\boldsymbol{n}\cdot\delta\boldsymbol{u} = 0. \tag{A.1.15}$$

This requires that flux lines do not pass through the surface of the superconductor.

A.2 Derivation of (4.23)

The kinetic energy density of the fifth term in (4.2) is written as

$$\frac{1}{2m^*}\left|-\mathrm{i}\hbar\mathrm{e}^{\mathrm{i}\varphi}\nabla|\Psi| + (\hbar\nabla\varphi + 2e\boldsymbol{A})\Psi\right|^2 = \frac{1}{2m^*}\left[\hbar^2(\nabla|\Psi|)^2 + (\hbar\nabla\varphi + 2e\boldsymbol{A})^2|\Psi|^2\right]. \tag{A.2.1}$$

Thus, using (4.20), the current density is

$$\boldsymbol{i} = \frac{2e}{m^*}|\Psi|^2(\hbar\nabla\varphi + 2e\boldsymbol{A}). \tag{A.2.2}$$

Hence, the kinetic energy density is

$$\frac{\hbar^2}{2m^*}(\nabla|\Psi|)^2 + \frac{m^*}{8e^2|\Psi|^2}\boldsymbol{i}^2. \tag{A.2.3}$$

Following (1.105) in [1], the current density is given by

$$\boldsymbol{i} = -\frac{H_{c2}}{2\kappa^2|\Psi_\infty|^2}\nabla\times\left(|\Psi|^2\boldsymbol{i}_z\right) = -\frac{H_{c2}}{2\kappa^2|\Psi_\infty|^2}\left(\frac{\partial|\Psi|^2}{\partial y}\boldsymbol{i}_x - \frac{\partial|\Psi|^2}{\partial x}\boldsymbol{i}_y\right). \tag{A.2.4}$$

Hence, the second term in (A.2.3) leads to

$$\frac{m^*H_{c2}^2}{32\kappa^4e^2|\Psi_\infty|^4|\Psi|^2}\left[\left(\frac{\partial|\Psi|^2}{\partial x}\right)^2 + \left(\frac{\partial|\Psi|^2}{\partial y}\right)^2\right] = \frac{m^*H_{c2}^2}{8\kappa^4e^2|\Psi_\infty|^4}(\nabla|\Psi|)^2 = \frac{\hbar^2}{2m^*}(\nabla|\Psi|)^2, \tag{A.2.5}$$

where we have used the relationships of $|\Psi_\infty|^2 = \mu_0H_c^2/|\alpha|$ and $|\alpha| = (2e\lambda\mu_0H_c)^2/m^*$ from (4.37) and (4.38). Thus, the sum of the condensation energy density and the kinetic energy density at high magnetic fields is written as

$$\alpha|\Psi|^2 + \frac{\hbar^2}{m^*}(\nabla|\Psi|)^2 = \mu_0H_c^2\left[-|\psi|^2 + 2\xi^2(\nabla|\psi|)^2\right], \tag{A.2.6}$$

where we have used $\psi = \Psi/|\Psi_\infty|$ and (4.6). Equation (4.32) is obtained by spatially averaging this equation.

A.3 Derivation of (4.42)

The current flows azimuthally around a stationary quantized flux line along the z–axis and its density at radius r from the center is given by (see (1.64) in [1])

$$j = \frac{\phi_0}{2\pi\mu_0\lambda^2 r}. \tag{A.3.1}$$

Hence, the azimuthal velocity of superconducting electrons is

$$v_{s\theta} = -\frac{j}{2e|\Psi_\infty|^2} = -\frac{\hbar}{m^*r}, \tag{A.3.2}$$

where (4.17) was used. Hence, the momentum of a superconducting electron is given by

$$\boldsymbol{p}_{\mathrm{s}} = m^* v_{\mathrm{s}\theta} \boldsymbol{i}_\theta = -\frac{\hbar}{r} \boldsymbol{i}_\theta, \tag{A.3.3}$$

where $\boldsymbol{i}_\theta$ is the azimuthal unit vector. It is assumed that the quantized flux line flows with velocity $\boldsymbol{v}$ along the x-axis, as discussed in Sect. 4.3. If the velocity of the superconducting electron is $\boldsymbol{v}_{\mathrm{s}}$, its gauge-invariant momentum is given by

$$m^* \boldsymbol{v}_{\mathrm{s}} = \boldsymbol{p}_{\mathrm{s}} + 2e\boldsymbol{A}. \tag{A.3.4}$$

If we approximate that the magnetic flux density B is almost uniform in the area where the current flows around the normal core of the quantized flux line, we have $\boldsymbol{A} = (Br/2)\boldsymbol{i}_\theta$. The force on the superconducting electron is denoted by $\boldsymbol{f}_{\mathrm{e}}$. Then, the equation of motion of the superconducting electron is

$$m^* \frac{\mathrm{d}\boldsymbol{v}_{\mathrm{s}}}{\mathrm{d}t} = \boldsymbol{f}_{\mathrm{e}}. \tag{A.3.5}$$

When the velocity of the quantized flux line is small enough, we can approximate as $\mathrm{d}/\mathrm{d}t \cong -(\boldsymbol{v} \cdot \nabla) = -v(\partial/\partial x)$ and (A.3.5) leads to

$$\boldsymbol{f}_{\mathrm{e}} = v \frac{\partial}{\partial x} \left(\frac{\hbar}{r} - eBr \right) \boldsymbol{i}_\theta. \tag{A.3.6}$$

Since this force is given by the electric field, the electric field is

$$\boldsymbol{e} = -\frac{\boldsymbol{f}_{\mathrm{e}}}{2e} = -v \frac{\partial}{\partial x} \left(\frac{\phi_0}{2\pi r} - \frac{Br}{2} \right) \boldsymbol{i}_\theta. \tag{A.3.7}$$

The relationships between the two-dimensional Cartesian coordinates (x, y) and the cylindrical coordinates (r, θ) are

$$x = r\cos\theta, \, y = r\sin\theta \tag{A.3.8}$$

and the unit vectors in the cylindrical coordinates are written as

$$\boldsymbol{i}_r = \boldsymbol{i}_x \cos\theta + \boldsymbol{i}_y \sin\theta, \, \boldsymbol{i}_\theta = -\boldsymbol{i}_x \sin\theta + \boldsymbol{i}_y \cos\theta. \tag{A.3.9}$$

Using these relationships, we have

$$\frac{\partial}{\partial x}(r\boldsymbol{i}_\theta) = \boldsymbol{i}_y, \, \frac{\partial}{\partial x}\left(\frac{1}{r} \boldsymbol{i}_\theta \right) = \frac{1}{r^2}(-\boldsymbol{i}_\theta \cos\theta + \boldsymbol{i}_r \sin\theta). \tag{A.3.10}$$

Thus, (4.32) is derived with $Bv\boldsymbol{i}_y = \boldsymbol{B} \times \boldsymbol{v}$.

A.4 Derivation of (5.78)

In the case where a static approximation holds, we can set

$$\Delta = \delta = \frac{a_\mathrm{f}(f_\mathrm{p} - 3f_\mathrm{pt})}{4f_\mathrm{pt}} \tag{A.4.1}$$

at $t = 0$ and

$$\Delta = vt_1 + \delta = \frac{a_\mathrm{f}(f_\mathrm{p} + f_\mathrm{pt})}{4f_\mathrm{pt}} \tag{A.4.2}$$

at $t = t_1$. Then, we obtain

$$vt_1 = a_\mathrm{f}. \tag{A.4.3}$$

If the second small term proportional to v^2 is neglected in (5.77), the pinning loss power density is given by

$$P_\mathrm{p} = \frac{N_\mathrm{p}\eta^*}{T}\left\{\left(\frac{f_\mathrm{pt}}{f_\mathrm{p}+f_\mathrm{pt}}\right)^2 \int_0^{t_1}\left[v + \frac{K_1}{\tau_1}\exp\left(-\frac{t}{\tau_1}\right)\right]^2 \mathrm{d}t \right.$$
$$\left. + \left(\frac{f_\mathrm{pt}}{f_\mathrm{p}-f_\mathrm{pt}}\right)^2 \int_{t_1}^{T}\left[v + \frac{K_2}{\tau_2}\exp\left(\frac{t-t_1}{\tau_2}\right)\right]^2 \mathrm{d}t\right\}. \tag{A.4.4}$$

Using the condition (5.75), the first integral in the braces is calculated as

$$v^2 t_1 + 2K_1 v\left[1 - \exp\left(-\frac{t_1}{\tau_1}\right)\right] + \frac{K_1^2}{2\tau_1}\left[1 - \exp\left(-\frac{2t_1}{\tau_1}\right)\right]$$
$$= \frac{a_\mathrm{f}(f_\mathrm{p}+f_\mathrm{pt})v}{f_\mathrm{p}} - v^2 t_1 + \frac{K_1^2}{2\tau_1} - \frac{1}{2\tau_1}\left[vt_1 - \frac{a_\mathrm{f}(f_\mathrm{p}+f_\mathrm{pt})}{2f_\mathrm{pt}} + K_1\right]^2. \tag{A.4.5}$$

Using (A.4.2) and (A.4.3) and neglecting small terms proportional to v, the quantity in (A.4.5) is reduced to

$$\frac{a_\mathrm{f}(f_\mathrm{p}+f_\mathrm{pt})(f_\mathrm{p}-f_\mathrm{pt})^2}{2\eta^* f_\mathrm{pt}^2}. \tag{A.4.6}$$

The second integral in the braces is calculated as

$$\frac{a_f(f_p - f_{pt})^3}{2\eta^* f_{pt}^2}. \tag{A.4.7}$$

Thus, the pinning loss power density is given by

$$P_p = \frac{N_p \eta^* v}{a_f} \cdot \frac{a_f}{2\eta^*}\left[\frac{(f_p - f_{pt})^2}{f_p + f_{pt}} + f_p - f_{pt}\right] = \frac{N_p f_p (f_p - f_{pt}) v}{f_p + f_{pt}}. \tag{A.4.8}$$

A.5 Derivation of (5.86)

Here, we discuss the structure of a partial flux line lattice that is treated representatively in the statistical treatment. For this purpose, the pinning correlation lengths are needed and the elastic moduli of the flux line lattice are explained. There are three independent elastic moduli and these are C_{11} for uniaxial compression, C_{44} for bending deformation, and C_{66} for shear (see Fig. A.1). These are respectively given by [2]

$$C_{11} \cong C_{44} = \frac{B^2}{\mu_0}, \tag{A.5.1}$$

$$C_{66} \cong \frac{\mu_0 H_c^2}{4} b(1-b)^2, \tag{A.5.2}$$

where $b = B/\mu_0 H_{c2}$ is the reduced field. The pinning correlation length is the characteristic distance over which the interaction between flux lines is shielded by flux pinning, and Campbell's penetration depth given by (5.49) is one of the pinning correlation lengths. Using (5.47), (5.49) is expressed as

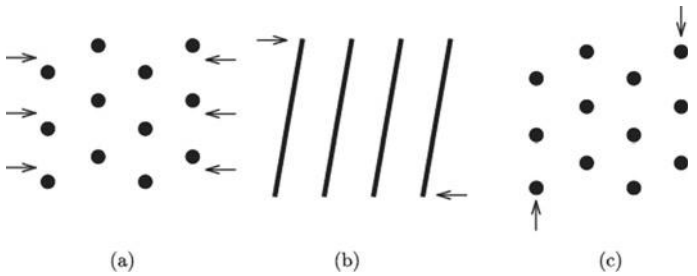

Fig. A.1 Deformation of flux line lattice for **a** uniaxial compression, **b** bending, and **c** shear

$$C_{11}\frac{\partial^2 u}{\partial x^2} = \alpha_{\mathrm{L}} u. \tag{A.5.3}$$

Thus, the pinning correlation length in the direction of the Lorentz force associated with the uniaxial compression, i.e., the magnetic pressure, is

$$L_{11} = \left(\frac{C_{11}}{\alpha_{\mathrm{L}}}\right)^{1/2} = \lambda_0^{'}. \tag{A.5.4}$$

The pinning correlation length along flux lines associated with bending deformation is given by

$$L_{44} = \left(\frac{C_{44}}{\alpha_{\mathrm{L}}}\right)^{1/2} \cong L_{11}. \tag{A.5.5}$$

The last one is the transverse pinning correlation length in the direction normal to the flux motion given by

$$L_{66} = \left(\frac{C_{66}}{\alpha_{\mathrm{L}}}\right)^{1/2}. \tag{A.5.6}$$

If we assume that the sizes of a partial flux line lattice along the direction of the Lorentz force, the transverse direction, and the longitudinal direction, denoted by L_x, L_y, and L_z are respectively proportional to the corresponding correlation lengths L_{11}, L_{66}, and L_{44}, we have

$$L_x = L_z = \left(\frac{C_{66}}{C_{44}}\right)^{1/6} d_{\mathrm{p}}, L_y = \left(\frac{C_{44}}{C_{66}}\right)^{1/3} d_{\mathrm{p}}. \tag{A.5.7}$$

Note that $L_x L_y L_z = d_{\mathrm{p}}^3 = N_{\mathrm{p}}^{-1}$.

Here we estimate K, defined in (5.81). In the case where interactions of all surrounding pinning centers become active, the surface of the region that we are treating as representative will be displaced by $x_0 - \Delta = u_0$ in the positive x-axis direction due to these interactions. As shown in Sect. 5.3, the flux lines in the surrounding region will be displaced as $u(x) = u_0 \exp(-x/L_{11})$ at a position of distance x from the surface, where $L_{11} = \lambda_0^{'}$. Thus, the surrounding pinning centers will push back with a force proportional to this displacement. Thus, the elastic force from the surrounding pinning centers can be estimated as

$$\alpha_{\mathrm{L}} L_y L_z \int_0^\infty u_0 \exp\left(-\frac{x}{L_{11}}\right) \mathrm{d}x = \alpha_{\mathrm{L}} L_y L_z L_{11} = \alpha_{\mathrm{L}}^{1/2} d_{\mathrm{p}}^2 \left(\frac{C_{44}^4}{C_{66}}\right)^{1/6} u_0, \tag{A.5.8}$$

where $L_y L_z$ is the area of the surface normal to the x-axis. Since this force is equal to Ku_0, we have

$$K = \alpha_{\mathrm{L}}^{1/2} d_{\mathrm{p}}^2 \left(\frac{C_{44}^4}{C_{66}} \right)^{1/6}. \tag{A.5.9}$$

Using this equation, the right-hand side of (5.84) is written as

$$K^2 \frac{a_{\mathrm{f}}}{\zeta d_{\mathrm{p}}^4} \left(\frac{C_{66}}{C_{44}^4} \right)^{1/3}. \tag{A.5.10}$$

Using (5.62), (5.82), and (5.85), the following equation is obtained:

$$K = \frac{k_{\mathrm{f}} t}{\left(k_{\mathrm{f}} a_{\mathrm{f}} / 4 f_{\mathrm{p}} \right) - t}. \tag{A.5.11}$$

Thus, (5.86) is obtained with

$$\beta = \frac{\zeta d_{\mathrm{p}}}{4 k_{\mathrm{f}}} \left(\frac{C_{44}^4}{C_{66}} \right)^{1/3}. \tag{A.5.12}$$

The spring constant k_{f} is given by the inverse compliance of a representative flux line for the lattice fixed at infinity as [3]

$$k_{\mathrm{f}}^{-1} = G'(0) = \frac{1}{4} \left(\frac{2}{\sqrt{3}\pi} \right)^{1/2} \frac{1}{a_{\mathrm{f}}} (C_{44} C_{66})^{-1/2}. \tag{A.5.13}$$

Thus, (5.87) is obtained from (A.5.12) and (A.5.13).

A.6 Derivation of (5.98)

Here we derive the condition of the minimum free energy given by (5.94) in volume V of the superconductor. The displacement of flux lines during minimization of the free energy is denoted by $\boldsymbol{u}$, and an additional small displacement is denoted by $\delta \boldsymbol{u}$. In this case the following condition should be satisfied:

$$\int_{\mathrm{V}} [\mathcal{F}(\boldsymbol{u} + \delta \boldsymbol{u}) - \mathcal{F}(\boldsymbol{u})] \mathrm{d}V = 0. \tag{A.6.1}$$

The first term is expanded as

$$\mathcal{F}(\boldsymbol{u} + \delta \boldsymbol{u}) = \mathcal{F}(\boldsymbol{u}) + \frac{\partial \mathcal{F}}{\partial \boldsymbol{u}} \cdot \delta \boldsymbol{u} + \frac{\partial \mathcal{F}}{\partial \boldsymbol{u}'} \cdot \delta \boldsymbol{u}', \tag{A.6.2}$$

where $\boldsymbol{u}'$ is defined as

$$\boldsymbol{u}' = \frac{\partial u}{\partial \zeta}\boldsymbol{i}_\zeta + \frac{\partial u}{\partial \xi}\boldsymbol{i}_\xi. \tag{A.6.3}$$

This is because $\mathcal{F}$ is also a function of the special derivative of $\boldsymbol{u}$, as can be seen in (5.97). Hence, (A.6.1) is written as

$$\int_{\mathrm{V}} \left(\frac{\partial \mathcal{F}}{\partial \boldsymbol{u}} \cdot \delta \boldsymbol{u} + \frac{\partial \mathcal{F}}{\partial \boldsymbol{u}'} \cdot \delta \boldsymbol{u}' \right) \mathrm{d}V = 0. \tag{A.6.4}$$

Here we use the formula for divergence of a product of scalar f and vector $\boldsymbol{g}$:

$$\nabla \cdot (f\boldsymbol{g}) = f \nabla \cdot \boldsymbol{g} + \nabla f \cdot \boldsymbol{g}. \tag{A.6.5}$$

Note that $\delta \boldsymbol{u}' = \nabla \delta u$ from (A.6.3). If we set $f = \delta u$ and $\boldsymbol{g} = \partial \mathcal{F}/\partial \boldsymbol{u}'$, the second term of (A.6.4) is written as

$$\frac{\partial \mathcal{F}}{\partial \boldsymbol{u}'} \cdot \delta \boldsymbol{u}' = \nabla \cdot \left(\delta u \frac{\partial \mathcal{F}}{\partial \boldsymbol{u}'} \right) - \delta u \nabla \cdot \frac{\partial \mathcal{F}}{\partial \boldsymbol{u}'}. \tag{A.6.6}$$

Using Gauss' theorem, the volume integral of the first term is

$$\int_{\mathrm{S}} \delta u \frac{\partial \mathcal{F}}{\partial \boldsymbol{u}'} \cdot \mathrm{d}\boldsymbol{S} = 0. \tag{A.6.7}$$

In the present isolated condition, we can assume that the displacement of flux lines δu is zero on the surface S of the superconductor. And we generally have $\delta u = \boldsymbol{i}_\xi \cdot \delta \boldsymbol{u}$. Thus, the second term of (A.6.6) is reduced to

$$-\delta \boldsymbol{u} \cdot \boldsymbol{i}_\xi \left[\frac{\partial}{\partial \zeta} \frac{\partial \mathcal{F}}{\partial (\partial u/\partial \zeta)} + \frac{\partial}{\partial \xi} \frac{\partial \mathcal{F}}{\partial (\partial u/\partial \xi)} \right]. \tag{A.6.8}$$

Hence, (A.6.4) is written as

$$\int_{\mathrm{V}} \left\{ \frac{\partial \mathcal{F}}{\partial \boldsymbol{u}} - \boldsymbol{i}_\xi \left[\frac{\partial}{\partial \zeta} \frac{\partial \mathcal{F}}{\partial (\partial u/\partial \zeta)} + \frac{\partial}{\partial \xi} \frac{\partial \mathcal{F}}{\partial (\partial u/\partial \xi)} \right] \right\} \cdot \delta \boldsymbol{u} \mathrm{d}V = 0. \tag{A.6.9}$$

The quantity inside the braces should be zero, so this condition is fulfilled for arbitrary $\delta \boldsymbol{u}$. Thus, (5.98) is derived.

A.7 Input Energy and Increase in Magnetic Energy

All the energy that comes into the superconductor can be obtained using Poynting's vector. A part of it appears as magnetic energy in the superconductor, but some part of it does not remain in the superconductor. It was shown in Sect. 5.7 that the energy that has disappeared is work done by the driving force. How shall we understand this phenomenon?

Here we discuss some practical cases. First we treat an irreversible phenomenon as described by the critical state model. In this case, it can be expected that the lost energy is exactly dissipated as a pinning loss. This will be proved here. Assume that a magnetic field with the magnetic flux density B_0 is applied along the z-axis parallel to a semi-infinite superconductor occupying $x \geq 0$. If the critical current density is denoted by J_c, the magnetic flux distribution inside the superconductor is described as

$$\begin{aligned} B(x) &= B_0 - \mu_0 J_c x; \ 0 \leq x \leq B_0/\mu_0 J_c, \\ &= 0; \qquad\qquad x > B_0/\mu_0 J_c. \end{aligned} \tag{A.7.1}$$

The induced electric field during this process is directed along the y-axis and is given by

$$E = -\int_{B_0/\mu_0 J_c}^{0} \frac{\partial B_0}{\partial t} \mathrm{d}x = \frac{B_0}{\mu_0 J_c} \frac{\partial B_0}{\partial t}. \tag{A.7.2}$$

Hence, Poynting's vector on the superconductor surface is EB_0/μ_0 in magnitude and directed into the superconductor. Thus, the energy that penetrates a unit cross-sectional area of the superconductor during increasing magnetic flux density from 0 to B_m is estimated as

$$U_{in} = \frac{1}{\mu_0^2 J_c} \int_0^{B_m} B_0^2 \mathrm{d}B_0 = \frac{B_m^3}{3\mu_0^2 J_c}. \tag{A.7.3}$$

On the other hand, the corresponding magnetic energy inside the superconductor in the final condition is

$$U_m = \frac{1}{2\mu_0} \int_0^{B_m/\mu_0 J_c} (B_m - \mu_0 J_c x)^2 \mathrm{d}x = \frac{B_m^3}{6\mu_0^2 J_c}, \tag{A.7.4}$$

which is smaller than the input energy. The loss power density during the process is

$$P(x) = E(x)J_c = J_c \frac{\partial B_0}{\partial t}\left(\frac{B_0}{\mu_0 J_c} - x\right), \tag{A.7.5}$$

and the loss energy per unit area of the superconductor surface is estimated as

$$W = \int_0^{B_m} \mathrm{d}B_0 \int_0^{B_0/\mu_0 J_c} J_c\left(\frac{B_0}{\mu_0 J_c} - x\right)\mathrm{d}x = \frac{1}{2\mu_0^2 J_c}\int_0^{B_m} B_0^2 \mathrm{d}B_0 = \frac{B_m^3}{6\mu_0^2 J_c}, \tag{A.7.6}$$

which is equal to the difference between the input energy and the magnetic energy. The reason for this result will be clear from (2.54). This is the reason why the loss energy can be estimated by measuring Poynting's vector [4].

Next we treat the case of reversible flux motion. We assume that a sufficiently high magnetic field of magnetic flux density B_m is applied again to the semi-infinite superconductor, and then, the external field is slightly reduced by Δb_0. The interior magnetic flux density is given by

$$B(x) = B_m - \mu_0 J_c x - \Delta b_0 \exp\left(-\frac{x}{\lambda_0'}\right). \tag{A.7.7}$$

The induced electric field with a decreasing magnetic field is

$$E(x) = \int_\infty^x \frac{\partial \Delta b_0}{\partial t}\exp\left(-\frac{x}{\lambda_0'}\right)\mathrm{d}x = -\lambda_0' \frac{\partial \Delta b_0}{\partial t}\exp\left(-\frac{x}{\lambda_0'}\right). \tag{A.7.8}$$

Poynting's vector on the superconductor surface is $(B_m - \Delta b_0)E(0)/\mu_0$ in magnitude and directed inwards. Thus, the energy that comes into the superconductor through the unit area as the magnetic field is decreased by b_0 is estimated as

$$\Delta U_{in} = -\frac{\lambda_0'}{\mu_0}\int_0^{b_0}(B_m - \Delta b_0)\mathrm{d}\Delta b_0 = -\frac{\lambda_0'}{\mu_0} b_0\left(B_m - \frac{b_0}{2}\right). \tag{A.7.9}$$

Namely, the energy substantially goes out the superconductor. The variation in the magnetic energy inside the superconductor is

$$\begin{aligned}\Delta U_m &= \frac{1}{2\mu_0}\int_0^\infty \left\{\left[B_m - \mu_0 J_c x - b_0 \exp\left(-\frac{x}{\lambda_0'}\right)\right]^2 - (B_m - \mu_0 J_c x)^2\right\}\mathrm{d}x \\ &= -\frac{\lambda_0'}{\mu_0} b_0\left(B_m - \mu_0 J_c \lambda_0' - \frac{b_0}{4}\right).\end{aligned} \tag{A.7.10}$$

Thus, we have

$$\Delta U_{\mathrm{in}} - \Delta U_{\mathrm{m}} = -\frac{\lambda_0'}{\mu_0} b_0 \left(\mu_0 J_{\mathrm{c}} \lambda_0' - \frac{b_0}{4} \right). \tag{A.7.11}$$

This means that the energy exceeding the decrease in the magnetic energy inside the superconductor goes out of the superconductor. It seems that a new form of energy is born. (Note that $b_0/\mu_0\lambda_0' < 2J_{\mathrm{c}}$ in the area of the reversible flux motion.) It can be shown that $\Delta U_{\mathrm{in}} - \Delta U_{\mathrm{m}}$ is equal to the work done by the driving force [5]. If the external magnetic field is increased from $B_{\mathrm{m}} - b_0$ to B_{m} after the above process, the inner magnetic flux distribution again obeys (A.7.7), but some energy disappears.

It is necessary to investigate the flux pinning mechanism that determines the flux distribution in the superconductor to understand the physics in such cases, where some energy seems to appear or disappear. Within the range of reversible flux motion, the pinning force is balanced with the driving force, but with some margin, because of the pinning force density below the critical value, and the work done by the driving force is stored as an increase in the pinning energy in the latter case. Since the pinning energy is not a magnetic energy but a thermodynamic energy, the magnetic energy disappears. In the former case, the pinning energy stored as the pinning energy in the initial process to increase the magnetic field to B_{m} partly goes out of the superconductor during the process of decreasing the magnetic field. In fact, it can be shown that the work done by the driving force is equal to the increase in the pinning energy [5]. On the other hand, the pinning energy reaches the upper limit in the critical state, and there is no room to store additional energy. Hence, the work done by the driving force is dissipated by the motion of depinned flux lines. This point will also be discussed from a different viewpoint in Appendix 8. In the case where there is no pinning effect, a uniform magnetic flux distribution is attained by the driving force, and the input energy is equal to the variation in the magnetic energy.

In the case of the longitudinal magnetic field effect treated in Sect. 6.3, the energy penetrating the superconductor during the process of introducing the force-free strain is the work done by the driving torque. In this process the magnetic energy does not change, and all of the input energy is stored as the pinning energy or dissipated. This clearly shows that the critical current density in the longitudinal magnetic field is also determined by the flux pinning mechanism.

A.8 Helmholtz Free Energy and Gibbs Free Energy

The Ginzburg-Landau free energy is a kind of Helmholtz free energy, and it is necessary to transform it to a Gibbs free energy by adding the Legendre term to discuss the transition under a magnetic field, as shown in Sect. 4.2. It should be noted that the Ginzburg-Landau equations do not change even under the Legendre transformation. The Gibbs energy density corresponding to the Ginzburg-Landau free energy density is

$$\mathcal{G} = \mathcal{F} - \boldsymbol{B} \cdot \boldsymbol{H}_0, \tag{A.8.1}$$

where $\boldsymbol{H}_0$ is the external magnetic field. The condition of the equilibrium state is obtained from $\partial \mathcal{G} / \partial \boldsymbol{B} = 0$, and it satisfies

$$\frac{\partial \mathcal{F}}{\partial \boldsymbol{B}} = \boldsymbol{H}_0. \tag{A.8.2}$$

The variation in the volume integral of the free energy density from (A.1.9) when the vector potential changes by $\delta \boldsymbol{A}$ is given by

$$-\int_{\mathrm{V}} (\boldsymbol{H}_0 \cdot \nabla \times \delta \boldsymbol{A}) \mathrm{d}V. \tag{A.8.3}$$

This is partially integrated, and neglecting the surface integral, we have

$$-\int_{\mathrm{V}} (\delta \boldsymbol{A} \cdot \nabla \times \boldsymbol{H}_0) \mathrm{d}V = 0. \tag{A.8.4}$$

Thus, the Ginzburg-Landau equation (4.4) does not change. Equation (4.3) does not change either.

The Gibbs free energy density should also be used for the electromagnetic phenomena in a non-isolated flux line system in a transverse magnetic field. For example, the Gibbs free energy density is given by

$$\mathcal{G} = \mathcal{F} - \boldsymbol{F} \cdot \boldsymbol{u} \tag{A.8.5}$$

when a force of density $\boldsymbol{F}$ is added to the flux line system, where $\boldsymbol{u}$ is the displacement of flux lines. This is minimized with respect to $\boldsymbol{u}$, and from the condition $\partial \mathcal{G} / \partial \boldsymbol{u} = 0$, we have

$$\boldsymbol{F} + \boldsymbol{F}_{\mathrm{p}} = 0, \tag{A.8.6}$$

where we used $\boldsymbol{F}_{\mathrm{p}} = -\partial \mathcal{F} / \partial \boldsymbol{u}$. The variation in the free energy density as a function of the displacement of the flux line system in the regime of reversible flux motion is illustrated in Fig. A.2. The spatial variation with period a comes from the first term of (A.8.5), including the pinning energy density, and the decrease with increasing displacement comes from the second term. Point A at which the energy density is locally a minimum gives the stable equilibrium position. The Legendre term for the second term in (A.8.5) is derived using Poynting's vector when we extend the flux line system from the isolated condition to the non-isolated one in the critical state theory in Sect. 5.7. Such a washboard pinning potential is usually assumed when discussing the flux creep phenomena.

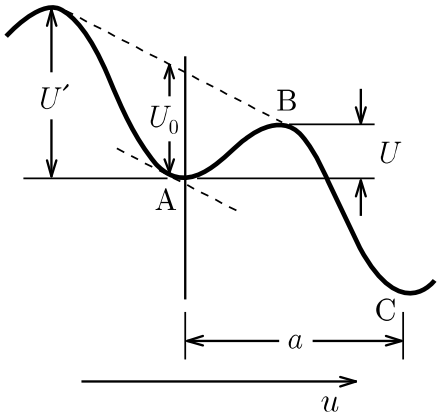

Fig. A.2 Energy that varies with period a with the displacement of flux lines u. The gradual decrease with increasing u comes from the work done by the Lorentz force. U_0 is the pinning potential, and U is the activation energy

It is also necessary to use the Gibbs free energy density to treat the non-isolated flux line system in the longitudinal magnetic field, and the free energy density to be minimized is

$$\mathcal{G} = \mathcal{F} - \boldsymbol{\Omega} \cdot \boldsymbol{\theta}, \tag{A.8.7}$$

where $\boldsymbol{\Omega}$ is the torque density and $\boldsymbol{\theta}$ is the rotation angle of the flux line system, with both of them vectors along the rotation axis. The free energy density is minimized with respect to $\boldsymbol{\theta}$, and we have

$$\boldsymbol{\Omega} + \boldsymbol{\Omega}_{\mathrm{p}} = 0, \tag{A.8.8}$$

where $\boldsymbol{\Omega}_{\mathrm{p}} = -\partial \mathcal{F}/\partial \boldsymbol{\theta}$ is the pinning torque density. The introduction of the second term in (A.8.7) is important. In the usual transverse magnetic field configuration, $\boldsymbol{F}$ in (A.8.5) is well known as the Lorentz force. On the other hand, $\boldsymbol{\Omega}$ in the longitudinal magnetic field is unknown, and we have to derive it using Poynting's vector.

The Legendre term to be added at the transformation is a part of the energy derived using Poynting's vector for the transverse magnetic field configuration or all of it for the rotating magnetic field in the longitudinal field configuration. In the former case, the remaining part of the energy is automatically included in the Helmholtz free energy as an increase in the magnetic energy (see Sect. 5.7). In the usual case of transportation of the current after application of the longitudinal magnetic field, the magnetic energy is similarly included, since the magnetic field strength on the surface is changed.

Table A.1 Comparison of different kinds of irreversibility

	Viscous loss	Pinning loss
Time reversal symmetry	No	Yes
Static stable state	No	Yes
Dissipation in steady state	Yes	No
Type of loss under variation	Copper loss	Iron loss

A.9 Two Kinds of Irreversibility

Here, we discuss two kinds of irreversibility. One of them is a general irreversibility arising from the breaking of time reversal symmetry, and the other is caused by different biased distributions of flux lines in the potential well due to the instability in flux motion accompanied by a hysteresis, as shown in Chap. 5. In the latter case, a reversible behavior is included, in which the time reversal symmetry is satisfied and the irreversibility is independent of the breaking of time reversal symmetry. If short, therefore, the irreversibility and energy dissipation are not identical in physics. This is because it is possible to change over from an irreversible state to a lossless reversible state. These two kinds of irreversibility are compared in Table A.1.

It is possible to theoretically derive the irreversibility of a closed magnetization curve and to insist that energy dissipation equal to the area of the closed loop should occur. Before the proof of the critical state theory, we could insist only that, if there is no energy dissipation, it contradicts the experimental results. It is possible now to say that if there is no energy dissipation, it contradicts the theoretical prediction. In addition, the energy dissipation based on the loss mechanism assuming the breaking of time reversal symmetry agrees with the energy dissipation calculated from the critical state theory.

A.10 Theoretical Systems of Flux Pinning

Flux pinning phenomena are roughly classified into the equilibrium state ($J = 0$), reversible state ($0 < J < J_c$), static critical state ($J = J_c$), quasi-static critical state ($J = J_{c+0}$),and dynamic state ($J > J_c$), depending on the current density. The theories that explain these phenomena except for in the equilibrium state are the coherent potential approximation theory [6, 7], the critical state theory, and the dynamic critical state model [8, 9] in this order (see Fig. A.3).

The former two theories are derived from first principles, namely, minimization of the energy, or do not contradict the principles. The dynamic critical state model is an expansion of the critical state theory to the dynamic state with the assumption of a viscous force. It should be noted that the condition of minimum energy dissipation is satisfied in the quasi-static and dynamic states. That is, the pinning loss appears in the superconductor, but it takes on a minimum value in these states. In addition,

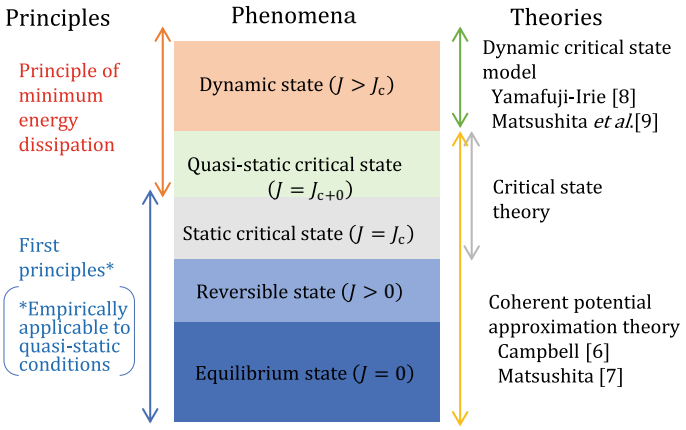

Fig. A.3 Flux pinning phenomena and theoretical systems

the principle of minimum energy dissipation seems to work in determination of the flux bundle size under the effect of flux creep or in sharing of pinning energy under the longitudinal magnetic field. This fact tells us that there is a possibility that this principle may be applied more widely, i.e., to a system with small energy dissipation, even though a dissipation mechanism is nonlinear. If the quantity associated with a flow such as the velocity of flux lines is denoted by ε, the energy dissipation is proportional to ε in the case of flux pinning, while it is proportional to ε^2 for the usual linear dissipation systems.

Although energy dissipation occurs in the quasi-static critical state, the state at each moment is equal to the prediction in the static critical state, and any variation with time occurs only through the variation in an external parameter such as magnetic field or current. Thus, the static state varies continuously with time. For this reason, first principles can be applied empirically and overlap with the principle of minimum energy dissipation in this region.

The same thing occurs in the case of longitudinal magnetic field effect, and the balance between the generalized force and flux pinning interactions is derived from the minimization of the energy. The force-free state is selected based on the current flow so as to satisfy the minimum energy dissipation, and the torque balance determines the state.

A.11 Analysis of Penetration of Flux Lines into a Superconducting Cylinder

Here, we analyze the penetration of flux lines into a cylindrical superconductor in a longitudinal magnetic field when current is applied, as treated in Sect. 6.1. The external magnetic field and self-field due to the current are denoted by H_e and H_I,

respectively. The magnetic field on the surface is given by

$$B = \mu_0\left(H_e^2 + H_I^2\right)^{1/2} \cong \mu_0 H_e\left[1 + \frac{1}{2}\left(\frac{H_I}{H_e}\right)^2\right]. \tag{A.11.1}$$

In the above, it is assumed that the self-field is sufficiently smaller than the external magnetic field. Hence, the increase in the magnetic flux density on the surface is $b_0 = \mu_0 H_I^2/2H_e$. Here we estimate the current at which one layer of flux lines penetrates the superconductor. This is in the situation where the displacement of flux lines on the surface reaches the flux line spacing, 380 nm. In the cylindrical coordinates, the continuity equation of flux lines (5.46) is written as

$$b = \frac{\mu_0 H_e}{R}\frac{\partial(Ru)}{\partial R}, \tag{A.11.2}$$

where R is a distance from the central axis and u is the displacement. It is assumed that b is uniform inside the superconductor. Since u is zero at the center ($R = 0$), the displacement of flux lines on the surface $R = R_0$ is obtained as

$$u_0 = \frac{b}{2\mu_0 H_e}R_0. \tag{A.11.3}$$

From the condition that this is equal to 380 nm, we have $b = 0.13 \times 10^{-4}$ [T], where $\mu_0 H_e = 14$ [mT] was used. Using (A.11.1), the self-field is found to be 0.43 mT, and the corresponding current is 1.72 A. If flux lines penetrate in a row, the magnetization may change discontinuously, although no discontinuous change has been observed. If it is assumed that a small number of flux lines penetrate continuously to make the change in the magnetization smooth, these flux lines must incline much more than the angle of the surface field to produce a self-field that satisfies the boundary condition by themselves. For example, if we assume that only a quarter of the flux lines in a row penetrate at 0.43 A, a quarter of the current needed for one row penetration (1.72 A), these flux lines must have a four times larger inclination than the surface field to produce the required self-field by themselves. This seems to be unrealistic. In addition, if a row of flux lines penetrates the superconductor translationally, all the current (1.72 A) must flow within the depth of one flux line spacing (380 nm) from the surface. In this case, the current density reaches 9.0×10^8 A m^{-2}, which is very much larger than the observed critical current density, 1.5×10^7 A m^{-2}. If such a situation is continued up to the critical current, where the self-field is 7.5 mT, the current is limited to within the depth of 0.12 mm from the surface. These situations are quite different from the concept of the critical state. It is expected that the current flows through the whole cross-section of the superconductor in the critical state, which requires that the inner flux lines must also rotate when new flux lines penetrate. This also explains the continuous variation in the magnetization.

A.12 On the Flux Cutting

Various contradictions that arise under the assumption that flux lines must move translationally have been evaded by assuming that flux cutting exists. Almost all of them can be reasonably explained, however, by the rotational motion of flux lines driven by the force-free torque, although it is not easy to directly identify which mechanism is at work from the experimental results that have been explained by the flux cutting model. This is the reason why the flux cutting model is used even now. Hence, it is necessary to examine it theoretically from various aspects. In this section the problems related to flux cutting are comprehensively argued. An argument will be presented following each viewpoint.

(1) **No inevitability of flux cutting**

All of the electromagnetic phenomena that were believed to be explained only by the flux cutting, such as the deviation of the induced electric field from Josephson's formula or the steady magnetization in the resistive state, as shown in Fig. 6.3, can be explained without the flux cutting. It is possible to raise other examples. This is because the flux cutting and flux rotation are equivalent to each other from the viewpoint of macroscopic electromagnetic phenomena.

This theoretical point was already presented in Sect. 6.1. That is, the flux cutting is a concept used to explain the phenomena by assuming Josephson's relationship for translational movement of each component of flux lines, although Josephson's formula does not hold.

As shown in Sects. 5.7 and 6.3, and Appendix A.7, when a current is induced in a superconductor by changing the external magnetic field, the energy that invades the superconductor exceeds the increase in the magnetic energy, and the excess energy, i.e., the work done by the driving force or torque to release the strain of flux lines in the regime of reversible flux motion, is stored as an increase in the pinning energy. If the rotational shear distortion of flux lines cannot be stabilized by the pinning interaction in the longitudinal magnetic field, such an energy balance cannot be explained, resulting in a theoretical contradiction. If it is assumed that flux cutting occurs in this situation, the excess energy is the magnetic energy itself of the interacting flux lines, as discussed in Sect. 6.1, and cannot be absorbed. Thus, there is no inevitability of flux cutting. Since this is in the regime of reversible flux motion, it is impossible to explain how the excess energy is dissipated due to flux cutting. In addition, the flux cutting cannot be the mechanism that determines fundamental phenomena such as the critical current density.

(2) **No possibility for flux cutting**

Some processes of flux cutting have been proposed, such as the inter-cutting process in which flux lines with different angles cut directly across each other, as shown in Fig. 6.7, and the intra-cutting process in which such flux lines recombine [6], although any real process of flux cutting has not been confirmed. In addition, the

mechanism for the work $\int \boldsymbol{E} \cdot \boldsymbol{J} \mathrm{d}t$ done by the general restoring force has not been clarified in association with energy conservation. In reality this is the work done by the torque, which exceeds the pinning interaction during the rotational motion of flux lines, similarly to the usual cases in the transverse magnetic field. We simply discuss the process of the flux cutting here, however, neglecting such an argument on the fundamental aspects. To realize the flux cutting, two flux lines with different angles must come close to each other against a strong repulsive force, but there is no force to make the flux lines come close to each other. Even if it were assumed that the flux cutting could happen, the theoretically estimated threshold value for the needed current density is too high for both the inter-cutting and the intra-cutting processes, and the observed critical current densities cannot be explained. It may be pointed out that flux cutting maybe easily take place at normal precipitates, etc. If this is so, however, the flux cutting maybe more easily occur in a superconductor with more pinning centers, resulting in a lower critical current density. The practical situation is the opposite, and such an insistence is meaningless. In reality, the flux cutting does not take place, since the rotational flux motion with no threshold occurs first.

Here, we introduce another experimental result that clearly shows that the flux cutting cannot take place. The experimental result shown in Fig. 6.15 clarifies that the magnetic flux distribution is exactly in the force-free state. The penetration depth of the AC magnetic flux approaches the value of about 10 μm in the limit of zero AC field amplitude, indicating that the motion of flux lines is in the regime of reversible flux pinning. Since the flux line spacing is about 90 nm under a DC magnetic field of 0.290 T, the variation in the external magnetic field reaches the distance of about 100 rows of flux lines from the surface in this situation. On the other hand, since the flux cutting is irreversible, the flux cutting process must be completed by the row behind to start the interaction with flux lines on the next row. That is, the penetration depth of the flux cutting is on the order of the flux line spacing, and the extension of such a reversible phenomenon to 10 μm cannot be explained [5]. In reality the rotational motion of flux lines occurs, and it can extend to the shielding distance of flux pinning in the reversible regime. Thus, the observed reversible phenomenon can be explained by the rotational motion of flux lines. Since energy dissipation does not occur by the mechanism of flux cutting in this regime, the energy is not conserved in the case of flux cutting, as discussed in Sect. 6.3, resulting in a contradiction.

In addition, relativity is not satisfied for the flux cutting between the case of rotating the external magnetic field and the case of rotating the superconductor in the opposite direction in a stationary external magnetic field (see p. 151 in [1]), although the details are not shown here.

(3) **No possibility of explanation by the flux cutting**

As described in Chap. 6, the following phenomena cannot be explained by the mechanism of flux cutting:

(a) the paramagnetic effect in the usual process of application of current after applying an external magnetic field,
(b) a critical current density that depends on the flux pinning strength, especially, very small critical current densities for weak pinning,

(c) the structure of electric fields in the resistive state, including the negative field that appears on the surface,
(d) the appearance of a radial electric field component in the resistive state, and
(e) the resistivity that follows the Bardeen-Stephen model.

(a) and (d) can be explained only by movement of the longitudinal magnetic flux component and cannot be explained by the flux cutting model, which assumes only the motion of the transverse component. (e) shows that the energy dissipation occurs in the whole length of the normal core in each flux line, while the energy dissipation may occur only in the region of cutting in the flux cutting model, resulting in appreciably smaller electrical resistivity than in the theoretical prediction of the Bardeen-Stephen model.

Other phenomena that cannot be explained by the flux cutting model are

(f) the occurrence of the longitudinal magnetic field effect, even when the external magnetic field and current are simultaneously increased so that the angle of the total magnetic field on the surface does not change, as shown in Fig. 6.22, and
(g) the helical flow of current to produce the longitudinal magnetic field in the resistive state when only the current is applied, as shown in Fig. 6.21.

Since the angle of the total magnetic field is not changed, the condition of the flux cutting is not fulfilled. In more detail, the process is quite opposite to the flux cutting, i.e., the appearance of flux lines with different angles from flux lines directed in the same direction, must occur to explain the phenomena in (f). It is also possible to point out as follows:

(h) The reason why the force-free state is realized cannot be explained, even though the flux pinning governs the phenomena.

These points, (f), (g), and (h), are explained by the principle of irreversible thermodynamics, in which the direction of current is determined so as to minimize the energy dissipation.

A.13 Magnetic Helicity in the Force-Free State

In the force-free state where the current density $\boldsymbol{J}$ is parallel to the magnetic flux density $\boldsymbol{B}$, it can be expressed as $\boldsymbol{J} = k\boldsymbol{B}$, using a scalar function k. In this case we have

$$\nabla \times \boldsymbol{J} = k\nabla \times \boldsymbol{B} - \boldsymbol{B} \times \nabla k = \mu_0 k^2 \boldsymbol{B} - \boldsymbol{B} \times \nabla k. \tag{A.13.1}$$

This quantity is not zero, since the first term is parallel to $\boldsymbol{B}$, and the second term is normal to $\boldsymbol{B}$. In fact, we have $\nabla \times \boldsymbol{J} = \left(\alpha_f^2/\mu_0\right)\boldsymbol{B}$ from (6.10) and (6.14). On the other hand, the static electric field must satisfy $\nabla \times \boldsymbol{E} = 0$. Hence, the electric resistivity must be zero. Thus, the static force-free state can be achieved only in superconductors.

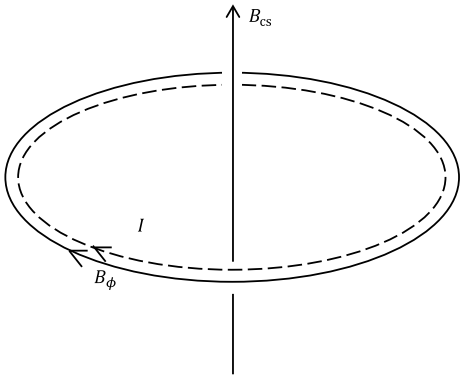

Fig. A.4 Magnetic fields B_ϕ produced by toroidal coils and B_{cs} produced by a central solenoid coil, and induced current I

When the magnetic helicity is not zero, we have $\boldsymbol{A} \cdot \boldsymbol{B} \neq 0$. In this case the vector potential $\boldsymbol{A}$ has a component parallel to $\boldsymbol{B}$. Since $\boldsymbol{A}$ is parallel to $\boldsymbol{J}$, as shown by (2.28) or (4.15), $\boldsymbol{J}$ has a force-free component parallel to $\boldsymbol{B}$. Thus, the perfect force-free state ($\boldsymbol{J} \| \boldsymbol{B}$) is the state with the maximum magnetic helicity ($\boldsymbol{A} \| \boldsymbol{B}$).

In a tokamak fusion reactor, a ring magnetic field (B_ϕ) is produced by a current flowing in toroidal coils placed in a doughnut shape, as illustrated in Fig. A.4. A normal pulsed magnetic field (B_{cs}) produced by a central solenoid coil induces a ring current I through a plasma inside the toroidal coils to heat up the plasma, resulting in fusion. In this case, a magnetic situation similar to that in a superconductor in a longitudinal magnetic field is realized. In fact, the force-free state is theoretically derived by minimizing the magnetic energy in the plasma under a fixed magnetic helicity [7, 8]. Although the induced current and magnetic helicity will surely decrease with time due to Joule heating, similar electromagnetic phenomena to the longitudinal magnetic field effect in the superconductor occur within a short period. There is no merit in achieving the force-free state in the plasma, however, such as an increase in the critical current density in the superconductor, and even the energy loss increases by making a longer current path. Thus, the energy dissipation is not minimized for the plasma. On the other hand, it is considered that the state of minimum energy that is achieved leads to a mechanical equilibrium.

A.14 Derivation of (6.41) and (6.42)

Since the magnetic flux density has no y-component, the continuity equation of magnetic flux is reduced to

$$\frac{\partial B_x}{\partial t} = -\frac{\partial}{\partial y}\left(B_x v_y\right) + \frac{\partial}{\partial z}(B_z v_x - B_x v_z), \tag{A.14.1}$$

$$\frac{\partial B_z}{\partial t} = -\frac{\partial}{\partial x}(B_z v_x - B_x v_z) - \frac{\partial}{\partial y}\left(B_z v_y\right). \tag{A.14.2}$$

Using (6.8) and (6.40), the second term on the right-hand side of (A.14.1) is written as

$$B\frac{\partial}{\partial z}(v_x \cos\theta - v_z \sin\theta) = -\frac{B}{\sin\theta} \cdot \frac{\partial v_z}{\partial z}. \tag{A.14.3}$$

This equation is reduced to

$$\frac{\partial B}{\partial t}\sin\theta + B\cos\theta\frac{\partial \theta}{\partial t} = -B\frac{\partial}{\partial y}\left(v_y \sin\theta\right) - \frac{B}{\sin\theta} \cdot \frac{\partial v_z}{\partial z}. \tag{A.14.4}$$

The first term on the right-hand side of (A.14.2) is written as

$$-B\frac{\partial}{\partial x}(v_x \cos\theta - v_z \sin\theta) = -\frac{B}{\cos\theta} \cdot \frac{\partial v_x}{\partial x}, \tag{A.14.5}$$

and this equation is reduced to

$$\frac{\partial B}{\partial t}\cos\theta - B\sin\theta\frac{\partial \theta}{\partial t} = -B\frac{\partial}{\partial y}\left(v_y \cos\theta\right) - \frac{B}{\cos\theta} \cdot \frac{\partial v_x}{\partial x}. \tag{A.14.6}$$

Summing (A.14.4) multiplied by $\sin\theta$ and (A.14.6) multiplied by $\cos\theta$, we have

$$\frac{\partial B}{\partial t} = -B\frac{\partial v_y}{\partial y}. \tag{A.14.7}$$

Subtracting (A.14.6) multiplied by $\sin\theta$ from (A.14.4) multiplied by $\cos\theta$, we have

$$\frac{\partial \theta}{\partial t} = \alpha_f v_y + \frac{1}{\sin\theta\cos\theta} \cdot \frac{\partial v_x}{\partial x}. \tag{A.14.8}$$

Thus, (6.41) and (6.42) are derived.

A.15 Proof of (6.45)

From the relationships of $\mu_0 H_e = B\cos\theta_0$ and $\mu_0 H_I = B\sin\theta_0$, we have

$$\frac{\partial \theta_0}{\partial t} = \frac{\partial \theta}{\partial t} = \frac{\mu_0}{B}\cos\theta_0 \frac{\partial H_I}{\partial t}, \frac{\partial B}{\partial t} = \mu_0 \sin\theta_0 \frac{\partial H_I}{\partial t}. \tag{A.15.1}$$

Using (6.49), (6.45) is written as

$$
\begin{aligned}
v_x &= r\frac{\mu_0}{B}\frac{\partial H_I}{\partial t}\cos\theta_0\cos\theta\left[1-\tan\theta_0\alpha_{\mathrm{f}}(d-y)\right],\\
v_y &= \frac{\mu_0}{B}\frac{\partial H_I}{\partial t}\sin\theta_0(d-y),\\
v_z &= -r\frac{\mu_0}{B}\frac{\partial H_I}{\partial t}\cos\theta_0\sin\theta\left[1-\tan\theta_0\alpha_{\mathrm{f}}(d-y)\right].
\end{aligned}
\tag{A.15.2}
$$

Then, we will directly check if the velocity given by (A.15.2) satisfies the continuity equation of magnetic flux. The variation of the x-component with time is given by

$$
\frac{\partial B_x}{\partial t} = -[\mathrm{rot}(\boldsymbol{B}\times\boldsymbol{v})]_x. \tag{A.15.3}
$$

The left-hand side is written as

$$
\frac{\partial B_x}{\partial t} = \frac{\partial B}{\partial t}\sin\theta + B\cos\theta\frac{\partial\theta}{\partial t} = \mu_0\frac{\partial H_I}{\partial t}\cos(\theta-\theta_0). \tag{A.15.4}
$$

After a tedious calculation the right-hand side is written as

$$
\begin{aligned}
-[\mathrm{rot}(\boldsymbol{B}\times\boldsymbol{v})]_x &= -B\frac{\partial}{\partial y}\left(v_y\sin\theta\right) + B\frac{\partial}{\partial z}(v_x\cos\theta - v_z\sin\theta)\\
&= \mu_0\frac{\partial H_I}{\partial t}\cos(\theta-\theta_0),
\end{aligned}
\tag{A.15.5}
$$

which is the same as (A.15.4). The variation of the z-component with time is given by

$$
\frac{\partial B_z}{\partial t} = -[\mathrm{rot}(\boldsymbol{B}\times\boldsymbol{v})]_z. \tag{A.15.6}
$$

The left-hand side is

$$
\frac{\partial B_z}{\partial t} = \frac{\partial B}{\partial t}\cos\theta - B\sin\theta\frac{\partial\theta}{\partial t} = -\mu_0\frac{\partial H_I}{\partial t}\sin(\theta-\theta_0) \tag{A.15.7}
$$

and the right-hand side is

$$
\begin{aligned}
-[\mathrm{rot}(\boldsymbol{B}\times\boldsymbol{v})]_z &= -B\frac{\partial}{\partial x}(v_x\cos\theta - v_z\sin\theta) - B\frac{\partial}{\partial y}\left(v_y\cos\theta\right)\\
&= -\mu_0\frac{\partial H_I}{\partial t}\sin(\theta-\theta_0),
\end{aligned}
\tag{A.15.8}
$$

which is the same as (A.15.7). Thus, (6.45) can be proved as the solution of the continuity equation of magnetic flux.

A.16 Derivation of (6.62) and (6.63)

The variation in the z-component of the magnetic flux density is

$$\frac{\partial B_z}{\partial t} = \frac{\partial H_I}{\partial t} \cdot \frac{\mu_0^2}{B}(H_I \cos\theta - H_e \sin\theta). \tag{A.16.1}$$

From the relationship $\partial A_x/\partial y = -B_z$ the variation in the z-conponent of the vector potential is given by

$$\delta A_z = -\delta H_I \frac{\mu_0^2}{B} \int (H_I \cos\theta - H_e \sin\theta) \mathrm{d}y. \tag{A.16.2}$$

Using $\mathrm{d}y = -(1/\alpha_f)\mathrm{d}\theta$ from (6.36), (A.16.2) is reduced to

$$\delta A_z = \frac{\mu_0^2}{\alpha_f B}(H_I \sin\theta + H_e \cos\theta)\delta H_I. \tag{A.16.3}$$

On the other hand, by integrating the second equation of (6.45) for a short period, the displacement of flux lines is calculated as

$$\delta u_y = \frac{\mu_0^2 H_I}{B^2}\delta H_I (d - y). \tag{A.16.4}$$

Since B_z is $B\cos\theta$, we have

$$\delta u_y B_z = \frac{\mu_0^2 H_I}{B}(d - y)\cos\theta \delta H_I. \tag{A.16.5}$$

A.17 Electromagnetic Phenomena in High-Temperature Superconductors

The characteristic points of electromagnetic phenomena in high-temperature superconductors are briefly introduced here. High-temperature superconductors have alternative layered structures composed of CuO_2 planes that show the superconductivity and almost insulating block layers that provide carriers to the CuO_2 planes. For this reason, these superconductors have large anisotropy with respect to the magnetic field angle. That is, the upper critical field is very high in the direction parallel to the CuO_2 plane, while it is relatively low in the direction parallel to the c-axis. This is caused by the anisotropy of the coherence length, which is extremely short along the c-axis.

Since the superconducting region is limited, the condensation energy is relatively low in spite of its very high critical temperature. This restricts the strength of flux pinning, resulting in low critical current densities. In addition, these superconductors are mostly used at high temperatures, the effect of thermal activation is big, and flux creep occurs easily, which allows pinned flux lines to easily escape from the pinning centers. Hence, the critical current density decreases even more, and the superconducting current, which has been believed to be a persistent current, decreases with time. Thus, the irreversibility field at which the critical current density goes to zero is much lower than the upper critical field at high temperatures. This trend is much stronger in superconductors with larger anisotropy, and Bi-2212 superconductor is a typical example. RE-123 (RE: rare earth element) superconductor has the lowest anisotropy among the high-temperature superconductors, and the effect of flux creep is not so strong. Hence, application of this superconductor is expected.

The flux pinning properties of high-temperature superconductors are complicated on the temperature versus magnetic field plane in comparison with metallic superconductors. This is caused by the fact that the situation of the pinned flux line lattice varies greatly. The variation depends strongly on the anisotropy, and the changes also depend on the kind or strength of the pinning centers. The energies that determine the behavior of the flux line system are the elastic energy U_E of the flux line lattice, the pinning energy U_P, and the thermal energy U_T. Hence, there are three kinds of transition that are determined mostly by two energies. These are the melting transition between U_E and U_T, the glass-liquid transition between U_P and U_T, and the order-disorder transition between U_E and U_P [9]. Thus, the mixed state in the phase diagram on the magnetic field vs. temperature plane is divided up in a complicated way, which is quite different from the simple mixed state discussed for metallic superconductors.

Another characteristic point is that the superconductivity depends quite sensitively on the carrier density. In polycrystalline superconductors, the superconductivity is easily broken at grain boundaries due to a large distortion or a local deviation from the stoichiometric composition that reduces the carrier density. For this reason, the density of the superconducting current that can tunnel through grain boundaries is quite low for polycrystalline superconductors. It is necessary to fabricate superconductors with highly aligned crystal axes to obtain a high critical current density as in metallic superconductors. Hence, tapes of RE-123 superconductor are now fabricated by using a highly developed thin film technique that can realize a polycrystalline long tape about 1 km in length with a highly aligned tri-axial structure. On the other hand, this property provides very strong pinning forces for point defects or dislocations, which are known as weak pinning centers in metallic superconductors, because the superconductivity will be lost in such defects due to variation in the carrier density. Such a high crystalline alignment is not achieved in Bi-2223 tapes, and their critical current density is lower by about two orders of magnitude in comparison with RE-123. But the thickness of the superconductor is much larger than that of RE-123 thin films, and the engineering critical current density divided by the cross-sectional area of the tape is not significantly different between the two superconductors.

References

1. T. Matsushita, *Flux Pinning in Superconductors*, 2 ed. (Springer, 2014), pp. 26, 151
2. E.H. Brandt, Phys. Rev. B **34**, 6514 (1986)
3. R. Labusch, Cryst. Lattice Defects **1**, 1 (1969)
4. F. Sumiyoshi, H. Kasahara, A. Kawagoe, K. Kubota, S. Akita, IEEE Trans. Appl. Supercond. **13**, 3663 (2003)
5. T. Matsushita, M. Kiuchi, Jpn. J. Appl. Phys. **57**, 103101 (2018)
6. A.M. Campbell, Philos. Mag. B **37**, 149 (1978)
7. T. Matsushita, E. Kusayanagi, K. Yamafuji, J. Phys. Soc. Jpn. **46**, 1101 (1979)
8. K. Yamafuji, F. Irie, Phys. Lett. **25A**, 387 (1967)
9. T. Matsushita, Physica C **214**, 100 (1993)
10. J.R. Clem, J. Low Temp. Phys., **38**, 353 (1980)
11. L. Woltjer, Proc. Natl. Acad. Sci. USA **44**, 489 (1958)
12. J.B. Taylor, Phys. Rev. Lett. **33**, 1139 (1974)
13. T. Matsushita, Physica C **243**, 312 (1995)

Index

T. Matsushita, *Superconductivity and Electromagnetism*, Springer Series in Solid-State Sciences 195, https://doi.org/10.1007/978-3-030-67568-4